Experimental and Computational Analysis of Polyglutamine-Mediated Cytotoxicity

Matthew Tang

Thesis submitted to the
Faculty of Graduate and Postdoctoral Studies
In partial fulfillment of the requirements for the degree of
Doctor of Philosophy in Biochemistry

Department of Biochemistry, Microbiology and Immunology
Faculty of Medicine
University of Ottawa

Abstract

Expanded polyglutamine proteins are known to be the causative agents of a number of human neurodegenerative diseases but the molecular basis of their cytoxicity is still poorly understood. Polyglutamine tracts may impede the activity of the proteasome, and evidence from single cell imaging suggests that the sequestration of polyglutamine proteins into inclusion bodies can reduce the proteasomal burden and promote cell survival, at least in the short term. The presence of misfolded protein also leads to activation of stress kinases such as p38MAPK, which can be cytotoxic. The relationships of these systems are not well understood. We have used fluorescent reporter systems imaged in living cells, and stochastic computer modeling to explore the relationships of expanded polyglutamine proteins, p38MAPK activation, generation of reactive oxygen species (ROS), proteasome inhibition, and inclusion body formation. In cells expressing a polyglutamine protein, inclusion body formation was preceded by proteasome inhibition but cytotoxicity was greatly reduced by administration of a p38MAPK inhibitor. Computer simulations suggested that without the generation of ROS, the proteasome inhibition and activation of p38MAPK would have significantly reduced toxicity. Our data suggest a vicious cycle of stress kinase activation and proteasome inhibition that is ultimately lethal to cells. There was close agreement between experimental data and the predictions of a stochastic computer model, supporting a central role for proteasome inhibition and p38MAPK activation in inclusion body formation and ROS-mediated cell death.

Acknowledgements

I am grateful to my supervisor Dr. Douglas Gray for his encouragement, advice, patience, and guidance during the course of my graduate studies at the University of Ottawa. I would like to sincerely thank him for the opportunity for this PhD research project, for his friendship, and for sharing his wisdom and enthusiasm for science. I am indebted to him for allowing me to explore my own curiosity in science.

I would like to extend my thanks to Drs. John Woulfe, Ian Lorimer, and Luc Sabourin for their role as thesis committee advisors, for their guidance, and constructive criticism (especially their insistence for me to focusing on one project at a time).

I am grateful to Maria and Mitch for being such great team players during our successfully collaborative effort in publishing our p38MAPK project. I would also like to thank Doug and Ian for allowing us the opportunity to pursue this project.

I would like to thank current and past members of the Gray laboratory (especially Mei, Madison, Sophie, Josée, and James) and all members of the Centre for Cancer Therapeutics (especially Ricardo, and Sylvie) for their friendship and support during my time in Ottawa. In addition, many thanks to my fellow lab rats from different labs (especially Jenn, Ian, Jude, Michelle, Laura, Sophie, and Nima) for their camaraderie and sharing their enthusiasm for scientific discovery – the labwork was fun, but the celebrations were even better.

I am indebted to Vivian for her strong emotional support and for her editorial help during the process of writing the thesis. In addition, I am grateful for the countless "home cooked" meals we enjoyed together.

Finally, I am forever grateful to my family especially Sephora, Mom, Dad, and Grandma for their unwavering support.

“Joy in looking and comprehending is nature’s most beautiful gift”

Albert Einstein

Table of Contents

LIST OF FIGURES

LIST OF TABLES

ABBREVIATIONS

Aβ	amyloid-β
AD	Alzheimer's disease
AFP	autofluorescent protein
ALS	amyotrophic lateral sclerosis
AP-1	activator protein-1
APP	amyloid precursor protein
AR	androgen receptor
ASK1	apoptosis signal-regulating kinase 1
ATF2	activating transcription factor 2
ATG	autophagy-related gene
ATP	adenosine triphosphate
ATM	ataxia telangiectasia mutated
Atx-1	ataxin-1
BACE	aspartyl proteases β-secretase
BSA	foetal bovine serum
BSO	buthionine sulphoximine
BRCA1	breast cancer 1, early onset
CACNA1A	calcium channel, voltage-dependent, P/Q type, α1A subunit
CBP	CREB-binding protein
CHIP	c-terminal of HSC-70
CHOP	C/EBP homologous protein
CMV	cytomegalovirus
CREB	cyclic AMP response element binding protein
C-terminal	carboxy-terminal
DAPI	4',6-diamidino-2-phenylindole
DNA	dioxyribonucleic acid
DRPLA	Dentatorubral-pallidoluysian atrophy
DUB	de-ubiquitinating enzymes
EDTA	ethyl diamine-tetra-acetic acid
EGFP	enhanced green fluorescent protein
ERK	extracellular signal-regulated kinase
Gly	glycine
GCP	golgi complex protein
GFP	green fluorescent protein
GPx	glutathione peroxidase
GSH	glutathione
HAT	histone acetyltransferase
Htt	huntingtin
HD	Huntington's disease
HDAC	histone deacetylase
HSP	heat shock protein
IRES	internal ribosome entry site
JNK	c-Jun N-terminal kinase
Kb	kilobase

kDa	kilodalton
LAMP-2A	lysosomal-associated membrane protein 2
Lys	lysine
mRFP	monomeric red fluorescent protein
MAPK	mitogen-activated protein kinase
MDa	megadalton
MEF2C	myocyte enhancer factor 2C
mRNA	messenger RNA
mTOR	mammalian target of rapamycin
NAC	N-acetylcysteine
NaCl	sodium chloride
NAF	sodium Fluoride
NaPPi	sodium pyrophosphate
NBR1	neighbour of BRCA1 gene 1
NP-40	nonidet P-40
NT	non-transgenic
N-terminal	amino-terminal
OPMD	oculopharyngeal muscular dystrophy
PABPN1	poly (A) binding protein nuclear 1
PBS	phosphate buffered saline
PD	Parkinson's disease
PI	proteasome inhibitor
PINK1	PTEN-induced putative kinase 1
PMSF	phenylmethylsulphonyl fluoride
Poly Q	polyglutamine
PP2A	protein phosphates 2A
PS-γ	presenilin-γ-secretase
PSP	progressive supranuclear palsy
PUMA	p53 upregulated modulator of apoptosis
RFP	red fluorescent protein
RNA	ribonucleic acid
ROS	reactive oxygen species
SBMA	spinobulbar muscular atrophy
SCA-1	spinocerebellar ataxia 1
SDS	sodium dodecyl sulfate
SDS-PAGE	sodium dodecyl sulfate polyacrylamide gel electrophoresis
Sp1	specificity protein 1
SV40	simian virus 40
TAK1	transforming growth factor β-activated kinase
TBP	TATA-binding protein
TBST	tris buffered saline with Tween-20
TDP-43	tar DNA-binding protein 43
TRIS	tris (hydrozymethyl) aminomethane
Ub	ubiquitin
UbC	ubiquitin C
UBP	ubiquitin specific protease

UCH	ubiquitin carboxy-terminal hydrolase
UPS	ubiquitin proteasome system
UV	ultraviolet
UVRAG	UV irradiation resistance-associated gene
VGCC	voltage gated calcium channels
Wt	wild-type
YFP	yellow fluorescent protein
3-NP	3-nitropropionic acid
8OHdG	8-Oxo-2'-deoxyguanosine

Chapter 1: Introduction

1.1 Neurodegenerative diseases

Neurodegenerative disorders such as Alzheimer's disease (AD), Parkinson's disease (PD), amyotrophic lateral sclerosis (ALS), Huntington's disease (HD), and spinocerebellar ataxias (SCA) are vicious illnesses characterized by the refractory decline and ultimate death of neurons (reviewed in (Orr, 2000; Ho et al., 2001; Selkoe, 2001; Fahn, 2003; Pasinelli and Brown, 2006)). Onset of these diseases typically occurs during the fourth or fifth decade of life and become progressively more severe with time. The clinical manifestations include cognitive, motor, and/or behavioural dysfunction (Harper, 1992; Orr, 2000). Although molecular genetics have identified specific genes that are associated with each neurodegenerative disease, the molecular characterization of cellular events leading to neuronal cell death remain elusive. To date, there are no effective therapeutic interventions.

Ageing is among the greatest risk factors for neurodegeneration. Age-related decline of the protein clearance mechanism is likely to result in the accumulation of oxidized or misfolded proteins followed by its deposition into abnormal structures (Grune et al., 2004; Vernace et al., 2007). These abnormal proteins may be the result of inherently high translational errors reported in eukaryotic systems (Schubert et al., 2000), elevated oxidation arising from progressive mitochondrial derangement (Hirai et al., 2001), or any number of environmental insults. It is conceivable the additional burden caused by the expression of toxic proteins associated with neurodegenerative diseases pushes the cell past a threshold of irreconcilable repair. Over the life course of the cell, the accumulation of abnormal proteins may simply overwhelm the cell and pathological consequences may ensue.

The diverse pathological derangements seen in the brains of post-mortem patients may reflect the unequal vulnerability of neurons to toxic entities associated with each disease. It has become clear a disruption of cellular homeostasis associated with protein quality control is a contributing factor to the abnormal deposition of proteins that have become a hallmark feature of neurodegenerative diseases (Figure

1) (Mayer et al., 1992; Lowe et al., 1993; Williams and Paulson, 2008).

1.1.1 Evidence of protein aggregates in Alzheimer's disease

More than a century has passed since Alois Alzheimer first described abnormal protein deposits in the form of neuritic plaques and neurofibrillary tangles (Goedert and Spillantini, 2006). Today, these abnormal structures continue to be defining characteristics of Alzheimer's disease (AD), a disease that has been recognized as the major form of age-related dementia (Allan et al., 2009), previously known as "senility". AD affects more than 20 million people giving it the distinction of being the most common neurodegenerative disorder in the world (reviewed in (Goedert and Spillantini, 2006)).

The major component of neuritic plaques was found to be insoluble deposits of amyloid fibrils formed from polymers of the amyloid-β protein (Aβ) (Glenner and Wong, 1984). Aβ is generated by the sequential proteolytic processing of the amyloid precursor protein (APP) by membrane resident proteases called aspartyl proteases β-secretase (BACE) and the presenilin-γ-secretase complex (PS-γ). The cleavage of APP creates two major species of Aβ consisting of 40 or 42-amino acid residues in length (De Strooper and Annaert, 2000; Vassar and Citron, 2000; Kimberly et al., 2003). Since Aβ42 contains two additional hydrophobic amino acids, it is more amyloidogenic and can polymerize into insoluble amyloid fibrils that aggregate into spherical plaques visible by microscopy

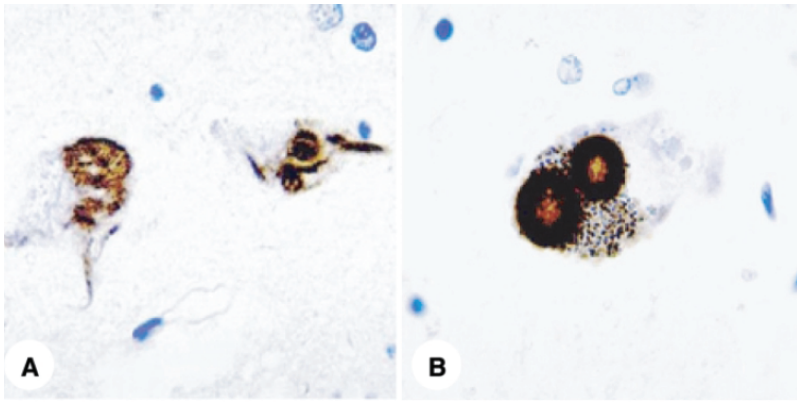

Gray *et al.*, SAGEKE, 2003

Figure 1. Abnormal protein deposits commonly found in neurodegenerative diseases

Immuohistochemical analysis of diseased brains from patients with Alzheimer's or Parkinson's disease showing positive staining for ubiquitin. A) Neurofibrillary tangles in cortical neurons from a patient with Alzheimer's disease. B) A pigmented dopaminergic neuron in the substantia nigra containing two intracytoplasmic Lewy bodies commonly found in patients with Parkinson's disease.

(Iwatsubo et al., 1994). Neuritic plaques are often found in the molecular layer of the dentate gyrus of the hippocampus, the amygdala, and the frontal, temporal, and parietal lobes (Selkoe, 1994, 2004).

Neurofibrillary tangles are the second group of abnormal protein deposit found in the brains of Alzheimer's patients (Figure 1). They are composed of twisted masses of helically wound protein filaments lying in the cytoplasm of neuronal cell bodies and neuritic processes (Selkoe, 2004). The tau protein, a highly stable microtubule-associated protein, has been identified as the main constituent protein of neurofibrillary tangles (Grundke-Iqbal et al., 1986). Hyperphosphorylation of tau results in its detachment from the microtubule and polymerization into insoluble cytoplasmic filaments that aggregate as neurofibrillary tangles (Barghorn and Mandelkow, 2002). Interestingly, tau deposits are also found in numerous other neurodegenerative diseases not associated with Aβ pathology, including progressive supranuclear palsy (PSP), corticobasal degeneration (CBD), Pick's disease (frontotemporal dementia), and Parkinson-dementia complex of Guam (reviewed in (Goedert and Spillantini, 2001; Lee et al., 2001)).

The majority of AD cases are sporadic with familial AD accounting for less than 1% of total cases (Blennow et al., 2006). The prevailing theory of AD posits that the deposition of Aβ triggers all cases of AD and precedes tau phosphorylation and tangle formation which ultimately leads to gradual synaptic and neuritic dysfunction (Hardy and Allsop, 1991). Indeed, genes identified in rare forms of familial AD seem to support the case for Aβ induced toxicity – an increase of Aβ42 has been reported in patients with mutations in the *presenilins* (Citron et al., 1997) and the *APP* gene (Citron et al., 1992; Suzuki et al., 1994).

Interestingly, the duplication of *APP* (which was previously mapped to chromosome 21 (Goate et al., 1989; Hardy et al., 1989)) in patients with Down's syndrome invariably leads an age-dependent development of Aβ plaques as well as neurofibrillary tangles (Lemere et al., 1996).

1.1.2 Evidence of protein aggregates in Parkinson's disease

Parkinson's disease (PD) is the second most common neurodegenerative disorder and is characterised by involuntary shaking (resting tremor), rigidity, and gait problems resulting from the loss of dopaminergic neurons in the substantia nigra and noradrenergic neurons located in the locus coeruleus (Braak et al., 2003). One of the histopathological hallmarks of PD is the presence of intracytoplasmic protein deposits called 'Lewy bodies' (Everett and Wood, 2004; Dickson et al., 2009) (Figure 1). The major constituent of Lewy bodies is α-synuclein. Normally localized to the presynaptic axon terminals and in the nucleus (Maroteaux et al., 1988), α-synuclein occurs physiologically as a folded tetramer of about 58 kDa (Bartels et al., 2011) that becomes destablizied to form amyloid-like filaments under conditions of oxidative stress (Ischiropoulos and Beckman, 2003). In addition, α-synuclein has been reported to form protofibrillar intermediates that may contribute to its cytotoxicity (Lansbury and Brice, 2002).

Although the majority of PD cases are sporadic, there have been several genes that have been identified whose mutations are linked to familial forms of PD. The first gene linked to PD was identified as *α-synuclein* (Polymeropoulos et al., 1997) which led to the discovery that the primary composition of Lewy bodies in sporadic cases of PD was wild-type α-synuclein (Spillantini et al., 1998). The genetic triplication of *α-synuclein* in a rare familial form of PD results in the over-expression of wild-type α-synuclein and results in a

pathological phenotype that closely resembles idiopathic PD (Singleton et al., 2003). *Parkin* and *UCH-L1* are genes that encode components of the intracellular protein degradation machinery responsible for removal of misfolded proteins including α-synuclein; these genes have also been implicated in familial forms of PD (Kitada et al., 1998; Shimura et al., 2000) and their loss of function in animal models have reproduced nigrostriatal defects and dopaminergic neuronal loss seen in human patients (Leroy et al., 1998; Goldberg et al., 2003; Setsuie et al., 2007). Taken together, heritable forms of PD implicate the aggregation of α-synuclein and dysfunctional protein quality control in the pathogenesis of PD.

1.1.3 Evidence of protein aggregates in polyglutamine disorders

Polyglutamine disorders are a large family of late onset neurodegenerative disorders encompassing at least 9 different diseases including five spinocerebellar ataxias (SCA-1, SCA-2, SCA-3, SCA-6, and SCA-7), spinobulbar muscular atrophy (SBMA), dentatorubral-pallidoluysian atrophy (DRPLA), and Huntington's disease (HD) (reviewed in (Everett and Wood, 2004)). They are inherited in an autosomal-dominant fashion and share common clinical and neuropathological features. Individuals afflicted by spinocerebellar ataxia initially display mild loss of limb and gait coordination, imperfect articulation of speech, and have difficulties with breathing and swallowing (Orr, 2000). As the disease progresses symptoms gradually worsen and the patient ultimately succumbs as a result of respiratory failure.

Polyglutamine disorders are caused by an expansion of CAG codons (encoding for glutamine) due to an error in replication in the coding region within a particular protein. During protein synthesis, the expanded CAG repeats results in the production of a mutant protein with an expanded polyglutamine tract causing a gain-of-toxic function that is

deleterious to neurons. The normal function of these proteins is largely unknown with the exception of SBMA (expanded repeat in the androgen receptor (AR), a steroid-hormone receptor (La Spada et al., 1991)), SCA-6 (a P/Q-type α1A calcium channel subunit called CACNA1A (Zhuchenko et al., 1997)), and SCA-17 (the general transcription factor TATA box binding protein (TBP) (Koide et al., 1999)). Typically, a polyglutamine expansion greater than 40 residues is sufficient to induce the disease while the length of the polyglutamine repeat is inversely related to the age of onset (Orr et al., 1993). Although the presence of the expanded glutamine tract is sufficient to cause pathology, each polyglutamine disorder is associated with a unique and unrelated protein (summarized in Table 1). The protein context surrounding the expanded glutamine repeat likely determines which neuronal cell population is at risk (Gatchel and Zoghbi, 2005). For example, in SCA-1 the pathologically expanded ataxin-1 protein is ubiquitously expressed in humans, yet the pathological features are solely manifested in Purkinje cell neurons residing in the cerebellum and to a lesser extent in neurons of the brainstem (Orr, 2000). Similarly in HD, ubiquitously expressed forms of mutant huntingtin protein causes the specific loss of medium spiny neurons in the striatum (Albin et al., 1990; Strong et al., 1993).

In addition to progressive neuronal loss, anatomical features of polyglutamine disorders include the presence of an inclusion body in the nucleus or cytoplasm of specific population of neurons that is afflicted during the course of disease (Davies et al., 1997). Inclusion bodies are microscopically visible protein deposits that have been reported to be exclusively found in the nucleus (SCA-1, SCA-7, and SCA-17), cytoplasm (SCA-2 and SCA-6), or both (in the case of HD, DRPLA, SBMA and SCA-3) (listed in Table 1 and

Disease	Gene name	Protein product	Normal repeat length	Pathogenic repeat length	Site of inclusion body	Reference
SCA-1	*SCA-1*	ataxin-1	6-39	40-82	N	(Matilla et al., 1993)
SCA-2	*SCA-2*	ataxin-2	15-24	32-200	C	(Pulst et al., 2005)
SCA-3	*SCA-3*	ataxin-3	13-36	61-84	C, N	(Padiath et al., 2005)
SCA-6	*CACNA1A*	$CACNA1_A$	4-20	20-29	C	(Zhuchenko et al., 1997)
SCA-7	*SCA-7*	ataxin-7	4-35	37-306	N	(Benton et al., 1998)
SCA-17	*SCA-17*	TBP	25-42	47-63	N	(Koide et al., 1999)
DRPLA	*DRPLA*	atrophin-1	7-34	49-88	C, N	(Komure et al., 1995)
SBMA	*AR*	androgen receptor	9-36	38-62	C, N	(La Spada et al., 1991)
HD	*HD*	huntingtin	11-34	40-121	C, N	(Nahhas et al., 2005)

Table 1. Characteristics of polyglutamine diseases

The characteristics of known polyglutamine diseases and their respective pathogenic gene and protein names are shown in the table. The polyglutamine repeat length of each protein in normal and disease states along with the location of inclusion bodies (cytoplasmic or nuclear) is also listed. Abbreviations: *CACNA1A*, calcium channel, voltage-dependent, P/Q type, α1A subunit; DRPLA, dentatorubral-pallidoluysian atrophy; HD, Huntington's disease; SBMA, spinobulbar muscular atrophy; SCA, spinocerebellar ataxia; TBP, TATA box binding protein; N, nuclear inclusion body; C, cytoplasmic inclusion body. Table adapted from (Gatchel and Zoghbi, 2005).

reviewed in (Gatchel and Zoghbi, 2005). The location, composition, and identity of the proteins which aggregate to form inclusion bodies have been instrumental towards the classification and diagnosis of neurodegenerative disorders (Woulfe, 2008). For example, the intracellular localization and perinuclear accumulation of expanded huntingtin has been reported in the striatum and cerebral cortex (Davies et al., 1997), whereas expanded ataxin-1 form inclusion bodies in Purkinje cells of the cerebellum (Orr, 2000).

There is increasing evidence that dysregulation of transcription may be a common mechanism of neurodegeneration in polyglutamine disorders (Cha, 2000; Sugars et al., 2004b). Transcriptional changes prior to any overt signs of pathology have been consistently reported in several mouse models including SCA-1 (Lin et al., 2000), HD (Luthi-Carter et al., 2002), and SCA-7 (Yoo et al., 2003). Although the molecular mechanisms leading to a decline of transcription is presently unclear, pathogenic expanded polyglutamine proteins are intrinsically linked to the nucleus. For example, the nuclear localization of expanded ataxin-1 was found to be critical in the pathogenesis of SCA-1 (Klement et al., 1998) and ataxin-1 was found to have intriguing RNA binding properties suggesting a role in RNA metabolism (Yue et al., 2001; Irwin et al., 2005). The mutant gene products of DRPLA (atrophin-1), SCA-3 (ataxin-3), and SCA-1 (ataxin-1) have all been implicated as transcriptional regulators (Zhang et al., 2002b; Tsai et al., 2004), while SCA-17 (TBP) and SBMA (android receptor) are themselves transcription factors (La Spada et al., 1991; Nakamura et al., 2001). In addition, several expanded polyglutamine proteins have been found to interact with other proteins containing short polyglutamine stretches including numerous transcription factors and transcriptional regulators such as CREB-binding protein (CBP) (Nucifora et al., 2001), TBP-associated factor (Dunah et al., 2002),

and Sp1 (Li et al., 2002). Intriguingly, TBP was found to co-localize with protein aggregates in brain tissues of SCA-1, SCA-2, SCA-3, and DRPLA patients, and it was suggested the polyglutamine tract is sufficient for the recruitment of TBP into these aggregates (Uchihara et al., 2001). TBP was also found to interact and co-aggregate with expanded huntingtin supporting a critical role of transcriptional dysregulation in polyglutamine disorders (Huang et al., 1998; Uchihara et al., 2001; Schaffar et al., 2004). Together, these data support a genetic gain-of-toxic function of expanded polyglutamine proteins which directly influences gene transcription suggesting an underlying pathogenesis of polyglutamine disorders. However, it remains unclear whether dysregulation of transcription caused by the inadvertent association of expanded polyglutamine proteins with transcription factors occurs prior to inclusion body formation or as the result of inclusion body formation.

1.2 Inclusion bodies – friend or foe?

Expanded polyglutamine proteins adopt a non-native conformation that is highly prone to self-associate leading to the formation of inclusion bodies. The observation that inclusion bodies contain ubiquitin, various heat-shock proteins, and components of the protein degradation machinery suggests a failed attempt of removing the inclusion bodies which may result in further inhibition of proteolysis (reviewed in (Ciechanover and Brundin, 2003)). In a similar manner, the sequestration of transcription factors such as CBP, Sp1, and TBP into inclusion bodies may be the cause of transcriptional dysregulation observed in polyglutamine diseases (Uchihara et al., 2001; Schaffar et al., 2004). In addition, the physical mass of an inclusion body is likely to create steric interference affecting axonal

transport or cellular processes (Gunawardena et al., 2003; Lee et al., 2004) and has also been reported to activate caspases and triggering apoptosis (Ross, 2002). All of these observations suggest that inclusion bodies are detrimental to neurons.

Considerable effort has been made to determine the significance of inclusion bodies with regards to disease progression in neurodegeneration. Circumstantial evidence suggests the accumulation of abnormal structures such as inclusion bodies in disease neurons play a major role in disease pathogenesis. However, this indictment relies heavily on guilt by association – arguments implicating inclusion bodies in neuronal cell death are inconclusive. All the while, new evidence has emerged to suggest inclusion bodies are not toxic entities, but may in-fact have a protective role. Consequently, whether inclusion bodies are pathogenic, protective, or merely an incidental entity remains controversial.

There is compelling evidence that inclusion bodies do not correlate with neuronal death (Saudou et al., 1998; Simeoni et al., 2000; Orr, 2001; Taylor et al., 2003). It has been shown in models of polyglutamine disease that inhibition of proteolysis occurs in the absence of inclusion body formation (Bennett et al., 2005) and interfering with the formation of inclusion bodies can significantly increase neuronal apoptosis (Klement et al., 1998; Saudou et al., 1998). Recently, elegant time lapse fluorescence microscopy experiments by Arrasate et al. demonstrated that cultured neurons forming inclusion bodies live longer than those that do not and the mere presence of inclusion bodies does not conclusively predict neuronal death (Arrasate et al., 2004). Similar work by Gong et al. showed that the detection of inclusion bodies does not coincide with cell death, while inclusion formation enhanced survival (Gong et al., 2008). Interestingly, the addition of pharmacological compounds to promote the formation of inclusion bodies was found to

ameliorate proteasomal dysfunction and reduced cellular pathology in cell models of HD and PD (Bodner et al., 2006). Together, these findings suggest the formation of inclusion bodies is a protective cellular mechanism.

1.3 Toxicity associated with aggregation intermediates

If inclusion bodies are not pathogenic entities, intermediate species prior to the formation of inclusion bodies are likely to be responsible for the toxicity associated with pathogenic proteins. Protein aggregation is a complex process involving several intermediates (reviewed in (Ross and Poirier, 2004) and (Takahashi et al., 2010)) (Figure 2). Expanded polyglutamine proteins in their monomeric form are likely misfolded and undergo conformational changes that increase their propensity to aggregate to form oligomers. The enhanced expression of chaperone proteins in attempts to refold the expanded proteins has been shown to limit their toxicity (Carmichael et al., 2000; Cummings et al., 2001; Kobayashi and Sobue, 2001). If the toxic proteins cannot be refolded, they will oligomerize to form protofibrils, leading to mature fibers before proceeding into an inclusion body. Previous studies have reported that oligomers and protofibrillar intermediates of expanded polyglutamine proteins induce greater toxicity than either polyglutamine monomers or inclusion bodies (Poirier et al., 2002; Sanchez et al., 2003; Takahashi et al., 2008). Recently, Lajoie and Snapp showed that the soluble polyglutamine oligomers are the predominant toxic species in polyglutamine disease pathogenesis and high levels of soluble oligomers induce greater cell death that was independent of inclusion body formation (Lajoie and Snapp, 2010).

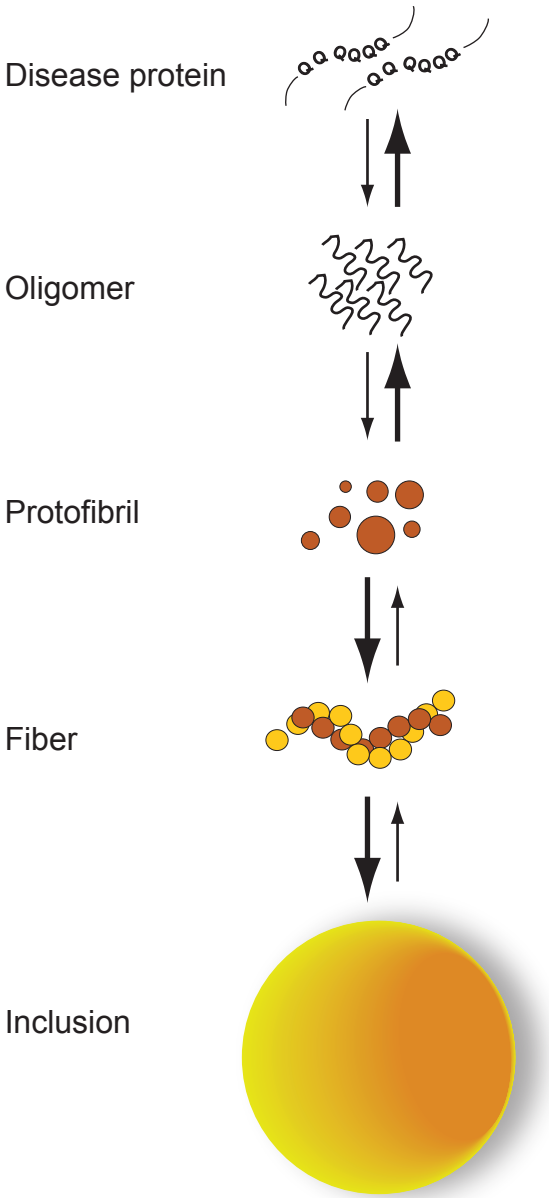
Disease protein
Q Q QQQ
Q Q QQQ
Oligomer
Protofibril
Fiber
Inclusion

Figure 2. Schematic diagram representing the aggregation of expanded polyglutamine proteins into an inclusion body

The formation of an inclusion body is a complex process involving several intermediates. Disease proteins containing an expanded polyglutamine tract exists as soluble monomers that are prone to misfolding. If the monomer cannot be refolded, their inherent tendency to interact with other monomers will result in the formation of oligomers. The aggregation of several oligomers leads to the formation of insoluble protofibrils, fibers, and finally an inclusion body. Figure adapted from (Ross and Poirier, 2004).

The observation of toxicity associated with oligomeric forms of huntingtin proteins is not exclusive to polyglutamine disorders. Intracellular Aβ was found to initiate neuronal dysfunction prior to its accumulation in extracellular plaques (Chui et al., 1999; Hsia et al., 1999) and the oligomeric intermediate of Aβ aggregation was later found to be the most toxic entity (Haass and Selkoe, 2007). In addition, the reduction of oligomer concentration by accelerating Aβ fibrillization has been shown to reduce functional deficits in mouse models (Cheng et al., 2007). Taken together, these experiments suggest the soluble oligomeric form of disease-associated proteins are the toxic entities that drive disease pathology. The formation of abnormal structures such as neuritic plaques or inclusion bodies may be a protective mechanism in attempt to reduce the concentration of the oligomeric species.

Although the intermolecular structure of expanded polyglutamine proteins and their intermediate aggregates have not been resolved, several groups have proposed various arrangements including anti-parallel β-sheets, parallel β-sheets, and head-to-tail cylindrical β-sheets (Perutz et al., 1994; Lathrop et al., 1998; Perutz et al., 2002). These proposed structures are all strikingly similar to amyloid fibrils that are associated with AD (Benzinger et al., 1998; Chen et al., 2002). Interestingly, the structural organization of α-synuclein fibrils has also been reported to have parallel β-sheet organization (Der-Sarkissian et al., 2003) and it is tempting to speculate that these disease proteins, at least in their oligomeric form, share a common amyloid-like structure that trigger neuronal dysfunction. Recently, an antibody was generated to recognize only oligomeric forms of Aβ and was found not only to interact with α-synuclein and expanded polyglutamine proteins, but was able to limit their toxicity (Kayed et al., 2003). If neurodegenerative diseases share a common

mechanism of pathogenicity based on their oligomeric structure, its targeted removal may emerge as a viable opportunity for therapeutic intervention.

1.4 Intracellular protein degradation

Efficient protein quality control mechanisms are essential in post-mitotic cells such as neurons because they do not have the ability to dilute potentially toxic proteins or aggregates by distributing their contents to daughter cells by means of cell division. Disease-associated mutant proteins such as Aβ, α-synuclein, and expanded polyglutamine proteins confer a gain-of-toxic function, become aggregation prone, and resist degradation. The failure to remove them may result in neuronal dysfunction and ultimately death of the neuron. Eukaryotic cells rely on two dominant intracellular protein degradation pathways: the ubiquitin-proteasome system removes short-lived nuclear and cytoplasmic proteins, whereas the process of bulk degradation of larger membrane proteins, cytoplasmic protein complexes, and organelles is accomplished by autophagy. What follows is a review of intracellular protein degradation pathways along with implications concerning neurodegeneration.

1.4.1 The ubiquitin-proteasome system

The ubiquitin-proteasome system (UPS) is responsible for the rapid and irreversible elimination of proteins (Figure 3) (reviewed in (Ciechanover and Brundin, 2003)). Ubiquitin is a ubiquitously expressed 76 amino acid protein which serves as a covalent tag to direct substrates for degradation (Ciechanover, 2005). The attachment of ubiquitin proceeds through a series of concerted steps involving ubiquitin metabolizing enzymes (E1, E2, and E3). Firstly, the ubiquitin activating enzyme E1 hydrolyses adenosine triphosphate

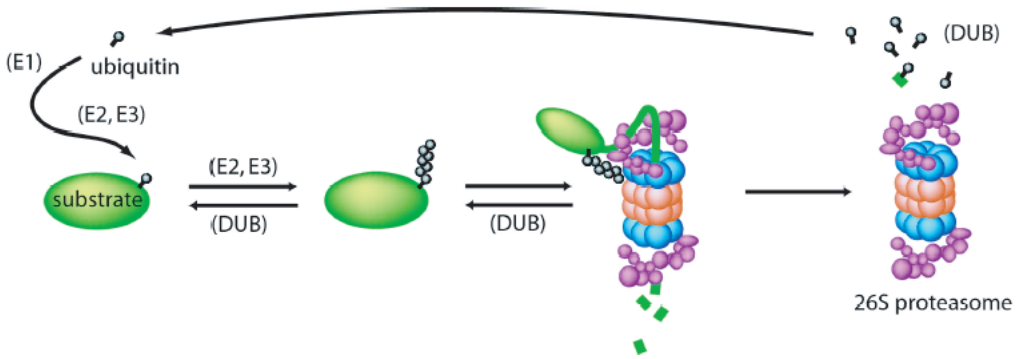

Gray et al, SAGEKE, 2003

Figure 3. Schematic diagram representing the ubiquitin-proteasome system

The covalent attachment of ubiquitin to a protein substrate (either a normal protein destined for degradation or a damaged or abnormally folded protein) proceeds via a three-step cascade. In the initial reaction, the C-terminal of ubiquitin is activated by the E1 ubiquitin activating enzyme. Substrate recognition and subsequent addition of ubiquitin molecules to the substrate is mediated through the activities of E2 and E3 activating enzymes, respectively. The addition of a ubiquitin molecule to the substrate is followed by successive addition of other ubiquitin moieties through the formation of an isopeptide bond between Lys48-Gly76 to form a polyubiquitin chain. Lys48-linked chains of 4 or more ubiquitin molecules are recognized by the proteasome where the substrate is unfolded and degraded by the proteolytic activities lining the inner rings of the protease. Deubiquitylating enzymes (DUBs) recycle ubiquitin by releasing ubiquitin from the polyubiquitin chain assembled on the substrate, yielding free ubiquitin monomers.

(ATP) to create a thioester linkage between its active site cysteine residue and the highly conserved G76 residue of the C-terminus of ubiquitin forming a high-energy thioester intermediate (E1-S~ubiquitin) (Ciechanover et al., 1981). Secondly, the activated ubiquitin moiety is transferred to the ubiquitin-carrier protein E2 via a transthiolation reaction. In contrast to the E1 activating enzymes, there exists a large family of approximately 40 E2 conjugases that can have diverse functions not necessarily pertaining to proteolysis (reviewed in (Jentsch et al., 1990)). The third and final step of the ubiquitylation involves the recruitment of E3 ubiquitin ligases by the E2 enzyme. As the most diverse component of the UPS, the E3 ligases are responsible for substrate-binding specificity as well as spatial and temporal control of ubiquitylation (Kim et al., 2007a). They cooperate with E2 enzymes to determine the length and topology of ubiquitin chains (Ye and Rape, 2009).

The removal and disassembly of the ubiquitin chain can serve to reverse the fate of a substrate that is otherwise destined for proteasomal degradation thereby affecting their steady state levels. Deubiquitylating (DUB) enzymes are thiol proteases that counteract the activities of E1, E2, and E3 enzymes (reviewed in (Amerik and Hochstrasser, 2004)) and play an active role in the recycling of monomeric ubiquitin (Hadari et al., 1992; Papa et al., 1999). There are two main families of DUB enzymes. Ubiquitin carboxy-terminal hydrolases (UCH) are a small group of enzymes that efficiently cleave ubiquitin from small peptides of proteins (Larsen et al., 1998). For example, UCH-L1 has been reported to cleave ubiquitin from small adducts and is thought to play a role in maintaining pools of monomeric ubiquitin (Osaka et al., 2003). The second family of DUBs consists of a much larger group of ubiquitin-specific processing proteases (UBPs) which are unrelated to the UCH family of proteases (Tobias and Varshavsky, 1991). They are much larger in size with

a molecular mass ranging from 50 – 250kDa (Soboleva and Baker, 2004) and have been shown to reverse the ubiquitylation of specific regulatory proteins and thereby preventing their degradation by the 26S proteasome (Huang et al., 1995; Cummins et al., 2004; Li et al., 2004).

1.4.2 Components of the ubiquitin-proteasome system associated with neurodegeneration

The observation that ubiquitin co-localized with abnormal protein deposits associated with neurodegenerative diseases (neurofibrillary tangles in AD, Lewy bodies in PD, and polyglutamine inclusion bodies in HD) suggested the UPS played a critical part in neurodegeneration ((Mori et al., 1987; Kuzuhara et al., 1988; DiFiglia et al., 1997) and reviewed in (Layfield et al., 2003)). Immunohistochemical analysis with anti-ubiquitin antibodies of pathological sections continues to be used for disease diagnosis by neuropathologists (Woulfe, 2008). Figure 1 show examples of immunohistochemical staining of neurofibrillary tangles and Lewy bodies using an anti-ubiquitin antibody.

The discovery of mutations within genes encoding components of the UPS resulting in heritable neurodegenerative diseases made it clear that intracellular protein degradation was intimately linked to the causation of disease. For example, mutations in the E3 ubiquitin-ligase UBE3A (also known as E6-AP) is encoded by the *UBE3A* gene and was found to cause Angelman syndrome, a disease characterized by mental retardation, seizures, and abnormal gait (Kishino et al., 1997). Parkin, an E3 ligase whose mutation causes autosomal recessive juvenile forms of PD (Kitada et al., 1998; Shimura et al., 2000), has been implicated in the proteasomal degradation of aberrant or misfolded proteins including α-synuclein (Shimura et al., 2001) and mutant ataxin-1 (Tsai et al., 2003); it has also been shown to be critical for the maintenance of mitochondrial homeostasis in dopaminergic

neurons (Park et al., 2006; Matsuda et al., 2010). The ubiquitin hydrolase enzyme UCH-L1 has also been associated with dominantly inherited PD (Leroy et al., 1998), although its function in PD pathogenesis is unclear. Interestingly, UCH-L1 has the potential to operate as a ubiquitin hydrolase and a E3 ubiquitin ligase (Liu et al., 2002). As a hydrolase, it has been shown to salvage monomeric ubiquitin within neurons (Osaka et al., 2003), whereas deletion of UCH-L1 in mice causes gracile axonal dystrophy in mice and is associated with the formation of ubiquitylated intraneuronal aggregates (Saigoh et al., 1999).

Further reports have highlighted the consequences of a dysfunctional UPS in neurodegeneration. Mutations of UBE3A (E6-AP) were found to enhance the toxicity in a mouse model of SCA-1 (Cummings et al., 1999), while the enhanced expression of CHIP (C-terminal of HSC-70), an E3 ligase that interacts with chaperone proteins to promote the degradation of misfolded proteins, has been shown to suppress the toxicity associated with polyglutamine protein aggregation including the mutant ataxin-1 and the androgen receptor (Al-Ramahi et al., 2006; Adachi et al., 2007; Mishra et al., 2008). Taken together, these findings make it clear that the UPS plays a central role in neurodegenerative diseases.

1.4.3 Targeting proteins to the proteasome

There are several ways E3 ligases can modify a targeted substrate with ubiquitin. Monoubiquitylation is the attachment of a single ubiquitin moiety and plays a role in gene expression and transcriptional control (Sun and Allis, 2002; Kao et al., 2004). The attachment of ubiquitin at multiple sites within a substrate (multiubiquitylation) has been associated with protein localization and modulating protein activities (Kerscher et al., 2006; Mukhopadhyay and Riezman, 2007). Alternatively, ubiquitin itself can serve as the attachment point on one of its seven lysine residues (Lys6, Lys11, Lys27, Lys29, Lys33,

Lys48, or Lys63) and the sequential attachment of further ubiquitin moieties generates a polyubiquitin chain. It is also possible to form chains of differing topology such as atypical forked or mixed ubiquitin chains (Ikeda and Dikic, 2008; Iwai and Tokunaga, 2009), however, the function of these chains remain unclear.

The successive attachment of ubiquitin at position Lys63 forms a linear polyubiquitin chain that has been shown to be involved in activating transcription factors, signal transduction, and DNA replication and repair complexes (Deng et al., 2000; Thrower et al., 2000; Hoege et al., 2002; Ulrich and Walden, 2010). By contrast, chain assembly using Lys48 results in a zigzag topology that functions as a signal for protein degradation by the 26S proteasome. Although monoubiquitylation and alternative linkages of polyubiquitin chains have been reported to target substrate proteins for removal (Baboshina and Haas, 1996; Hofmann and Pickart, 2001; Boutet et al., 2007; Saeki et al., 2009), the 26S proteasome undoubtedly has a preference for Lys48 linked polyubiquitin chains and possesses a physical affinity to substrates modified by four or more ubiquitin molecules (Thrower et al., 2000; Glickman and Ciechanover, 2002).

1.4.4 The 26S proteasome

The 26S proteasome (named for its sedimentation coefficient by density gradient centrifugation) is a large cylindrical multicatalytic protease complex that is charged with the destruction of ubiquitylated proteins into short peptides (Figure 4). The highly conserved 2.5MDa proteasome complex can be functionally divided into two major sub-assemblies: the cylindrical 20S core particle responsible for peptide bond cleavage and the 19S regulatory particle charged with the task of unfolding the substrate and feeding it into the core for degradation (reviewed in (Pickart and Cohen, 2004) and (Finley, 2009)).

A

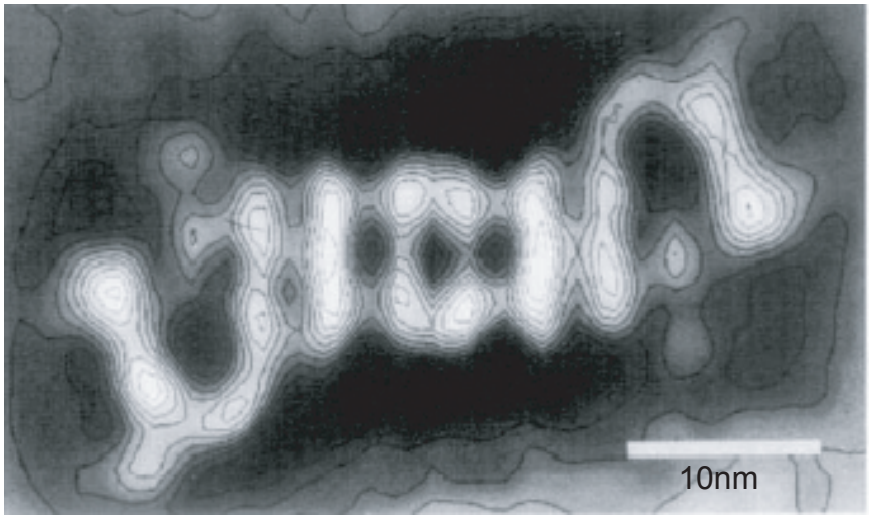

Yoshimura et al, 1993

B

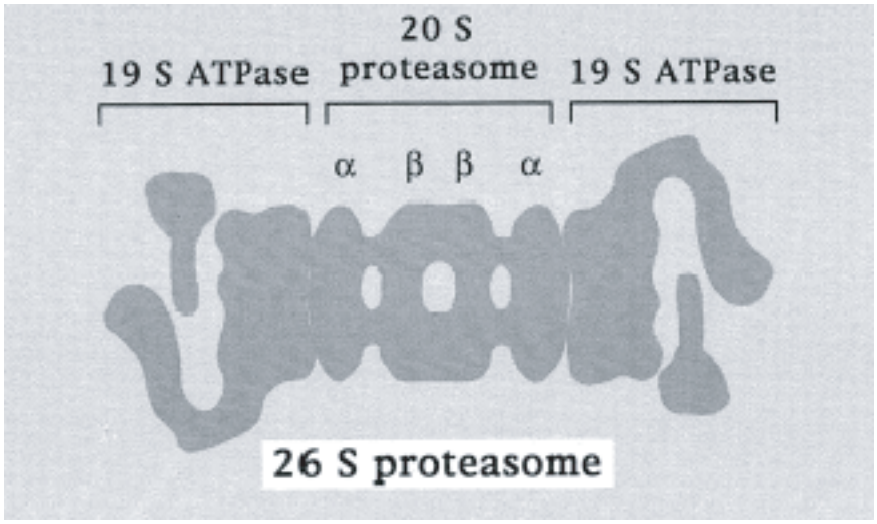

Kessel et al, 1995

Figure 4. The eukaryotic 26S proteasome

A) Electron micrograph of the eukaryotic 26S proteasome isolated from rat liver. The structure consists of two 19S regulatory particles flanked on either end of the 20S catalytic core. B) Schematic representation of (A) showing the lid and base components of the 19S regulatory particle.

The 19S regulatory unit does not possess proteolytic activity and is found at the ends of the 20S core particle. It is composed of 19 subunits that make up the lid and base components which control substrate access to the catalytic chamber (Hershko and Ciechanover, 1998). Protein-unfoldase activity at the base of the regulatory particle unfolds and threads the substrate into the narrow channel opening of the catalytic chamber of the 20S core particle (Smith et al., 2005). This ensures controlled and efficient hydrolysis and the progressive degradation of the substrate into small peptides thereby limiting the generation of incomplete reactions.

The 20S core particle is a barrel-like structure with four stacked 7-membered rings. It is composed of two distinct subunits: the ß-type subunits which contain the catalytic activities and the α-type subunits which are required for structural reasons totaling 28 different subunits (reviewed in (Hilt and Wolf, 1995) and (Groll et al., 1997)). The proteolytic activity is sequestered within the internal space of the catalytic core. There are three subunits containing proteolytic active sites (β-1, β-2, and β-5) (Heinemeyer et al., 1991) which exhibit three distinct activities associated with the 20S proteasome: the trypsin-like, the chymotrypsin-like, and the post-glutamyl peptidyl hydrolytic (PGPH) activities which cleave after basic, large hydrophobic, and acidic residues, respectively (Orlowski et al., 1993).

1.4.5 Proteasome efficiency and neurodegenerative diseases

The decline in proteolytic efficiency with age has previously been reported in many tissues (Carrard et al., 2002; Keller et al., 2002; Ferrington et al., 2005). Transcriptional studies have shown a decline in mRNAs of UPS components in the ageing mouse brain (Lee et al., 2000; Blalock et al., 2003). Recently, a comprehensive study of the structure and

function of the proteasome isolated from mouse liver showed a 40% decrease in proteolytic activity in the 12-month-old mice compared to that of 6-month-old littermates (Rodriguez et al., 2010). By analyzing the three peptidolytic activities of the proteasome in conjunction with intracellular distribution, they showed a profound decline of proteasome function in the nuclear fractions (Rodriguez et al., 2010). Such a decline in proteasome function in the nucleus could ultimately lead to compromised cellular signalling and transcriptional dysregulation. Interestingly, the impairment of the proteasome has also been reported in several neurodegenerative diseases including AD (Keller et al., 2000), PD (McNaught et al., 2001), and polyglutamine models (Bence et al., 2001; Ortega et al., 2010). However, it is unclear if proteasome inhibition is the result of the failure to degrade monomeric forms of the toxic proteins or the inability to degrade oligomeric species and inclusion bodies.

The efficiency of the proteasome in degrading disease proteins such as expanded polyglutamine proteins is controversial. Several groups have reported that expanded polyglutamine proteins act as proteasome inhibitors (Verhoef et al., 2002; Venkatraman et al., 2004), while other have shown they are completely and efficiently degraded (Michalik and Van Broeckhoven, 2004; Bennett et al., 2005). Experiments using an inducible mouse model of HD in combination with a UPS reporter mouse detected proteasomal inhibition when the mutant huntingtin protein was expressed (Ortega et al., 2010). Yet, the continual expression of mutant huntingtin in UPS reporter mice showed an accumulation of ubiquitin conjugates without global UPS impairment (Maynard et al., 2009), supporting the previous observation that failed to detect proteasome inhibition in the brains of HD mice (Diaz-Hernandez et al., 2003).

There are indications that the UPS is fully functional in the early stages of polyglutamine disorders. In inducible mouse models of HD and SCA-1, the cessation of expression of the mutant polyglutamine proteins led to clearance of aggregates and inclusion bodies which correlated with the recovery of motor co-ordination (Yamamoto et al., 2000; Martin-Aparicio et al., 2001; Zu et al., 2004). This suggests that neurons may have the ability to repair damage caused by the expression of toxic proteins including the removal of inclusion bodies. However, it is unclear which proteolytic process is actually responsible for this observation (the UPS, autophagy, or both). It is tempting to speculate that proteolytic systems may co-operate to maintain cellular homeostasis – should the UPS become unable to cope with the accumulating backlog of misfolded proteins, the activation of autophagy may prove to be the next viable option (Rideout et al., 2004). Not surprisingly, there has been much interest in the role of autophagy in neurodegeneration (Komatsu et al., 2006a; Rubinsztein, 2006).

1.4.6 The autophagy-lysosome pathway

The word autophagy is derived from the Greek meaning to self-eat. It is an intracellular degradation process by which cells break down their own components using the lysosomal degradation pathway (Figure 5) (reviewed in (Kim and Klionsky, 2000; Cuervo, 2004; Yorimitsu and Klionsky, 2005)). Unlike the UPS, which rapidly degrades ubiquitylated substrates, autophagy is a slower generally non-selective degradation system that mediates the remove of insoluble misfolded protein substrates in the cytosol (Ding and Yin, 2008), entire organelles (such as defective or damaged mitochondria and peroxisomes), or parts of organelles (such as regions of Golgi and endoplasmic reticulum) (Lemasters et al., 2002; Bellu and Kiel, 2003).

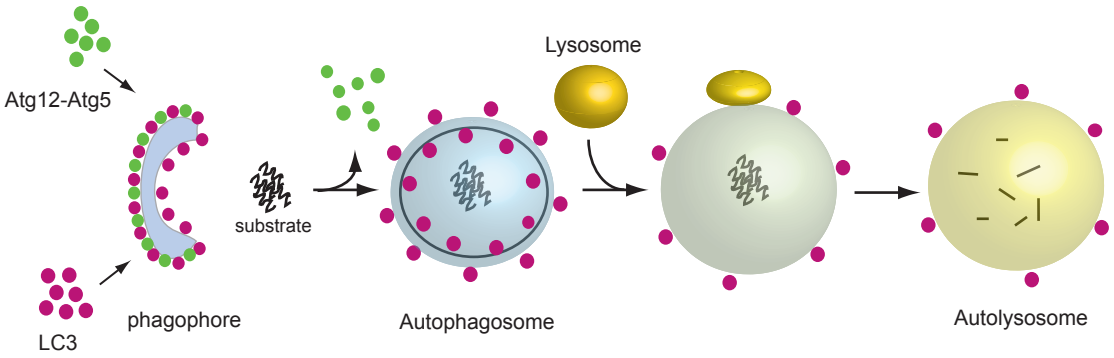
Atg12-Atg5
LC3
phagophore
substrate
Autophagosome
Lysosome
Autolysosome

Figure 5. Schematic diagram representing macroautophagy

The bulk degradation of cytoplasmic protein complexes or organelles begins with a vesicle nucleation event, which forms a double-membrane structure called the phagophore. Vesicle elongation is accomplished by the localization of the Atg12-Atg5 complex and LC3 to the phagophore forming an autophagosome. The Atg12-Atg5 complex dissociates from the autophagosome while LC3 remains on the membrane. The autophagosome fuses with the lysosome to form the autolysosome, where their contents are degraded by acidic lysosomal hydrolases and are recycled in the form of amino acids, fatty acids, sugars, or nucleotides. Figure adapted from (Ravikumar et al., 2009).

There are three major forms of autophagy. The first is microautophagy which involves the lysosomal membrane invaginating to engulf cytosolic proteins which are then taken into the lysosome vacuole (Muller et al., 2000). The second is chaperone-mediated autophagy. Proteins that contain a pentapeptide motif Lys-Phe-Glu-Arg-Gln (KFERQ) are recognized by the cytosolic chaperone HSC70, forming a chaperone-substrate complex (Massey et al., 2004). This complex is transported to the lysosome where it is recognized by the lysosomal membrane receptor LAMP-2A resulting in the translocation of the substrate across the lysosomal membrane into the lysosomal lumen (Massey et al., 2004). The third is macroautophagy (generally known as autophagy), which involves the sequestration of cytosolic components into a double or multilamellar cytosolic vesicle, called an autophagosome (Yorimitsu and Klionsky, 2005). The origin of this membrane is unknown but is believed to be sourced from the endoplasmic reticulum (ER), Golgi complex, and even the mitochondria. The autophagosome then fuses with the outer membrane of the lysosome, which is enriched in numerous digestive enzymes that subsequently degrade the sequestered material (Klionsky and Ohsumi, 1999; Yorimitsu and Klionsky, 2005).

There are approximately 35 autophagy-related (*ATG*) genes that are necessary for autophagosome formation, elongation and expansion of the phagophore membrane, and the maturation and fusion of the autophagosome to the lysosome (Klionsky et al., 2003; Yorimitsu and Klionsky, 2005). Two genes, *ATG5* and *ATG7*, have been identified to be essential for autophagy – the activities of Atg5 and Atg7 catalyze a conjugation event involving several other Atg proteins including LC3 to form the Atg12-Atg5 protein complex required for autophagosome formation (Hara et al., 2006; Komatsu et al., 2006b).

The Atg1 kinase complex is primarily involved in autophagy induction, while Atg6 and Atg14 participate in vesicle nucleation. The Atg11-Atg19 complex is required for cargo recognition while the LC3-Atg12 complex is required for cargo recognition and packaging. The most characterized gene is *Beclin 1*, whose product has been shown to be critical for the formation of the autophagosome. Originally identified as an interaction partner of the anti-apoptotic protein Bcl-2 (Liang et al., 1998), Beclin 1 interacts with Vps34, a class III phosphatidylinositol-3-kinase (PI3K) to form an autophagy-regulating macromolecular complex. The formation of the autophagosomes is accomplished through the recruitment of other Atg proteins (Suzuki et al., 2001; Itakura et al., 2008). The binding of Beclin 1 to Bcl-2 prevents its interaction with Vps34 resulting in the inhibition of autophagy. During nutrient deprivation Beclin 1 dissociates from Bcl-2 and interacts with proteins that positively regulate autophagy (Maiuri et al., 2007). Positive regulators of Beclin 1 have been identified that promote autophagy including UVRAG (UV irradiation resistance-associated gene) (Liang et al., 2007), Bif-1 (also known as Endophilin B1), and AMBRA1 (a protein recently found to be critical for normal neural tube development) (Fimia et al., 2007).

Autophagy has been shown to be necessary for proper neuronal development, plasticity, and homeostasis (Wang et al., 2006; Fimia et al., 2007; Komatsu et al., 2007). Autophagy occurs at a basal level in normal growing cells but can be significantly induced in times of cellular stress such as nutrient deficiency, heat or oxidative stress, and/or the accumulation of damaged cellular components. Autophagy can serve as an important survival mechanism by removing potentially toxic components and damaged organelles and recycling amino acids, lipids, carbohydrates, and nucleotides (Yorimitsu and Klionsky,

2005). The master negative regulator of autophagy is TOR (target of rapamycin), a serine/threonine protein kinase that monitors energy status, growth factors, and nutrients availability (Levine and Klionsky, 2004). Under nutrient rich conditions, TOR suppresses autophagy by directly interacting with the complex responsible for autophagosome induction (Mizushima, 2010). Under starvation conditions, however, TOR is inhibited resulting in the activation of autophagy (Noda and Ohsumi, 1998; Mizushima, 2010).

1.5 The link between UPS and autophagy

The removal of cellular material by autophagy has long been considered to be independent of the UPS. However, there is new evidence that suggest co-operation between both protein clearance pathways. There are several proteins that are substrates of both the UPS and the autophagy-lysosome system (Fuertes et al., 2003b; Fuertes et al., 2003a; Wooten et al., 2008). Recent evidence suggests that the posttranslational modification of substrates by ubiquitin can also serve as a signal for selective autophagy (reviewed in (Korolchuk et al., 2010)). The use of adaptor molecules has been proposed to facilitate the autophagic degradation of ubiquitylated proteins and suggests a selectivity in the sequestration of autophagic cargo (Kirkin et al., 2009b). For example, p62 (SQSTM1/A170) and NBR1 (neighbour of BRCA1 gene 1) have been reported to act as adaptor proteins for the autophagic degradation of ubiquitylated substrates and organelles (Kim et al., 2008; Lamark et al., 2009). Both p62 and NBR1 contain ubiquitin association (UBA) domains and preferentially bind Lys63- as opposed to Lys48-linked chains (Tan et al., 2007; Waters et al., 2009) and have affinity for the autophagic membrane (Pankiv et al., 2007). Thus, it has been proposed that p62 and/or NBR1 sequester ubiquitylated substrates

(via its UBA domains) forming a complex that is recognized by the autophagic machinery which then engulf and degrade the entire complex (Kirkin et al., 2009a). The role of adaptor molecules such as p62 may identify substrate for autophagy and may be important in selective autophagy for ubiquitylated substrates.

1.6 Autophagy and neurodegeneration

The ability to remove insoluble cytosolic proteins before they aggregate to toxic levels has become pertinent in the context of neurodegenerative diseases. The observation that neural-specific autophagy-deficient mice develop symptoms of neurodegeneration including deficits in motor functions with neuronal pathology (including the presence of ubiquitylated inclusion bodies) suggests that polyubiquitylated proteins are substrates for autophagy (Hara et al., 2006; Komatsu et al., 2006b). Recently, the disease protein linked to Lafora disease, an autosomal recessive neurodegenerative disease, was found to be a regulator of autophagy (Knecht et al., 2010). The loss of laforin results in the increased activity of mTOR (mammalian target of rapamycin) leading to a deficiency in autophagy resulting in the accumulation of intracellular inclusion bodies called Lafora bodies. Autophagy may therefore have a critical role in the removal of protein aggregates (previously destined for the UPS) before they reach a toxic level. Dysfunctional autophagy has been reported in several neurodegenerative diseases. For example, an increased number of autophagic vacuoles has been reported in many HD models and HD patients (Kegel et al., 2000). The neurons of AD patients have been reported to have many autophagosomes containing Aβ (Boland et al., 2008) and reduced levels of Beclin 1 (Pickford et al., 2008), suggesting a failed clearance attempt by autophagy. In PD, it has been shown that pink 1

and parkin modulate mitochondrial trafficking and their clearance by autophagy through signalling via Lys63-linked polyubiquitylated signals (Vives-Bauza et al., 2010).

Interestingly, the induction of autophagy has been shown to degrade disease proteins associated with neurodegenerative disorders including expanded polyglutamine proteins, mutant forms of α-synuclein, and tau (Webb et al., 2003; Ravikumar et al., 2004; Berger et al., 2006; Shibata et al., 2006). Although the wild-type forms of these proteins are normally degraded by the proteasome, their mutations incur toxic properties that are much more resistant to degradation and therefore must rely on autophagy for their removal. In addition, mTOR was found to be sequestered into aggregates suggesting a potential mechanism for the upregulation of autophagy (Ravikumar et al., 2004), while the acute inhibition of the proteasome was found to activate autophagy (Iwata et al., 2005). Thus, the upregulation of autophagy using pharmacological compounds (such as rapamycin or rilmenidine) may provide a protective role against the progression of neurodegenerative diseases and may be a therapeutic treatment (reviewed in (Bove et al., 2011)).

1.7 Reactive oxygen species and neurodegeneration

The accumulation of aggregates caused by the expression of disease proteins may be a potential generator of oxidative stress. Abnormal aggregates can influence normal cellular metabolism and the deposition of abnormal proteins induces oxidative stress and mitochondrial dysfunction. Reactive oxygen species (ROS) are the natural by-product of enzymatic reactions and are produced from the mitochondrial electron transport chain during the production of ATP. However, gradual mitochondrial dysfunction results in a decreased production of ATP along with an increase in the production of ROS such as

superoxide anions (O_2^-) and hydrogen peroxide (H_2O_2) (reviewed in (Ding et al., 2006)). The cell has several antioxidant mechanisms in which to control oxidative stress. The particularly damaging superoxide anions are rapidly converted to hydrogen peroxide (H_2O_2) by copper/zinc superoxide dismutase (SOD1) in the cytoplasm and mitochondrial intermembrane space, or manganese superoxide dismutase (SOD2) which is located in the mitochondrial matrix (Zhang and Gutterman, 2007). Finally, antioxidant molecules such as glutathione peroxidise (GPx) or catalases reduces H_2O_2 to form water (Zhang and Gutterman, 2007). If these antioxidant measures are not successful in counterbalancing ROS and/or the dysfunctional mitochondria are not removed, a condition of oxidative stress may ensue and wreak havoc on cellular components. Proteins damaged as a result of oxidative stress must be removed by the proteasome. It has been suggested that the proteasome not only is a target of oxidative stress, (by damaging subunits that make up the proteasome) but also a mediator of oxidative stress (Ding et al., 2006). If the proteasome becomes overburdened, the failure to removed oxidized proteins may induce mitochondrial dysfunction resulting in the further production of ROS. Oxidative damage within the CNS include lipid oxidation, protein oxidation, and DNA oxidation (reviewed in (Ding et al., 2006)). Lipid oxidation results in the formation of three groups of oxidative products: 2-alkenals and ketoaldehydes are the least reactive oxidation products, while 4-hydroxy-2-alkenals is the most reactive (Ding et al., 2006). The cytotoxicity of 4-hydroxy-2-alkenals is primarily due to their propensity to form covalent bonds with the cysteine, histidine, and lysine residues, the consequence of which has been reported to be inhibition of the proteasome (Ferrington and Kapphahn, 2004). In addition, proteins cross-linked with 4-hydroxy-2-alkenals are also able to inhibit proteasome function (Friguet and Szweda, 1997).

Elevated levels of ROS can also result in protein oxidation. The direct oxidation of lysine, arginine, proline, and threonine residues of proteins results in the formation of protein carbonyls (reviewed in (Sohal, 2002)). This can alter the tertiary structure of the protein exposing hydrophobic residues increasing its propensity to form potentially deleterious protein-protein interactions (Beckman and Ames, 1998). Finally, nucleotide base damage and DNA and RNA strand breaks have been shown to be a result of oxidative damage caused by proteasomal inhibition (Bohr, 2002; Ding et al., 2004).

Not surprisingly, oxidative damage has been reported in several neurodegenerative diseases. Perhaps the best example is the mutation of *SOD1* in familial forms of ALS (Rosen et al., 1993), a mutation that was found to mediate neuronal toxicity associated with high levels of mitochondrial superoxides (Zimmerman et al., 2007). Oxidative stress has been also been associated with AD, with several reports indicating an increase in the levels of DNA oxidation products such as 8-hydoxydeoxyguanosine (8OHdG) in the mitochondria and nucleus, presence of oxidized proteins, and carbonyl toxicity (Markesbery, 1997; Smith et al., 1997; Picklo et al., 2002). There are many examples of oxidative stress in PD. Brains of patients with PD have increased oxidative damage and defective mitochondrial function (Alam et al., 1997; Nunomura et al., 2007), while parkin-deficient mice show mitochondrial dysfunction and oxidative damage (Palacino et al., 2004). Interestingly, familial forms of PD have been associated with genes involving oxidative stress and mitochondrial functions. These include *PARK7*, a redox-sensitive chaperone protein also known as DJ-1 which localizes to the mitochondria during oxidative stress (Bonifati et al., 2003), and *PINK1*, a mitochondrion-targeted serine/threonine kinase linked to the maintenance of mitochondrial structure and function (Valente et al., 2004). Finally, the expression of mutant huntingtin

has been shown to cause excitotoxicity and damage to the mitochondria, leading to the increase generation of destructive oxygen free radicals and to alterations in energy production (Beal, 2005). In addition, oxidative stress markers such as 8OHdG, lipid peroxidation and nitrotyrosine has been reported in human and animal models of polyglutamine diseases (Browne et al., 1999; Bogdanov et al., 2001). The importance of mitochondrial function was highlighted by the discovery that the administration of mitochondrial toxins, such as 3-nitropropionic acid (3-NP) in animals and humans causes progressive striatal degeneration resulting in the presentation of clinical and pathophysiological features of HD (Ludolph et al., 1992; Borlongan et al., 1997). The evidence suggest alterations in energy metabolism or mitochondrial function contribute to cell death in polyglutamine diseases (Grunewald and Beal, 1999).

1.8 Stress-inducible kinases and neurodegenerative diseases

The presence of misfolded proteins or abnormal structures such as inclusion bodies and the production of reactive oxygen species may trigger stress-activated kinase signalling pathways. Mitogen-activated protein kinases (MAPKs) are serine/threonine kinases that serve to integrate diverse signal cascades to regulate cellular activities such as gene expression, mitosis, metabolism, and apoptosis (reviewed in (Robinson and Cobb, 1997; Johnson and Lapadat, 2002; Cargnello and Roux, 2011)). They are part of an intricate cascade of kinases that ensures a rapid response to stress-signals that can mediate cellular fate. MAPKs functions in distinct pathways and are therefore divided into sub-groups based on their biological activities and sequence similarities.

There are three families of MAPKs that have been extensively characterized. They include the extracellular signal-regulated kinases (ERK), c-Jun N-terminal protein kinases (JNK), and the p38MAP kinases (p38MAPK). MAPKs have a unique phosphorylation motif that requires dual phosphorylation on the flexible loop region called the 'phosphorylation lip'. Upstream MAPKs kinases (MAPKKs) catalyze the conserved threonine and tyrosine dual phosphorylation on the phosphorylation lip which is unique for each family (Songyang et al., 1994; Songyang et al., 1996). The phosphorylation motif of ERK enzymes consists of Thr-Glu-Tyr, for the JNK enzymes it is Thr-Pro-Tyr, while the p38MAPK have a Thr-Gly-Tyr motif. ERK enzymes (ERK1 and ERK2) respond to growth factors such as epidermal growth factor (EGF), nerve growth factor (NGF), and insulin, and have been reported to regulate meiosis, mitosis, and post-mitotic function in differentiated cells (Boulton et al., 1990). They play a central role in the control of cell proliferation – ERK1/2 activity is rapidly stimulated by mitogenic agents and a sustained activity of ERK1/2 is required for efficient G1 to S phase progression (Meloche and Pouyssegur, 2007). ERK1/2 has also be shown to stabilize c-Fos protein through direct phosphorylation, thereby allowing c-Fos to associate with c-Jun and form transcriptionally active AP-1 complex (Shaulian and Karin, 2001). JNK and p38MAPK enzymes are known to respond to cytokines and cellular stress. They can regulate stress-dependent apoptosis including transcriptional changes affecting death receptors, survival pathways, or pro- and anti-apoptotic Bcl-2 family proteins (Tournier et al., 2000; Cuenda and Rousseau, 2007). JNK has also been shown to participate in signalling pathways activated by inflammatory cytokines and has been implicated in obesity-induced insulin resistance diabetes (Hirosumi et al., 2002), while the p38MAPK pathway is activated in response to stresses including UV

radiation, heat shock, oxidative stress, and osmotic stress (Clerk et al., 1998; Ono and Han, 2000). There are four p38MAPK enzymes isoforms (α, β, γ, and δ): the α-and β-isoform are most abundant in the central nervous system, the expression of β-isoform is found in all tissues, while the expression of δ is restriced to non-CNS tissues (Jiang et al., 1996). Kinases that have been identified to activate p38MAPK include MKK3/6, ASK1, Tpl2, and TAK1 (reviewed in (Cargnello and Roux, 2011)). Downstream targets of p38MAPK include transcription factors (ATF2, MEF2C, and CHOP (Cohen, 1997)) and other kinases including MAPKAPK2 and MAPKAPK3, which in turn phosphorylate other proteins including HSP27 (Stokoe et al., 1992), ATF1 (Tan et al., 1996), or MNK1(Fukunaga and Hunter, 1997).

The activation of the p38MAPK pathway has been previously shown to induce apoptotic death of neurons in tissue culture (Gunn-Moore and Tavare, 1998; Namgung and Xia, 2001; Yeste-Velasco et al., 2009). Recently, the activation of p38MAPK has also been reported in several neurodegenerative diseases including PD (Hunot et al., 2004; Cha et al., 2005), ALS (Raoul et al., 2002; Dewil et al., 2007), AD (Zhu et al., 2000; Zhu et al., 2001; Sun et al., 2003), and polyglutamine disorders (Nishitoh et al., 2002), suggesting the activation of stress-inducible kinases may be a common mechanism of pathogenicity that play a critical role in modulating neurodegenerative disease.

1.9 Aims of the research

The accumulations of abnormal and misfolded proteins forming an inclusion body have become the hallmark feature of neurodegenerative diseases, yet there remains controversy over whether these abnormal structures are protective, detrimental, or relatively

benign. The formation of inclusion bodies may be accelerated by inefficient protein degradation that may promote activation of stress signalling pathways. Each of these events may promote the generation of reactive oxygen species which may exacerbate the problem by damaging more proteins, possibly damaging components of the UPS itself, but in either case further impeding the function of cellular proteolysis systems. We hypothesize that multiple factors contribute to the demise of neurons in the context of neurodegenerative diseases. To test this hypothesis and to determine how these events are related and which are critical, we generated a live cell imaging system in which inclusion formation and proteolytic efficiency can be evaluated, and created a stochastic computer model incorporating the same components. These systems were used to explore the kinetics of inclusion formation and proteasome inhibition in the presence or absence of pharmacological agents targeting specific components of the UPS and MAPK signalling pathways.

CHAPTER 2: MATERIALS AND METHODS

2.1 Eukaryotic expression vectors

The pEGFP-N1 expression construct was purchased from Clontech (Palo Alto, California, USA). HttQ25 and HttQ103 expression constructs containing a synthetic insert encoding exon 1 or human Huntingtin containing a polyglutamine tract of either 25Q or 103Q fused to the yellow fluorescent reporter protein (YFP) were generous gifts from Dr. Ron Kopito (Stanford University). These are designated HttQ25YFP or HttQ103YFP. A red fluorescent proteasome reporter was generated by PCR-mediated transfer of the degron sequence ((a 16 amino acid sequence consisting of ACKNWFSSLSHFVIHL) from the GFP^u reporter (Bence et al.; the gift of Dr. Ron Kopito) to the C terminus of the monomeric red fluorescent protein (the gift of Dr. Robert Campbell, University of Alberta). To simultaneously express the expanded YFP-tagged polyglutamine proteins and the red fluorescent proteasome reporter the former was inserted into NheI site upstream of the internal ribosome entry site (IRES) in the vector pIRES (Clontech, Palo Alto, California, USA) and the latter was inserted between the Xba I and Sal I sites downstream of the IRES element. The resulting construct was designated HttQ103YFP-pIRES-$mRFP^u$. The wild type and kinase dead p38MAPK variants were generous gifts from Dr. J. Hans (The Scripps Research Institute, La Jolla, CA). The hyper-active p38MAPK construct was a gift from Dr. Oded Livnah (The Hebrew University of Jerusalem).

2.2 Cell culture and transfections

The human U87MG glioblastoma cells (a gift from Dr. I. Lorimer at the Ottawa Hospital Research Institute) were maintained in Dulbecco's modified Eagle's medium (DMEM) and supplemented with 10% FBS and maintained in a 37°C incubator with 5% CO_2. For transient transfections, cells were plated in either 96- or 6 well dishes 24hours

prior to transfections. Subsequently, they were transfected using GeneJuice Transfection Reagent (Novagen, Madison, WI, USA) as per the supplier's protocol. 0.5µg or 3.0µg of plasmid DNA was used in each well of a 96 or 6 well dish, respectively. For p38MAPK inhibition experiments, cells were pre-treated for 2h with 20µM SKF86002 (Calbiochem) prior to transfection with various expression constructs. ERK inhibition experiments were performed in a similar manner using the MEK inhibitor U0126 at a final concentration of 20 µM (Promega, Madison, WI, USA). For proteasome inhibition experiments, cells were treated with Proteasome Inhibitor I (Calbiochem), a reversible inhibitor of the chymotrypsin-like activity of the multicatalytic proteinase complex, 24h post-transfection at a final concentration of 25µM. Fluorescent detection was analyzed by flow cytometry using a Beckman Coulter Quanta SC MPL. Data and analysis were done using Quanta Analysis software (Beckman Coulter, Inc., Brea, CA, USA).

2.3 Survival analysis

Cell viability was assessed by MTT or flow cytometry using propidium iodide exclusion. For MTT assays, cells in 96 well microtitre plates were transfected with the GFP control vector, HttQ25YFP or HttQ103YFP. 24 hours post-transfection of the plasmid DNA cell survival was assessed using the MTT (3-(4,5-dimethylthiazol-2-yl)-2,5-diphenyltetrazolium bromide) assay. Cells were exposed to 25 µl of MTT (5 mg/ml in sterile PBS, Sigma-Aldrich, Canada) and incubated for 2–3 h at 37°C and 5% CO2. The formazan product was formed and dissolved by adding 100 µl of lysis buffer (20% SDS (BioShop Canada Inc., Burlington, ON, Canada)) and DMF (VWR International, Mississauga, ON, Canada). Absorbance was measured at 570 nm in a Dynex MRX microplate reader. Background values were determined by carrying out the assay in wells

containing media without cells. For flow cytometry experiments, adherent and non-adherent cells were transfected with various constructs for 30 hours, harvested and stained with Propidium Iodide.

2.4 Glutathione analysis

Cell lysates from U87MG cells overexpressing wild type p38MAPK or kinase dead p38MAPK were analyzed for reduced GSH content using a luciferase kit (GSH-Glo) from Promega (Madison, WI). $1x10^5$ cells were seeded in 96-well plates and transfected with 0.5µg of DNA for 48 hours. Cells were collected and analyzed for reduced GSH using a GloMax-Multi Microplate Multimode Reader (Promega, Madison, WI) following the manufacture's protocol.

2.5 Proteasome activity assay using fluorogenic substrates

U87MG cells were cultured in 6-well dishes prior to transfection with pcDNA3 empty control vector, p38wild-type, or p38Kinase-dead expression vectors. 48 hours later, the cells were lysed with 250 µl of buffer (20 mM Tris-HCl, pH 7.0, 1 mM EDTA and 3 mM sodium azide). Lysis was achieved by three freeze thaw cycles using dry ice and room temperature. Extracts were spun at 5000g for 5 minutes to pellet cellular debris and protein quantification was carried out using the protein assay from Bio-Rad Laboratories (Mississauga On). 60 µg of cell extract was diluted in a total volume of 300 µl of lysis buffer. The fluorogenic substrates II and III that assay for the peptidylglutamyl and chymotrypsin-like activities of the proteasome (Calbiochem, San Diego, California, USA) were also diluted in lysis buffer at a final concentration of 10 µM. An equal volume of buffer containing the fluorogenic substrate was added to the extract and each sample was dispensed into six 100 µl samples in a 96-well microtitre dish. For p38MAPK inhibition assays, cells were pre-treated for 2h with 20µM SKF86002 prior to transfection with various

expression constructs. A control sample consisted of a mock transfected cell lysate incubated in the presence of Proteasome Inhibitor I, a specific inhibitor of the chymotrypsin-like activity of the proteasome, at a final concentration of 50 μM. Fluorescence (λem: 445 nm) was measured at various time points for up to 16 hours using a fluorimeter (Fluoroskan Ascent FL, Thermo Laboratory Systems).

2.6 Proteasome inhibition analysis using GFP^u

To establish stable cell lines expressing the proteasome reporter GFP^u, 3T3 cells were co-transfected with a PGK-driven puromycin resistance gene (gift of Dr. M. McBurney, Ottawa Hospital Research Institute) and the EGFP containing a CL1 degron (ACKNWFSSLSHFVIHL) previously described by Bence et al. 2001 (1:6 ratio). Cells stably expressing the proteasome reporter GFP^u were selected over 2 weeks in a final concentration of 2.0μg/ml. For proteasome assays, wild type p38MAPK, kinase dead p38MAPK, or pcDNA were transfected into 3T3-GFP^u cells for 48 hours. Cells were collected and analyzed for GFP^u expression by flow cytometry (Beckman Coulter Quanta SC MPL). Mean GFP intensity was analyzed using the Quanta Analysis software and subsequently graphed using Excel (Microsoft).

2.7 Measurement of reactive oxygen species (ROS)

For intracellular ROS levels measurement $5x10^4$ cells were plated in 24-well dishes. 24 hours post transfection, cells were stained with 2',7'-dichlorodihydrofluorescein diacetate (H2DCFDA; Sigma, USA). Cells were loaded with 20 μM H2DCFDA at 37°C for 30 min followed by rinsing three times with Hank's Balanced Salt Solution (HBSS) buffer. Fluorescence was detected using the SynergyMx plate reader using the excitation/emission filter set settings of 485/530.

2.8 Preparation of cell extracts and Western blot analysis

2.8.1 Cultured cells

The cells were washed 3 times with PBS and trypsinized for 5 minutes at 37°C. Cells were then collected in culture medium, centrifuged at 3000g for 5 minutes and resuspended in protein lysis buffer (20 mM Tris-HCl (pH 7.5), 150 mM NaCl, 1% Nonidet P-40 (Sigma, St. Louis, Missouri, USA), 0.5 mM EDTA, 20% glycerol) containing the following protease and phosphates inhibitors: 1 mM phenylmethylsulfonyl fluoride, 5 µg/mL leupeptin (Sigma, St. Louis, Missouri, USA), 2 µg/mL aprotinin (Sigma, St. Louis, Missouri, USA), 200 µM sodium Fluoride (NaF) and 200 µM sodium pyrophosphate (NaPPi). The cells were incubated on ice for 30 minutes and then centrifuged at 14 000rpm for 20 minutes at 4°C to pellet cellular debris. The soluble fractions were recovered and the protein concentration was determined using the Bradford protein assay (Bio-Rad Laboratories (Canada) Inc., Mississauga, Ontario, Canada). 20 or 30 µg of cytoplasmic extracts were then resolved on a two-phase SDS-polyacrylamide gel (15 and 8%) and electroblotted onto a hybond C nitrocellulose membrane (Amersham Pharmacia Biotech, Baie D'Urfé, Québec, Canada). The membranes were stained with Ponceau S (Sigma, St. Louis, Missouri, USA) prior to western blotting with the appropriate antibody to ensure the complete transfer of the proteins. Primary and secondary antibodies were diluted in 5% skim milk in TBST (10 mM Tris-HCl (pH7.6), 150 mM NaCl and 1%Tween-20) for 1 hour at room temperature. The membranes were washed 3 times with TBST prior to incubation with the appropriate secondary antibody. The proteins were detected by a horseradish peroxidase method and SuperSignal West Pico Chemiluminescent Substrate reagents (Pierce, Rockford, IL, USA) and were visualized using the GeneGnome (Syngene, Frederick, MD, USA).

2.8.2 Animal tissues

The use of animals in these experiments followed the guidelines of the Animal Care Committee of the University of Ottawa and was approved under protocol number ME-212.The origin of the B05 transgenic line carrying an expanded polyglutamine in the Ataxin -1 allele with 82 CAG repeats and the A02 line with a CAG repeat of 30 codons was described in a paper from the laboratory of Dr. Harry Orr, Minnesota ((Burright et al., 1995)), from whom the lines were obtained. Animals were anaesthetized using CO2 and sacrificed by cervical dislocation. Whole brains or cerebella of non-transgenic and transgenic animals were excised and homogenized in PBS (whole brain) or protein lysis buffer (cerebella) containing 1% NP-40, and the protease and phosphatase inhibitors previously described. The homogenates were then sonicated on ice (3x10 sec). The extracts were centrifuged for 30 minutes at 4°C to pellet cellular debris. Protein quantification and western analysis was carried out as previously described.

2.9 Immunohistochemistry

Cerebella from age-matched nontransgenic, A02 and B05 transgenic mice were excised and fixed in 10% phosphate-buffered formalin overnight at room temperature. Tissues were paraffin-embedded and sagitally sectioned using a microtome at a thickness of 5µm. Deparaffinized sections were heated in a solution of 10 mM sodium citrate (pH 6.0) in 700W microwave for 10 minutes. Endogenous peroxidase activity was blocked by incubating in methanol containing 3% hydrogen peroxide for 20 minutes. Sections were washed with 0.1 M PBS (pH 7.4) and incubated for 30 minutes with 1.5% normal goat serum (Santa Cruz Biotechnologies Inc, SC, CA, USA) to block nonspecific binding. Sections were then incubated overnight at 4°C with the phospho-p38MAPK antibody (Cell

Signaling Technology, Beverly, MA, USA). The reaction product was visualized with the ABC system (DAKO Diagnostics Canada Inc.).

2.10 Time-lapse microscopy

$7.5x10^4$ U87MG glioblastoma cells were seeded onto a Delta T4 culture dish system (Bioptechs, Butler, PA) and maintained in a 37°C incubator with 5% CO_2 for 24h hours. Cells were transfected with 2ug of plasmid DNA encoding HttQ103YFP-pIRES-mRFP^u for 24 hours before being transferred onto a heated stage maintained at 37°C and at 5% CO_2 using a Delta T4 culture dish temperature controller and cell perfusion system (Bioptechs, Butler, PA). For p38MAPK inhibition experiments, cells were pre-treated for 2h with SKF86002 for a final concentration of 20µM. For proteasome inhibition experiments, cells were treated with Proteasome Inhibitor I (Calbiochem), a specific inhibitor of the chymotrypsin-like activity of the proteasome, 24h post-transfection at a final concentration of 25µM. For buthionine sulphoximide (BSO)-induced depletion of glutathione experiments, cells were treated 24h post-transfection with BSO (Sigma) 24h post-transfection at a final concentration of 5mM. Microscopy was performed 24 hours post-transfection on a Zeiss Axiovert 200M inverted fluorescent microscope for a total of 24 hours. Fully automated multidimensional acquisition was controlled using Axiovision 4.8 software. Images were acquired using a 10X objective (EC Plan-Neofluar) with a side-mounted AxiocamHRm camera. Yellow fluorescent protein or red fluorescent protein was excited using the Zeiss Colibri LED illumination system (LEDmodule 505nm or LED module 590nm) and detected using the appropriate filters (46HEYFP or 61HEGFP/HcRED, respectively). Fixed exposure times were as follows: Brightfield phase contrast 1ms; YFP

100ms; RFP 188ms. Images were taken at 10 minute intervals for 24 hours and compiled into movie files using Axiovision 4.8 software (Carl Zeiss, Thornwood, NY).

2.11 Antibodies

Western blot analysis was performed using the mouse monocolonal phospho-p38MAPK, phosopho-ERK ½ and the rabbit polyclonal antibodies recognizing p38MAPK antibody, phospho-HSP27, total HSP27, phospho-ATF2 and total ATF2 was purchased from Cell Signaling Technology (Beverly, MA, USA). Pan ERK monoclonal antibody ((1/1000) was from Transduction Laboratories (Lexington, KY, USA). GFP, HttQ25YFP and HttQ103YFP was detected using the rabbit polyclonal GFP antibody (1/2000) (reactive to all variants of *Aequorea victoria* GFP such as YFP, CFP and EGFP) which was purchased from Abcam (Abcam, Cambridge, MA). The mouse monoclonal actin antibody (1/10 000) was purchased from Sigma-Aldrich. EGFP (1/2000) were detected with rabbit polyclonal antibodies purchased from Santa Cruz Biotechnologies (Santa Cruz, CA). The horseradish peroxidase conjugated mouse (1/5000) and rabbit secondary antibodies (1/5000) were purchased from Bio-Rad and Pierce respectively.

2.12 Statistical analysis

Unless otherwise indicated, all values are represented as the average of three independent experiments performed in triplicate, with error bars indicating standard error of the mean. Statistical significance was determined by a two tailed Student's t-test. Values were considered significant when $P<0.05$.

2.13 Mathematical model

All mathematical modeling was designed and performed by Dr. Carole Proctor at the University of Newcastle, Newcastle upon Tyne, United Kingdom. In the model we assume that the addition of the polyQ gene to the cell resulted in continuous synthesis of the polyQ protein. It is also degraded by the proteasome so that total levels remain fairly constant with a half-life of about 20 hours . We set the levels of polyQ sythesis and degradation so that the half-life would be 20 hours if the proteasome did not become inhibited by aggregates. Two molecules of polyQ interact to form a small aggregate (AggPolyQ1). We assume that ROS affects the aggregation kinetics if it rises above basal levels. The aggregate can grow in size by the addition of further polyQ proteins in a reversible manner. However, when the aggregate reaches a certain threshold size, we assume that disaggregation can no longer take place and that instead an inclusion forms (SeqAggP). This threshold represents the seed and is assumed to be of size six based on data for amyloid fibril polymerization . Since mutant huntingtin forms amyloid-like filaments, it is reasonable to assume that it has similar aggregation kinetics. A very recent study shows that mutant huntingtin forms three major pools: monomers, oligomers and inclusion bodies . Interestingly, the study showed that the pool of oligomers as a proportion of total huntingtin did not change over a time period of 3 days despite continued conversion of monomer to inclusion bodies. We also compared the levels of oligomers (represented by the species AggPolyQ[i], where i=1-5) in our simulation output in cells which formed inclusion bodies (Appendix 1. Figure S2) and discuss the results in the Text S1 section. It has been shown that small aggregates bind to proteasomes and inhibit proteasomal function . Therefore, we assume that AggPolyQ can bind to the proteasome and so reduce the pool of available proteasomes. However we assume that inclusions do not interfere with the degradation machinery. We also include a species to

represent mRFPu and assume that this is turned over with a half-life of about 30 minutes . We assume that ROS is continuously generated and removed with a half-life of 1 hour but that basal levels are low (about 10 molecules). We assume that small aggregates may generate ROS, so that the level of ROS is dependent on the amount of small aggregates (either bound to the proteasome or free pools). We also assume that the presence of inclusions will increase levels of ROS but with a much smaller effect than small aggregates. We represent p38MAPK in two forms: unphosphorylated (p38) and phosphorylated (p38-P) with p38-P being the active state. We assume that high levels of ROS activate p38MAPK and that high levels of p38-P initiate a signalling cascade that results in cell death. We set the rate of this reaction so that it is unlikely to occur when p38-P levels are low and the probability of the reaction occurring increases with increasing levels of p38-P. However, since the model is stochastic, it is possible that even low levels of p38-P will occasionally signal for cell death. We also assume that if the level of proteasomes bound by aggregates increases above a threshold of about 50%, then another signalling pathway leads to cell death due to the accumulation of the pro-apoptotic protein p53. As in the p38 death pathway, cell death due to aggregates inhibiting the proteasome may occur even when levels of AggP Proteasome are fairly low. The reactions for the cell death pathways are shown in AppendixTable S2 in AppendixText S1. After cell death occurs, a dummy parameter k_{alive} is set to zero to prevent further reactions occurring, and a dummy species to record the cause of cell death is set to 1. This makes it possible to plot the time of cell death, the cause of death and to count the number of cell deaths of each type in multiple simulations.

We also assume that proteasomes bound by AggP, polyQ or mRFPu may be sequestered into inclusions if degradation does not take place. If AggP is sequestered into inclusions,

then this will help alleviate the increase in ROS due to protein aggregation, since we assume that small aggregates lead to greater ROS generation than inclusions.

We also include a generic pool of protein (NatP) which can misfold to become (MisP). We assume that misfolded protein can be either refolded, ubiquitinated and degraded or at high concentrations it may start to aggregate. Once an inclusion forms, misfolded protein may be sequestered into the inclusion body, including MisP bound to proteasomes.

CHAPTER 3: RESULTS

3.1 In vitro analysis of expanded polyglutamine proteins

3.1.1 The expression of HttQ103 alters morphology and is accompanied by inclusion body formation

The cleavage of full-length huntingtin with an expanded polyglutamine tract by caspase- or calpain-mediated events has previously been shown to produce N-terminal fragments that are sufficient to generate cytotoxicity (Mangiarini et al., 1996). For this reason, constructs encoding exon 1 of the huntingtin protein, containing a non-pathological polyglutamine tract of 25 glutamines (hereafter referred to as HttQ25) and a pathological polyglutamine tract of 103 glutamines (hereafter referred to as HttQ103), fused to a yellow fluorescent protein (YFP) reporter system, have commonly been used to investigate the cytotoxic effects of expanded polyglutamine proteins in cell culture models (Sugars et al., 2004a; Swayne et al., 2005). In addition, mice expressing the N-terminal fragment of the huntingtin protein with an expanded polyglutamine tract develop a progressive neurological phenotype with motor symptoms resembling those with HD (Cha et al., 1998; Carter et al., 1999). To investigate the cytotoxicity of N-terminal huntingtin protein fragment with an expanded polyglutamine tract, U87MG glioblastoma cells (chosen for their flat morphology and high transfection efficiency) were transiently transfected with GFP, HttQ25, or HttQ103 and imaged by phase contrast and fluorescence microscopy. Cells expressing HttQ103 showed a significant increase in the number of shrunken, rounded, and detached cells when observed under phase contrast microscopy in comparison to cells expressing HttQ25 or GFP (Figure 6A, upper panel). Under fluorescence microscopy, cells expressing HttQ103 were found to accumulate visible nuclear inclusion bodies as early as 24 hours post-transfection while no such inclusions were observed in cells expressing HttQ25 or GFP (Figure 6A,

A

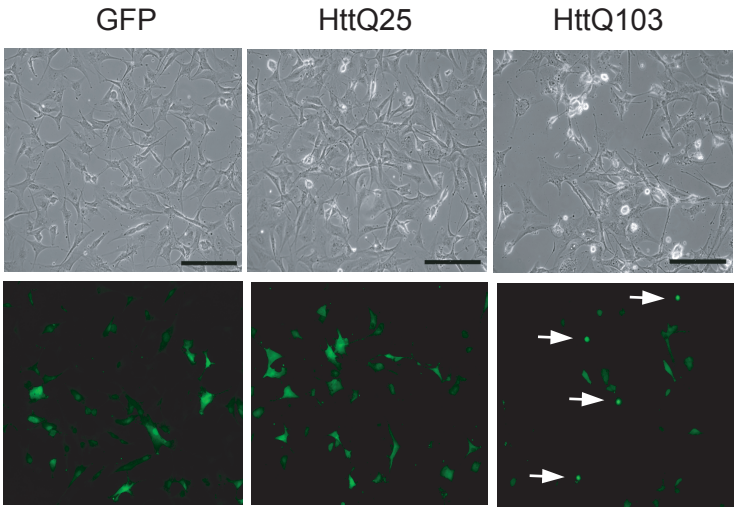
GFP
HttQ25
HttQ103

B

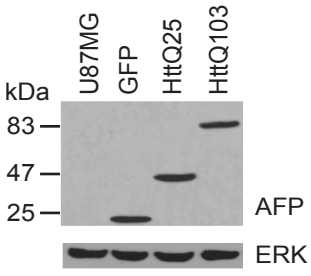
U87MG
GFP
HttQ25
HttQ103
kDa
83
47
25
AFP
ERK

Figure 6. Cell morphology of cells expressing HttQ25 or HttQ103

A) U87MG cells expressing GFP, HttQ25, or HttQ103 for 24 hours were visualized under white light (upper panel) or fluorescence (bottom panel) in the same field of view to assess cell morphology and transfection efficiency. Arrowheads demonstrate nuclear inclusion bodies in HttQ103-expressing cells. Scale bars represent 100μm. B) Western blot analysis of cell extracts from cells transfected with GFP, HttQ25, or HttQ103 with an antibody raised against AFP (autofluorescent protein). No significant difference in the protein levels of GFP, HttQ25, or HttQ103 were observed in extracts from transfected cells. The membrane was re-probed with an antibody directed against total ERK, which served as a loading control.

bottom panel). This is consistent with previous observations of inclusion body formation in the expression of polyglutamine expanded proteins in other cell lines, such as the PC12 (derived from a pheochromocytoma rat adrenal medulla) cell line (Gong et al., 2008) and the SH-SY5Y (human neuroblastoma) cell line (Wyttenbach et al., 2000), suggesting a similar mechanism of cytotoxicity associated with expression of polyglutamine proteins. The transfection efficiency of the huntingtin proteins in U87MG cells was estimated at ~ 80% as assessed by fluorescence microscopy (Figure 6A). Similar levels of GFP, HttQ25, and HttQ103 expression were confirmed by Western blot analysis of extracts from transfected cells with an antibody specific for the fluorescent protein reporter as is shown in Figure 6B.

3.1.2 The expression of HttQ103 induces cell death and is associated with oxidative stress

The progressive loss of neurons has been reported to be associated with high amounts of oxidative damage in several neurodegenerative diseases including HD, AD, and PD (Wyttenbach et al., 2002; Beal, 2005). We quantified cell death by analyzing cell viability of U87MG cells transfected with GFP, HttQ25, or HttQ103 by the MTT assay 24 hours post-transfection to determine if the change in cell morphology in cells expressing HttQ103 is associated with cell death. Cells expressing HttQ103 had ~ 30% less surviving cells compared to the cells expressing HttQ25 or GFP, while the cell survival was found to be similar between the HttQ25 and GFP controls (Figure 7). Similar cell viability results were obtained by flow cytometric analysis (Appendix 2 Supplemental Figure 1). To determine if oxidative stress may have accompanied decreased cell survival of HttQ103-expressing cells, we measured the amount of reactive oxygen species (ROS) and levels of reduced glutathione (GSH). U87MG cells were transfected with GFP, HttQ25, or HttQ103

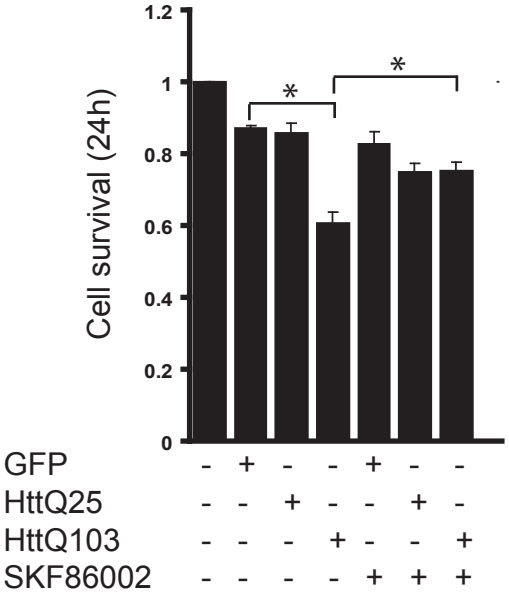
1.2
1
0.8
0.6
0.4
0.2
0
Cell survival (24h)
*
*
GFP - + - - + - -
HttQ25 - - + - - + -
HttQ103 - - - + - - +
SKF86002 - - - - + + +

Figure 7. Cell survival analysis of polyglutamine-expressing cells treated with SKF86002

Inhibition of p38MAPK activation by treatment with SKF86002 rescues cells from expanded polyglutamine cytotoxicity. U87MG cells were treated with SKF86002 for 2 hours prior to transfection with GFP, HttQ25, or HttQ103. Cell survival was assessed by the MTT assay 24 hours post-transfection. The analysis revealed a decrease in survival of HttQ103-expressing cells compared to cells expressing GFP or HttQ25, which was reversed by treatment with SKF86002. Data represents the average of three independent experiments, with error bars indicating standard error of the mean (*$p<0.01$).

for 24 hours and assessed for ROS and GSH content. The analysis revealed that cells expressing HttQ103 had a significant increase in the ROS (Figure 8A, Appendix 2 Supplemental Figure 2), as well as a decrease of GSH by ~ 30% in comparison to the GFP control (Figure 8B). These data suggest that the expression of HttQ103 induces oxidative stress which may contribute to its cytotoxicity.

3.1.3 The expression of HttQ103 induces activation of p38MAPK

The observation that the expression of HttQ103 increases oxidative stress suggested that expanded polyglutamine proteins may be affecting stress-inducible pro-apoptotic pathways. Stress-activated kinases have previously been reported to be activated in AD; the activation of p38MAPK has been shown to mediate Aβ cytotoxicity in cell culture systems (Zhu et al., 2005) and has been found to be activated in brains of patients with AD (Zhu et al., 2001; Sun et al., 2003). In addition, ASK1, a kinase directly upstream of p38MAPK, is highly responsive to oxidative stresses and has been implicated in the mutant Cu/Zn superoxide dismutase $SOD1^{G93A}$ transgenic model of ALS (Nishitoh et al., 2008). Although the activation of the p38MAPK pathway in response to environmental and genotoxic stress is well characterized (Papoutsaki et al., 2005; Colognato et al., 2006), its role in polyglutamine disorders has not been defined. To investigate the role of this kinase, we began by analysing its activity in response to HttQ103 expression. Cell extracts from U87MG cells expressing GFP, HttQ25, or HttQ103 were analysed by Western blot using a phospho-p38MAPK antibody 24 hours post-transfection. The analysis show an 1.8 fold increase of phospho-p38MAPK levels in cells expressing HttQ103 compared to untransfected and GFP controls (Figure 9, Appendix 2 Supplemental Figure 3), suggesting

A

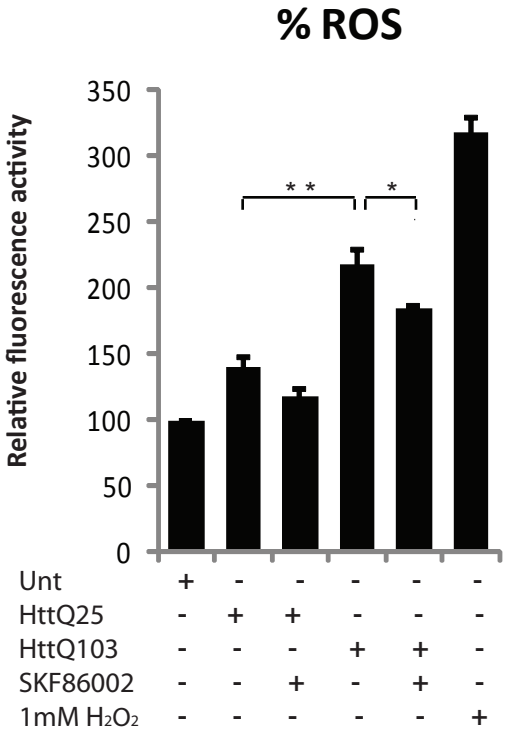
% ROS
Relative fluorescence activity
350
300
250
200
150
100
50
0
* *
*
Unt + - - - - -
HttQ25 - + + - - -
HttQ103 - - - + + -
SKF86002 - - + - + -
1mM H2O2 - - - - - +

B

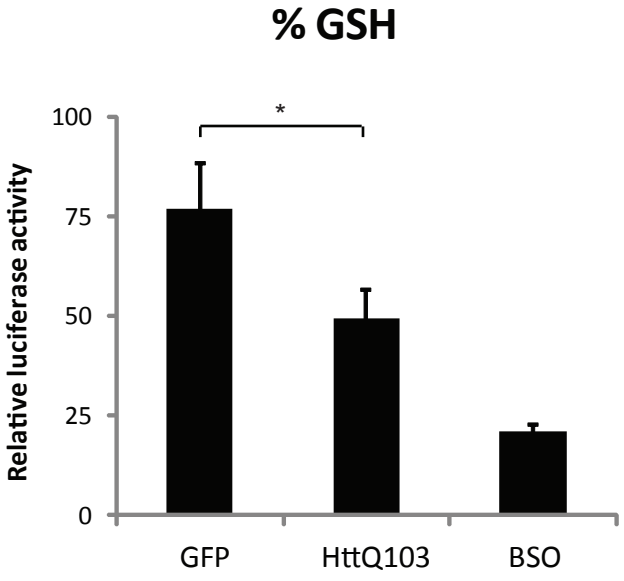
% GSH
Relative luciferase activity
100
75
50
25
0
*
GFP
HttQ103
BSO

Figure 8. Analysis of ROS and GSH in cells expressing expanded polyglutamine proteins

Expression of expanded polyglutamine proteins results in an increase generation of reactive oxygen species (ROS) and lowers reduced glutathione (GSH) levels. A) Polyglutamine-expressing cells were analyzed for ROS using the ROS-sensitive fluorophore, hydroxyphenyl fluorescein. An increase in ROS was detected in expanded polyglutamine-expressing cells when compared to the untransfected control. Cells treated with SKF86002 were found to have a lower percentage of ROS relative to their non-treated counterparts. Cells treated with hydrogen peroxide (H_2O_2) served as a positive control. Data represents experiments done in triplicate with error bars indicating standard error of the mean (*$p<0.02$, **$p<0.02$). B) Lysates from cells expressing GFP or HttQ103 were assayed for reduced GSH content. Cells transfected with HttQ103 had lower levels of reduced GSH when compared to the GFP control. Treatment with buthionine sulphoximine (BSO) served as a positive control. Data represents experiments done in triplicate with error bars representing standard error of the mean (*$p<0.05$).

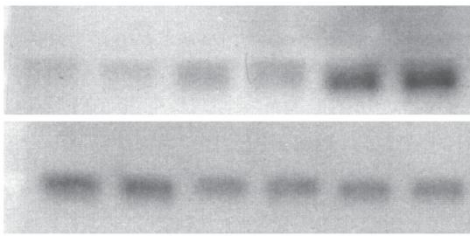

Unt	+	-	-	-	-	-
GFP	-	+	-	-	-	-
HttQ25	-	-	+	+	-	-
HttQ103	-	-	-	-	+	+

Figure 9. Western blot analysis of phosporylated-p38MAPK protein levels from cells expressing polyglutamine proteins

Western blot analysis of duplicate cell extracts from U87MG cells expressing GFP, HttQ25, or HttQ103 with the phospho-p38MAPK antibody. The analysis revealed a slight increase of phospho-p38MAPK levels in HttQ25-expressing cells and a strong induction of phospho-p38MAPK in HttQ103-expressing cells 24 hours post-transfection. The antibody raised against total p38MAPK was used to detect total p38MAPK levels, which served as a loading control.

that p38MAPK is activated in response to the enhanced expression of HttQ103 and its activation may be the basis for the increased cell death observed in HttQ103-expressing cells.

3.1.4 Pharmacological blockade of p38MAPK rescues cells from HttQ103-induced toxicity

If the activation of p38MAPK is triggering cell death pathways in HttQ103-expressing cells, it is predicted that its inhibition would correlate with an increase in cell survival. To determine if blocking the activation of p38MAPK by inhibiting its phosphorylation may rescue cells from polyglutamine-induced toxicity, we treated cells with SKF86002, a specific p38MAPK inhibitor. Cell viability was assessed in cells pre-treated with SKF86002 prior to transfection with GFP, HttQ25, or HttQ103. The inhibition of p38MAPK resulted in a significant rescue of HttQ103-expressing cells such that their survival was comparable to HttQ25 or GFP transfected cells treated with the inhibitor (Figure 7, Appendix 2 Supplemental Figure 1). This suggests that the activation of p38MAPK mediates polyglutamine-induced cytotoxicity. In addition, the increased survival with SKF86002 treatment was found to coincide with a decrease in ROS levels in HttQ103-expressing cells (Figure 8A). The activation of p38MAPK has been shown to phosphorylate several downstream targets including other kinases (MAPKAPK2/3) and transcription factors (ATF2, MEF2C, and CHOP) (Stokoe et al., 1992; Cohen, 1997). It was therefore expected that in our system the activation of p38MAPK would result in the phosphorylation of downstream targets. To confirm the activation of p38MAPK and its inhibition by SKF86002, the extracts from HttQ103-expressing cells were analysed by Western blot analysis with the phospho-HSP27 antibody, a downstream target of p38MAPK. The

analysis in Figure 10 (and Appendix 2 Supplemental Figure 4) showed that HSP27 phosphorylation was not detected in SKF86002-treated or untransfected controls, suggesting a complete inhibition of p38MAPK activity. As expected, cell extracts expressing HttQ103 not treated with the inhibitor was found to have a 6.8 fold increase of HSP27 phosphorylation when compared to untransfected controls,which is consistent with the activation of p38MAPK. Although the HttQ25 protein contains a polyglutamine tract below the threshold length for pathogenicity, a 4.3 fold increase of phosphorylated-HSP27 was detected (Figure 10, Appendix 2 Supplemental Figure 4), suggesting that the overexpression of the N-terminal fragment of huntingtin containing a short (non-pathological) polyglutamine tract may be sufficient to activate p38MAPK at a low and nontoxic level.

3.1.5 Genetic modulation of the p38MAPK pathway inhibits the activation of p38MAPK in cells expressing HttQ103

Having established that the pharmacological inhibition of p38MAPK significantly rescued cytotoxicity associated with the expression of HttQ103, we sought to determine if the activation of p38MAPK could be modulated by genetic means. Dominant negative mutants of kinases are often used to corroborate findings from pharmacological kinase inhibitor experiments to demonstrate that the observed effects are not attributed to off-target activities. To determine if the activation of the p38MAPK pathway caused by the expression of HttQ103 could be modulated by genetic means, U87MG cells were co-transfected with HttQ25 or HttQ103 plasmids in conjunction with constructs encoding either wild-type p38MAPK alpha (p38Wt), a constitutively-active variant (p38Active), or its dominant negative kinase-dead counterpart (p38KD), and analyzed by Western blot. The over-expression of p38Wt and p38Acitive in U87MG cells was found to reduce cell survival by

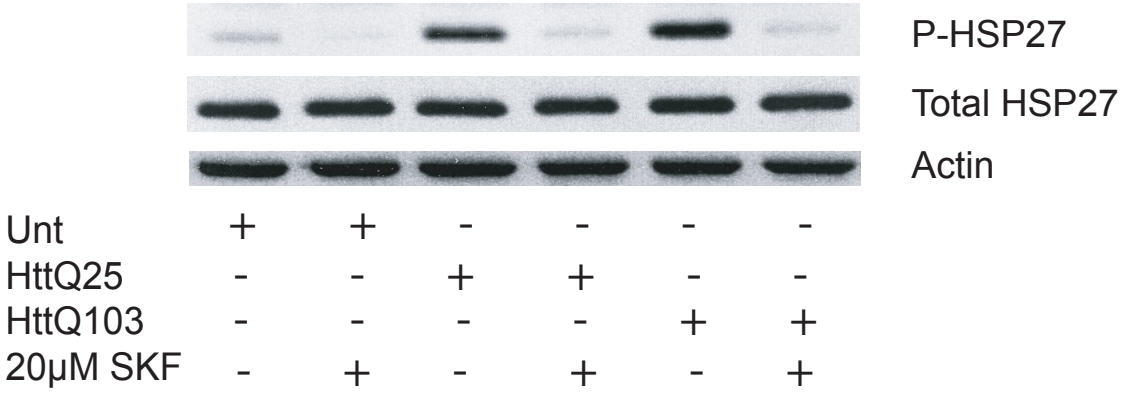
P-HSP27
Total HSP27
Actin
Unt + + - - - -
HttQ25 - - + + - -
HttQ103 - - - - + +
20μM SKF - + - + - +

Figure 10. Western blot analysis of phosphorylated-HSP27 protein levels from polyglutamine-expressing cells

Western blot analysis of protein levels of phospho-HSP27, a downstream target of p38MAPK, of lysates from U87MG cells expressing HttQ25 or HttQ103 with or without the p38MAPK inhibitor SKF86002. Phosphorylation of HSP27 is abrogated in SKF86002-treated cells. Total HSP27 and actin levels served as loading controls.

~30% and ~40%, respectively (Appendix 2 Supplemental Figure 5). In addition, these expression constructs have previously been used to investigate the contribution of p38MAPK signalling in cultured cells (Wang et al., 2000; Ge et al., 2002; Askari et al., 2007) and has been used to establish the role of p38MAPK in Aβ cytotoxicity (Zhu et al., 2005). Western blot analysis revealed a two fold reduction of phsopho-HSP27 from cell extracts co- transfected with p38KD and HttQ25 or HttQ103 when compared to cells co-expressing HttQ25 and the empty vector control pcDNA (Figure 11 and Appendix 2 Supplemental Figure 6), suggesting the expression of p38KD is capable of modulating the activity of p38MAPK. Extracts from cells co-transfected with p38Wt or p38Active in conjunction with the expression of HttQ25 or HttQ103 showed the highest levels of HSP27 phosphorylation (Figure 11). This suggested that the enhanced expression of p38Wt or p38Active in conjunction with HttQ25 or HttQ103 is sufficient to induce the phosphorylation of HSP27. Consistent with previous results, HttQ103 co-transfected with the empty control vector showed an increase of 1.5 fold in HSP27 activation when compared to HttQ25 co-transfected with empty control vector (Figure 11 and Appendix2 Supplemental Figure 6). Taken together, the data shown in Figure 10 and 11 revealed that the phosphorylation of HSP27 was significantly abrogated by treatment of transfected cells with a pharmacological inhibitor of p38MAPK (Figure 10) or the co-expression of HttQ103 with a dominant negative (p38KD) variant of p38MAPK (Figure 11), confirming that the phosphorylation of HSP27 was due to the activation of the p38MAPK pathway by HttQ103.

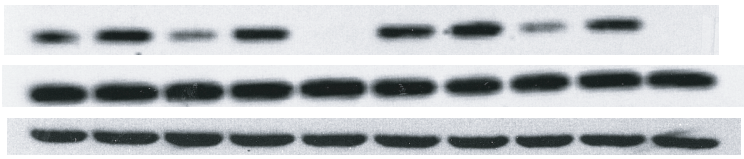

HttQ25	+	+	+	+	+	-	-	-	-	-
HttQ103	-	-	-	-	-	+	+	+	+	+
pcDNA	+	-	-	-	-	+	-	-	-	-
p38 Wt	-	+	-	-	-	-	+	-	-	-
p38 KD	-	-	+	-	-	-	-	+	-	-
p38 Active	-	-	-	+	-	-	-	-	+	-
20μM SKF	-	-	-	-	+	-	-	-	-	+

Figure 11. Western blot analysis of phosphorylated-HSP27 protein levels in cells co-transfected with polyglutamine and p38MAPK expression constructs

Western blot analysis with the phospho-HSP27 antibody of cell extracts from U87MG cells co-transfected with pcDNA empty vector (pcDNA), wild-type p38MAPK (p38 Wt), kinase-dead p38MAPK (p38 KD), or hyper-active p38MAPK (p38 Active) expression constructs in cells expressing HttQ25 or HttQ103. The analysis revealed that phospho-HSP27 levels were reduced in extracts from HttQ25- or HttQ103-expressing cells when co-transfected with p38 KD. A complete abrogation of HSP27 phosphorylation was shown in cells treated with SKF86002. Total HSP27 and actin levels served as loading controls.

3.1.6 Full-length expanded human ataxin-1 protein induces cell toxicity in a p38MAPK-dependent manner

Although polyglutamine disorders encompass several disorders that are caused by the expansion of a polyglutamine tract within unique and unrelated proteins, they share common neuropathological features. The polyglutamine expansion has been shown to cause a gain-of-toxic function that is deleterious to neurons. To determine whether the activation of p38MAPK pathways in HttQ103-expressing cells represented a general mechanism of expanded polyglutamine toxicity, we investigated the effects of enhanced expression of the expanded *Ataxin-1* gene product with a polyglutamine tract of 83 glutamines (hereafter referred to as AtxQ83) that causes spinocerebellar ataxia type-1 (SCA-1) (Orr et al., 1993). The length of the polyglutamine repeat in normal unaffected humans is from 6 to 40 residues. Mice expressing full-length human ataxin-1 with a polyglutamine tract of 30 glutamines (hereafter referred to as AtxQ30) show no phenotype effects, while the expression of AtxQ83 causes behavioural and pathological changes reminiscent of SCA-1 in humans (Burright et al., 1995). The expression of AtxQ30 was therefore used as a control for the expanded AtxQ83 protein. Western blot analysis revealed a 1.6 fold increase in p38MAPK activation in cell extracts from AtxQ83-expressing cells when compared to AtxQ30-expressing cell extracts (Figure 12A, Appendix 2 Supplemental Figure 7). The analysis also revealed a moderate induction of phosphorylated-p38MAPK in Atx30-expressing cells, suggesting that while shorter than the threshold length necessary to induce cytotoxicity, a polyglutamine tract of 30 glutamines within ataxin-1 may be sufficient to activate p38MAPK at a low and nontoxic level. This data is consistent with the moderate increase of phosphorylated-HSP27expression in cells expressing HttQ25 shown in Figure 10.

A

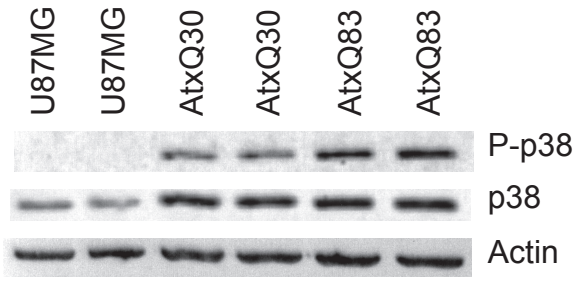
U87MG
U87MG
AtxQ30
AtxQ30
AtxQ83
AtxQ83
P-p38
p38
Actin

B

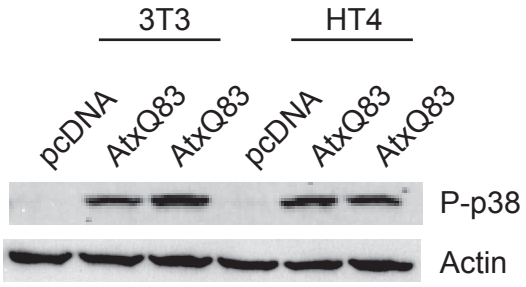
3T3
HT4
pcDNA
AtxQ83
AtxQ83
pcDNA
AtxQ83
AtxQ83
P-p38
Actin

Figure 12. Western blot analysis of phosporylated-p38MAPK protein levels from cells expressing expanded ataxin-1 protein

A) Western blot analysis of duplicate cell extracts from U87MG cells expressing AtxQ30 or AtxQ83 with the phospho-p38MAPK antibody. An increase in phosphorylated p38MAPK levels was observed in lysates from AtxQ83-expressing cells when compared to lysates from mock transfected or AtxQ30-expressing cells. The analysis of total p38MAPK revealed an increase in lysates from AtxQ30- or AtxQ83-transfected cells when compared to mock transfected cells. Actin levels served as a loading control. B) HT4 and NIH-3T3 cells were transiently transfected in duplicate with the AtxQ83 construct. Cell extracts were analyzed by western blot analysis with the phospho-p38MAPK antibody revealing an increase of phospho-p38MAPK protein levels in both cell lines expressing AtxQ83. No induction of phospho-p38MAPK was observed in cell extracts from either HT4 or NIH-3T3 cells expressing a pcDNA empty vector control. Actin levels served as a loading control.

To determine if the cytotoxicity associated with Atx83 could be rescued by blocking the activity of p38MAPK, cell viability was analysed in AtxQ83-expressing cells treated with a pharmacological inhibitor of p38MAPK, or co-expressed with a dominant negative mutant kinase. Figure 13 show the results of the MTT assay revealing a decrease in cell survival by ~ 40% in cells expressing AtxQ83, whereas AtxQ83-expressing cells treated with SKF86002 had similar cell survival comparable to that of AtxQ30-expressing cells and non-transfected counterparts treated with SKF86002 (Figure 13). Similarly, the expression of the kinase dead p38MAPK increased the survival of AtxQ83 expressing cells (Appendix 2 Supplemental Figure 8). These data are in agreement with the improved cell survival observed in HttQ103-expressing cells treated with SKF86002 shown in Figure 7 and suggest the activation of p38MAPK is a common pathogenic mechanism in polyglutamine disorders.

3.1.7 The expression of AtxQ83 activates p38MAPK in several cell lines

The use of U87MG cells was chosen for the current set of experiments for their ease of handling and transfection efficiency. Several reports have shown disease features, such as inclusion body formation, in several different cell lines including COS-7, PC12, and SH-SY5Y (Wyttenbach et al., 2000; Chun et al., 2002; Gong et al., 2008). This suggests that expanded polyglutamine proteins exhibit common pathological mechanisms of irrespective of cell type. To ensure the activation of p38MAPK by polyglutamine expanded proteins was not specific to the U87MG cell type, AtxQ30 and AtxQ83 were transfected into NIH-3T3 mouse fibroblasts and HT4 mouse neuroblastoma cells and analysed for the expression of p38MAPK. Western blot analysis revealed an increase in p38MAPK activation in both NIH-3T3 and HT4 cell lines expressing AtxQ83 (Figure 12B). This is consistent with the previous observations of AtxQ83 expression in U87MG cells and suggests that the

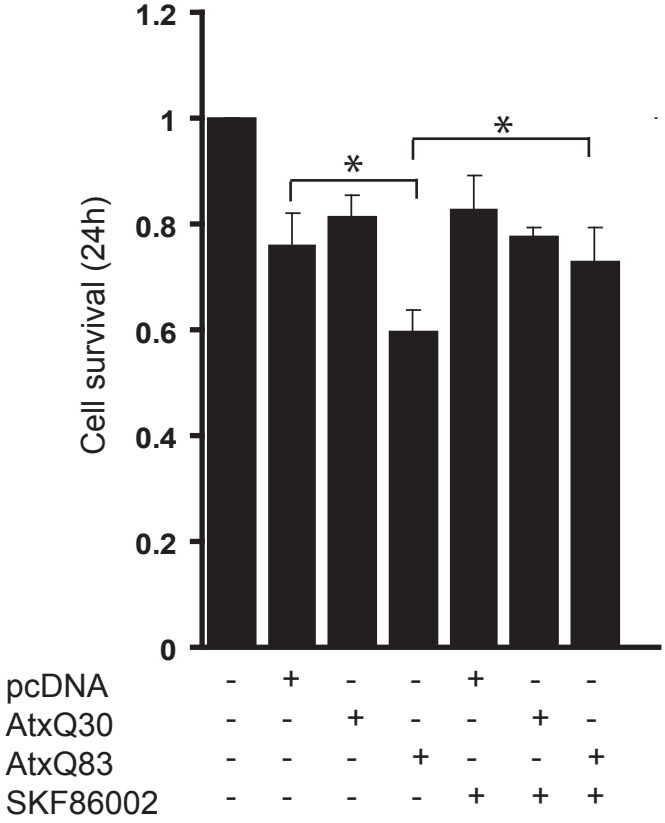
1.2
1
0.8
0.6
0.4
0.2
0
Cell survival (24h)
*
*
pcDNA - + - - + - -
AtxQ30 - - + - - + -
AtxQ83 - - - + - - +
SKF86002 - - - - + + +

Figure 13. Cell survival analysis of AtxQ30- or AtxQ83-expressing cells treated with SKF86002

U87MG cells were treated with SKF86002 for 2 hours prior to transfection with pcDNA empty vector, AtxQ30, or AtxQ83. Cell survival was assessed by the MTT assay 24 hours post-transfection. The analysis revealed a decrease in survival of AtxQ83-expressing cells compared to cells expressing the pcDNA empty vector control, which was reversed by treatment with SKF86002. Data represents the average of three independent experiments, with error bars indicating standard error of the mean (*$p<0.01$).

activation of p38MAPK represents a universal mechanism of polyglutamine cytotoxicity that is independent of cell type.

3.2 *In vivo* analysis of the p38MAPK pathway in a mouse model of SCA-1

3.2.1 Evidence of p38MAPK activation in the cerebella of SCA-1 transgenic mice

To determine if our observations of p38MAPK activation in tissue culture models of polyglutamine disorders is translatable to animal models, the *in vivo* induction of p38MAPK was examined in the previously characterized B05 mouse model of SCA-1. In this mouse model, a human ataxin-1 cDNA with an expanded CAG tract encoding 83 glutamines is specifically expressed in Purkinje neurons (reviewed in (Orr, 2000)). B05 mice develop severe ataxia and progressive Purkinje cell pathology starting at 3 months of age (Burright et al., 1995; Clark et al., 1997). In contrast, the A02 transgenic mouse strain expressing a similar construct with a non-pathological expansion of 30 glutamines show no signs of altered neurological function or Purkinje cell pathology. If p38MAPK is mediating neuronal toxicity, it is predicted that its activation would coincide with the beginning of neurological deficits. Consistent with this premise, Western blot analysis of cerebellar protein extracts from aged-matched 3-month-old mice with the phospho-p38MAPK antibody revealed enhanced phosphorylation of p38MAPK in extracts from B05 mice (Figure 14). In agreement with the findings in cultured cells, the phosphorylation of p38MAPK in extracts from A02 mice was found to be lower than that detected in B05 extracts, but slightly increased when compared to extracts from non-transgenic controls (Figure 14A and 14B, Appendix 2 Supplemental Figure 9). Importantly, the B05 mice were

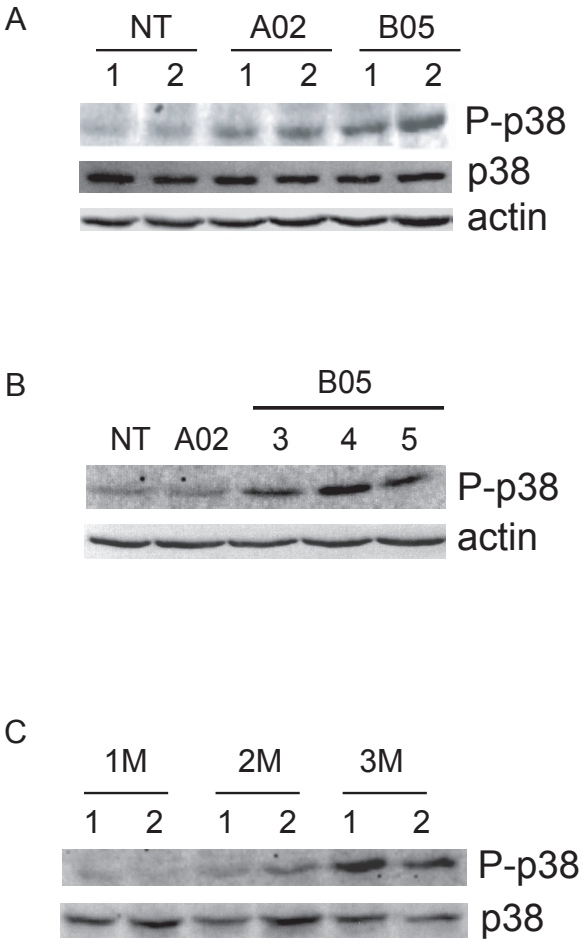
A
NT
A02
B05
1 2 1 2 1 2
P-p38
p38
actin
B
B05
NT A02 3 4 5
P-p38
actin
C
1M
2M
3M
1 2 1 2 1 2
P-p38
p38

Figure 14. Western blot analysis of phosporylated-p38MAPK in the cerebella of 3-month-old SCA-1 mice

A) Western blot analysis of duplicate cerebellar extracts from 3-month-old non-transgenic (NT), A02, and B05 mice with the phospho-p38MAPK antibody. An increase of phosphorylated p38MAPK protein was detected in extracts from B05 mice when compared to NT or A02 mice. The membrane was re-probed for total p38MAPK and actin to confirm equal loading. B) Western blot analysis of three cerebellar extracts from 3-month-old B05 mice (numbered 3, 4, and 5) revealed an increase of phosphorylated p38MAPK levels when compared to NT or A02 mice. Actin levels served as a loading control. C) Western blot analysis of duplicate cerebellar extracts from B05 mice at 1, 2, and 3 months of age with the phospho-p38MAPK antibody. The analysis revealed a detectable induction in p38MAPK activation in lysates from mice at 3 months of age. The membrane was re-probed with a total p38MAPK antibody, which served as a loading control.

observed to have a 5 fold induction in p38MAPK phosphorylation at 3 months of age, while mice at 1 and 2 months of age showed little or no detectable p38MAPK phosphorylation (Figure 14C). These data suggest that the activation of p38MAPK correlates well with the onset of behavioural and anatomical anomalies in the mouse model of SCA-1.

3.2.2 Detection of p38MAPK activation in the Purkinje neurons of 3-month-old SCA-1 mice

To determine if the activation of p38MAPK was localized to the Purkinje neurons, sagittal sections from the cerebella of 3-month-old B05 mice were analysed by immunohistochemistry (Figure 15). The localization of phosphorylated p38MAPK was found to be primarily localized to the cytoplasm and nucleus of Purkinje neurons (Figure 15, panel i). No detection of phosphorylated p38MAPK was evident in cerebella sections stained with secondary antibody alone (Figure 15, panel iii), while non-transgenic mice had low levels of phospho-p38MAPK (Figure 15, panel ii). These results suggest that the increase in the levels of activated p38MAPK (as detected by Western blot analysis) could be attributed to the expanded polyglutamine expression in Purkinje neurons.

3.3 Analysis of the ubiquitin-proteasome system in expanded polyglutamine-expressing cells

3.3.1 Proteasome inhibition sensitizes HttQ103-expressing cells

The HttQ103 protein is known to inhibit proteasome activity in a cell-based assay (Bence et al., 2001). To determine if the cytotoxicity of the expanded polyglutamine proteins could be enhanced by further proteasome inhibition, a pharmacological proteasome inhibitor (PI) that inhibits chymotrypsin-like activity of the multicatalytic proteinase complex was added to HttQ25 and HttQ103-transfected cells. At 30 hours post-transfection,

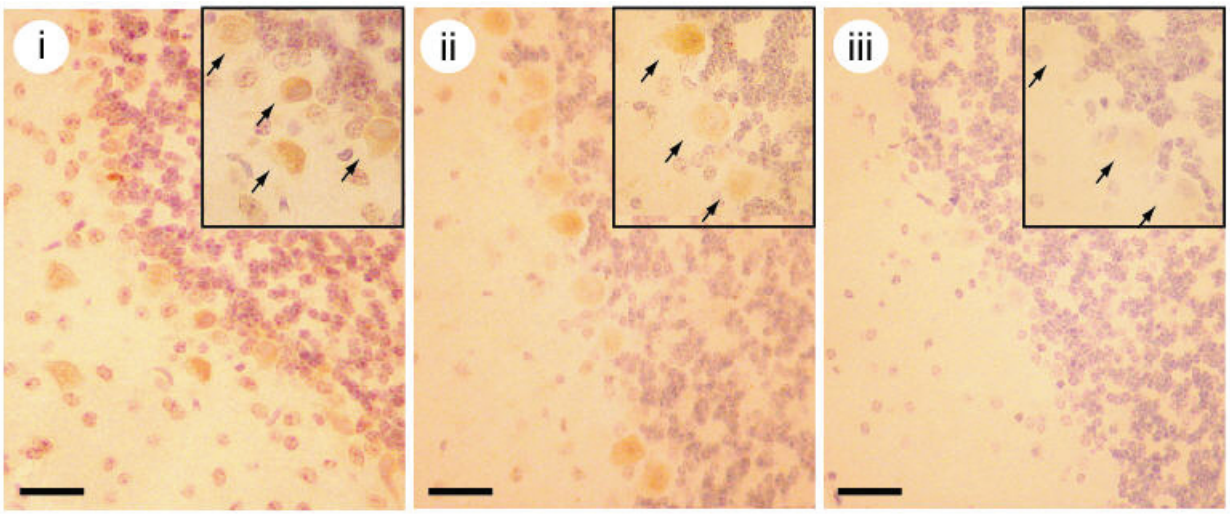
i
ii
iii

Figure 15. Immunohistochemical detection of phosphorylated-p38MAPK in a 3-month-old SCA-1 mouse

Immunohistochemical analysis of mice cerebella using the phospho-p38MAPK antibody. Panel i) a sagittal section of the cerebellum from a B05 mouse and ii) non-transgenic mouse at 3 months of age. Immunoreactivity was detected in the cytoplasm and nucleus of Purkinje cells of B05 and non-transgenic mice. Panel iii) a sagittal section from a B05 mouse stained with the secondary antibody alone, demonstrating the absence of immunoreactivity by omission of the primary antibody. Scale bars represent 25µm.

flow cytometry was performed using propidium iodide exclusion; cells were pre-treated with PI for 6 hours prior to assessing cell death. Consistent with previous results, HttQ103-expressing cells exhibited the highest levels of death (25%, Figure16), whereas the death associated with HttQ25 expression was similar to that of GFP (10-12%). Treatment of HttQ25- and HttQ103-expressing cells with SKF86002 resulted in a decrease in cell death that was most pronounced in cells expressing HttQ103 (Figure 16). PI-treated U87MG cells expressing HttQ103 had a significant increase in cell death (~ 30%) when compared to their untreated counterparts (Figure 16) and was found to be 15% greater than PI-treated HttQ25-expressing cells. Under the same experimental conditions the amount of cell death induced by proteasome inhibition in untransfected cells was approximately 5% (not shown), roughly equivalent to the increase in cell death mediated by proteasome inhibition in cells expressing HttQ25 and HttQ103. Under these conditions proteasomes cannot therefore be fully inhibited by expression of the polyglutamine proteins alone – if the proteasomes were completely inhibited the addition of PI would have no effect on cell survival. The pharmacological data shown in Figure 16 support the argument that the cytotoxicity of expanded polyglutamine proteins is mediated by proteasome inhibition and p38MAPK activation, but do not reveal whether these activities are independent.

3.3.2 Engineering a bicistronic reporter system to detect proteasome inhibition of polyglutamine proteins

Fluorescent ubiquitin-proteasome reporters have previously been used to monitor the activity of the ubiquitin-proteasome system (UPS) in living cells (Dantuma et al., 2000; Bence et al., 2001) and organisms (Lindsten et al., 2003; Bett et al., 2009; Maynard et al., 2009). To simultaneously assess functioning of the UPS and inclusion body formation at a

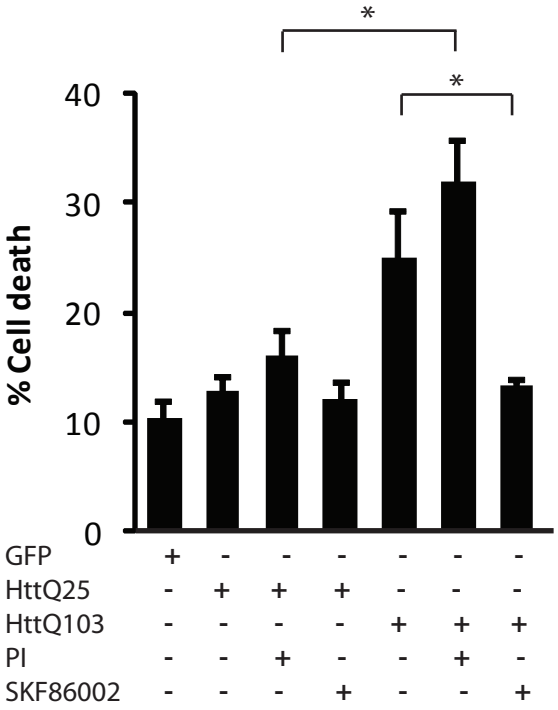
*
*
40
30
20
10
0
% Cell death
GFP + - - - - - -
HttQ25 - + + + - - -
HttQ103 - - - - + + +
PI - - + - - + -
SKF86002 - - - + - - +

Figure 16. Treatment with proteasome inhibitor sensitizes polyglutamine-expressing cells

Cell viability of U87MG cells expressing GFP, HttQ25, or HttQ103 treated with proteasome inhibitor (PI) or the p38MAPK inhibitor (SKF86002) was assessed by flow cytometry analysis using propidium iodide exclusion 30 hours post-transfection. The survival of SKF86002-treated HttQ103-expressing cells was significantly improved when compared to the untreated counterpart. Treatment with proteasome inhibitor resulted in a significant increase in cell death in cells expressing HttQ103 when compared to cells expressing HttQ25. Experiments were done in triplicate. Error bars represent the standard error of the mean (*$p<0.05$).

single cell level, a bicistronic construct that encodes a short or expanded polyglutamine protein and a fluorescent proteasome substrate reporter on the same transcript was created and designated HttQ25YFP-pIRES-mRFP^{u} and HttQ103YFP-pIRES-mRFP^{u}, respectively (Figure 17A and 18A). The fluorescent proteasome reporter was created by fusing the constitutively active CL1 degradation signal (a 16 amino acid sequence consisting of ACKNWFSSLSHFVIHL) to the C-terminus of the monomeric red fluorescent protein (mRFP) to create a destabilized version of mRFP (designated mRFP^{u}). The mRFP^{u} variant is similar to the GFP^{u} reporter system previously described in Bence et al. (Bence et al., 2001). Under normal conditions mRFP^{u} is quickly degraded by the 26S proteasome, but during conditions of proteasomal impairment the turnover of mRFP^{u} is reduced leading to an accumulation of mRFP^{u} that is visible by fluorescence microscopy.

Fluorescence microscope images of U87MG cells transfected with HttQ25YFP-pIRES-mRFP^{u} for 24 hours showed diffuse HttQ25 expression in the cytoplasm and nucleus along with very low detection of mRFP^{u} (Figure 17B). The low levels of mRFP^{u} suggest the expression of HttQ25 does not result in proteasome inhibition. In contrast, cells transfected with HttQ103YFP-pIRES-mRFP^{u} showed an increase in mRFP^{u} levels when compared to cells expressing HttQ25YFP-pIRES-mRFP^{u} (comparison of Figure 17B and 18B). Inclusion bodies were detected in cells expressing HttQ103YFP-pIRES-mRFP^{u} which was accompanied with higher levels of mRFP^{u} fluorescence (Figure 18B). No inclusion bodies were detected in cells expressing HttQ25YFP-pIRES-mRFP^{u} (Figure 17B). The data suggests a relationship between inclusion body formation and proteasome impairment, but provide little information with regards to the temporal order of events.

A

B

YFP RFP merge

Figure 17. Engineering a bicistronic reporter to detect proteasome inhibition by HttQ25

A bicistronic reporter can be used to detect proteasome inhibition by polyglutamine proteins. A) Schematic representation of the bicistronic expression construct engineered to simultaneously express the huntingtin-derived protein HttQ25 fused to the yellow fluorescent protein (YFP) and an intrinsic proteasome activity reporter ($mRFP^u$) downstream of an attenuated internal ribosome entry site (IRES). This construct is designated HttQ25YFP-pIRES-$mRFP^u$. B) Representative images of cells expressing HttQ25YFP-pIRES-$mRFP^u$ visualized under fluorescence 24 hours post-transfection. Visualization using the yellow channel revealed HttQ25 expression in the cytoplasm and nucleus of the transfected cells. Visualization under the red channel showed low levels of $mRFP^u$ expression evenly distributed throughout the cytoplasm and nucleus of the cell.

A

B

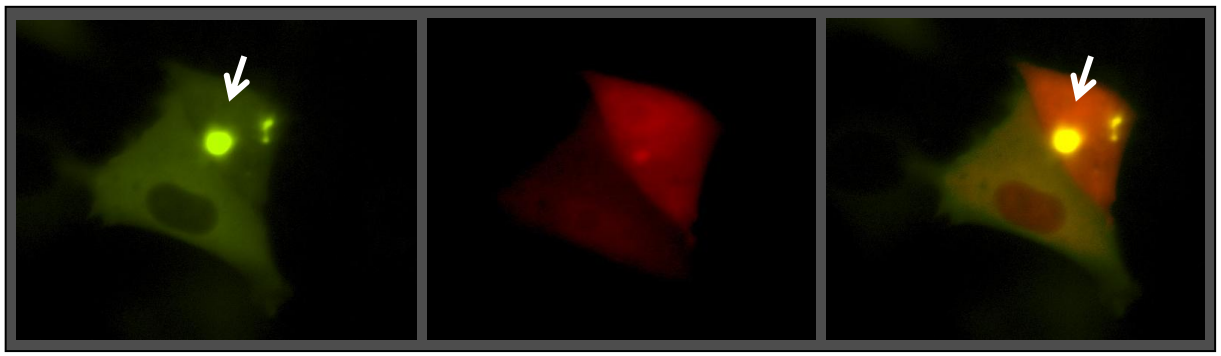

YFP RFP merge

Figure 18. Engineering a bicistronic reporter to detect proteasome inhibition by HttQ103

A bicistronic reporter can be used to detect proteasome inhibition by polyglutamine proteins. A) Schematic representation of the bicistronic expression construct engineered to simultaneously express the huntingtin-derived protein HttQ103 fused to the yellow fluorescent protein (YFP) and an intrinsic proteasome activity reporter ($mRFP^u$) downstream of an attenuated internal ribosome entry site (IRES). This construct is designated HttQ103YFP-pIRES-$mRFP^u$. B) Representative images of cells expressing HttQ103YFP-pIRES-$mRFP^u$ visualized under fluorescence 24 hours post-transfection. An inclusion body (depicted by the white arrow) is visible in the yellow channel and corresponds to an increase in $mRFP^u$ detected in the red channel. The cell without an inclusion body is shown to have lower levels of $mRFP^u$ fluorescence.

3.3.3 Time lapse imaging of single cells provide temporal information of inclusion body formation and proteasome inhibition

The analysis of fixed cells can reveal many changes associated with HttQ103 expression including alterations of morphology and the appearance of inclusion bodies, but offer little information with respect to primary or secondary events leading up to these observations. In order to study the cause-and-effect relationships between inclusion body formation and proteasome inhibition in expanded polyglutamine-mediated cytotoxicity, U87MG cells were transfected with HttQ103YFP-pIRES-mRFP^{u} and were imaged at 30 minute intervals from 24 to 48 hours post-transfection (Figure 19). Single cell analysis of the time lapse images visualized under brightfield revealed a change in morphology associated with cell death at 48 hours (Figure 19, panel 1). Inclusion body formation was detected at approximately 33 hours post-transfection (Figure 19, panel 2), while the detection of mRFP^{u} was evident at 27 hours and gradually increased to a plateau at 33 hours, where it remained constant (Figure 19, panel 3). These data suggest time lapse microscopy of cells simultaneously expressing HttQ103 and a fluorescent proteasome reporter can provide temporal information with regards to inclusion body formation and proteasome inhibition that could not be obtained from fixed cells.

HttQ103

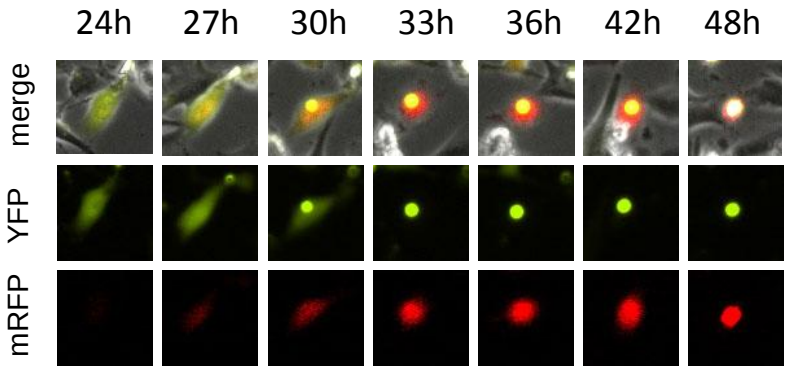

Figure 19. Single cell analysis of time lapse images provides temporal information regarding the formation of inclusion bodies and proteasome inhibition

U87MG cells transfected with HttQ103YFP-pIRES-mRFP^{u} were visualized over the course of 24 hours. Live cell imaging was initiated at 24 hours post-transfection with images acquired at 30 minute intervals. Selected frames are shown at time points indicated on the top. The formation of an inclusion body is evident in the yellow channel at 30 hours. Although an inclusion body appears at 30 hours, the cell appears to be viable based on its morphology. mRFP^{u} was detected in the red channel prior to the formation of an inclusion body. Merged images, including cells visualized under brightfield field, yellow channel, and red channel, are shown on the top panel; cells visualized using the yellow channel is shown in the second panel; and cells visualized using the red channel is shown in the third panel.

3.4 Inclusion body formation is promoted by p38MAPK activity and proteasome dysfunction

3.4.1 Single cell analysis

It was previously suggested in Figure 16 that the activities of the UPS and p38MAPK activation are critical components that mediate the toxicity associated with expanded polyglutamine proteins. To investigate the temporal order of events leading to HttQ103-induced cellular and proteasome toxicities and to dissect the role of p38MAPK in these events, U87MG cells were transfected with HttQ103YFP-pIRES-mRFP^{u} and were imaged starting at 24 post-transfection (Figure 20). To increase the resolution of the data set, the frequency of image acquisition was increased to 10 minute intervals. To quantify proteasome activity the values of mRFP^{u} intensity were graphed as a function of time. The analysis revealed an increase in mRFP^{u} fluorescence prior to the formation of an inclusion body, which was followed by a period of constant mRFP^{u} intensity (Figure 20, panel 1). The single cell analysis revealed that HttQ103-induced cell death is preceded by gradual UPS impairment. Once this impairment reaches a threshold level, inclusion bodies begin to form and their formation correlated with a momentary recovery of UPS efficiency as measured by mRFP^{u} intensity. The data suggests that inclusion body formation rescues proteasome dysfunction in HttQ103YFP-expressing cells and are consistent with previously published findings in primary neuron cultures (Arrasate et al., 2004).

The cell viability data shown in Figure 16 also suggests that the functionality of the UPS is not fully compromised in cells expressing HttQ103. Since HttQ103 is a substrate of the UPS, the addition of PI is predicted to delay its degradation but it is unclear what effect this may have on the formation of inclusion bodies. To examine the extent in which inclusion body formation was dependent on UPS dysfunction, U87MG cells expressing

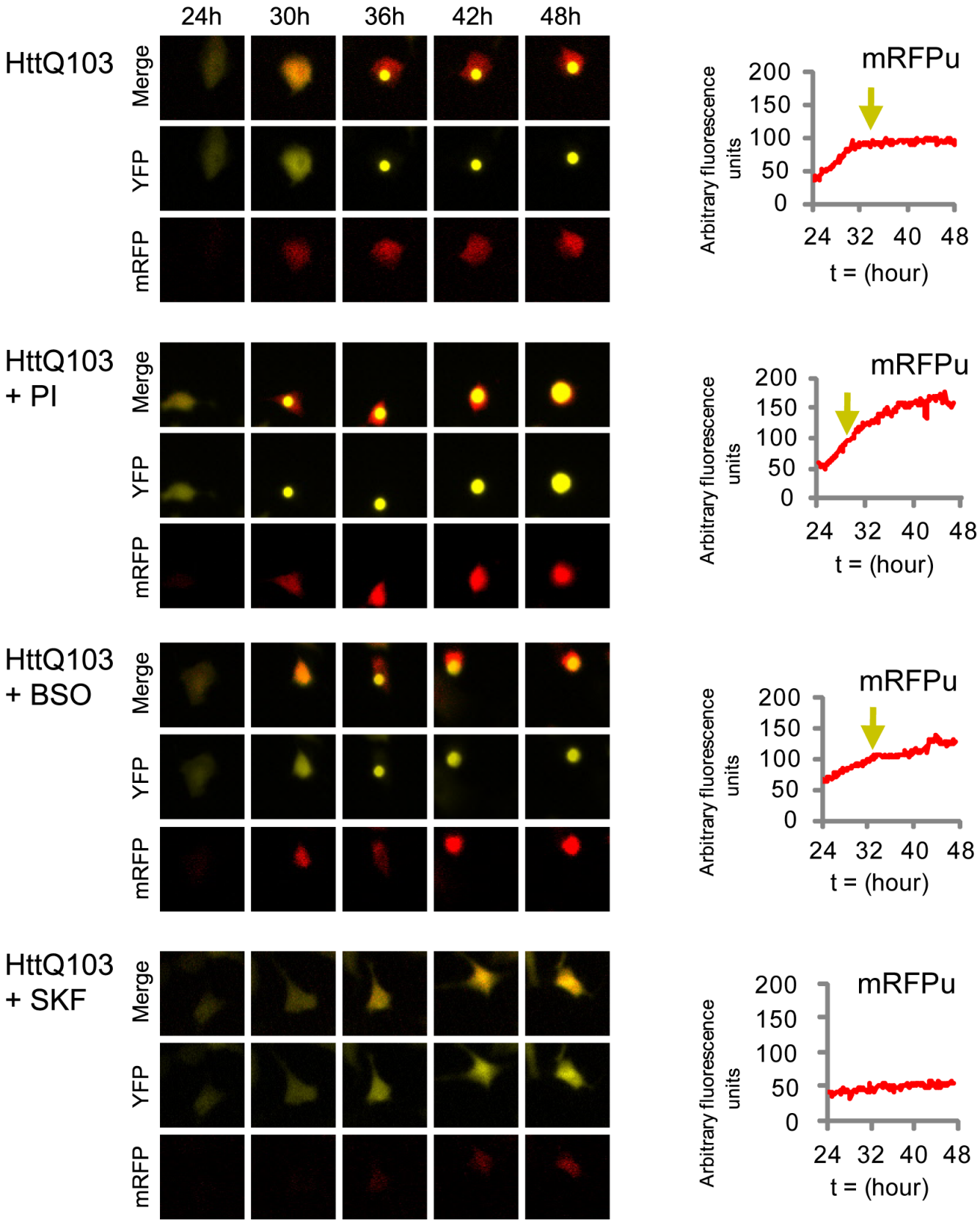
24h
30h
36h
42h
48h
HttQ103
Merge
YFP
mRFP
mRFPu
Arbitrary fluorescence units
200
150
100
50
0
24 32 40 48
t = (hour)
HttQ103
+ PI
HttQ103
+ BSO
HttQ103
+ SKF

Figure 20. Expression of HttQ103 results in the formation of inclusion bodies that are preceded by increased levels of the proteasome reporter protein mRFP^{u}

Single cell analysis of inclusion body formation and ubiquitin-proteasome system impairment induced by the expression of the HttQ103 protein. U87MG cells expressing HttQ103YFP-pIRES-mRFP^{u} were imaged over the course of 24 hours to simultaneously follow inclusion body formation and ubiquitin-proteasome system impairment. Cells were either left untreated (panel 1) or treated with proteasome inhibitor (PI, panel 2), buthionine sulphoximine (BSO, panel 3), or the p38MAPK inhibitor (SKF86002, panel 4) and visualized under fluorescence at 10 minute intervals. The accumulation of mRFP^{u} was quantified using densitometry values from a single cell for each condition, which revealed detectible levels of mRFP^{u} prior to the formation of an inclusion body (represented by the yellow arrow). Treatment with proteasome inhibitor resulted in earlier inclusion body formation and correlated with increased levels of mRFP^{u}. BSO treatment also increased mRFP^{u} levels but did not significantly accelerate the timing of inclusion body formation. Treatment with SKF86002 resulted in the overall lower levels of mRFP^{u} and a delay in inclusion body formation. Single cells used for the analysis were isolated from the population of cells described in Figures 21- 24. Comparative single cell analysis of inclusion body formation corresponds to time points in which 40% of the transfected cells had formed inclusion bodies.

HttQ103YFP-pIRES-mRFP^{u} were treated with PI and were imaged as previously described. As expected PI treatment resulted in a rapid and persistent increase in mRFP^{u} intensity which is consistent with the accumulation of the proteasome fluorescent reporter. Under these conditions inclusion body formation was accelerated relative to the untreated control – the majority of inclusion bodies were detected at 30 hours post-transfection compared to 36 hours in untreated cells (Figure 20, panel 1 compared to panel 2). Therefore, the formation of inclusion bodies is promoted by PI treatment in HttQ103-expressing cells suggesting a direct relationship between proteasome inhibition and inclusion body formation.

Damaged proteins are normally eliminated by the UPS. We speculated that an increase in cellular ROS levels would lead to oxidative damage to proteins and inflict an additional burden on proteasomes that may affect the kinetics of inclusion body formation. To test this hypothesis, we depleted GSH levels in HttQ103YFP-pIRES-mRFP^{u}-transfected cells by treatment with buthionine sulphoximine (BSO) at 24 hours post-transfection. In BSO-treated cells, we observed a constant increase in mRFP^{u} intensity (Figure 20, panel 3) consistent with a cumulative UPS burden. However, in contrast to PI treatment, no difference was found in the detection of inclusion bodies compared to untreated cells (Figure 20, panel 1 compared to panel 3). Taken together, these data suggest that BSO treatment increases UPS burden but not inclusion body formation in HttQ103-expressing cells.

Having previously established that the activation of p38MAPK in HttQ103-expressing cells contributes to toxicity, we sought to determine what effects inhibition of p38MAPK signalling pathways would have on inclusion body formation and UPS

dysfunction. U87MG cells expressing HttQ103YFP-pIRES-mRFP^{u} were pre-treated with SKF86002 and imaged as described previously. These cells exhibited a low level of mRFP^{u} fluorescence along with a delay in inclusion body formation (Figure 20, panel 4). The mRFP^{u} fluorescence remained low and did not feature a rapid increase as seen in the untreated control. These data suggest that inhibition of the p38MAPK pathway decouples the proteasome inhibition from HttQ103 protein expression, resulting in delayed formation of inclusion bodies.

3.4.2 Quantification of inclusion body formation and proteasome inhibition of multiple time lapse experiments

To quantify inclusion body formation and proteasome inhibition, we analyzed many cells from three independent experiments corresponding to PI, BSO, SKF86002 treatment, or untreated controls. Time lapse imaging of U87MG cells expressing HttQ103YFP-pIRES-mRFP^{u} was initiated at 24 hours post-transfection with images acquired at 10 minute intervals. The brightfield or fluorescence emanating from the YFP and RFP channels were merged to create a movie file (Appendix 1). Images corresponding to the start (24 hours), half way point (36 hours), and the end of the experiment (48 hours) were compiled into a composite for each treatment condition – time lapse composites for untreated, PI-, BSO-, and SKF86002-treated cells are shown in Figures 21-24, respectively. The expression of HttQ103 is shown to be diffuse throughout the cell. Only a few cells forming an inclusion body were detected at 24 hours (Figure 21, panel 3). At 36 hours, many more inclusion bodies were detected and this was accompanied with a notable accumulation of mRFP^{u}. Based on their morphology, many cells with inclusion bodies appear to be viable throughout the experiment. Cells treated with PI shown in Figure 22 demonstrated a rapid and progressive accumulation of mRFP^{u} that coincided with the detection of a greater number of

HttQ103

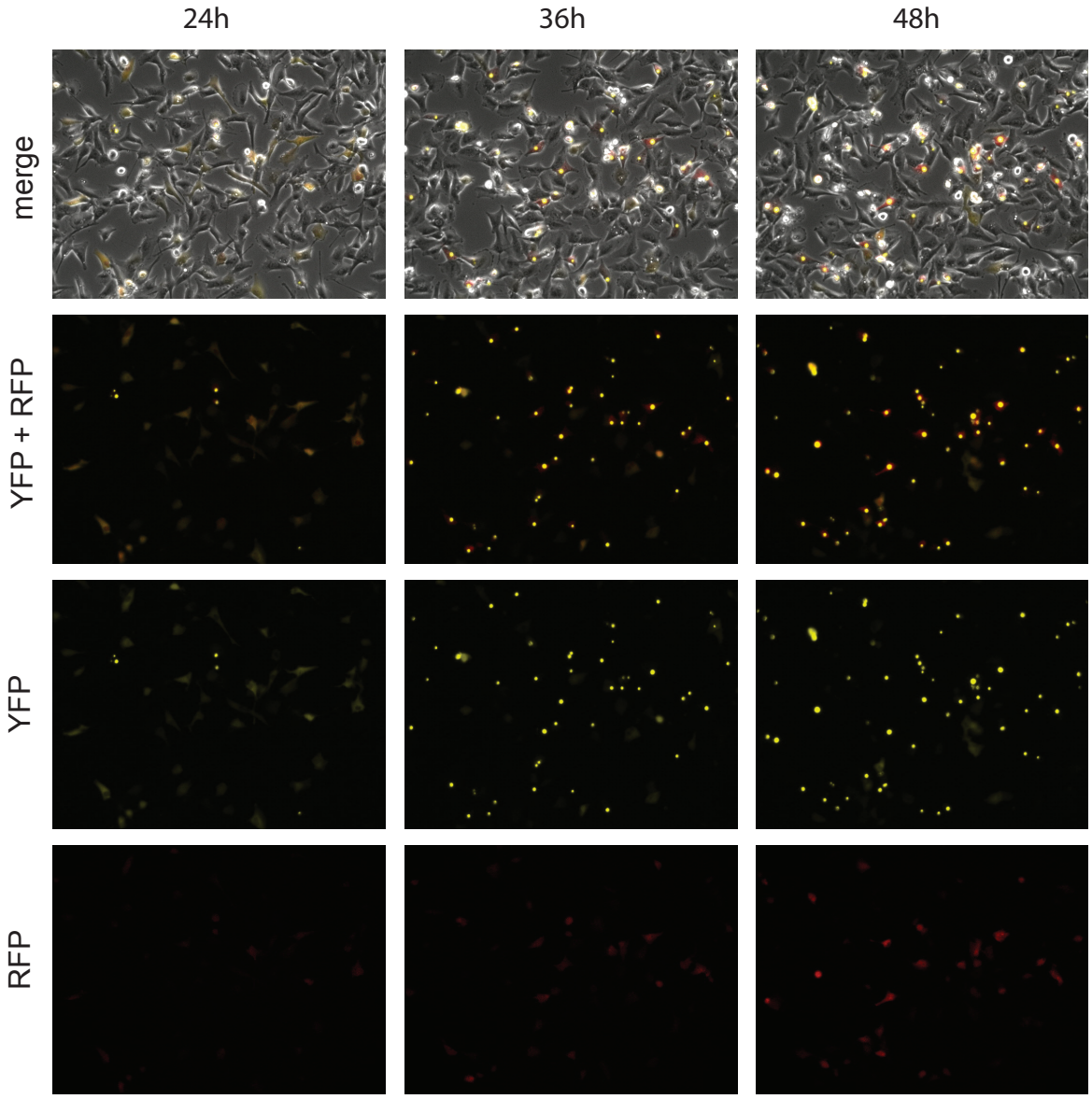

Figure 21. Time lapse imaging of multiple cells expressing HttQ103YFP-pIRES-mRFP^{u}

Time lapse imaging of U87MG cells transfected with HttQ103YFP-pIRES-mRFP^{u} was initiated at 24 hours post-transfection. Images were acquired every 10 minutes using a 10X objective for a total of 24 hours. Selected frames at 24, 36, and 48 hours post-transfection are shown. Cells were visualized under white light and filters that detect YFP or mRFP. At 24 hours, detectable levels of HttQ103 are visible through the cell. At 36 hours (the half way point) many cells begin to form inclusion bodies and have notable accumulation of the red reporter protein (indicative of proteasome inhibition). At 48 hours, many cells have formed inclusion bodies and appear to be viable.

HttQ103 + PI

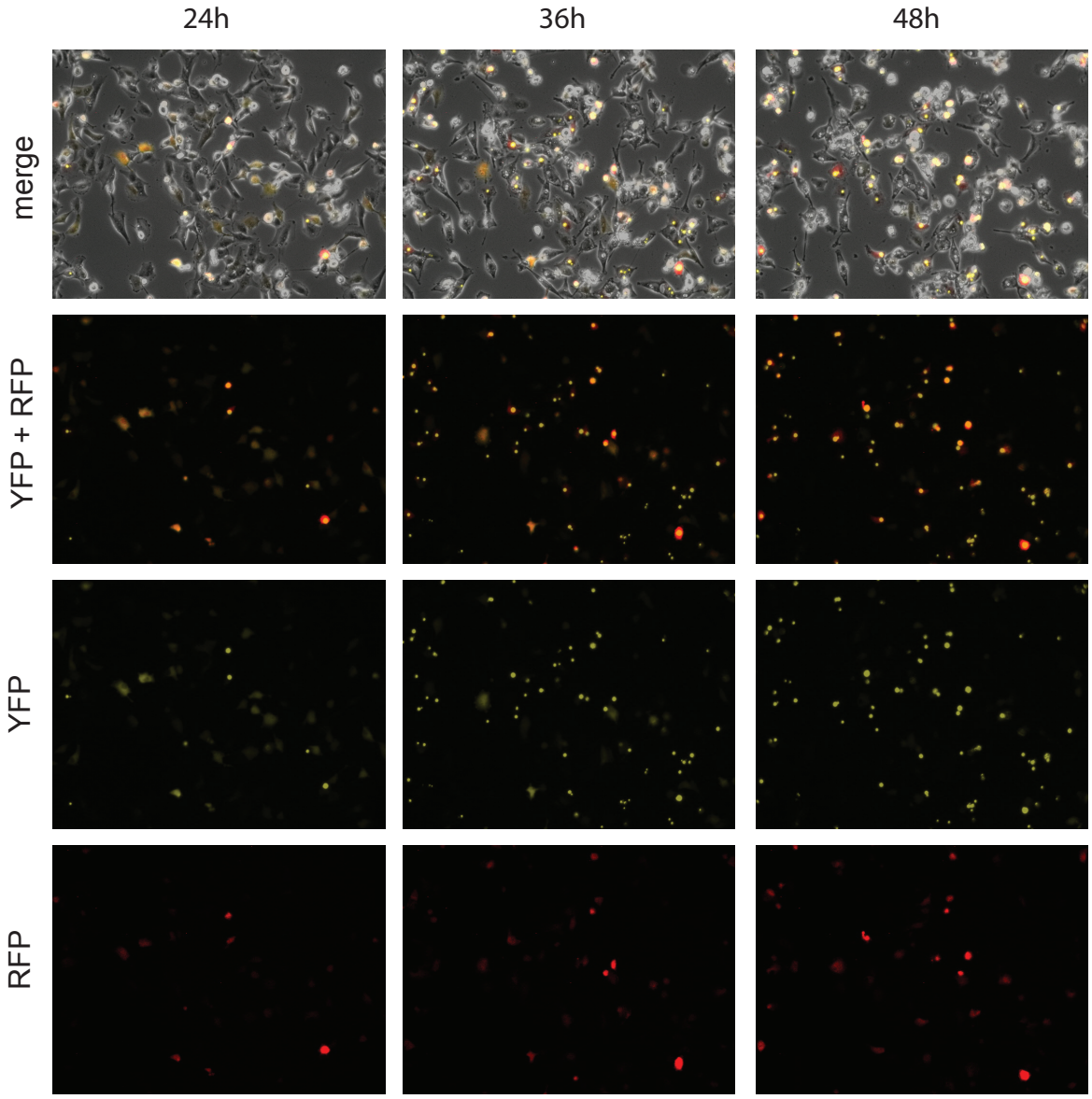

Figure 22. Time lapse imaging of multiple cells expressing HttQ103YFP-pIRES-mRFP^{u} treated with proteasome inhibitor

Time lapse imaging of U87MG cells transfected with HttQ103YFP-pIRES-mRFP^{u} and treated with proteasome inhibitor (PI). Images were acquired every 10 minutes using a 10X objective for a total of 24 hours. Selected frames at 24, 36, and 48 hours post-transfection are shown. The accumulation of the mRFP^{u} reporter protein (red colour) coinciding with a greater number of cells forming an inclusion body is seen at 36 hours compared to untreated cells (in Figure 21). At 48 hours, there is considerably more inclusion bodies and cell death as compared to untreated cells (in Figure 21).

HttQ103 + BSO

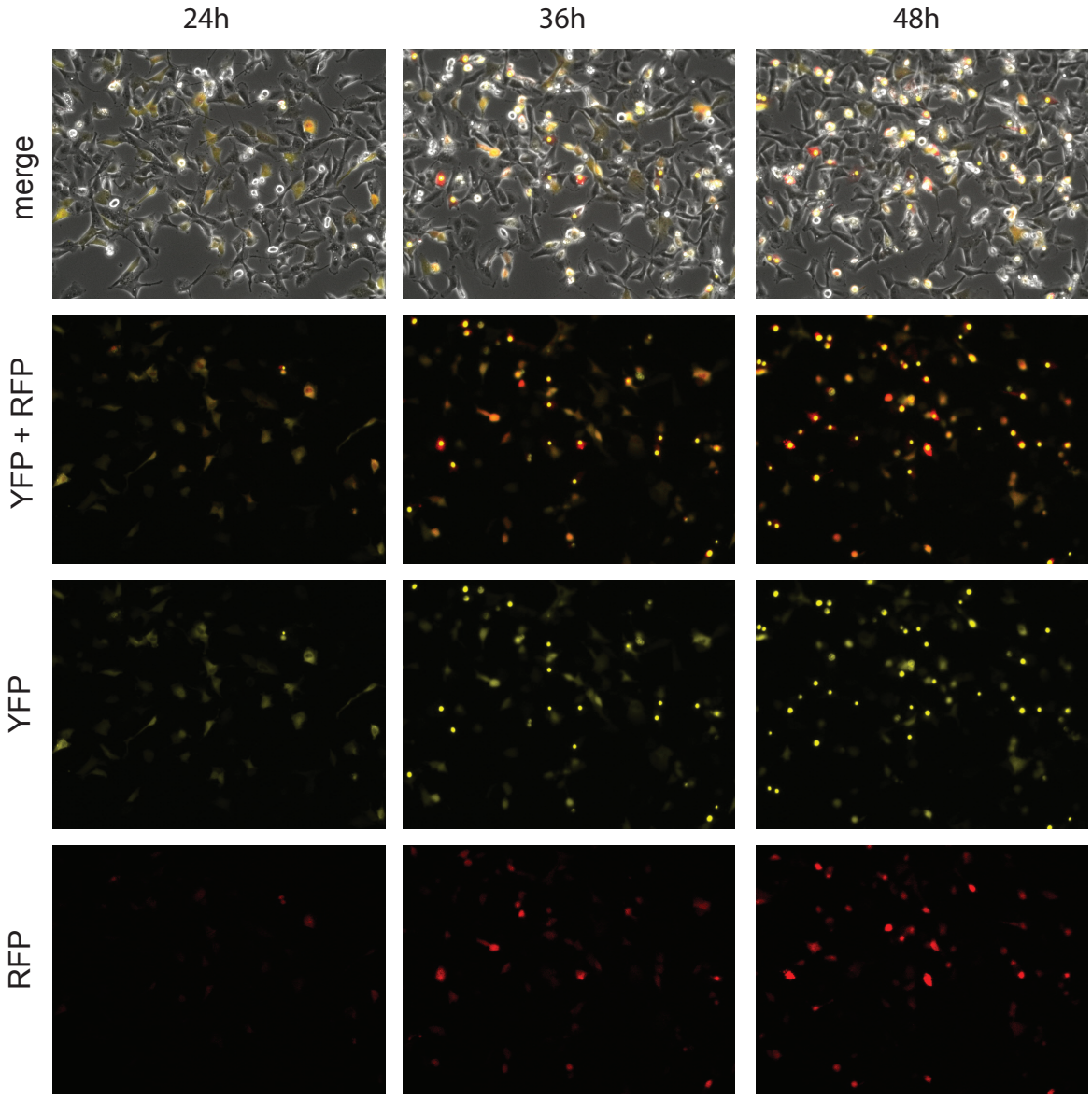

Figure 23. Time lapse imaging of multiple cells expressing HttQ103YFP-pIRES-mRFP^{u} treated with buthionine sulphoximine

Time lapse imaging of U87MG cells transfected with HttQ103YFP-pIRES-mRFP^{u} and treated with buthionine sulphoximine (BSO). Images were acquired every 10 minutes using a 10X objective for a total of 24 hours. Selected frames at 24, 36, and 48 hours post-transfection are shown. Cells were visualized under white light and filters that detect YFP or RFP. At 36 and 48 hours, cells treated with BSO displayed an increase accumulation of the mRFP^{u} reporter protein (red colour) but the frequency of inclusion body formation is not notably different than in untreated cells (in Figure 21).

HttQ103 + SKF

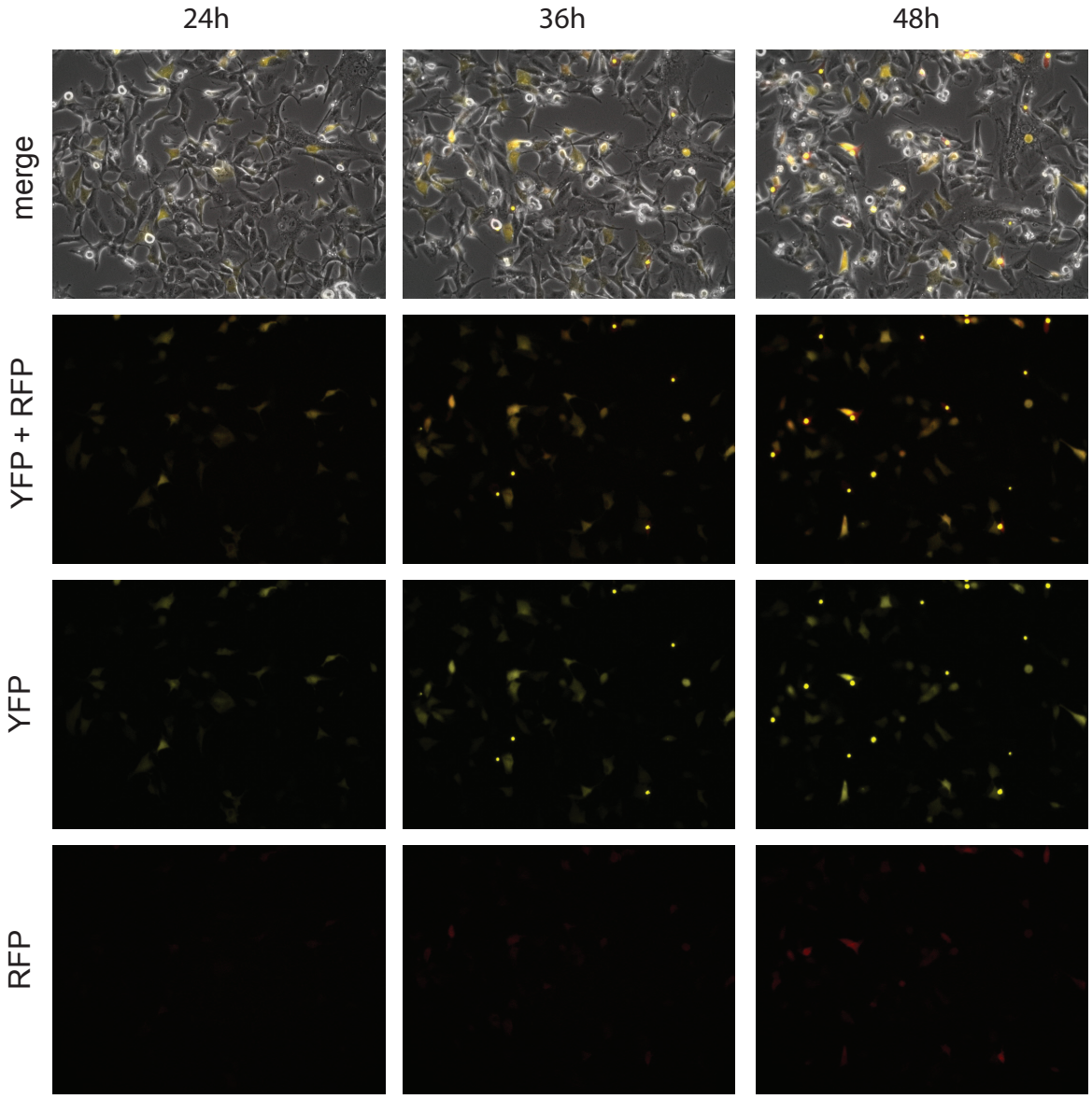

Figure 24. Time lapse imaging of multiple cells expressing HttQ103YFP-pIRES-mRFP^{u} treated with SKF86002

Time lapse imaging of U87MG cells transfected with HttQ103YFP-pIRES-mRFP^{u} treated with SKF86002 two hours prior to transfection. Images were acquired every 10 minutes using a 10X objective for a total of 24 hours. Selected frames at 24, 36, and 48 hours post-transfection are shown. A decrease in inclusion body formation is seen compared to untreated cells (in Figure 21) and the levels of the mRFP^{u} reporter protein (red colour) remain low.

inclusion bodies at 36 and 48 hours compared to untreated cells (Figure 22 compared to Figure 21). In addition, a significant increase in the number of shrunken, rounded, and detached cells were observed under phase contrast microscopy (Figure 22, panel 1). Similarly, cells treated with BSO displayed a rapid and progressive accumulation of the $mRFP^{u}$ reporter protein consistent with proteasomal burden (Figure 23, panel 4), but the frequency of inclusion body formation was not found to be notably different compared to untreated cells (Figure 23 compared to Figure 21). In contrast, cells pre-treated with SKF86002 shown in Figure 24 were found to have the fewest number of inclusion bodies among treated and untreated cells (Figure 24 compared to Figure 21, 22, and 23). In addition, the levels of the $mRFP^{u}$ reporter protein remained lower than in untreated cells and do not increase until late in the movie (Figure 24).

Inclusion body formation was quantified by recording the number of cells with inclusion bodies at 6 hour intervals starting at 24 hours post-transfection. The percentage of cells with inclusion bodies was graphed as a function of time and is shown in Figure 25. At 36 hours, ~ 35% of untreated cells were found to have inclusion bodies which increased to ~ 60% by 48 hours. Treatment with BSO did not significantly affect inclusion body formation, whereas treatment with PI generated the greatest number of inclusion bodies (~ 70% at 36 hours and ~ 85% at 48 hours). The rapid increase in the frequency of inclusion bodies with PI treatment suggests proteasome inhibition directly influences the formation of inclusion bodies. In contrast, cells treated with SKF86002 had the fewest number of inclusion bodies. Only 10% of SKF86002-treated cells were found to have inclusion bodies at 36 hours which increases slightly to 20% by 48 hours.

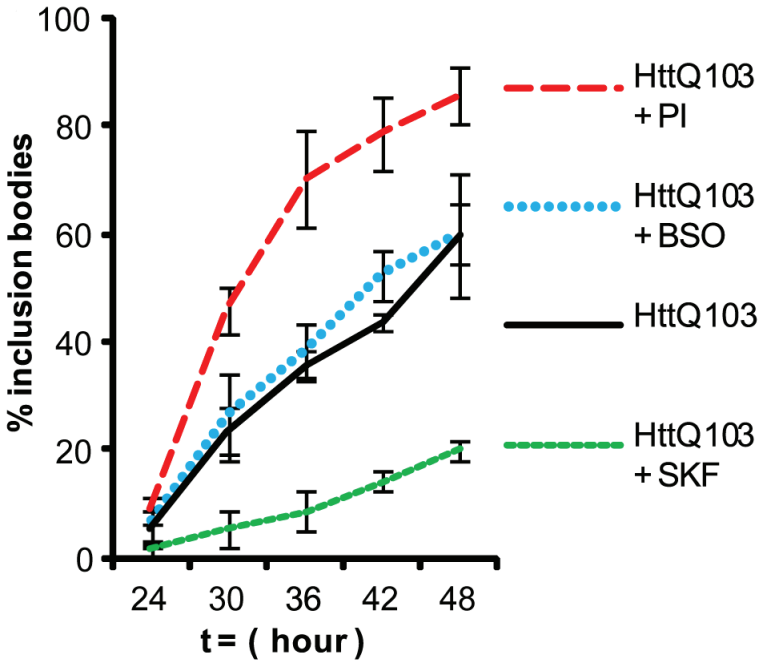
100
80
60
40
20
0
% inclusion bodies
24
30
36
42
48
t = (hour)
HttQ103
+ PI
HttQ103
+ BSO
HttQ103
HttQ103
+ SKF

Figure 25. Multiple live cell analysis of inclusion body formation

The percentage of inclusion body formation in cells expressing HttQ103 for each treatment was recorded every 6 hours beginning at 24 hours post-transfection for 24 hours. Treatment with proteasome inhibitor (PI) generated the greatest number of inclusion bodies compared to untreated cells while SKF86002-treated cells were found to have the fewest inclusion bodies. Experiments were performed in triplicate with over 50 cells analyzed in each condition. Error bars indicate standard error of the mean.

Similarly, we quantified the average mRFP^u fluorescence from many U87MG cells expressing HttQ103YFP-pIRES-mRFP^u and graphed the fluorescence intensities as a function of time (Figure 26). Treatments with PI and BSO were found to generate the highest amounts of mRFP^u fluorescence compared to the untreated control. In addition, the mRFP^u fluorescence of PI- and BSO-treated cells demonstrated a linear relationship (evident by the constant rate of change) throughout the experiment. This suggests that cells treated with PI or BSO did not show any recovery of UPS function during the course of the experiment. In contrast, untreated cells displayed an initial increase of mRFP^u from 24 to 36 hours that was followed by a period of constant mRFP^u fluorescence intensity. This suggests that a momentary recovery of UPS function may have occurred at 36 hours. Finally, SKF86002-treated cells resulted in the lowest levels of mRFP^u throughout the length of the experiment in comparison to untreated cells. This suggests that SKF86002 treatment decouples the proteasome inhibition associated with the expression of expanded polyglutamine proteins. These findings from multiple cells were consistent with the mRFP^u fluorescence levels observed in the single cell analysis.

3.5 Treatment with SKF86002 or PI does not change inclusion formation kinetics

The rate-limiting step of inclusion body formation is a nucleation event caused by the aggregation of expanded polyglutamine proteins (Colby et al., 2006). This nucleation event seeds the rapid addition of monomeric and oligomeric HttQ103 species and results in the formation of a mature inclusion body (Legleiter et al., 2010). It was shown that SKF86002-treated cells expressing HttQ103YFP-pIRES-mRFP^u formed the fewest number of inclusion bodies. It is possible treatment with SKF86002 may impede the rate of which soluble

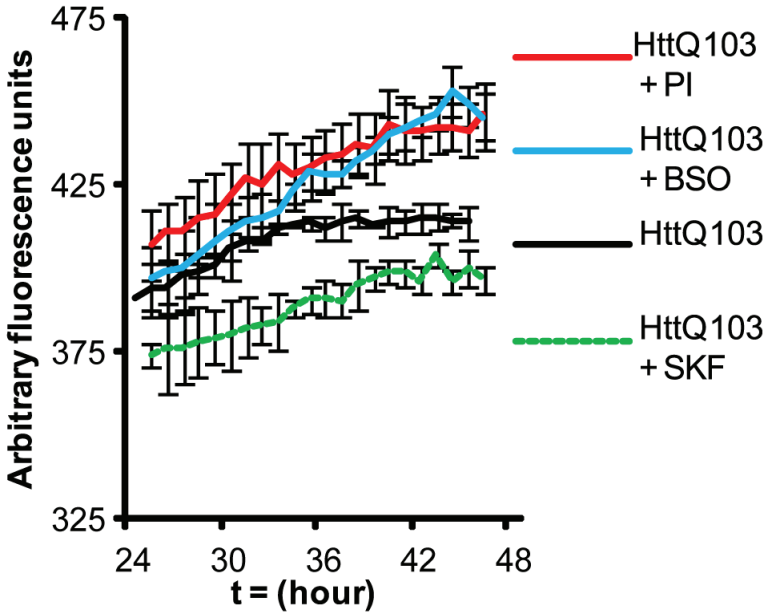
475
425
375
325
Arbitrary fluorescence units
24
30
36
42
48
t = (hour)
HttQ103
+ PI
HttQ103
+ BSO
HttQ103
HttQ103
+ SKF

Figure 26. Multiple live cell analysis of proteasome inhibition

The average $mRFP^u$ intensity values for multiple cells expressing HttQ103 for each treatment was quantified every hour beginning at 24 hours post-transfection for 24 hours. Treatment with proteasome inhibitor (PI) and buthionine sulphoximine (BSO) generated the highest levels of $mRFP^u$ expression in comparison to untreated cells. Experiments were performed in triplicate with over 50 cells analyzed in each condition. Error bars indicate standard error of the mean.

HttQ103 species are sequestered into an inclusion body. Conversely, treatment with PI may accelerate the formation of an inclusion body. To determine if the treatment with PI, SKF86002, or BSO had any effect on the formation kinetics of individual inclusion bodies, we recorded the time interval starting from the initial seeding event to the formation of a mature inclusion body. The formation of an inclusion body in U87MG cells expressing HttQ103YFP-pIRES-mRFP^{u} treated with PI, SKF86002, BSO, or no treatment is shown in Figure 27A. Initially, the expression of HttQ103 is found in the cytoplasm and nucleus of the cell. A nucleation event close to the nuclear membrane causes a rapid sequestration of HttQ103 proteins which form a large mature inclusion body. The time required to form a full inclusion body starting from the initial seeding event was found to be ~ 35 minutes for untreated, PI-, and SKF86002-treated cells, while cells treated with BSO was found to take ~ 29 minutes (Figure 27B). Although the total number of inclusion bodies was found to be greatest for PI-treated cells and fewest in SKF86002-treated cells, the time required form an inclusion body was not noticeably different. However, an increase in the rate of inclusion body formation was revealed under conditions of oxidative stress (BSO-treated cells).

3.6 Treatment with SKF86002 does not affect expression levels of HttQ103

The cytotoxicity associated with the expanded huntingtin protein has been suggested to be dependent on its expression levels and many laboratories have demonstrated that the reduction in the concentration of HttQ103 (either by its physical removal or transcriptional suppression) greatly reduces cytotoxicity (Martin-Aparicio et al., 2001; Ravikumar et al., 2002). To determine if the expression levels of HttQ103 was affected by the treatment with SKF86002, extracts from cells expressing HttQ25, HttQ103, or HttQ103YFP-pIRES-mRFP^{u} treated with or without SKF86002 was analysed by Western blot analysis (Figure 28). Since

A

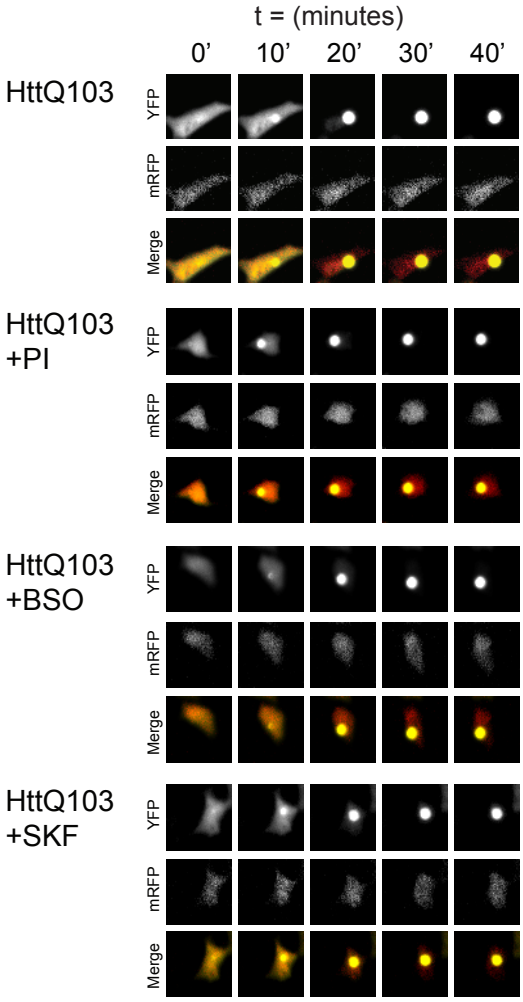
t = (minutes)
0’
10’
20’
30’
40’
HttQ103
HttQ103 +PI
HttQ103 +BSO
HttQ103 +SKF
YFP
mRFP
Merge

B

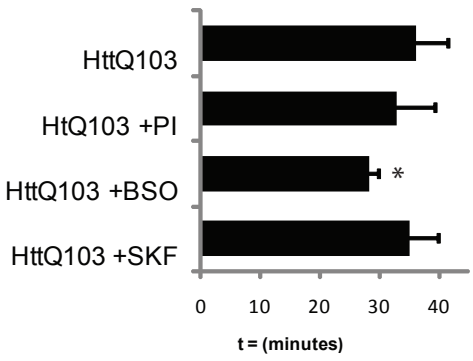
HttQ103
HtQ103 +PI
HttQ103 +BSO
HttQ103 +SKF
*
0
10
20
30
40
t = (minutes)

Figure 27. Analysis of inclusion body formation kinetics

Analysis of the time required to form an inclusion body beginning from the initial seeding event. A) Time lapse imaging of inclusion body formation in U87MG cells expressing HttQ103YFP-pIRES-mRFP^{u} treated with proteasome inhibitor (PI), buthionine sulphoximine (BSO), SKF86002, or no treatment. Inclusion body formation in a single cell can be seen in the yellow channel. The detection of the proteasome reporter protein mRFP^{u} can be seen in the red channel, which illustrates the periphery of the cell. B) Quantification of the time required for the formation of an inclusion body for each condition is shown. No difference in inclusion body formation kinetics was found in cells treated with PI or SKF86002 compared to untreated cells, while BSO-treated cells were found to form an inclusion body at a slightly faster rate. Data represents three independent experiments with approximately 20 cells analyzed in each condition. Error bars represent the standard error of the mean (* $p<0.05$).

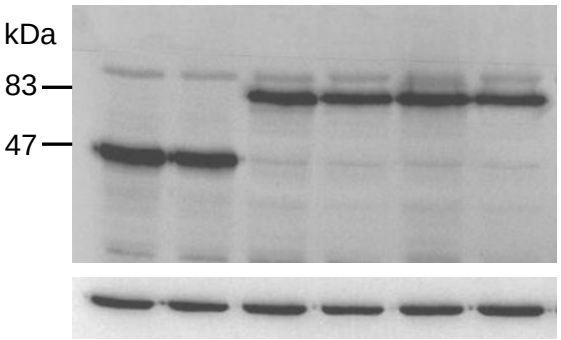

HttQ25	+	+	-	-	-	-
HttQ103	-	-	+	+	-	-
HttQ103YFPpIRESmRFP^{u}	-	-	-	-	+	+
SKF	-	+	-	+	-	+

Figure 28. Treatment with SKF86002 does not affect polyglutamine protein expression levels

Western blot analysis of cell extracts from U87MG cells expressing HttQ25, HttQ103, or HttQ103YFP-pIRES-mRFP^{u} with or without the p38MAPK inhibitor SKF86002. The analysis of YFP using an antibody that recognizes both YFP and GFP revealed no changes in the expression level of the huntingtin YFP-fusion protein in SKF86002-treated cells. Actin levels served as a loading control.

HttQ103 is fused to YFP, it is possible to determine the expression levels of HttQ103 using a GFP antibody that can also recognize YFP. The analysis in Figure 28 showed no difference in expression levels of HttQ25 or HttQ103 from treated or non-treated cell extracts. This suggests that SKF86002 treatment does not affect the expression of HttQ103 – the amelioration of cell survival, reduction in inclusion body formation, and the delayed proteasome impairment observed in SFK86002-treated cells cannot therefore be attributed to a decrease in expression levels of HttQ103.

3.7 Activation of p38MAPK contributes to ROS production but not direct proteasome inhibition

3.7.1 Enhanced expression of wild-type p38MAPK lowers reduced glutathione levels

Based on the single cell analysis data, we speculated that the activation of p38MAPK and UPS impairment were contributing to the production of ROS and that SKF86002 may be counteracting this cellular response. A genetic approach was adopted to test this hypothesis, utilizing transfected cells with the expression vectors encoding wild-type or kinase-dead p38MAPK. Whereas pharmacological inhibition may affect multiple p38MAPK isoforms, any modulation of cellular response observed with the genetic approach would be attributable to the alpha isoform of p38MAPK exclusively. It was previously confirmed in Figure 11 that these expression vectors were capable of modulating p38MAPK activity using phosphorylation of HSP27 as a proxy marker. To investigate the relationship of p38MAPK and production of ROS, U87MG cells were transfected with the p38MAPK expression vectors or with an empty vector control construct for 48 hours and then assayed for GSH content, a marker of oxidative status within cells. The overexpression of wild-type p38MAPK resulted in a significant decrease in GSH levels whereas the GSH

content in cells expressing kinase-dead p38MAPK was less affected in comparison to the empty vector control (Figure 29). This suggested that the enhanced expression of wild-type p38MAPK can promote oxidative stress.

3.7.2 Enhanced expression of wild-type p38MAPK results in the increase of the proteasome reporter GFP^{u}

To determine if the overexpression of wild-type p38MAPK resulted in dysfunction of the UPS, the p38MAPK expression constructs were transfected into a cell line stably expressing GFP^{u}, a well-characterized proteasome sensor (Bence et al., 2001). For these experiments, a stable NIH-3T3 cell line expressing GFP^{u} previously generated in the lab was used (the GFP^{u} reporter is expressed at a lower level in the stable cell line and does not accumulate as an artefact of transfection-mediated overexpression). By flow cytometric analysis, it was found that cells overexpressing wild-type p38MAPK exhibited the highest levels of GFP^{u} intensity compared to the cells expressing the kinase-dead p38MAPK or the empty vector, which were similar (Figure 30). These data suggested that the activation of p38MAPK was negatively affecting UPS function.

3.7.3 Enhanced expression of p38MAPK does not directly inhibit the proteasome

To test whether the inhibition of the proteasome was a direct affect of p38MAPK activation, U87MG cells were transfected with the same set of p38MAPK plasmids and their proteasome activity was assayed using fluorogenic substrates. No significant difference in peptidylglutamyl- or chymotrypsin-specific activity was found (Figure 31), suggesting that the proteasome remains functional during p38MAPK activation. Taken together, these data shown in Figures 29-31 indicate that the expression of p38MAPK does affect the oxidative status of cells, but does not directly inhibit the proteasome.

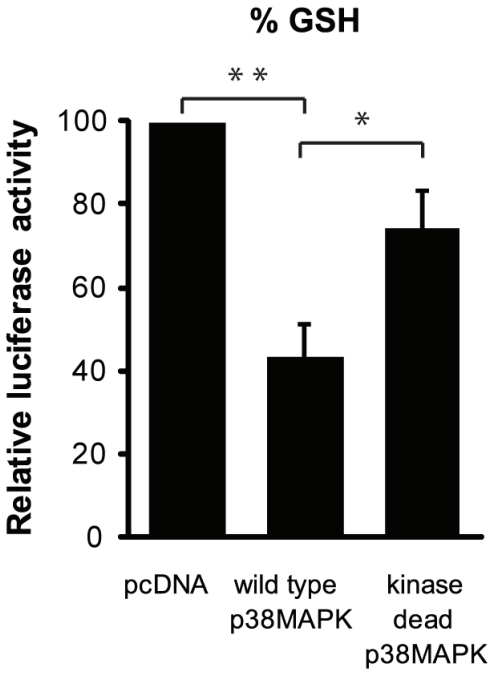
% GSH
* *
*
Relative luciferase activity
100
80
60
40
20
0
pcDNA
wild type p38MAPK
kinase dead p38MAPK

Figure 29. Effects of p38MAPK activity on reduced GSH levels

Lysates from U87MG cells overexpressing wild-type p38MAPK, kinase-dead p38MAPK, or pcDNA control plasmids were assayed for reduced glutathione (GSH) content 48 hours post-transfection. Cells transfected with wild-type p38MAPK had lower levels of reduced GSH when compared to the pcDNA empty vector control (**$p<0.05$) and kinase-dead p38MAPK-expressing cells (*$p=0.06$). Lysates were assayed in triplicate. Error bars represent standard error of the mean.

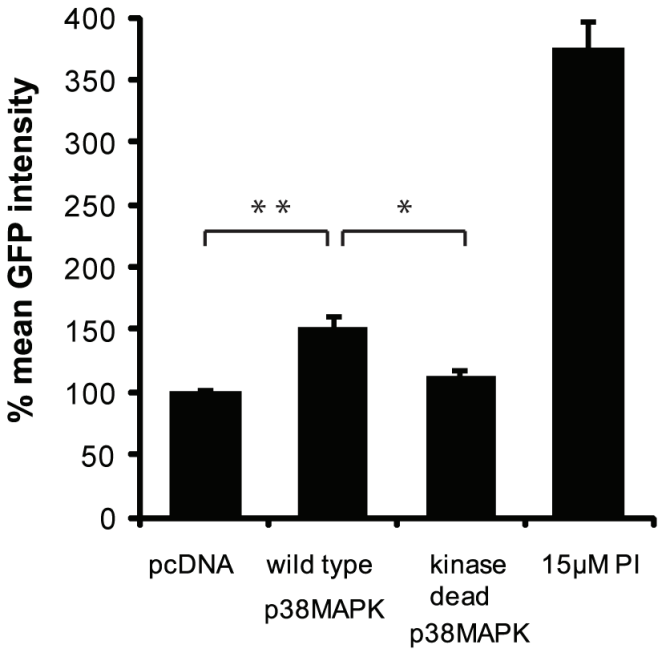
% mean GFP intensity
400
350
300
250
200
150
100
50
0
* *
*
pcDNA
wild type p38MAPK
kinase dead p38MAPK
15μM PI

Figure 30. Effects of p38MAPK activity on the proteasome reporter GFP^{u}

Activation of the p38MAPK pathway leads to proteasomal inhibition. Wild-type p38MAPK or kinase-dead p38MAPK were transfected into NIH-3T3 cells stably expressing the proteasome reporter GFP^{u}. Cells were collected at 48 hours post-transfection and GFP^{u} intensity was analyzed by flow cytometric analysis. Cells overexpressing wild-type p38MAPK had significantly higher levels of GFP^{u} accumulation when compared to cells expressing kinase-dead p38MAPK (*$p<0.05$) and pcDNA empty vector control (**$p<0.01$). Proteasome inhibitor treatment served as a positive control. Experiments were done in triplicate. Error bar represents standard error of the mean.

A

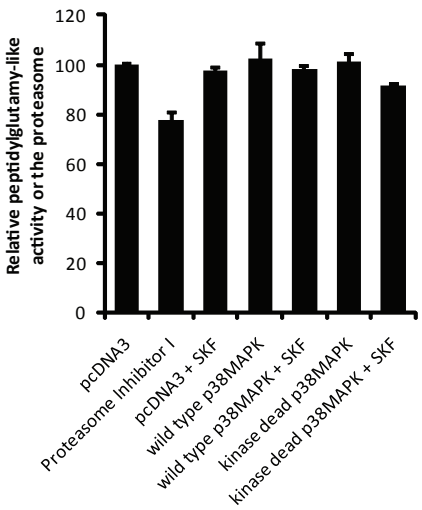
Relative peptidylglutamy-like activity or the proteasome
120
100
80
60
40
20
0
pcDNA3
Proteasome Inhibitor I
pcDNA3 + SKF
wild type p38MAPK
wild type p38MAPK + SKF
kinase dead p38MAPK
kinase dead p38MAPK + SKF

B

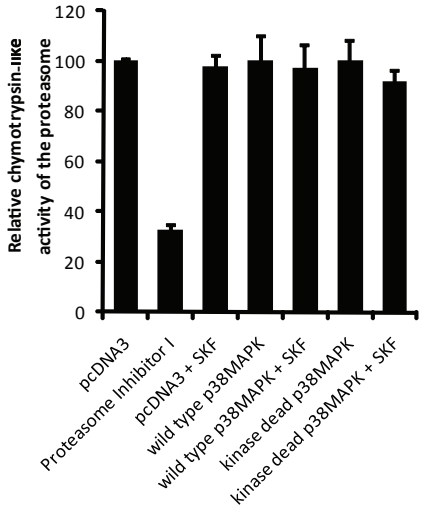
Relative chymotrypsin-like activity of the proteasome
120
100
80
60
40
20
0
pcDNA3
Proteasome Inhibitor I
pcDNA3 + SKF
wild type p38MAPK
wild type p38MAPK + SKF
kinase dead p38MAPK
kinase dead p38MAPK + SKF

Figure 31. Expression of p38MAPK does not directly inhibit the proteasome

U87MG cells transfected with wild-type p38MAPK, kinase-dead p38MAPK, or pcDNA empty vector control plasmids and assayed for their ability to process a peptidylglutamyl- (A) or chymotrypsin-specific (B) fluorogenic substrate. Cells were lysed 48 hours post-transfection and assayed in triplicate. The relative activity of the proteasome was measured 12 hours after the addition of the substrate. No change in the peptidylglutamyl- or chymotrypsin-activity was observed. Proteasome inhibitor (PI) added to lysates was used as a control to demonstrate the specificity of the PI for the chymotrypsin-like activity of the proteasome. Data was normalized to the proteasome activity in lysates from cells transfected with the pcDNA empty vector control. Experiments were performed in triplicate with error bars representing the standard error of the mean.

3.8 Creating a stochastic computer model of polyglutamine-induced cytotoxicity

3.8.1 The critical role of p38MAPK is supported by mathematical modeling

It must be clearly stated that all the computer modeling results were generated by our collaborator, Dr. Carole Proctor, at the University of Newcastle. Dr. Proctor has previously built a stochastic computer model to study age-related decline of proteolysis (Proctor et al., 2007). Our objective was to adapt this relatively simple mathematical model and incorporate components thought to be critical for polyglutamine-mediated cytotoxicity. If the model could recapitulate our laboratory findings, it would validate all the critical components of polyglutamine-induced cell death identified in the laboratory. However, if the simulated data from the mathematical model were at odds with actual laboratory data it would suggest that some critical component must have been overlooked or one or more of the starting assumptions must be invalid. The stochastic computer model was constructed using the Systems Biology Markup Language as described in the Materials and Methods section (details of molecular species and reactions are given in the Appendix 1) and is represented schematically in Figure 32. A stochastic process is one whose behaviour is non-deterministic, in that a systems subsequent state is determined by both process's predictable action and by a random element. Initially, the model was fitted using experimental results, including percentage of cell death, percentage of inclusion body formation, and $mRFP^{u}$ levels from U87MG cells expressing HttQ103. When the kinetics of aggregation, cell death, and $mRFP^{u}$ accumulation were established, additional modeling events were added to represent proteasome inhibitor treatment, ROS production, and p38MAPK activation. Figure 33 shows the results from the computer model simulation. The model predicted that treatment with PI would lead to reduced cell death at 30 hours (Figure 33A), suggesting a short term benefit from reduced levels of small aggregates possibly as the result of an

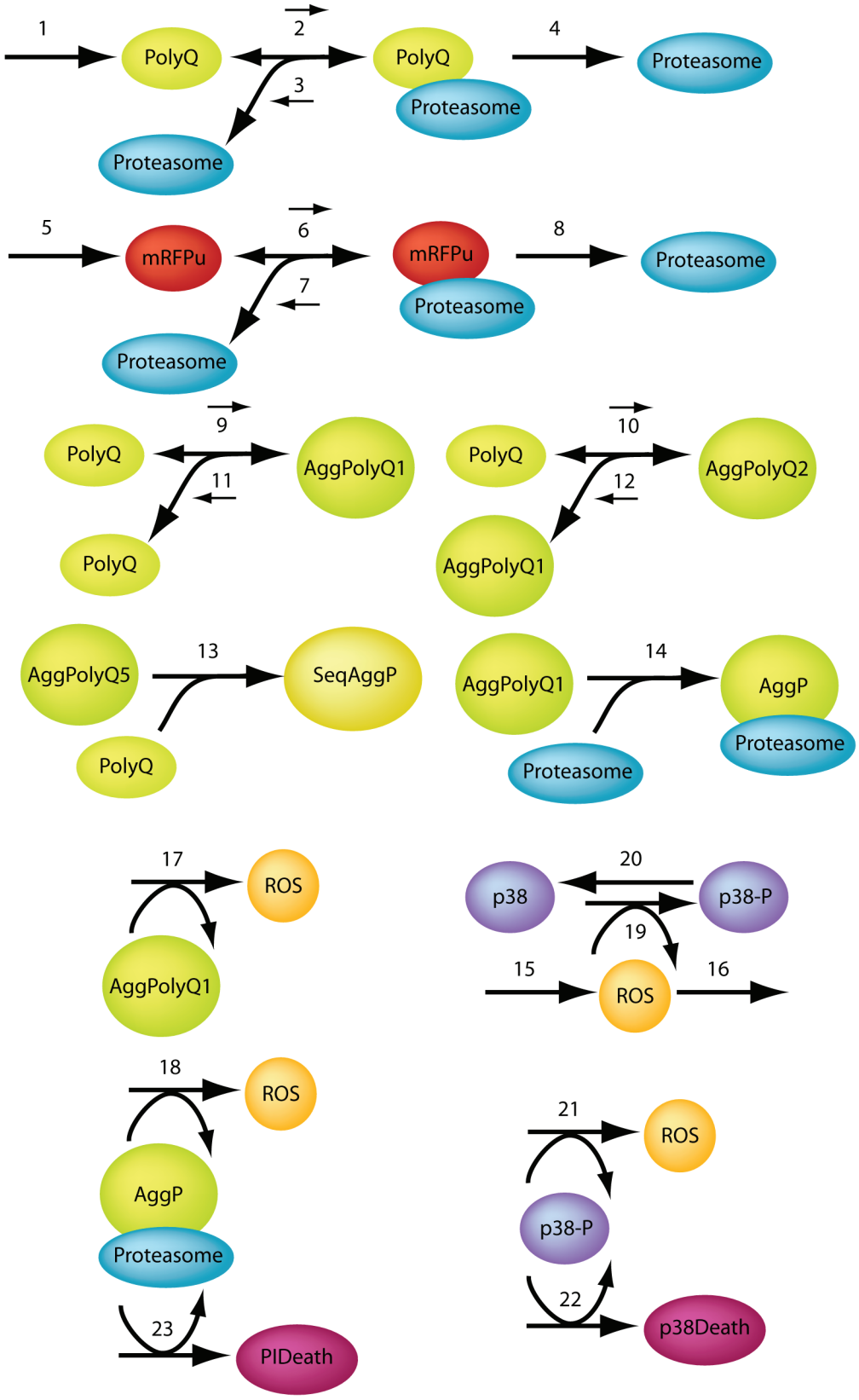
1
PolyQ
2
PolyQ
3
Proteasome
Proteasome
4
Proteasome
5
mRFPu
6
mRFPu
7
Proteasome
Proteasome
8
Proteasome
9
PolyQ
AggPolyQ1
11
PolyQ
10
PolyQ
AggPolyQ2
12
AggPolyQ1
AggPolyQ5
13
SeqAggP
PolyQ
AggPolyQ1
14
AggP
Proteasome
Proteasome
17
ROS
AggPolyQ1
p38
20
p38-P
19
15
ROS
16
18
ROS
AggP
Proteasome
23
PIDeath
21
ROS
p38-P
22
p38Death

Figure 32. A network diagram of the molecular relationships simulated in the stochastic computer model

A schematic representation of the stochastic computer model designed and simulated by Carole Proctor at the University of Newcastle. This model was constructed using the Systems Biology Markup Language (described in the Material and Methods). The molecular species and its interactions between them are shown. The model assumptions are described in the Appendix 1, along with a list of molecular species (Appendix 1 Table 2) and reaction parameters (Appendix 1 Table 3).

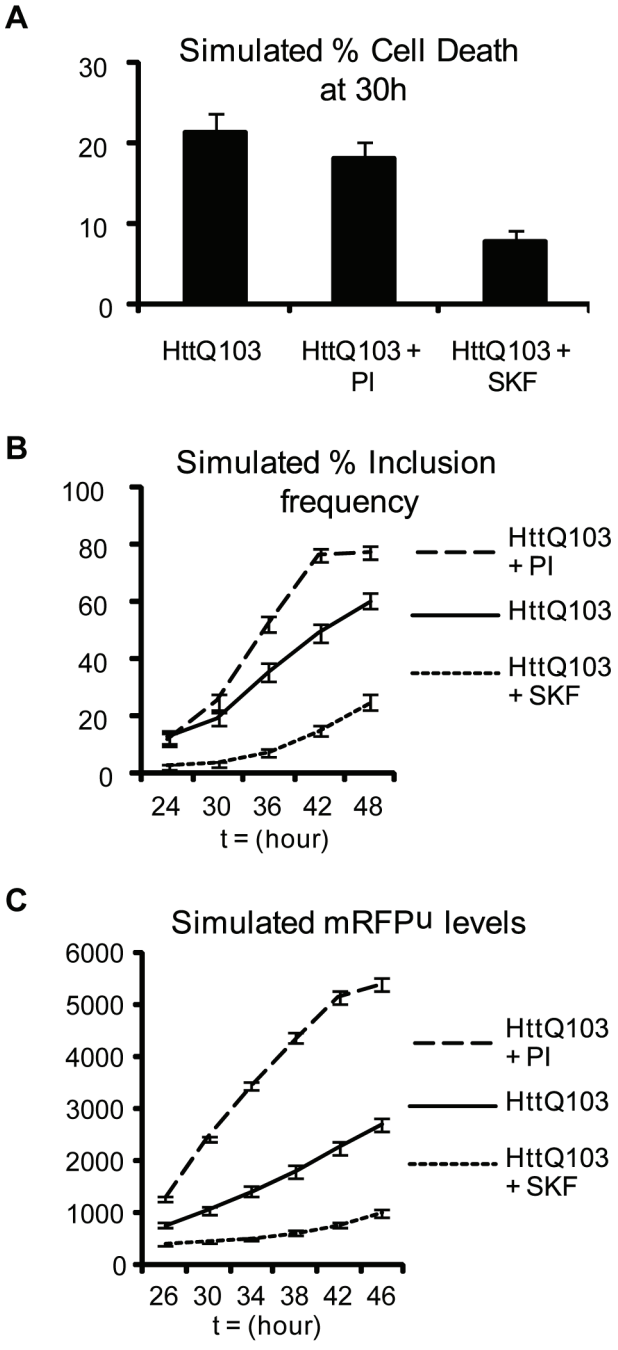
A
Simulated % Cell Death at 30h
30
20
10
0
HttQ103
HttQ103 + PI
HttQ103 + SKF
B
Simulated % Inclusion frequency
100
80
60
40
20
0
24 30 36 42 48
t = (hour)
HttQ103 + PI
HttQ103
HttQ103 + SKF
C
Simulated mRFPu levels
6000
5000
4000
3000
2000
1000
0
26 30 34 38 42 46
t = (hour)
HttQ103 + PI
HttQ103
HttQ103 + SKF

Figure 33. Simulations generated by a stochastic computer model of polyglutamine-expressing cells

Simulations results from a stochastic computer model of HttQ103-expressing cells treated with proteasome inhibitor (PI), p38MAPK inhibitor (SKF), or no treatment are in close agreement with the experimental data. A) Computer model predictions for percent cell death at 30 hours in 300 simulations of each computer experiment. Treatment with proteasome inhibitor (PI) was predicted to have slightly fewer cell death events, while the p38MAPK inhibitor was predicted to have the least cell death events in comparison to untreated cells. B) Computer model predictions for kinetics of inclusion body formation at each time point from 300 simulations for each computer experiment. The number of inclusion bodies was predicted to be greatest with PI treatment in comparison with untreated cells, while p38MAPK inhibition was predicted to have the fewest number of inclusion body formed. C) Computer model predictions for accumulation of $mRFP^{u}$. The mean level of $mRFP^{u}$ for 300 simulations of each computer experiment was calculated for each of the time points shown. The model predicts a rapid rise in $mRFP^{u}$ levels with PI treatment compared to untreated cells. The inhibition of p38MAPK was predicted to have low levels of $mRFP^{u}$ and remained low throughout the simulation. The y-axis shows the number of molecules predicted by the simulations. Error bars for the model predictions represents standard error of the mean.

increase in inclusion body formation (Figure 33B). However, this is contrary to the experimental data indicating increased cell death with PI treatment (shown in Figure 16), suggesting the effects of proteasome inhibition may be more complex than is currently accounted for in the model. In agreement with experimental results, the computer model predicted an increase in $mRFP^u$ levels with PI treatment (Figure 33C). The model also correctly predicts that inhibition of p38MAPK activity should lead to a much lower cell death (Figure 33A) and a decrease in inclusion body formation (Figure 33B) compared to untreated cells. In addition, the simulation predicts an increase in inclusion body formation from 36-48 hours in cells treated with SKF (Figure 33B), with a rate of increase similar to untreated cells (note that the lines are parallel for untreated and p38MAPK inhibited activity during this time interval). This increase in inclusion body formation when p38MAPK activity is inhibited is likely the result of ROS generated from the accumulated aggregated protein (parameter #17 and 18, Figure 32). Critically, the computer model predicted a reduced accumulation of $mRFP^u$ in cells with inhibited p38MAPK activity compared to non-treated cells (Figure 33C). Overall the simulations and experimental data are in good agreement, indicating that the model describes the important molecular relationships of the system as portrayed in Figure 32.

3.8.2 p38MAPK-dependent ROS generation is a critical component of the mathematical model

The ability to simulate outcomes of experiments that cannot be performed in the laboratory is an advantage of developing a stochastic computer model. For example, we have identified the generation of ROS from three sources (aggregation of expanded polyglutamine proteins, proteasome inhibition, and p38MAPK activation) as critical components of polyglutamine-induced cytotoxicity. To determine the predicted outcome

should p38MAPK *not* be involved in generating more ROS we removed the reaction for ROS generation via p38MAPK from the model (parameter #21, Figure 32) and repeated the computer simulations (Figure 34). Without p38MAPK-generated ROS, less cell death was predicted under all conditions (Figure 33A compared to Figure 34A). The new simulations also predicted a lower frequency of inclusion body formation in untreated cells with no significant difference in the numbers of inclusion bodies that were predicted at early time points between untreated and cells treated with p38MAPK inhibitor (Figure 33B compared to Figure 34B).

Modifications of the computer model was made by re-fitting the model for HttQ103-expression without treatment and no p38MAPK to ROS feedback loop, using the experimental data for cell death and inclusion body formation (Figure 34C and D). Since the model predicted less cell death and a lower frequency of inclusion body formation than the experimental data (Figure 34A and B compared to Figure 16 and Figure 25, respectively), we increased the parameters for inclusion formation (parameter #13, Figure 32) and cell death by proteasome inhibition and p38MAPK (parameter #22 and #23, Figure 32). We also increased the parameter for ROS generation via p38MAPK (parameter #21, Figure 32) since this had the effect of increasing both the number of cell death and the levels of inclusion bodies (Figure 33A and B compared to Figure 34A and B, respectively). We then ran the model to predict the effects of proteasome inhibition and p38MAPK inhibition. The new model was not able to reproduce the decline in cell death or the lower levels of inclusion bodies when p38MAPK is inhibited (Figure 34C and D compared to Figure 33A and B). Therefore, the new model indicates that a feedback loop from p38MAPK to ROS is likely required to explain the experimental data.

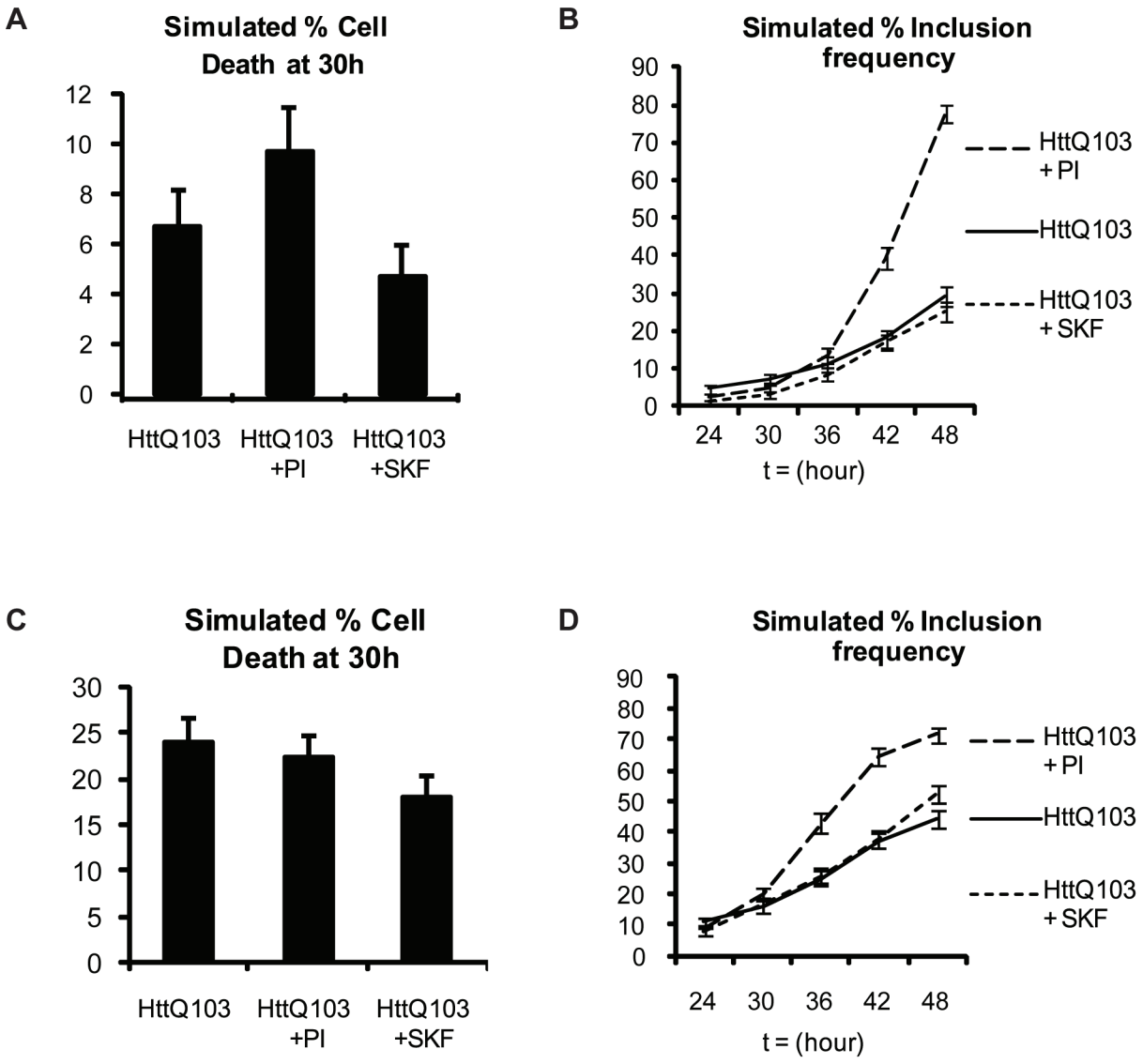
A
Simulated % Cell Death at 30h
12
10
8
6
4
2
0
HttQ103
HttQ103 +PI
HttQ103 +SKF
B
Simulated % Inclusion frequency
90
80
70
60
50
40
30
20
10
0
24
30
36
42
48
t = (hour)
HttQ103 + PI
HttQ103
HttQ103 + SKF
C
Simulated % Cell Death at 30h
30
25
20
15
10
5
0
HttQ103
HttQ103 +PI
HttQ103 +SKF
D
Simulated % Inclusion frequency
90
80
70
60
50
40
30
20
10
0
24
30
36
42
48
t = (hour)
HttQ103 + PI
HttQ103
HttQ103 + SKF

Figure 34. Simulated effects of p38MAPK activation without ROS generation

A and B) New stochastic computer model simulations are no longer in agreement with the experimental data when the reaction for reactive oxygen species (ROS) generation via p38MAPK is removed from the model. A) New computer simulation predicts that cell death will be reduced in all conditions compared to the original computer simulation in which p38MAPK derived-ROS was present (Figure 33, panel A). B) New computer simulations predict no significant differences in the number of inclusion bodies at each time point between untreated polyglutamine-expressing cells and cells treated with the p38MAPK inhibitor (SKF). Similarly, no significant difference is predicted in the number of inclusion bodies at early time points between untreated cells and cells treated with a proteasome inhibitor (PI). At later time points (≥42 hours) more inclusion bodies are predicted for the PI-treated cells due to the accumulation of misfolded protein which cannot be degraded. C and D) Refitting the new stochastic computer model to experimental data of untreated HttQ103-expressing cells does not correctly predict cell death or levels of inclusion body formation in cells treated with the p38MAPK inhibitor. C) New computer model simulations predict more cell deaths but no significant differences between treatments. D) New computer simulations show no significant differences between untreated and treated cells at early time points. At 48 hours, the model predicts a small but significant increase in the number of inclusion bodies for cells treated with the p38MAPK inhibitor compared to untreated cells, indicating that the model no longer fits the experimental data. The error bars represent the standard error of the percentage given by $\sqrt{p(100-p)/n}$ where n is the number of simulation runs (n=300) and p is the percentage of cells.

CHAPTER 4: DISCUSSION

4.1 The cytotoxicity of expanded polyglutamine proteins is mediated by p38MAPK

4.1.1 Elevated ROS levels triggers the activation of stress-activated kinases

Elucidating the molecular mechanism of neurodegenerative diseases has proven to be extremely challenging. Although neurodegenerative diseases share many common features, the pathogenesis of most, if not all, remains a mystery. The inability to distinguish between primary and secondary events observed in disease progression makes it difficult to ascribe cause-and-effect relationships. In the attempt to gain insight relating to the molecular mechanisms of neurodegeneration we sought to identify critical components associated with polyglutamine-induced cytotoxicity.

Alterations in energy metabolism or mitochondrial function has been previously been reported in polyglutamine disorders (Grunewald and Beal, 1999). For example, the expression of mutant huntingtin causes excitotoxicity and damage to the mitochondria, leading to the increase generation of destructive oxygen free radicals and a compromise in energy production (Beal, 2005). Wild-type and expanded huntingtin fragments have been shown to localize to the outer membrane of the mitochondria and disrupt the mitochondrial fusion-fission machinery (Wang 2009), which results in an increase of ROS (Firdaus et al., 2006a; Quintanilla and Johnson, 2009). Not surprisingly, an increase in oxidative stress markers, including 8OHdG, lipid peroxidation, nitrotyrosine, and DNA damage have been reported in human (Browne et al., 1999; Hersch et al., 2006) and animal models (Tabrizi et al., 2000; Bogdanov et al., 2001) of polyglutamine disorders. In addition to being toxic to the cell, ROS can act as a second messenger in the intracellular signal transduction pathways to mediate cellular responses including apoptosis (Matsuzawa and Ichijo, 2008). We

showed that the expression of expanded polyglutamine proteins result in the elevation of ROS levels (Figure 8) and the activation of the stress-inducible kinase p38MAPK (Figure 9). Using expression constructs encoding an expanded polyglutamine tract appended to exon 1 of the huntingtin or full-length ataxin-1 proteins, we showed that the activation of the p38MAPK pathway is a critical component of neurodegeneration. Activated p38MAPK was found to be upregulated in cultured mammalian cells of different origins (glioblastomas, fibroblasts, and cells of neuronal lineage) (Figure 12) and in the cerebellar Purkinje neurons of a SCA-1 mouse model of neurodegeneration (Figure 15). These observations are consistent with other reports of p38MAPK activation in neurodegenerative diseases, including PD (Hunot et al., 2004; Cha et al., 2005), ALS (Raoul et al., 2002; Dewil et al., 2007), AD (Zhu et al., 2000; Zhu et al., 2001; Sun et al., 2003), and other polyglutamine disorders (Nishitoh et al., 2002), suggesting stress-inducible kinases may be a common mechanism of pathogenicity that modulates neurodegenerative disease. ASK1 (apoptosis signal-regulating kinase 1) is a MAP3K which is directly upstream of the p38MAPK pathway and has been reported to mediate apoptotic death associated with Aβ toxicity (Behl et al., 1994; Hensley et al., 1994) as well as polyglutamine-induced toxicity (Cho et al., 2009). Although we did not investigate the status of ASK1 in our system, it is likely the activation of p38MAPK is mediated through ASK1. The activation of the p38MAPK pathway has previously been shown to induce apoptosis of neurons in cell culture (Gunn-Moore and Tavare, 1998; Namgung and Xia, 2001; Yeste-Velasco et al., 2009). Specifically, p38MAPK activates the transcription factor p53 resulting in the upregulation of the pro-apoptotic protein Bax (Hsu et al., 2007). The enhanced phosphorylation and transcriptional activity of p53 has recently been shown to cause mitochondrial-mediated

apoptosis in a neuronal cell culture model of SCA-3 (Chou et al., 2011). The binding activity of p53 to Bax was found to be significantly enhanced in cultured cerebellar neurons expressing expanded ataxin-3, resulting in the increase of PUMA (p53 upregulated modulator of apoptosis), while the intraperitoneal administration of a p53 inhibitor rescued neuronal death in the pontine nuclei of SCA-3 transgenic mice (Chou et al., 2011). In addition, evidence of apoptotic neurons has been reported in the brains of a mouse (Zhang et al., 2008) and swine models of HD (Yang et al., 2010). Taken together, these data suggests that the mitochondrial apoptotic cascade activated in neurodegenerative diseases is mediated by the p38MAPK pathway. Therefore, it is conceivable that the amelioration of cell survival by pharmacological or genetic inhibition of p38MAPK, which we observed in our cell culture model of expanded polyglutamine proteins, is a direct result of suppressing apoptosis.

The JNK pathway is also activated by various types of oxidative stress and has been associated with the activation of apoptosis (Xia et al., 1995; Zhou et al., 1995). The JNK pathway has previously been shown to mediate cell death in cell culture models of HD (Apostol et al., 2006) and AD (Tare et al., 2011) suggesting a role for JNK in neurodegenerative diseases. The treatment with pharmacological inhibitors of JNK was recently shown to protect neurons in a mouse model of PD (Chambers et al., 2011) and AD (Braithwaite et al., 2010). However, the targeted deletion of *JNK3* did not attenuate cell death in the mitochondrial toxin 3-nitropropionic acid (3-NP)-induced mouse model of HD (Junyent et al., 2011). Although the activation of JNK3 was previously found to play an important role in HD pathogenesis (Garcia et al., 2002), *JNK3* null mice did not confer neuroprotection in comparison to wild-type mice. This suggests that the JNK pathway is not

the primary mechanism of neuronal death induced by 3-NP treatment (Junyent et al., 2011). Although we cannot officially rule out the effects of JNK in our studies, our data favours the activation of the p38MAPK as the primary cause of cell death in HD.

The activation of ERK has been proposed to oppose the functions of the JNK/p38MAPK pathway by promoting cell survival pathways (Xia et al., 1995). Although the ERK pathway is most commonly linked to the regulation of cell proliferation, ERK-mediated survival signals were shown to promote the survival of polyglutamine-expressing PC12 cells (Apostol et al., 2006). In addition, the ERK pathway has been shown to protect against oxidative stress-mediated by upregulating cell superoxide dismutase in cell culture models of ageing (Yan et al., 2007). However, there is evidence that the activation of ERK-mediated signalling compromise neuronal viability (Cheung and Slack, 2004; Subramaniam et al., 2004; Subramaniam and Unsicker, 2006). We have previously shown in our polyglutamine cell culture model that there was an absence of the induction of the ERK pathway, while the inhibition of p38MAPK was found to be sufficient to block cell death regardless of the presence or absence of activated ERK (Tsirigotis et al., 2008). This suggests that it may be sufficient to block p38MAPK signalling to promote the survival of neurons in neurodegenerative diseases. It is likely that the total balance between the magnitude and/or duration of p38MAPK, JNK, or ERK activation plays a critical role in determining the fate of neurodegenerative diseases (Matsuzawa and Ichijo, 2001; Subramaniam and Unsicker, 2010). Our data suggests that the sustained activation of p38MAPK is a critical component of polyglutamine-induced cytotoxicity.

4.1.2 The activation of p38MAPK contributes to ROS production

The protective features of p38MAPK inhibition may also be attributed to a decrease in oxidative stress. HSP27 is a regulator of intracellular redox state (Preville et al., 1999; Arrigo, 2001). It is phosphorylated by MAPKAPK2 and MAPKAPK3 kinases, which are directly downstream of p38MAPK (Stokoe et al., 1992). HSP27 has been shown to protect against oxidative stress by maintaining glutathione in its reduced form (Arrigo et al., 2005) and decreasing the uptake of iron (Arrigo et al., 2005; Chen et al., 2006). Interestingly, the protective effects of HSP27 is regulated by its phosphorylation status (Mehlen et al., 1997; Rogalla et al., 1999). In its non-phosphorylated state, HSP27 forms large oligomers that protect cells from oxidative stress by binding to cytochrome c and inhibiting the formation of the apoptosome (Bruey et al., 2000; Paul et al., 2002). We showed that the pharmacological or genetic inhibition of p38MAPK significantly decreases the phosphorylation state of HSP27 (Figure 10 and 11). Conversely, the expression of p38MAPK (either by the enhanced expression of p38MAPK isoforms or HttQ103) was found to increase HSP27 phosphorylation, which correlated with a decrease in reduced GSH levels. It was previously reported that the treatment with N-acetylcysteine (NAC) or glutathione-ethylester significantly reduced ROS levels, which corresponded to the reduction in cell death of polyglutamine-expressing cells (Wyttenbach et al., 2002). Consistent with its ability to modulate oxidative stress, the enhanced expression of HSP27 was found to reduce the toxicity associated with polyglutamine-expressing cells via a mechanism involving the reduction of ROS levels (Wyttenbach et al., 2002), although the rescue of cell death was not accompanied by a reduction of inclusion bodies (Chai et al., 1999; Jana et al., 2000; Wyttenbach et al., 2002). In contrast, we showed that the inhibition of p38MAPK in cells expressing expanded polyglutamine proteins not only increased cell

survival (Figure 7), but also decreased ROS levels (Figure 8) and the frequency of inclusion body formation (Figure 25). Furthermore, the genetic enhancement of p38MAPK expression was found to decrease levels of GSH (Figure 29). Taken together, the data suggests that p38MAPK activation contributes to the production of ROS in cells expressing polyglutamine proteins. The inhibition of p38MAPK can therefore modulate ROS production by significantly decreasing the phosphorylation state of HSP27.

4.1.3 The influence of p38MAPK activation on transcription

The dysregulation of transcription has previously been reported in several polyglutamine disorders (Cha, 2000; Sugars et al., 2004b). The loss of transcriptional control in several mouse models of polyglutamine diseases was evident prior to the overt appearance of pathology (Lin et al., 2000; Luthi-Carter et al., 2002; Yoo et al., 2003). The nuclear localization of expanded huntingtin (Saudou et al., 1998) or ataxin-1 (Klement et al., 1998) was found to be critical for pathogenesis and it is conceivable that the nuclear localization of expanded polyglutamine proteins interferes with transcription factors leading to cellular toxicity. Expanded polyglutamine proteins have the ability to bind and sequester transcriptional activators, such as p300/CBP (CREB-binding protein) (Everett and Wood, 2004; Cong et al., 2005; Tsuda et al., 2005), and this loss was shown to reduce the expression of a set of target genes involving neuronal homeostasis (Nucifora et al., 2001; Chiang et al., 2005). Interestingly, p300 is degraded by the proteasome in response to p38MAPK activation (Poizat et al., 2005). In addition, the partial inhibition of proteolysis was shown to delay the loss of p300/CBP in a mouse model of SCA-1, which correlated with behavioural and morphological improvements (Tsirigotis et al., 2006). We showed that the activation of p38MAPK occurs at 3 months of age in the mouse model of SCA-1 (Figure 14), a time point which correlates well with the onset of behavioural and anatomical

anomalies (Orr, 2000). It is possible that the accelerated degradation of p300/CBP caused by p38MAPK activation contributes to the disruption of transcriptional control and neuronal homeostasis. p300/CBP are histone acetyltransferases (HATs) and their activities are in opposition to histone deacetylases (HDACs). The loss of HAT activity is predicted to be restored by the inhibition of HDACs. Indeed, the administration of pharmacological agents targeting HDACs was shown to delay disease progression in the fly (Steffan et al., 2001; Ghosh and Feany, 2004) and mouse models of polyglutamine diseases (Ferrante et al., 2003; Hockly et al., 2003). Taken together, the pharmacological blockade of p38MAPK may influence the activity of p300/CBP in polyglutamine disorders. Thus, HATs such as p300/CBP may be promising downstream targets of p38MAPK and deserve to be investigated further.

4.2 Proteasome inhibition is associated with the expression of polyglutamine proteins

The use of fluorescent-tagged proteins to study cellular processes in living systems by fluorescence microscopy is well established and has been an important tool for the study of protein localization and aggregation (reviewed in (Zhang et al., 2002a)). They have frequently been used to study the cytotoxic effects of expanded polyglutamine proteins in cell culture models (Bence et al., 2001; Arrasate et al., 2004; Bennett et al., 2005). We have developed an imaging platform to simultaneously follow the expression of an expanded polyglutamine protein and proteasome function using fluorescent reporter systems. The objective was to study the temporal relationship between inclusion body formation, proteasome inhibition, and cell death in HttQ103-expressing cells.

There is sufficient evidence of protein aggregation in neurodegenerative diseases to suggest that disease proteins negatively impact the efficiency of the UPS (Spillantini et al., 1998; Everett and Wood, 2004; Goedert and Spillantini, 2006). Numerous studies have reported proteasome inhibition in many neurodegenerative diseases, including AD, PD, and HD (Keller et al., 2000; McNaught et al., 2001; Bennett et al., 2005). However, there has been considerable effort made to understand how the expression of a disease associated protein causes UPS dysfunction. Substrates targeted for degradation by the UPS are unfolded before they can pass through the narrow opening of the catalytic core of proteasome (Hershko and Ciechanover, 1998). It has previously been shown that if the substrate is blocked from entering the central pore, it remains bound to the proteasome, thereby preventing other substrates from being unfolded and degraded (Navon and Goldberg, 2001). If expanded polyglutamine proteins are resistant to degradation by the proteasome, it is conceivable they will sequester and physically block the proteasome complex preventing the entrance of further substrates into the catalytic core of the proteasome. Consistent with this view, it has been reported that polyglutamine proteins are inefficiently degraded and sequestered irreversibly within aggregates (Holmberg et al., 2004) or are capable of inhibiting the 26S proteasome (Diaz-Hernandez et al., 2006). In addition, Venkatraman et al. have shown that proteasomes are incapable of digesting polyglutamine chains greater than 25 residues in length, and the failure to release the polyglutamine chain can result in the loss of proteasome function (Venkatraman et al., 2004). Thus, the presence of expanded polyglutamine proteins is thought to interfere with UPS function by sequestering or directly clogging the proteasome. However, there is growing evidence that this model of "proteasome choking" is incorrect. Synthetic

polyglutamine proteins consisting of EGFP (enhanced green fluorescent proteins) fusion proteins containing non-pathological or expanded polyglutamine tracts were found to be efficiently degraded by the 26S proteasome with no difference in the rate of degradation of either synthetic polyglutamine proteins (Michalik and Van Broeckhoven, 2004). In addition, soluble oligomeric polyglutamine aggregates or highly aggregated fibrillar species did not inhibit the proteasome in an *in vitro* proteasome activity assay, even in excessive molar quantities relative to proteasomes (Bennett et al., 2005). These data suggests that soluble expanded polyglutamine proteins are readily unfolded and efficiently degraded by the proteasome, and the activity of the proteasome is unaffected by the presence of aggregated or fibrillar species of expanded polyglutamine proteins. Critically, Bennett et al. demonstrated that the localization of expanded polyglutamine proteins to either the cytoplasm or the nucleus resulted in severe UPS dysfunction in both compartments and is independent of the sequestration of protein aggregates into inclusion bodies (Bennett et al., 2005). In addition, they reasoned that, although proteasomes and components of the UPS are localized to the inclusion bodies, only a minor fraction of the proteasomes are actually depleted from nuclear or cytoplasmic pools (Bennett et al., 2005). For these reasons, it is unlikely that the dysfunction of the UPS is caused by the direct sequestration or choking of proteasomes. Instead, protein aggregates may cause UPS dysfunction indirectly by influencing the activity or distribution of UPS modulators. For example, the depletion of free ubiquitin pools (Ryu et al., 2008) or the activation of caspases (Sun et al., 2004) (resulting in irreversible inhibition of proteasomes during apoptosis) may contribute to the decreased the efficiency of the UPS. Consistent with the idea that inclusion body formation is not required for UPS impairment, we found that the expression of polyglutamine proteins

caused a gradual inhibition of the UPS and once this inhibition reached a threshold level, an inclusion body began to form (Figure 20). Treatment with proteasome inhibitor increased the timing of inclusion body formation suggesting that UPS impairment triggers inclusion body formation. However, the direct mechanism in which expanded polyglutamine proteins affect the UPS prior to inclusion body formation is presently unclear. We showed that the sequestration of diffuse HttQ103 species into an inclusion body coincided with a partial and temporary recovery of the UPS, which is consistent with previously published findings in primary neuron cultures (Arrasate et al., 2004). Furthermore, it has previously been shown that small intermediate forms of aggregates (and not fibrillar forms) are more toxic to cells (Bucciantini et al., 2002) and it is possible that intermediate forms of aggregates can negatively impact the UPS. Taken together, our data support a protective role for inclusion body formation (at least in the short term; the longer term effects of inclusion bodies were not assessed in our cell culture system).

4.3 Elevated ROS levels is associated with the expression of polyglutamine proteins

The expression of expanded polyglutamine proteins can disrupt the membrane of the mitochondria and contribute to oxidative stress (Quintanilla and Johnson, 2009). For example, expanded huntingtin protein has been shown to be localized to the outer mitochondrial membrane and was found to affect the opening of the mitochondrial permeability transition pore (Choo et al., 2004). Although the precise mechanism in which expanded huntingtin proteins disrupts mitochondrial function is unclear, mitochondrial energy metabolism deficits are strongly correlated with the length of the polyglutamine tract in the huntingtin protein (Seong et al., 2005). Functional neuroimaging studies have

revealed evidence of impaired energy metabolism in the brains of HD patients by magnetic resonance spectroscopy (MRS) imaging (Jenkins et al., 1993; Garseth et al., 2000). In addition, a significant decrease in the activities of several mitochondrial complexes have been reported (Gu et al., 1996; Browne et al., 1999). It has become clear that mitochondrial and energetic deficits are major components of HD pathogenesis and it is conceivable that mitochondrial alterations cause an increase in ROS levels (reviewed in (Browne, 2008)). Since the primary source of ROS in the neuron is mitochondrial, mitochondrial dysfunction is likely to impact the functionality of the UPS. Therefore, we cannot exclude the possibility that the dysfunction of the UPS observed in our experiments may be the result of elevated levels of ROS. Oxidized proteins as well as cross-linked proteins and lipids can directly inhibit the proteasome (Terman and Brunk, 2004) and the proteasome is itself an important regulator of oxidative damage in neurons (Ding et al., 2006). Proteasome inhibition has been shown to induce oxidative protein modifications in addition to increasing oxidative stress levels and mitochondrial dysfunction (Demasi and Davies, 2003; Ding et al., 2006). An increase in oxidative stress would therefore result in further oxidative damage to proteins that the proteasome is responsible for removing. This is predicted to cause an accumulation of oxidatively damaged proteins, which would exacerbate the burden on the proteasome and create a cycle of ROS production.

4.4 Experimental and stochastic computer modeling supports a vicious cycle of polyglutamine-induced cytotoxicity

Using pharmacological agents that target specific components of the UPS and MAPK signalling pathways, it was found that the expression of expanded polyglutamine proteins activates p38MAPK, which contributes to the progression of inclusion body formation,

proteasome inhibition, and production of ROS. The experimental data in conjunction with a stochastic computer model supports a vicious cycle of polyglutamine cytotoxicity. The proposed model in Figure 35 suggests that the initial event that triggers the vicious cycle of expanded polyglutamine cytotoxicity is the inhibition of the proteasome by small aggregates of misfolded proteins, resulting in the increase of oxidative stress within the cell. Increased ROS levels can oxidized proteins and can result in the inhibition of the proteasome (reviewed in (Ding et al., 2006)). Elevated ROS levels can also trigger the activation of kinases in signalling pathways, including ASK1, MKK3, and MKK6 that are directly upstream of the stress-activated kinase p38MAPK (Nishitoh et al., 2002; Ho et al., 2005; Fernandes et al., 2009). For example, we found evidence of p38MAPK activation in both *in vitro* cell culture models and in an *in vivo* model of polyglutamine disease, which may be further exacerbated by promoting downstream ROS production. By damaging other cellular proteins, the ROS would provide an additional burden to the UPS, which is responsible for the proteolytic degradation of damaged or abnormal proteins. Increased proteasome inhibition would lead to further accumulation of misfolded proteins, ultimately coalescing into inclusion bodies. The sequestration of misfolded or intermediate species of HttQ103 that are thought to be most inhibitory to the proteasome may temporarily alleviate proteasome inhibition, at least in the short term. However, inclusion bodies have been reported to concentrate iron and promote the generation of ROS (Firdaus et al., 2006b). An increase in the levels of iron and ferritin has also been reported in the brain during the course of HD (Simmons et al., 2007). Electron microscope studies have also shown that inclusion bodies are the centers of oxidative events and the purification of inclusion bodies revealed high levels of oxidized proteins (Firdaus et al., 2006b). ROS generated from

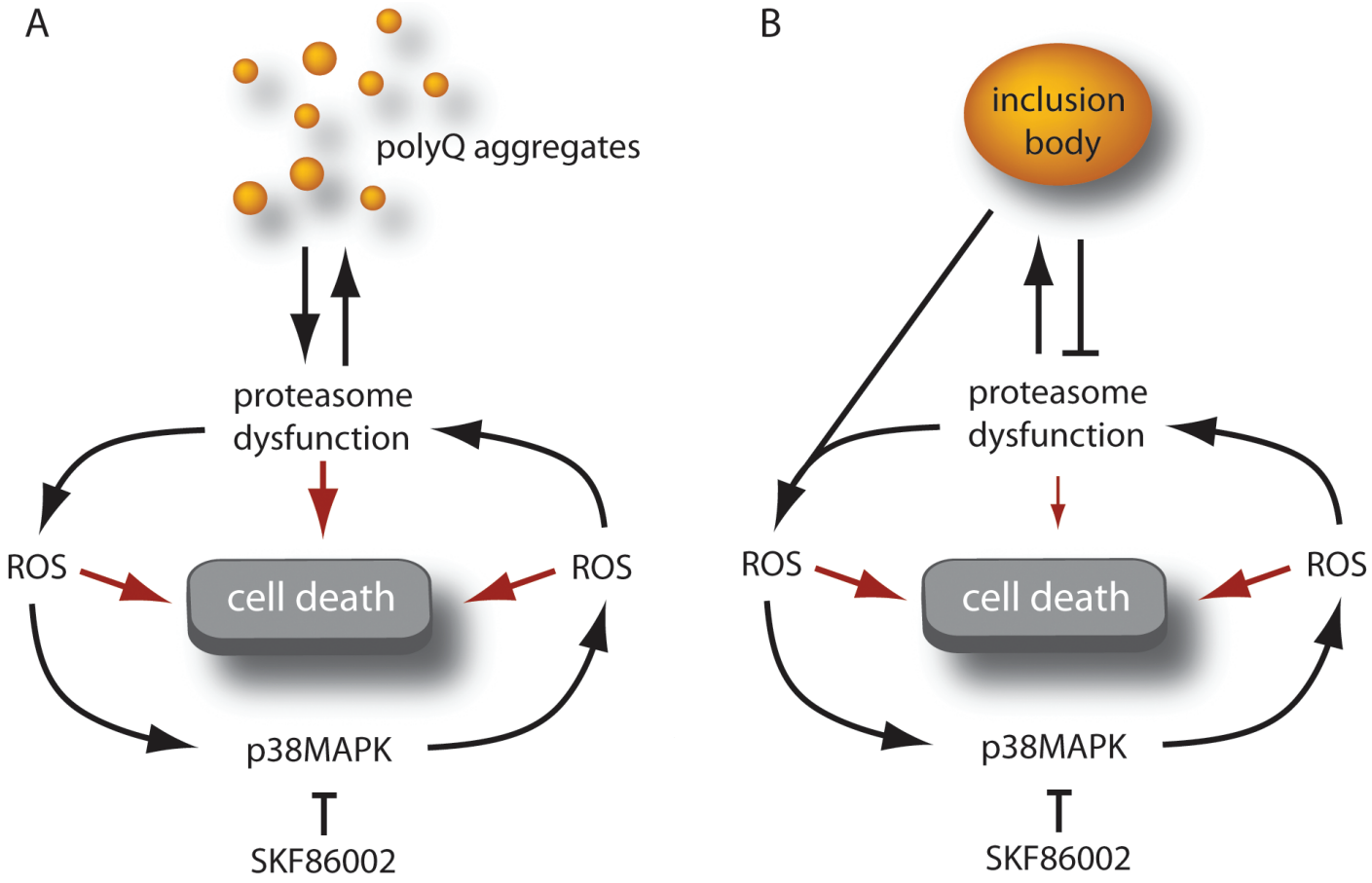
A
polyQ aggregates
proteasome
dysfunction
ROS
cell death
ROS
p38MAPK
SKF86002
B
inclusion
body
proteasome
dysfunction
ROS
cell death
ROS
p38MAPK
SKF86002

Figure 35. Proposed model of expanded polyglutamine induced cytotoxicity

A) Expression of expanded polyglutamine proteins leads to proteasome inhibition, promoting the generation of reactive oxygen species (ROS). This in turn leads to p38MAPK activation (which can be blocked by treatment of cells with SKF86002) and the further generation of ROS through a mechanism which is likely to involve the mitochondria. An increased burden of oxidatively damaged proteins leads to further proteasome impairment, and yet more ROS generation. B) Proteasome impairment ultimately leads to inclusion body formation, which temporarily reduces ubiquitin-proteasome system dysfunction. Inclusion bodies perpetuate ROS production through concentration of iron, ensuring continued activation of p38MAPK. Pharmacological inhibitors of p38MAPK such as SKF86002 can preclude the initiation of the vicious cycle or potentially interrupt it at a later stage.

inclusion bodies would ensure yet more damage and conditions that will sustain p38MAPK activation. Whether or not there is self-amplification of the vicious cycle as a consequence of increasing ROS production, we postulate that it is sustained p38MAPK activity and proteasome inhibition that will ultimately lead to cell death.

4.5 Mathematical model supports the vicious cycle model

Stochastic mathematical models have previously been used to understand biological systems, including chaperone proteins in their role of ageing (Proctor et al., 2005), maintenance of protein homeostasis (Passos et al., 2010; Proctor and Lorimer, 2011), and cellular senescence (Passos et al., 2010). To study the effects of polyglutamine protein cytotoxicity, we used a previously published model of the UPS (Proctor et al., 2007) and extended it to include the turnover and aggregation of polyglutamine proteins. The model predictions were found to be in close agreement with the experimental data, suggesting that we have identified and incorporated the critical components for polyglutamine-induced cytotoxicity in the system (the network diagram is shown in Figure 32). However, some discrepancies between the model predictions and experimental data were found regarding cell death at early time points under conditions of proteasome inhibition. The model predicted less cell death in conditions of proteasome inhibition (Figure 33A). It is possible that the model is exaggerating the protective benefits of inclusion body formation. For example, the model assumes that the level of ROS is dependent on the amount of small aggregates and that the ROS generated by inclusion bodies is less than that of small aggregates. Thus, the removal of small aggregates is likely to be beneficial to the cell as a result of producing less ROS and therefore provide temporary relief to the UPS. However,

inclusion bodies have been shown to bind to heavy metals, such as iron, which can increase oxidative stress and cytotoxicity (Firdaus et al., 2006b). We assumed in the model that small aggregates generated more ROS than inclusion bodies. If we increase the parameters of inclusion body-dependent ROS generation, it is likely that the model would predict more cell death under conditions of proteasome inhibition. Alternatively, there could be a missing element in the model. For example, the turnover of pro-apoptotic proteins, including the transcription factor p53, which may be compromised, could result in greater cell death not predicted in the model. Parameters of p53 and pro-apoptotic proteins have previously been modelled (Proctor and Gray, 2008) and could easily be incorporated into the current model which may correct our predicted cell death outcomes. Asides from this irregularity, the computer model was in close agreement with the experimental data with regards to the percentage of inclusion body formation and proteasome inhibition, suggesting our assertion of critical components involved in polyglutamine-induced cytotoxicity (shown in Figure 32) is correct. An advantage of computer modelling over laboratory experiments is that it is easy to manipulate the system on a computer, whereas the same experiment in the laboratory may be impossible or very costly to perform. For example, although it would be difficult to prove experimentally that ROS generated by p38MAPK is required, the hypothesis could easily be tested in the mathematical model by simply removing the reaction of p38MAPK-dependent ROS generation and repeating the simulations. The model confirmed that p38MAPK is involved in generating more ROS because when the feedback loop was broken the model output no longer fitted the experimental data (Figure 34).

The data discussed herein describe a vicious cycle of cell death continually propelled by the generation of ROS. The importance of ROS in protein misfolding disorders is not a

new concept; indeed the cytotoxicity of elevated ROS generated by mutant huntingtin has been convincingly demonstrated by the laboratory of Rubinsztein (Wyttenbach et al., 2002). Intriguingly, the proteasome is itself an important regulator of oxidative damage in neurons and proteasome inhibition is known to induce mitochondrial dysfunction and promote oxidative damage to DNA and protein (reviewed in (Ding et al., 2006)). Once some threshold of polyglutamine-mediated proteasome inhibition is reached, it seems entirely plausible that a self-perpetuating loop of ROS generation and p38MAPK activation could lock the cell into a dysfunctional state. Indeed, a directly analogous positive feedback loop involving ROS and p38MAPK activation was recently proposed for the induction of senescence in mammalian cells. By combining bioinformatics, stochastic computer modeling, and direct experimental interventions, Passos et al. have provided convincing evidence that sustained activation of p38MAPK is required for the generation of mitochondrial ROS, which by generating DNA damage ensures the continued activation of p38MAPK in senescent cells (Passos et al., 2010). The ROS generated as a consequence of proteasome inhibition also appears to be of mitochondrial origin (Sullivan et al., 2004), so the cascade of events in cells expressing misfolded protein may be very similar to that in cells in which the initiating event is exposure to ionizing radiation (as was the case in the Passos paper). If a similar loop were operating in cells expressing expanded polyglutamine proteins, one might expect to find ROS-mediated DNA damage leading to activation of ATM (ataxia telangiectasia mutated) and phosphorylation of histone H2AX, as has indeed been documented in cells from Huntington's disease and SCA-2 patients (Giuliano et al., 2003). The activation of ATM and the formation of H2AX repair foci appears to precede the formation of inclusion body (Illuzzi et al., 2009), but may be coincident with p38MAPK

activation and the generation of ROS. If our model is correct, treatment of cells with the p38MAPK inhibitor should reduce the number of H2AX foci in cells expressing HttQ103.

4.6 The role of inclusion bodies in polyglutamine disorders

4.6.1 Inclusion bodies and neuronal survival

The significance of inclusion bodies in the pathogenesis of polyglutamine disorders is highly contested. Considerable effort has been made to determine if inclusion bodies are pathogenic, protective, or merely an incidental entity. The formation of an inclusion body may be an adaptive survival mechanism. It was previously shown that cultured neurons that form inclusion bodies live longer than those that do not (Arrasate et al., 2004). Our data is consistent with the literature, which suggests that the partial improvement of proteasome function coinciding with the formation of an inclusion body may be partially responsible for prolonged survival (Figure 20) (Arrasate et al., 2004; Mitra et al., 2009). We also showed that the formation of inclusion bodies reduces the expression of HttQ103 to very low or undetectable levels. The formation of an inclusion body may be a coping mechanism to mitigate the cytotoxic conformations of expanded polyglutamine proteins. In addition to improving proteasome function, inclusion body formation may be limiting the cytotoxicity associated with HttQ103 expression, including its role in the loss of transcriptional control by binding to transcription factors (Schaffar et al., 2004) or in the increase of ROS caused by the disruption of mitochondrial function (Wang et al., 2009a; Song et al., 2011). Recently, a comprehensive single-cell analysis showed that the concentration of HttQ103 prior to the formation of an inclusion body has a diminished impact on its instantaneous risk of cell death (Miller et al., 2010). It has been suggested that the formation of an inclusion

body is an adaptive response that represents a new "cellular epoch" for neuronal survival (Miller et al., 2010) and this phenomenon may explain the protective effects of inclusion bodies reported elsewhere (Taylor et al., 2003; Arrasate et al., 2004; Bodner et al., 2006; Gong et al., 2008).

Although the formation of inclusion bodies may provide a short term protective mechanism (through improved proteasome function or the sequestration of diffuse forms of mutant polyglutamine peptides), the longer term implications of inclusion bodies in neurodegenerative diseases must be considered. For example, the size of an inclusion body can be very large such that it can fill the entire axonal cross-sectional diameter of a neuron (Li et al., 2003). Inclusion bodies can physically block neuronal processes, including vesicular transport and mitochondrial mobility, resulting in the impairment of mitochondrial transport and the accumulation of mitochondria adjacent to the inclusion body (Trushina et al., 2004; Chang et al., 2006). Therefore, the long term consequence of impaired mitochondrial transport is likely to involve the depletion of available mitochondria resulting in insufficient ATP for cellular processes, mitochondrial dysfunction, increased production of ROS, and induction of apoptosis (Chang et al., 2006). This would be yet another source of ROS to further the vicious cycle of cell death described in Figure 35.

Several components of the proteasome, including regulatory and catalytic subunits as well as ubiquitin conjugation enzymes, has also been reported to be sequestered in inclusion bodies (Jana et al., 2001) resulting in the impairment of the UPS (Bence et al., 2001). A transient alleviation by inclusion bodies of the polyglutamine-mediated proteasome burden was recently demonstrated *in vivo* in an inducible model of HD (Ortega et al., 2010), but no long term impairment of proteasome function was observed in the brains of these mice. If

the inclusion bodies concentrates iron and promotes ROS generation through Fenton chemistry (Firdaus et al., 2006b), the inclusion bodies, once formed, might ensure the perpetuation of the vicious cycle proposed in Figure 35. The failure to detect this effect in older mice expressing a polyglutamine protein may relate to the inability of the reporter system to detect less than a 40% decrease in proteasome inhibition (Ortega et al., 2010) or may relate to differences between the mouse model and the human disease.

In human polyglutamine disorders, the disease may progress over years if not decades, and the later consequences of inclusion body formation might therefore be more severe. Clinical evidence supports a deleterious role for inclusion bodies in human disease. Neurons with inclusion bodies appear much more compromised than those without, although it is difficult to distinguish between neuronal dysfunction and neuronal death (Woulfe, 2007). In addition, inclusion bodies have been shown to sequester transcription factors, chaperone proteins, and other nuclear factors which may contribute to the transcriptional dysregulation reported in neurodegenerative diseases (Cummings et al., 1998; Nucifora et al., 2001). In polyglutamine repeat diseases such as HD, frontotemporal lobar degeneration, and RNA-mediated diseases such as myotonic dystrophy, inclusion-mediated titration of transcription factors (like CBP), tar DNA-binding protein 43 (TDP-43), and RNA splicing factors (for example muscleblind), respectively, may represent an important molecular mechanism of disease (Woulfe, 2007). Added to these effects would be the deleterious effects we ascribe to the ROS-mediated vicious cycle.

The cytotoxicity associated with inclusion bodies is not a polyglutamine-specific process. Expansion of a polyalanine tract has also been reported to form inclusion bodies which is associated with cell death (Fan et al., 2001) . For example, oculopharyngeal

muscular dystrophy (OPMD) is a late-onset neuromuscular disorder that belongs to a family of nine polyalanine disorders that is characterized by progressive eyelid ptosis, swallowing difficulties, and proximal limb muscle weakness (Brais et al., 1998; Brown and Brown, 2004). OPMD is caused by an abnormal expansion of the polyglutamine tract within the coding region of the poly(A) binding protein nuclear 1 (PABPN1) (Brais et al., 1998). The histopathological hallmark of OPMD is the presence of nuclear inclusion bodies that are immunoreactive for PABPN1, ubiquitin, nuclear factors, and proteasomal subunits (Becher et al., 2000; Calado et al., 2000), suggesting a similar neurodegenerative mechanism involving the cytotoxicity associated with inclusion bodies found in expanded polyglutamine disorders. In addition, the disruption of inclusion bodies by administrating anti-aggregation drugs was found to attenuate muscle weakness in a mouse model of OPMD (Davies et al., 2006), although there are reports that mutant PABPN1 can cause cytotoxicity through a gain-of-toxic function by sequestering poly(A) mRNA (Brais et al., 1998; Brais et al., 1999; Calado et al., 2000). A more direct evidence for a toxic role of inclusion bodies was demonstrated using a protein chimera composed of GFP fused to an internal fragment of the golgi complex protein (GCP-170) (Fu et al., 2005). This chimera protein was found to be capable of forming inclusion bodies that recruited molecular chaperones and UPS components. In addition, the sequestration of transcription factors including CBP and p53 resulted in the repression of p53 transcriptional activity causing cell death. These data suggests that the toxicity associated with inclusion bodies formed by polyglutamine-independent proteins is analogous to inclusion bodies formed by polyglutamine proteins, and supports a detrimental role for inclusion bodies in neurodegenerative diseases.

4.6.2 The kinetics of inclusion body formation

We observed a greater number of inclusion bodies at an earlier time point for HttQ103-expressing cells treated with proteasome inhibitor (Figure 20), suggesting that the rate of reaction of inclusion body formation is directly dependent on the concentration of HttQ103. This is consistent with the finding that higher expression of an expanded polyglutamine protein leads to earlier inclusion body formation (Arrasate et al., 2004). However, we found no difference in the length of time required to form a mature inclusion body starting from the initial seeding event between HttQ103-expressing cells treated with proteasome inhibitor, SKF86002, and the untreated control (Figure 27). A comprehensive time lapse *in situ* atomic force microscopy study by Legleiter et al. offered detailed mechanistic steps of inclusion body formation. They revealed several distinct conformations of expanded huntingtin monomeric species and that the formation of fibrils is dependent on a major structural transition of oligomeric species. They noted a gradual increase of oligomeric species prior to the formation of fibrils. Once the fibrils were formed, fibril elongation was facilitated by the addition of both oligomeric and monomeric species (Legleiter et al., 2010). It is likely that the initial seeding event seen in our studies corresponds to the major structural transition of oligomeric species into fibrils described in Legleiter et al. Our data suggests that the rate at which oligomeric or monomeric HttQ103 species are sequestered into an inclusion body is independent of proteasome function or p38MAPK activation. However, the rate at which HttQ103 species were sequestered into the inclusion body was found to be slightly higher in BSO-treated cells, although it did not affect the timing of inclusion body formation. This suggests an increasing concentration of oxidized proteins may increase the kinetics of inclusion body formation after the initial seeding event, but does not affect the rate-limiting step of inclusion body formation. Taken

together, the data suggests that the seeding of an inclusion body is the rate-limiting step of inclusion body formation, which is followed by the addition and sequestration of all other HttQ103 species forming a mature inclusion body.

4.7 A role for autophagy in polyglutamine disorders

The data suggests that the expression of expanded polyglutamine proteins negatively impact the UPS and that the targeted removal of soluble and intermediate species of expanded polyglutamine proteins may be an effective way to releave proteasome inhibition and cell toxicity associated with polyglutamine disorders. It is conceivable that enhanced levels of autophagy may also contribute to the protective effects of the p38MAPK inhibitor we have observed. Although the effects may be dependent on cell type, there is evidence that the alpha isoform of p38MAPK inhibits autophagy (Webber and Tooze, 2010) (note that this is the same isoform utilized in our genetic experiments, and may be the target of primary importance to all of the interventions described herein). Low level inhibition of the proteasome is known to promote autophagy (Ding et al., 2003), but as proteasome inhibition increases the activation of p38MAPK may limit autophagic clearance of protein aggregates. Enhancement of autophagy has been proposed as a therapeutic strategy for the treatment of polyglutamine disorders such as HD (Sarkar et al., 2008). In addition, pharmacological blockade of p38MAPK may provide benefits by multiple mechanisms. It may break the vicious cycle of ROS generation while promoting autophagy-mediated clearance of aggregates in cells already compromised for proteasome function.

Although the failure of the UPS has received much attention in neurodegeneration, there is mounting evidence that defective autophagic degradation may also contribute to

pathogenesis (Wong and Cuervo, 2010). It has been suggested that the UPS is initially more efficient at clearing soluble polyglutamine proteins in the brain (Li et al., 2010). However, should the UPS become compromised the cell would rely on the activation of autophagy to remove misfolded proteins (Ravikumar et al., 2002; Ding et al., 2003; Iwata et al., 2005). The failure of the autophagy pathway would lead to a dire situation and leave the neuron with no functional protein clearance mechanism, leaving the formation of an inclusion body its last recourse. Consistent with this idea is the observation that p62, an adaptor protein for autophagic degradation that has been shown to bind to polyubiquitylated protein aggregates (Lamark et al., 2009), was found to be co-localized with inclusion bodies (Pikkarainen et al., 2011). It is conceivable that the enhancement of autophagy would be beneficial and provide a therapeutic treatment strategy for neurodegenerative diseases (Bove et al., 2011). By restoring the cells ability to clear toxic species of HttQ103, it would limit the ability of HttQ103 to exert its toxic effects on transcriptional control (by adverse interactions with transcription factors (Schaffar et al., 2004)) or the mitochondria (resulting a disruption of mitochondrial function ensuring an increase of ROS (Wang et al., 2009a; Song et al., 2011). In addition, since mitochondrial turnover is predominantly mediated by autophagy (Kim et al., 2007b), the enhancement of autophagy would ensure the removal of damaged mitochondria and may pre-empt the excessive production of ROS. Finally, it has previously been shown in inducible mouse models of HD that neurons have the ability to recover and return to normal homeostasis including the recovery of motor co-ordination and the clearance of inclusion bodies (Yamamoto et al., 2000; Martin-Aparicio et al., 2001). Enhancement of autophagy would facilitate the removal of monomeric and aggregated species of polyglutamine proteins and therefore would indirectly lead to the clearance of

inclusion bodies by reversing the reaction equilibrium towards inclusion body formation (Rubinsztein, 2006). The clearance of inclusion bodies would also prevent deleterious effects associated with inclusion bodies including the sequestration of transcription factors (Schaffar et al., 2004), components of the UPS (Waelter et al., 2001), chaperones (Cummings et al., 1998), and sites of ROS generation (Firdaus et al., 2006b). Taken together, it is very likely the enhancement of autophagy would be increase neuron survival by break the vicious cycle of ROS generation described in Figure 35.

The administration of rapamycin to enhanced autophagy has been reported to improve the clearance of protein aggregates and survival in cell culture (Ravikumar et al., 2002; Tsvetkov et al., 2010), fly (Ravikumar et al., 2004; Sarkar et al., 2008; Wang et al., 2009b), and animal (Ravikumar et al., 2004; Rose et al., 2010) models of HD. The idea of increasing autophagy as a therapeutic strategy is not limited to polyglutamine diseases – enhancement of autophagy has been shown to attenuate dopaminergic neuron loss in mouse models of PD (Dehay et al., 2010; Malagelada et al., 2010), as well as decrease intraneuronal accumulation of pathogenic Aβ42 and attenuate tau pathology in mouse models of AD (Spilman et al., 2010; Caccamo et al., 2011). However, strategy may not be beneficial for all neurodegenerative diseases. It was recently reported that the treatment with rapamycin in mouse models of familial ALS resulted in exacerbation of ALS pathology, including greater motor neuron loss, increased accumulation of autophagosomes, and more severe mitochondrial impairment and caspase-3 activation (Gill et al., 2009; Zhang et al., 2011). Although it is unclear why the enhancement of autophagy would accelerate the pathology in ALS, studies in other neurodegeneration models show promising

findings for enhanced autophagy as a potential therapeutic strategy for neurodegenerative diseases.

4.8 Conclusion

The abnormal accumulation of proteins, visible as inclusion bodies, has become a hallmark of polyglutamine disorders. It is believed that their presence plays a central role in cytotoxicity, however, recent efforts to distinguish between primary and secondary events during disease pathogenesis have revealed a beneficial role for inclusion bodies. In this study, it was determined that critical components of expanded polyglutamine-induced cytotoxicity occur prior to the formation of inclusion bodies and that the formation of inclusion bodies is protective. By combining stochastic computer modeling and experimental data, we identified three critical components of expanded polyglutamine-induced cytotoxicity. The data described herein provides evidence of a vicious cycle of cell death involving a self-perpetuating loop of ROS generation, p38MAPK activation, and proteasome inhibition that may lock the cell in a dysfunctional state. It was found that breaking the vicious cycle using p38MAPK inhibitors precludes further damage and proteasome inhibition, which significantly improved cell survival.

The identification of critical components in expanded polyglutamine-induced cytotoxicity may assist in the development of therapies for polyglutamine disorders. Any therapeutic intervention will likely be most beneficial in treating patients before their neurons become locked into a dysfunctional state – the goal would be to extend the number of years prior to the manifestation of symptoms. Since the mechanism of neuronal death involves three critical components, the treatment should reflect this and therefore a

combinatorial therapy may provide the best strategy for delaying the onset of symptoms. Early therapeutic intervention is plausible for genetically transmitted diseases in which there is complete penetrance and reliable genetic testing (disorders like Huntington's disease where inheritance of the disease-associated allele can be confirmed with confidence, and where in the absence of intervention there will be inevitable decline). The data supports a vicious cycle of ROS generation, p38MAPK activation, and proteasome inhibition. By targeting each of the critical components, such as inhibiting p38MAPK activation (using inhibitors such as SKF86002), increasing the removal of oligomeric forms of the toxic protein (by enhancing autophagy), and reducing ROS (by suppressing mitochondrial-respiration or treatment with antioxidants), it would delay the vicious cycle of cell death. It should be possible to test this three-pronged therapeutic approach in animal models of polyglutamine disorders. Furthermore, since proteasome inhibition, p38MAPK activation, and ROS generation may be a general mechanism of cytotoxicity in neurodegenerative diseases, the proposed three-pronged therapeutic may have greater therapeutic benefits and extend beyond expanded polyglutamine disorders.

REFERENCES

Adachi H, Waza M, Tokui K, Katsuno M, Minamiyama M, Tanaka F, Doyu M, Sobue G (2007) CHIP overexpression reduces mutant androgen receptor protein and ameliorates phenotypes of the spinal and bulbar muscular atrophy transgenic mouse model. J Neurosci 27:5115-5126.

Alam ZI, Jenner A, Daniel SE, Lees AJ, Cairns N, Marsden CD, Jenner P, Halliwell B (1997) Oxidative DNA damage in the parkinsonian brain: an apparent selective increase in 8-hydroxyguanine levels in substantia nigra. J Neurochem 69:1196-1203.

Albin RL, Young AB, Penney JB, Handelin B, Balfour R, Anderson KD, Markel DS, Tourtellotte WW, Reiner A (1990) Abnormalities of striatal projection neurons and N-methyl-D-aspartate receptors in presymptomatic Huntington's disease. N Engl J Med 322:1293-1298.

Allan LM, Ballard CG, Rowan EN, Kenny RA (2009) Incidence and prediction of falls in dementia: a prospective study in older people. PLoS One 4:e5521.

Al-Ramahi I, Lam YC, Chen HK, de Gouyon B, Zhang M, Perez AM, Branco J, de Haro M, Patterson C, Zoghbi HY, Botas J (2006) CHIP protects from the neurotoxicity of expanded and wild-type ataxin-1 and promotes their ubiquitination and degradation. J Biol Chem 281:26714-26724.

Amerik AY, Hochstrasser M (2004) Mechanism and function of deubiquitinating enzymes. Biochimica et Biophysica Acta (BBA) - Molecular Cell Research 1695:189-207.

Apostol BL, Illes K, Pallos J, Bodai L, Wu J, Strand A, Schweitzer ES, Olson JM, Kazantsev A, Marsh JL, Thompson LM (2006) Mutant huntingtin alters MAPK signaling pathways in PC12 and striatal cells: ERK1/2 protects against mutant huntingtin-associated toxicity

10.1093/hmg/ddi443. Human Molecular Genetics 15:273-285.

Arrasate M, Mitra S, Schweitzer ES, Segal MR, Finkbeiner S (2004) Inclusion body formation reduces levels of mutant huntingtin and the risk of neuronal death. 431:805-810.

Arrigo AP (2001) Hsp27: novel regulator of intracellular redox state. IUBMB Life 52:303-307.

Arrigo AP, Firdaus WJ, Mellier G, Moulin M, Paul C, Diaz-latoud C, Kretz-remy C (2005) Cytotoxic effects induced by oxidative stress in cultured mammalian cells and protection provided by Hsp27 expression. Methods 35:126-138.

Askari N, Diskin R, Avitzour M, Capone R, Livnah O, Engelberg D (2007) Hyperactive variants of p38alpha induce, whereas hyperactive variants of p38gamma suppress, activating protein 1-mediated transcription. J Biol Chem 282:91-99.

Baboshina OV, Haas AL (1996) Novel multiubiquitin chain linkages catalyzed by the conjugating enzymes E2EPF and RAD6 are recognized by 26 S proteasome subunit 5. J Biol Chem 271:2823-2831.

Barghorn S, Mandelkow E (2002) Toward a unified scheme for the aggregation of tau into Alzheimer paired helical filaments. Biochemistry 41:14885-14896.

Bartels T, Choi JG, Selkoe DJ (2011) alpha-Synuclein occurs physiologically as a helically folded tetramer that resists aggregation. Nature 477:107-110.

Beal MF (2005) Mitochondria take center stage in aging and neurodegeneration. Ann Neurol 58:495-505.

Becher MW, Kotzuk JA, Davis LE, Bear DG (2000) Intranuclear inclusions in oculopharyngeal muscular dystrophy contain poly(A) binding protein 2. Ann Neurol 48:812-815.
Beckman KB, Ames BN (1998) The free radical theory of aging matures. Physiol Rev 78:547-581.
Behl C, Davis JB, Lesley R, Schubert D (1994) Hydrogen peroxide mediates amyloid beta protein toxicity. Cell 77:817-827.
Bellu AR, Kiel JA (2003) Selective degradation of peroxisomes in yeasts. Microsc Res Tech 61:161-170.
Bence NF, Sampat RM, Kopito RR (2001) Impairment of the ubiquitin-proteasome system by protein aggregation. Science 292:1552-1555.
Bennett EJ, Bence NF, Jayakumar R, Kopito RR (2005) Global impairment of the ubiquitin-proteasome system by nuclear or cytoplasmic protein aggregates precedes inclusion body formation. Mol Cell 17:351-365.
Benzinger TL, Gregory DM, Burkoth TS, Miller-Auer H, Lynn DG, Botto RE, Meredith SC (1998) Propagating structure of Alzheimer's beta-amyloid(10-35) is parallel beta-sheet with residues in exact register. Proc Natl Acad Sci U S A 95:13407-13412.
Berger Z, Ravikumar B, Menzies FM, Oroz LG, Underwood BR, Pangalos MN, Schmitt I, Wullner U, Evert BO, O'Kane CJ, Rubinsztein DC (2006) Rapamycin alleviates toxicity of different aggregate-prone proteins. Hum Mol Genet 15:433-442.
Bett JS, Cook C, Petrucelli L, Bates GP (2009) The ubiquitin-proteasome reporter GFPu does not accumulate in neurons of the R6/2 transgenic mouse model of Huntington's disease. PLoS One 4:e5128.
Blalock EM, Chen KC, Sharrow K, Herman JP, Porter NM, Foster TC, Landfield PW (2003) Gene microarrays in hippocampal aging: statistical profiling identifies novel processes correlated with cognitive impairment. J Neurosci 23:3807-3819.
Blennow K, de Leon MJ, Zetterberg H (2006) Alzheimer's disease. Lancet 368:387-403.
Bodner RA, Outeiro TF, Altmann S, Maxwell MM, Cho SH, Hyman BT, McLean PJ, Young AB, Housman DE, Kazantsev AG (2006) Pharmacological promotion of inclusion formation: a therapeutic approach for Huntington's and Parkinson's diseases. Proc Natl Acad Sci U S A 103:4246-4251.
Bogdanov MB, Andreassen OA, Dedeoglu A, Ferrante RJ, Beal MF (2001) Increased oxidative damage to DNA in a transgenic mouse model of Huntington's disease. J Neurochem 79:1246-1249.
Bohr VA (2002) Repair of oxidative DNA damage in nuclear and mitochondrial DNA, and some changes with aging in mammalian cells. Free Radic Biol Med 32:804-812.
Boland B, Kumar A, Lee S, Platt FM, Wegiel J, Yu WH, Nixon RA (2008) Autophagy induction and autophagosome clearance in neurons: relationship to autophagic pathology in Alzheimer's disease. J Neurosci 28:6926-6937.
Bonifati V, Rizzu P, Squitieri F, Krieger E, Vanacore N, van Swieten JC, Brice A, van Duijn CM, Oostra B, Meco G, Heutink P (2003) DJ-1(PARK7), a novel gene for autosomal recessive, early onset parkinsonism. Neurol Sci 24:159-160.
Borlongan CV, Koutouzis TK, Sanberg PR (1997) 3-Nitropropionic acid animal model and Huntington's disease. Neurosci Biobehav Rev 21:289-293.

Boulton TG, Yancopoulos GD, Gregory JS, Slaughter C, Moomaw C, Hsu J, Cobb MH (1990) An insulin-stimulated protein kinase similar to yeast kinases involved in cell cycle control. Science 249:64-67.
Boutet SC, Disatnik MH, Chan LS, Iori K, Rando TA (2007) Regulation of Pax3 by proteasomal degradation of monoubiquitinated protein in skeletal muscle progenitors. Cell 130:349-362.
Bove J, Martinez-Vicente M, Vila M (2011) Fighting neurodegeneration with rapamycin: mechanistic insights. Nat Rev Neurosci 12:437-452.
Braak H, Del Tredici K, Rub U, de Vos RA, Jansen Steur EN, Braak E (2003) Staging of brain pathology related to sporadic Parkinson's disease. Neurobiol Aging 24:197-211.
Brais B, Rouleau GA, Bouchard JP, Fardeau M, Tome FM (1999) Oculopharyngeal muscular dystrophy. Semin Neurol 19:59-66.
Brais B, Bouchard JP, Xie YG, Rochefort DL, Chretien N, Tome FM, Lafreniere RG, Rommens JM, Uyama E, Nohira O, Blumen S, Korczyn AD, Heutink P, Mathieu J, Duranceau A, Codere F, Fardeau M, Rouleau GA (1998) Short GCG expansions in the PABP2 gene cause oculopharyngeal muscular dystrophy. Nat Genet 18:164-167.
Braithwaite SP, Schmid RS, He DN, Sung ML, Cho S, Resnick L, Monaghan MM, Hirst WD, Essrich C, Reinhart PH, Lo DC (2010) Inhibition of c-Jun kinase provides neuroprotection in a model of Alzheimer's disease. Neurobiol Dis 39:311-317.
Brown LY, Brown SA (2004) Alanine tracts: the expanding story of human illness and trinucleotide repeats. Trends Genet 20:51-58.
Browne SE (2008) Mitochondria and Huntington's disease pathogenesis: insight from genetic and chemical models. Ann N Y Acad Sci 1147:358-382.
Browne SE, Ferrante RJ, Beal MF (1999) Oxidative stress in Huntington's disease. Brain Pathol 9:147-163.
Bruey JM, Ducasse C, Bonniaud P, Ravagnan L, Susin SA, Diaz-Latoud C, Gurbuxani S, Arrigo AP, Kroemer G, Solary E, Garrido C (2000) Hsp27 negatively regulates cell death by interacting with cytochrome c. Nat Cell Biol 2:645-652.
Bucciantini M, Giannoni E, Chiti F, Baroni F, Formigli L, Zurdo J, Taddei N, Ramponi G, Dobson CM, Stefani M (2002) Inherent toxicity of aggregates implies a common mechanism for protein misfolding diseases. Nature 416:507-511.
Burright EN, Clark HB, Servadio A, Matilla T, Feddersen RM, Yunis WS, Duvick LA, Zoghbi HY, Orr HT (1995) SCA1 transgenic mice: a model for neurodegeneration caused by an expanded CAG trinucleotide repeat. Cell 82:937-948.
Caccamo A, Majumder S, Richardson A, Strong R, Oddo S (2011) Molecular interplay between mammalian target of rapamycin (mTOR), amyloid-beta, and Tau: effects on cognitive impairments. J Biol Chem 285:13107-13120.
Calado A, Tome FM, Brais B, Rouleau GA, Kuhn U, Wahle E, Carmo-Fonseca M (2000) Nuclear inclusions in oculopharyngeal muscular dystrophy consist of poly(A) binding protein 2 aggregates which sequester poly(A) RNA. Hum Mol Genet 9:2321-2328.
Cargnello M, Roux PP (2011) Activation and function of the MAPKs and their substrates, the MAPK-activated protein kinases. Microbiol Mol Biol Rev 75:50-83.
Carmichael J, Chatellier J, Woolfson A, Milstein C, Fersht AR, Rubinsztein DC (2000) Bacterial and yeast chaperones reduce both aggregate formation and cell death in mammalian cell models of Huntington's disease. Proc Natl Acad Sci U S A 97:9701-9705.

Carrard G, Bulteau AL, Petropoulos I, Friguet B (2002) Impairment of proteasome structure and function in aging. Int J Biochem Cell Biol 34:1461-1474.
Carter RJ, Lione LA, Humby T, Mangiarini L, Mahal A, Bates GP, Dunnett SB, Morton AJ (1999) Characterization of Progressive Motor Deficits in Mice Transgenic for the Human Huntington's Disease Mutation. J Neurosci 19:3248-3257.
Cha GH, Kim S, Park J, Lee E, Kim M, Lee SB, Kim JM, Chung J, Cho KS (2005) Parkin negatively regulates JNK pathway in the dopaminergic neurons of Drosophila. Proc Natl Acad Sci U S A 102:10345-10350.
Cha JH (2000) Transcriptional dysregulation in Huntington's disease. Trends Neurosci 23:387-392.
Cha J-HJ, Kosinski CM, Kerner JA, Alsdorf SA, Mangiarini L, Davies SW, Penney JB, Bates GP, Young AB (1998) Altered brain neurotransmitter receptors in transgenic mice expressing a portion of an abnormal human Huntington disease gene
10.1073/pnas.95.11.6480. Proceedings of the National Academy of Sciences 95:6480-6485.
Chai Y, Koppenhafer SL, Bonini NM, Paulson HL (1999) Analysis of the role of heat shock protein (Hsp) molecular chaperones in polyglutamine disease. J Neurosci 19:10338-10347.
Chambers JW, Pachori A, Howard S, Ganno M, Hansen D, Jr., Kamenecka T, Song X, Duckett D, Chen W, Ling YY, Cherry L, Cameron MD, Lin L, Ruiz CH, Lograsso P (2011) Small Molecule c-jun-N-terminal Kinase (JNK) Inhibitors Protect Dopaminergic Neurons in a Model of Parkinson's Disease. ACS Chem Neurosci 2:198-206.
Chang DT, Rintoul GL, Pandipati S, Reynolds IJ (2006) Mutant huntingtin aggregates impair mitochondrial movement and trafficking in cortical neurons. Neurobiol Dis 22:388-400.
Chen H, Zheng C, Zhang Y, Chang YZ, Qian ZM, Shen X (2006) Heat shock protein 27 downregulates the transferrin receptor 1-mediated iron uptake. Int J Biochem Cell Biol 38:1402-1416.
Chen S, Berthelier V, Hamilton JB, O'Nuallain B, Wetzel R (2002) Amyloid-like features of polyglutamine aggregates and their assembly kinetics. Biochemistry 41:7391-7399.
Cheng IH, Scearce-Levie K, Legleiter J, Palop JJ, Gerstein H, Bien-Ly N, Puolivali J, Lesne S, Ashe KH, Muchowski PJ, Mucke L (2007) Accelerating amyloid-beta fibrillization reduces oligomer levels and functional deficits in Alzheimer disease mouse models. J Biol Chem 282:23818-23828.
Cheung EC, Slack RS (2004) Emerging role for ERK as a key regulator of neuronal apoptosis. Sci STKE 2004:PE45.
Chiang MC, Lee YC, Huang CL, Chern Y (2005) cAMP-response element-binding protein contributes to suppression of the A2A adenosine receptor promoter by mutant Huntingtin with expanded polyglutamine residues. J Biol Chem 280:14331-14340.
Cho KJ, Lee BI, Cheon SY, Kim HW, Kim HJ, Kim GW (2009) Inhibition of apoptosis signal-regulating kinase 1 reduces endoplasmic reticulum stress and nuclear huntingtin fragments in a mouse model of Huntington disease. Neuroscience 163:1128-1134.
Choo YS, Johnson GV, MacDonald M, Detloff PJ, Lesort M (2004) Mutant huntingtin directly increases susceptibility of mitochondria to the calcium-induced permeability transition and cytochrome c release. Hum Mol Genet 13:1407-1420.

Chou AH, Lin AC, Hong KY, Hu SH, Chen YL, Chen JY, Wang HL (2011) p53 activation mediates polyglutamine-expanded ataxin-3 upregulation of Bax expression in cerebellar and pontine nuclei neurons. Neurochem Int 58:145-152.
Chui DH, Tanahashi H, Ozawa K, Ikeda S, Checler F, Ueda O, Suzuki H, Araki W, Inoue H, Shirotani K, Takahashi K, Gallyas F, Tabira T (1999) Transgenic mice with Alzheimer presenilin 1 mutations show accelerated neurodegeneration without amyloid plaque formation. Nat Med 5:560-564.
Chun W, Lesort M, Lee M, Johnson GV (2002) Mutant huntingtin aggregates do not sensitize cells to apoptotic stressors. FEBS Lett 515:61-65.
Ciechanover A (2005) Proteolysis: from the lysosome to ubiquitin and the proteasome. Nat Rev Mol Cell Biol 6:79-87.
Ciechanover A, Brundin P (2003) The ubiquitin proteasome system in neurodegenerative diseases: sometimes the chicken, sometimes the egg. Neuron 40:427-446.
Ciechanover A, Heller H, Katz-Etzion R, Hershko A (1981) Activation of the heat-stable polypeptide of the ATP-dependent proteolytic system. Proc Natl Acad Sci U S A 78:761-765.
Citron M, Oltersdorf T, Haass C, McConlogue L, Hung AY, Seubert P, Vigo-Pelfrey C, Lieberburg I, Selkoe DJ (1992) Mutation of the beta-amyloid precursor protein in familial Alzheimer's disease increases beta-protein production. Nature 360:672-674.
Citron M, Westaway D, Xia W, Carlson G, Diehl T, Levesque G, Johnson-Wood K, Lee M, Seubert P, Davis A, Kholodenko D, Motter R, Sherrington R, Perry B, Yao H, Strome R, Lieberburg I, Rommens J, Kim S, Schenk D, Fraser P, St George Hyslop P, Selkoe DJ (1997) Mutant presenilins of Alzheimer's disease increase production of 42-residue amyloid beta-protein in both transfected cells and transgenic mice. Nat Med 3:67-72.
Clark HB, Burright EN, Yunis WS, Larson S, Wilcox C, Hartman B, Matilla A, Zoghbi HY, Orr HT (1997) Purkinje cell expression of a mutant allele of SCA1 in transgenic mice leads to disparate effects on motor behaviors, followed by a progressive cerebellar dysfunction and histological alterations. J Neurosci 17:7385-7395.
Clerk A, Michael A, Sugden PH (1998) Stimulation of multiple mitogen-activated protein kinase sub-families by oxidative stress and phosphorylation of the small heat shock protein, HSP25/27, in neonatal ventricular myocytes. Biochem J 333 (Pt 3):581-589.
Cohen P (1997) The search for physiological substrates of MAP and SAP kinases in mammalian cells. Trends Cell Biol 7:353-361.
Colby DW, Cassady JP, Lin GC, Ingram VM, Wittrup KD (2006) Stochastic kinetics of intracellular huntingtin aggregate formation. Nat Chem Biol 2:319-323.
Colognato R, Laurenza I, Fontana I, Coppede F, Siciliano G, Coecke S, Aruoma OI, Benzi L, Migliore L (2006) Modulation of hydrogen peroxide-induced DNA damage, MAPKs activation and cell death in PC12 by ergothioneine. Clin Nutr 25:135-145.
Cong SY, Pepers BA, Evert BO, Rubinsztein DC, Roos RA, van Ommen GJ, Dorsman JC (2005) Mutant huntingtin represses CBP, but not p300, by binding and protein degradation. Mol Cell Neurosci 30:560-571.
Cuenda A, Rousseau S (2007) p38 MAP-kinases pathway regulation, function and role in human diseases. Biochim Biophys Acta 1773:1358-1375.
Cuervo AM (2004) Autophagy: many paths to the same end. Mol Cell Biochem 263:55-72.

Cummings CJ, Mancini MA, Antalffy B, DeFranco DB, Orr HT, Zoghbi HY (1998) Chaperone suppression of aggregation and altered subcellular proteasome localization imply protein misfolding in SCA1. Nat Genet 19:148-154.
Cummings CJ, Sun Y, Opal P, Antalffy B, Mestril R, Orr HT, Dillmann WH, Zoghbi HY (2001) Over-expression of inducible HSP70 chaperone suppresses neuropathology and improves motor function in SCA1 mice. Hum Mol Genet 10:1511-1518.
Cummings CJ, Reinstein E, Sun Y, Antalffy B, Jiang Y, Ciechanover A, Orr HT, Beaudet AL, Zoghbi HY (1999) Mutation of the E6-AP ubiquitin ligase reduces nuclear inclusion frequency while accelerating polyglutamine-induced pathology in SCA1 mice. Neuron 24:879-892.
Cummins JM, Rago C, Kohli M, Kinzler KW, Lengauer C, Vogelstein B (2004) Tumour suppression: disruption of HAUSP gene stabilizes p53. Nature 428:1 p following 486.
Dantuma NP, Lindsten K, Glas R, Jellne M, Masucci MG (2000) Short-lived green fluorescent proteins for quantifying ubiquitin/proteasome-dependent proteolysis in living cells. Nat Biotechnol 18:538-543.
Davies JE, Berger Z, Rubinsztein DC (2006) Oculopharyngeal muscular dystrophy: potential therapies for an aggregate-associated disorder. Int J Biochem Cell Biol 38:1457-1462.
Davies SW, Turmaine M, Cozens BA, DiFiglia M, Sharp AH, Ross CA, Scherzinger E, Wanker EE, Mangiarini L, Bates GP (1997) Formation of neuronal intranuclear inclusions underlies the neurological dysfunction in mice transgenic for the HD mutation. Cell 90:537-548.
De Strooper B, Annaert W (2000) Proteolytic processing and cell biological functions of the amyloid precursor protein. J Cell Sci 113 (Pt 11):1857-1870.
Dehay B, Bove J, Rodriguez-Muela N, Perier C, Recasens A, Boya P, Vila M (2010) Pathogenic lysosomal depletion in Parkinson's disease. J Neurosci 30:12535-12544.
Demasi M, Davies KJ (2003) Proteasome inhibitors induce intracellular protein aggregation and cell death by an oxygen-dependent mechanism. FEBS Lett 542:89-94.
Deng L, Wang C, Spencer E, Yang L, Braun A, You J, Slaughter C, Pickart C, Chen ZJ (2000) Activation of the IkappaB kinase complex by TRAF6 requires a dimeric ubiquitin-conjugating enzyme complex and a unique polyubiquitin chain. Cell 103:351-361.
Der-Sarkissian A, Jao CC, Chen J, Langen R (2003) Structural organization of alpha-synuclein fibrils studied by site-directed spin labeling. J Biol Chem 278:37530-37535.
Dewil M, dela Cruz VF, Van Den Bosch L, Robberecht W (2007) Inhibition of p38 mitogen activated protein kinase activation and mutant SOD1(G93A)-induced motor neuron death. Neurobiol Dis 26:332-341.
Diaz-Hernandez M, Valera AG, Moran MA, Gomez-Ramos P, Alvarez-Castelao B, Castano JG, Hernandez F, Lucas JJ (2006) Inhibition of 26S proteasome activity by huntingtin filaments but not inclusion bodies isolated from mouse and human brain. J Neurochem 98:1585-1596.
Diaz-Hernandez M, Hernandez F, Martin-Aparicio E, Gomez-Ramos P, Moran MA, Castano JG, Ferrer I, Avila J, Lucas JJ (2003) Neuronal induction of the immunoproteasome in Huntington's disease. J Neurosci 23:11653-11661.
Dickson DW, Braak H, Duda JE, Duyckaerts C, Gasser T, Halliday GM, Hardy J, Leverenz JB, Del Tredici K, Wszolek ZK, Litvan I (2009) Neuropathological assessment of Parkinson's disease: refining the diagnostic criteria. Lancet Neurol 8:1150-1157.

DiFiglia M, Sapp E, Chase KO, Davies SW, Bates GP, Vonsattel JP, Aronin N (1997) Aggregation of huntingtin in neuronal intranuclear inclusions and dystrophic neurites in brain. Science 277:1990-1993.

Ding Q, Dimayuga E, Keller JN (2006) Proteasome regulation of oxidative stress in aging and age-related diseases of the CNS. Antioxid Redox Signal 8:163-172.

Ding Q, Dimayuga E, Markesbery WR, Keller JN (2004) Proteasome inhibition increases DNA and RNA oxidation in astrocyte and neuron cultures. J Neurochem 91:1211-1218.

Ding Q, Dimayuga E, Martin S, Bruce-Keller AJ, Nukala V, Cuervo AM, Keller JN (2003) Characterization of chronic low-level proteasome inhibition on neural homeostasis. J Neurochem 86:489-497.

Ding WX, Yin XM (2008) Sorting, recognition and activation of the misfolded protein degradation pathways through macroautophagy and the proteasome. Autophagy 4:141-150.

Dunah AW, Jeong H, Griffin A, Kim YM, Standaert DG, Hersch SM, Mouradian MM, Young AB, Tanese N, Krainc D (2002) Sp1 and TAFII130 transcriptional activity disrupted in early Huntington's disease. Science 296:2238-2243.

Everett CM, Wood NW (2004) Trinucleotide repeats and neurodegenerative disease. Brain 127:2385-2405.

Fahn S (2003) Description of Parkinson's disease as a clinical syndrome. Ann N Y Acad Sci 991:1-14.

Fan X, Dion P, Laganiere J, Brais B, Rouleau GA (2001) Oligomerization of polyalanine expanded PABPN1 facilitates nuclear protein aggregation that is associated with cell death. Hum Mol Genet 10:2341-2351.

Fernandes AF, Bian Q, Jiang JK, Thomas CJ, Taylor A, Pereira P, Shang F (2009) Proteasome inactivation promotes p38 mitogen-activated protein kinase-dependent phosphatidylinositol 3-kinase activation and increases interleukin-8 production in retinal pigment epithelial cells. Mol Biol Cell 20:3690-3699.

Ferrante RJ, Kubilus JK, Lee J, Ryu H, Beesen A, Zucker B, Smith K, Kowall NW, Ratan RR, Luthi-Carter R, Hersch SM (2003) Histone deacetylase inhibition by sodium butyrate chemotherapy ameliorates the neurodegenerative phenotype in Huntington's disease mice. J Neurosci 23:9418-9427.

Ferrington DA, Kapphahn RJ (2004) Catalytic site-specific inhibition of the 20S proteasome by 4-hydroxynonenal. FEBS Lett 578:217-223.

Ferrington DA, Husom AD, Thompson LV (2005) Altered proteasome structure, function, and oxidation in aged muscle. Faseb J 19:644-646.

Fimia GM, Stoykova A, Romagnoli A, Giunta L, Di Bartolomeo S, Nardacci R, Corazzari M, Fuoco C, Ucar A, Schwartz P, Gruss P, Piacentini M, Chowdhury K, Cecconi F (2007) Ambra1 regulates autophagy and development of the nervous system. Nature 447:1121-1125.

Finley D (2009) Recognition and Processing of Ubiquitin-Protein Conjugates by the Proteasome

doi:10.1146/annurev.biochem.78.081507.101607. Annual Review of Biochemistry 78:477-513.

Firdaus WJ, Wyttenbach A, Diaz-Latoud C, Currie RW, Arrigo AP (2006a) Analysis of oxidative events induced by expanded polyglutamine huntingtin exon 1 that are

differentially restored by expression of heat shock proteins or treatment with an antioxidant. Febs J 273:3076-3093.
Firdaus WJ, Wyttenbach A, Giuliano P, Kretz-Remy C, Currie RW, Arrigo AP (2006b) Huntingtin inclusion bodies are iron-dependent centers of oxidative events. Febs J 273:5428-5441.
Friguet B, Szweda LI (1997) Inhibition of the multicatalytic proteinase (proteasome) by 4-hydroxy-2-nonenal cross-linked protein. FEBS Lett 405:21-25.
Fu L, Gao YS, Sztul E (2005) Transcriptional repression and cell death induced by nuclear aggregates of non-polyglutamine protein. Neurobiol Dis 20:656-665.
Fuertes G, Villarroya A, Knecht E (2003a) Role of proteasomes in the degradation of short-lived proteins in human fibroblasts under various growth conditions. Int J Biochem Cell Biol 35:651-664.
Fuertes G, Martin De Llano JJ, Villarroya A, Rivett AJ, Knecht E (2003b) Changes in the proteolytic activities of proteasomes and lysosomes in human fibroblasts produced by serum withdrawal, amino-acid deprivation and confluent conditions. Biochem J 375:75-86.
Fukunaga R, Hunter T (1997) MNK1, a new MAP kinase-activated protein kinase, isolated by a novel expression screening method for identifying protein kinase substrates. Embo J 16:1921-1933.
Garcia M, Vanhoutte P, Pages C, Besson MJ, Brouillet E, Caboche J (2002) The mitochondrial toxin 3-nitropropionic acid induces striatal neurodegeneration via a c-Jun N-terminal kinase/c-Jun module. J Neurosci 22:2174-2184.
Garseth M, Sonnewald U, White LR, Rod M, Zwart JA, Nygaard O, Aasly J (2000) Proton magnetic resonance spectroscopy of cerebrospinal fluid in neurodegenerative disease: indication of glial energy impairment in Huntington chorea, but not Parkinson disease. J Neurosci Res 60:779-782.
Gatchel JR, Zoghbi HY (2005) Diseases of unstable repeat expansion: mechanisms and common principles. Nat Rev Genet 6:743-755.
Ge B, Gram H, Di Padova F, Huang B, New L, Ulevitch RJ, Luo Y, Han J (2002) MAPKK-independent activation of p38alpha mediated by TAB1-dependent autophosphorylation of p38alpha. Science 295:1291-1294.
Ghosh S, Feany MB (2004) Comparison of pathways controlling toxicity in the eye and brain in Drosophila models of human neurodegenerative diseases. Hum Mol Genet 13:2011-2018.
Gill A, Kidd J, Vieira F, Thompson K, Perrin S (2009) No benefit from chronic lithium dosing in a sibling-matched, gender balanced, investigator-blinded trial using a standard mouse model of familial ALS. PLoS One 4:e6489.
Giuliano P, De Cristofaro T, Affaitati A, Pizzulo GM, Feliciello A, Criscuolo C, De Michele G, Filla A, Avvedimento EV, Varrone S (2003) DNA damage induced by polyglutamine-expanded proteins. Hum Mol Genet 12:2301-2309.
Glenner GG, Wong CW (1984) Alzheimer's disease: initial report of the purification and characterization of a novel cerebrovascular amyloid protein. Biochem Biophys Res Commun 120:885-890.
Glickman MH, Ciechanover A (2002) The Ubiquitin-Proteasome Proteolytic Pathway: Destruction for the Sake of Construction. Physiol Rev 82:373-428.

Goate AM, Haynes AR, Owen MJ, Farrall M, James LA, Lai LY, Mullan MJ, Roques P, Rossor MN, Williamson R, et al. (1989) Predisposing locus for Alzheimer's disease on chromosome 21. Lancet 1:352-355.
Goedert M, Spillantini MG (2001) Tau gene mutations and neurodegeneration. Biochem Soc Symp:59-71.
Goedert M, Spillantini MG (2006) A century of Alzheimer's disease. Science 314:777-781.
Goldberg MS, Fleming SM, Palacino JJ, Cepeda C, Lam HA, Bhatnagar A, Meloni EG, Wu N, Ackerson LC, Klapstein GJ, Gajendiran M, Roth BL, Chesselet MF, Maidment NT, Levine MS, Shen J (2003) Parkin-deficient mice exhibit nigrostriatal deficits but not loss of dopaminergic neurons. J Biol Chem 278:43628-43635.
Gong B, Lim MC, Wanderer J, Wyttenbach A, Morton AJ (2008) Time-lapse analysis of aggregate formation in an inducible PC12 cell model of Huntington's disease reveals time-dependent aggregate formation that transiently delays cell death. Brain Res Bull 75:146-157.
Groll M, Ditzel L, Lowe J, Stock D, Bochtler M, Bartunik HD, Huber R (1997) Structure of 20S proteasome from yeast at 2.4 A resolution. Nature 386:463-471.
Grundke-Iqbal I, Iqbal K, Tung YC, Quinlan M, Wisniewski HM, Binder LI (1986) Abnormal phosphorylation of the microtubule-associated protein tau (tau) in Alzheimer cytoskeletal pathology. Proc Natl Acad Sci U S A 83:4913-4917.
Grune T, Jung T, Merker K, Davies KJ (2004) Decreased proteolysis caused by protein aggregates, inclusion bodies, plaques, lipofuscin, ceroid, and 'aggresomes' during oxidative stress, aging, and disease. Int J Biochem Cell Biol 36:2519-2530.
Grunewald T, Beal MF (1999) Bioenergetics in Huntington's disease. Ann N Y Acad Sci 893:203-213.
Gu M, Gash MT, Mann VM, Javoy-Agid F, Cooper JM, Schapira AH (1996) Mitochondrial defect in Huntington's disease caudate nucleus. Ann Neurol 39:385-389.
Gunawardena S, Her LS, Brusch RG, Laymon RA, Niesman IR, Gordesky-Gold B, Sintasath L, Bonini NM, Goldstein LS (2003) Disruption of axonal transport by loss of huntingtin or expression of pathogenic polyQ proteins in Drosophila. Neuron 40:25-40.
Gunn-Moore FJ, Tavare JM (1998) Apoptosis of cerebellar granule cells induced by serum withdrawal, glutamate or beta-amyloid, is independent of Jun kinase or p38 mitogen activated protein kinase activation. Neurosci Lett 250:53-56.
Haass C, Selkoe DJ (2007) Soluble protein oligomers in neurodegeneration: lessons from the Alzheimer's amyloid beta-peptide. Nat Rev Mol Cell Biol 8:101-112.
Hadari T, Warms JV, Rose IA, Hershko A (1992) A ubiquitin C-terminal isopeptidase that acts on polyubiquitin chains. Role in protein degradation. J Biol Chem 267:719-727.
Hara T, Nakamura K, Matsui M, Yamamoto A, Nakahara Y, Suzuki-Migishima R, Yokoyama M, Mishima K, Saito I, Okano H, Mizushima N (2006) Suppression of basal autophagy in neural cells causes neurodegenerative disease in mice. Nature 441:885-889.
Hardy J, Allsop D (1991) Amyloid deposition as the central event in the aetiology of Alzheimer's disease. Trends Pharmacol Sci 12:383-388.
Hardy JA, Owen MJ, Goate AM, James LA, Haynes AR, Rossor MN, Roques P, Mullan MJ (1989) Molecular genetics of Alzheimer's disease. Biochem Soc Trans 17:75-76.
Harper PS (1992) The epidemiology of Huntington's disease. Hum Genet 89:365-376.

Heinemeyer W, Kleinschmidt JA, Saidowsky J, Escher C, Wolf DH (1991) Proteinase yscE, the yeast proteasome/multicatalytic-multifunctional proteinase: mutants unravel its function in stress induced proteolysis and uncover its necessity for cell survival. Embo J 10:555-562.

Hensley K, Carney JM, Mattson MP, Aksenova M, Harris M, Wu JF, Floyd RA, Butterfield DA (1994) A model for beta-amyloid aggregation and neurotoxicity based on free radical generation by the peptide: relevance to Alzheimer disease. Proc Natl Acad Sci U S A 91:3270-3274.

Hersch SM, Gevorkian S, Marder K, Moskowitz C, Feigin A, Cox M, Como P, Zimmerman C, Lin M, Zhang L, Ulug AM, Beal MF, Matson W, Bogdanov M, Ebbel E, Zaleta A, Kaneko Y, Jenkins B, Hevelone N, Zhang H, Yu H, Schoenfeld D, Ferrante R, Rosas HD (2006) Creatine in Huntington disease is safe, tolerable, bioavailable in brain and reduces serum 8OH2'dG. Neurology 66:250-252.

Hershko A, Ciechanover A (1998) The ubiquitin system. Annu Rev Biochem 67:425-479.

Hilt W, Wolf DH (1995) Proteasomes of the yeast S. cerevisiae: genes, structure and functions. Mol Biol Rep 21:3-10.

Hirai K, Aliev G, Nunomura A, Fujioka H, Russell RL, Atwood CS, Johnson AB, Kress Y, Vinters HV, Tabaton M, Shimohama S, Cash AD, Siedlak SL, Harris PL, Jones PK, Petersen RB, Perry G, Smith MA (2001) Mitochondrial abnormalities in Alzheimer's disease. J Neurosci 21:3017-3023.

Hirosumi J, Tuncman G, Chang L, Gorgun CZ, Uysal KT, Maeda K, Karin M, Hotamisligil GS (2002) A central role for JNK in obesity and insulin resistance. Nature 420:333-336.

Ho AK, McNeil L, Terriff D, Price DM, Chik CL (2005) Role of protein turnover in the activation of p38 mitogen-activated protein kinase in rat pinealocytes. Biochem Pharmacol 70:1840-1850.

Ho LW, Carmichael J, Swartz J, Wyttenbach A, Rankin J, Rubinsztein DC (2001) The molecular biology of Huntington's disease. Psychol Med 31:3-14.

Hockly E, Richon VM, Woodman B, Smith DL, Zhou X, Rosa E, Sathasivam K, Ghazi-Noori S, Mahal A, Lowden PA, Steffan JS, Marsh JL, Thompson LM, Lewis CM, Marks PA, Bates GP (2003) Suberoylanilide hydroxamic acid, a histone deacetylase inhibitor, ameliorates motor deficits in a mouse model of Huntington's disease. Proc Natl Acad Sci U S A 100:2041-2046.

Hoege C, Pfander B, Moldovan G-L, Pyrowolakis G, Jentsch S (2002) RAD6-dependent DNA repair is linked to modification of PCNA by ubiquitin and SUMO. Nature 419:135-141.

Hofmann RM, Pickart CM (2001) In vitro assembly and recognition of Lys-63 polyubiquitin chains. J Biol Chem 276:27936-27943.

Holmberg CI, Staniszewski KE, Mensah KN, Matouschek A, Morimoto RI (2004) Inefficient degradation of truncated polyglutamine proteins by the proteasome. Embo J 23:4307-4318.

Hsia AY, Masliah E, McConlogue L, Yu GQ, Tatsuno G, Hu K, Kholodenko D, Malenka RC, Nicoll RA, Mucke L (1999) Plaque-independent disruption of neural circuits in Alzheimer's disease mouse models. Proc Natl Acad Sci U S A 96:3228-3233.

Hsu MJ, Hsu CY, Chen BC, Chen MC, Ou G, Lin CH (2007) Apoptosis signal-regulating kinase 1 in amyloid beta peptide-induced cerebral endothelial cell apoptosis. J Neurosci 27:5719-5729.
Huang CC, Faber PW, Persichetti F, Mittal V, Vonsattel JP, MacDonald ME, Gusella JF (1998) Amyloid formation by mutant huntingtin: threshold, progressivity and recruitment of normal polyglutamine proteins. Somat Cell Mol Genet 24:217-233.
Huang Y, Baker RT, Fischer-Vize JA (1995) Control of cell fate by a deubiquitinating enzyme encoded by the fat facets gene. Science 270:1828-1831.
Hunot S, Vila M, Teismann P, Davis RJ, Hirsch EC, Przedborski S, Rakic P, Flavell RA (2004) JNK-mediated induction of cyclooxygenase 2 is required for neurodegeneration in a mouse model of Parkinson's disease. Proc Natl Acad Sci U S A 101:665-670.
Ikeda F, Dikic I (2008) Atypical ubiquitin chains: new molecular signals. 'Protein Modifications: Beyond the Usual Suspects' review series. EMBO Rep 9:536-542.
Illuzzi J, Yerkes S, Parekh-Olmedo H, Kmiec EB (2009) DNA breakage and induction of DNA damage response proteins precede the appearance of visible mutant huntingtin aggregates. J Neurosci Res 87:733-747.
Irwin S, Vandelft M, Pinchev D, Howell JL, Graczyk J, Orr HT, Truant R (2005) RNA association and nucleocytoplasmic shuttling by ataxin-1. J Cell Sci 118:233-242.
Ischiropoulos H, Beckman JS (2003) Oxidative stress and nitration in neurodegeneration: cause, effect, or association? J Clin Invest 111:163-169.
Itakura E, Kishi C, Inoue K, Mizushima N (2008) Beclin 1 forms two distinct phosphatidylinositol 3-kinase complexes with mammalian Atg14 and UVRAG. Mol Biol Cell 19:5360-5372.
Iwai K, Tokunaga F (2009) Linear polyubiquitination: a new regulator of NF-kappaB activation. EMBO Rep 10:706-713.
Iwata A, Christianson JC, Bucci M, Ellerby LM, Nukina N, Forno LS, Kopito RR (2005) Increased susceptibility of cytoplasmic over nuclear polyglutamine aggregates to autophagic degradation. Proc Natl Acad Sci U S A 102:13135-13140.
Iwatsubo T, Odaka A, Suzuki N, Mizusawa H, Nukina N, Ihara Y (1994) Visualization of A beta 42(43) and A beta 40 in senile plaques with end-specific A beta monoclonals: evidence that an initially deposited species is A beta 42(43). Neuron 13:45-53.
Jana NR, Tanaka M, Wang G, Nukina N (2000) Polyglutamine length-dependent interaction of Hsp40 and Hsp70 family chaperones with truncated N-terminal huntingtin: their role in suppression of aggregation and cellular toxicity. Hum Mol Genet 9:2009-2018.
Jana NR, Zemskov EA, Wang G, Nukina N (2001) Altered proteasomal function due to the expression of polyglutamine-expanded truncated N-terminal huntingtin induces apoptosis by caspase activation through mitochondrial cytochrome c release. Hum Mol Genet 10:1049-1059.
Jenkins BG, Koroshetz WJ, Beal MF, Rosen BR (1993) Evidence for impairment of energy metabolism in vivo in Huntington's disease using localized 1H NMR spectroscopy. Neurology 43:2689-2695.
Jentsch S, Seufert W, Sommer T, Reins HA (1990) Ubiquitin-conjugating enzymes: novel regulators of eukaryotic cells. Trends Biochem Sci 15:195-198.
Jiang Y, Chen C, Li Z, Guo W, Gegner JA, Lin S, Han J (1996) Characterization of the structure and function of a new mitogen-activated protein kinase (p38beta). J Biol Chem 271:17920-17926.

Johnson GL, Lapadat R (2002) Mitogen-activated protein kinase pathways mediated by ERK, JNK, and p38 protein kinases. Science 298:1911-1912.
Junyent F, de Lemos L, Verdaguer E, Pallas M, Folch J, Beas-Zarate C, Camins A, Auladell C (2011) Lack of Jnk3 Does Not Protect against Neurodegeneration Induced by 3-Nitropropionic Acid. Neuropathol Appl Neurobiol.
Kao C-F, Hillyer C, Tsukuda T, Henry K, Berger S, Osley MA (2004) Rad6 plays a role in transcriptional activation through ubiquitylation of histone H2B. Genes Dev 18:184-195.
Kayed R, Head E, Thompson JL, McIntire TM, Milton SC, Cotman CW, Glabe CG (2003) Common structure of soluble amyloid oligomers implies common mechanism of pathogenesis. Science 300:486-489.
Kegel KB, Kim M, Sapp E, McIntyre C, Castano JG, Aronin N, DiFiglia M (2000) Huntingtin expression stimulates endosomal-lysosomal activity, endosome tubulation, and autophagy. J Neurosci 20:7268-7278.
Keller JN, Hanni KB, Markesbery WR (2000) Impaired proteasome function in Alzheimer's disease. J Neurochem 75:436-439.
Keller JN, Gee J, Ding Q (2002) The proteasome in brain aging. Ageing Res Rev 1:279-293.
Kerscher O, Felberbaum R, Hochstrasser M (2006) Modification of proteins by ubiquitin and ubiquitin-like proteins. Annu Rev Cell Dev Biol 22:159-180.
Kim HT, Kim KP, Lledias F, Kisselev AF, Scaglione KM, Skowyra D, Gygi SP, Goldberg AL (2007a) Certain pairs of ubiquitin-conjugating enzymes (E2s) and ubiquitin-protein ligases (E3s) synthesize nondegradable forked ubiquitin chains containing all possible isopeptide linkages. J Biol Chem 282:17375-17386.
Kim I, Rodriguez-Enriquez S, Lemasters JJ (2007b) Selective degradation of mitochondria by mitophagy. Arch Biochem Biophys 462:245-253.
Kim J, Klionsky DJ (2000) Autophagy, cytoplasm-to-vacuole targeting pathway, and pexophagy in yeast and mammalian cells. Annu Rev Biochem 69:303-342.
Kim PK, Hailey DW, Mullen RT, Lippincott-Schwartz J (2008) Ubiquitin signals autophagic degradation of cytosolic proteins and peroxisomes. Proc Natl Acad Sci U S A 105:20567-20574.
Kimberly WT, LaVoie MJ, Ostaszewski BL, Ye W, Wolfe MS, Selkoe DJ (2003) Gamma-secretase is a membrane protein complex comprised of presenilin, nicastrin, Aph-1, and Pen-2. Proc Natl Acad Sci U S A 100:6382-6387.
Kirkin V, McEwan DG, Novak I, Dikic I (2009a) A role for ubiquitin in selective autophagy. Mol Cell 34:259-269.
Kirkin V, Lamark T, Johansen T, Dikic I (2009b) NBR1 cooperates with p62 in selective autophagy of ubiquitinated targets. Autophagy 5:732-733.
Kishino T, Lalande M, Wagstaff J (1997) UBE3A/E6-AP mutations cause Angelman syndrome. Nat Genet 15:70-73.
Kitada T, Asakawa S, Hattori N, Matsumine H, Yamamura Y, Minoshima S, Yokochi M, Mizuno Y, Shimizu N (1998) Mutations in the parkin gene cause autosomal recessive juvenile parkinsonism. 392:605-608.
Klement IA, Skinner PJ, Kaytor MD, Yi H, Hersch SM, Clark HB, Zoghbi HY, Orr HT (1998) Ataxin-1 nuclear localization and aggregation: role in polyglutamine-induced disease in SCA1 transgenic mice. Cell 95:41-53.

Klionsky DJ, Ohsumi Y (1999) Vacuolar import of proteins and organelles from the cytoplasm. Annu Rev Cell Dev Biol 15:1-32.
Klionsky DJ, Cregg JM, Dunn WA, Jr., Emr SD, Sakai Y, Sandoval IV, Sibirny A, Subramani S, Thumm M, Veenhuis M, Ohsumi Y (2003) A unified nomenclature for yeast autophagy-related genes. Dev Cell 5:539-545.
Knecht E, Aguado C, Sarkar S, Korolchuk VI, Criado-Garcia O, Vernia S, Boya P, Sanz P, Rodriguez de Cordoba S, Rubinsztein DC (2010) Impaired autophagy in Lafora disease. Autophagy 6:991-993.
Kobayashi Y, Sobue G (2001) Protective effect of chaperones on polyglutamine diseases. Brain Research Bulletin 56:165-168.
Koide R, Kobayashi S, Shimohata T, Ikeuchi T, Maruyama M, Saito M, Yamada M, Takahashi H, Tsuji S (1999) A neurological disease caused by an expanded CAG trinucleotide repeat in the TATA-binding protein gene: a new polyglutamine disease? Hum Mol Genet 8:2047-2053.
Komatsu M, Kominami E, Tanaka K (2006a) Autophagy and neurodegeneration. Autophagy 2:315-317.
Komatsu M, Wang QJ, Holstein GR, Friedrich VL, Jr., Iwata J, Kominami E, Chait BT, Tanaka K, Yue Z (2007) Essential role for autophagy protein Atg7 in the maintenance of axonal homeostasis and the prevention of axonal degeneration. Proc Natl Acad Sci U S A 104:14489-14494.
Komatsu M, Waguri S, Chiba T, Murata S, Iwata J, Tanida I, Ueno T, Koike M, Uchiyama Y, Kominami E, Tanaka K (2006b) Loss of autophagy in the central nervous system causes neurodegeneration in mice. Nature 441:880-884.
Korolchuk VI, Menzies FM, Rubinsztein DC (2010) Mechanisms of cross-talk between the ubiquitin-proteasome and autophagy-lysosome systems. FEBS Lett 584:1393-1398.
Kuzuhara S, Mori H, Izumiyama N, Yoshimura M, Ihara Y (1988) Lewy bodies are ubiquitinated. A light and electron microscopic immunocytochemical study. Acta Neuropathol 75:345-353.
La Spada AR, Wilson EM, Lubahn DB, Harding AE, Fischbeck KH (1991) Androgen receptor gene mutations in X-linked spinal and bulbar muscular atrophy. Nature 352:77-79.
Lajoie P, Snapp EL (2010) Formation and toxicity of soluble polyglutamine oligomers in living cells. PLoS One 5:e15245.
Lamark T, Kirkin V, Dikic I, Johansen T (2009) NBR1 and p62 as cargo receptors for selective autophagy of ubiquitinated targets. Cell Cycle 8:1986-1990.
Lansbury PT, Jr., Brice A (2002) Genetics of Parkinson's disease and biochemical studies of implicated gene products. Curr Opin Cell Biol 14:653-660.
Larsen CN, Krantz BA, Wilkinson KD (1998) Substrate specificity of deubiquitinating enzymes: ubiquitin C-terminal hydrolases. Biochemistry 37:3358-3368.
Lathrop RH, Casale M, Tobias DJ, Marsh JL, Thompson LM (1998) Modeling protein homopolymeric repeats: possible polyglutamine structural motifs for Huntington's disease. Proc Int Conf Intell Syst Mol Biol 6:105-114.
Layfield R, Cavey JR, Lowe J (2003) Role of ubiquitin-mediated proteolysis in the pathogenesis of neurodegenerative disorders. Ageing Res Rev 2:343-356.
Lee CK, Weindruch R, Prolla TA (2000) Gene-expression profile of the ageing brain in mice. Nat Genet 25:294-297.

Lee VM, Goedert M, Trojanowski JQ (2001) Neurodegenerative tauopathies. Annu Rev Neurosci 24:1121-1159.
Lee WC, Yoshihara M, Littleton JT (2004) Cytoplasmic aggregates trap polyglutamine-containing proteins and block axonal transport in a Drosophila model of Huntington's disease. Proc Natl Acad Sci U S A 101:3224-3229.
Legleiter J, Mitchell E, Lotz GP, Sapp E, Ng C, DiFiglia M, Thompson LM, Muchowski PJ (2010) Mutant huntingtin fragments form oligomers in a polyglutamine length-dependent manner in vitro and in vivo. J Biol Chem 285:14777-14790.
Lemasters JJ, Qian T, He L, Kim JS, Elmore SP, Cascio WE, Brenner DA (2002) Role of mitochondrial inner membrane permeabilization in necrotic cell death, apoptosis, and autophagy. Antioxid Redox Signal 4:769-781.
Lemere CA, Blusztajn JK, Yamaguchi H, Wisniewski T, Saido TC, Selkoe DJ (1996) Sequence of deposition of heterogeneous amyloid beta-peptides and APO E in Down syndrome: implications for initial events in amyloid plaque formation. Neurobiol Dis 3:16-32.
Leroy E, Boyer R, Auburger G, Leube B, Ulm G, Mezey E, Harta G, Brownstein MJ, Jonnalagada S, Chernova T, Dehejia A, Lavedan C, Gasser T, Steinbach PJ, Wilkinson KD, Polymeropoulos MH (1998) The ubiquitin pathway in Parkinson's disease. Nature 395:451-452.
Levine B, Klionsky DJ (2004) Development by self-digestion: molecular mechanisms and biological functions of autophagy. Dev Cell 6:463-477.
Li H, Wyman T, Yu ZX, Li SH, Li XJ (2003) Abnormal association of mutant huntingtin with synaptic vesicles inhibits glutamate release. Hum Mol Genet 12:2021-2030.
Li M, Brooks CL, Kon N, Gu W (2004) A dynamic role of HAUSP in the p53-Mdm2 pathway. Mol Cell 13:879-886.
Li SH, Cheng AL, Zhou H, Lam S, Rao M, Li H, Li XJ (2002) Interaction of Huntington disease protein with transcriptional activator Sp1. Mol Cell Biol 22:1277-1287.
Li X, Wang CE, Huang S, Xu X, Li XJ, Li H, Li S (2010) Inhibiting the ubiquitin-proteasome system leads to preferential accumulation of toxic N-terminal mutant huntingtin fragments. Hum Mol Genet 19:2445-2455.
Liang C, Feng P, Ku B, Oh BH, Jung JU (2007) UVRAG: a new player in autophagy and tumor cell growth. Autophagy 3:69-71.
Liang XH, Kleeman LK, Jiang HH, Gordon G, Goldman JE, Berry G, Herman B, Levine B (1998) Protection against fatal Sindbis virus encephalitis by beclin, a novel Bcl-2-interacting protein. J Virol 72:8586-8596.
Lin X, Antalffy B, Kang D, Orr HT, Zoghbi HY (2000) Polyglutamine expansion down-regulates specific neuronal genes before pathologic changes in SCA1. Nat Neurosci 3:157-163.
Lindsten K, Menendez-Benito V, Masucci MG, Dantuma NP (2003) A transgenic mouse model of the ubiquitin/proteasome system. Nat Biotechnol 21:897-902.
Liu Y, Fallon L, Lashuel HA, Liu Z, Lansbury PT, Jr. (2002) The UCH-L1 gene encodes two opposing enzymatic activities that affect alpha-synuclein degradation and Parkinson's disease susceptibility. Cell 111:209-218.
Lowe J, Mayer RJ, Landon M (1993) Ubiquitin in neurodegenerative diseases. Brain Pathol 3:55-65.

Ludolph AC, Seelig M, Ludolph AG, Sabri MI, Spencer PS (1992) ATP deficits and neuronal degeneration induced by 3-nitropropionic acid. Ann N Y Acad Sci 648:300-302.
Luthi-Carter R, Hanson SA, Strand AD, Bergstrom DA, Chun W, Peters NL, Woods AM, Chan EY, Kooperberg C, Krainc et a (2002) Dysregulation of gene expression in the R6/2 model of polyglutamine disease: parallel changes in muscle and brain. Human Molecular Genetics 11:1911-1926.
Maiuri MC, Le Toumelin G, Criollo A, Rain JC, Gautier F, Juin P, Tasdemir E, Pierron G, Troulinaki K, Tavernarakis N, Hickman JA, Geneste O, Kroemer G (2007) Functional and physical interaction between Bcl-X(L) and a BH3-like domain in Beclin-1. Embo J 26:2527-2539.
Malagelada C, Jin ZH, Jackson-Lewis V, Przedborski S, Greene LA (2010) Rapamycin protects against neuron death in in vitro and in vivo models of Parkinson's disease. J Neurosci 30:1166-1175.
Mangiarini L, Sathasivam K, Seller M, Cozens B, Harper A, Hetherington C, Lawton M, Trottier Y, Lehrach H, Davies SW, Bates GP (1996) Exon 1 of the HD gene with an expanded CAG repeat is sufficient to cause a progressive neurological phenotype in transgenic mice. Cell 87:493-506.
Markesbery WR (1997) Oxidative stress hypothesis in Alzheimer's disease. Free Radic Biol Med 23:134-147.
Maroteaux L, Campanelli JT, Scheller RH (1988) Synuclein: a neuron-specific protein localized to the nucleus and presynaptic nerve terminal. J Neurosci 8:2804-2815.
Martin-Aparicio E, Yamamoto A, Hernandez F, Hen R, Avila J, Lucas JJ (2001) Proteasomal-dependent aggregate reversal and absence of cell death in a conditional mouse model of Huntington's disease. J Neurosci 21:8772-8781.
Massey A, Kiffin R, Cuervo AM (2004) Pathophysiology of chaperone-mediated autophagy. Int J Biochem Cell Biol 36:2420-2434.
Matsuda N, Sato S, Shiba K, Okatsu K, Saisho K, Gautier CA, Sou YS, Saiki S, Kawajiri S, Sato F, Kimura M, Komatsu M, Hattori N, Tanaka K (2010) PINK1 stabilized by mitochondrial depolarization recruits Parkin to damaged mitochondria and activates latent Parkin for mitophagy. J Cell Biol 189:211-221.
Matsuzawa A, Ichijo H (2001) Molecular mechanisms of the decision between life and death: regulation of apoptosis by apoptosis signal-regulating kinase 1. J Biochem 130:1-8.
Matsuzawa A, Ichijo H (2008) Redox control of cell fate by MAP kinase: physiological roles of ASK1-MAP kinase pathway in stress signaling. Biochim Biophys Acta 1780:1325-1336.
Mayer RJ, Laszlo L, Middleton A, Landon M, Hope J, Lowe J (1992) Ubiquitin, lysosomes and neurodegenerative diseases. Biochem Soc Trans 20:645-648.
Maynard CJ, Bottcher C, Ortega Z, Smith R, Florea BI, Diaz-Hernandez M, Brundin P, Overkleeft HS, Li JY, Lucas JJ, Dantuma NP (2009) Accumulation of ubiquitin conjugates in a polyglutamine disease model occurs without global ubiquitin/proteasome system impairment. Proc Natl Acad Sci U S A 106:13986-13991.
McNaught KS, Olanow CW, Halliwell B, Isacson O, Jenner P (2001) Failure of the ubiquitin-proteasome system in Parkinson's disease. Nat Rev Neurosci 2:589-594.
Mehlen P, Hickey E, Weber LA, Arrigo AP (1997) Large unphosphorylated aggregates as the active form of hsp27 which controls intracellular reactive oxygen species and

glutathione levels and generates a protection against TNFalpha in NIH-3T3-ras cells. Biochem Biophys Res Commun 241:187-192.
Meloche S, Pouyssegur J (2007) The ERK1/2 mitogen-activated protein kinase pathway as a master regulator of the G1- to S-phase transition. Oncogene 26:3227-3239.
Michalik A, Van Broeckhoven C (2004) Proteasome degrades soluble expanded polyglutamine completely and efficiently. Neurobiology of Disease 16:202-211.
Miller J, Arrasate M, Shaby BA, Mitra S, Masliah E, Finkbeiner S (2010) Quantitative relationships between huntingtin levels, polyglutamine length, inclusion body formation, and neuronal death provide novel insight into huntington's disease molecular pathogenesis. J Neurosci 30:10541-10550.
Mishra A, Dikshit P, Purkayastha S, Sharma J, Nukina N, Jana NR (2008) E6-AP promotes misfolded polyglutamine proteins for proteasomal degradation and suppresses polyglutamine protein aggregation and toxicity. J Biol Chem 283:7648-7656.
Mitra S, Tsvetkov AS, Finkbeiner S (2009) Single neuron ubiquitin-proteasome dynamics accompanying inclusion body formation in huntington disease. J Biol Chem 284:4398-4403.
Mizushima N (2010) The role of the Atg1/ULK1 complex in autophagy regulation. Curr Opin Cell Biol 22:132-139.
Mori H, Kondo J, Ihara Y (1987) Ubiquitin is a component of paired helical filaments in Alzheimer's disease. Science 235:1641-1644.
Mukhopadhyay D, Riezman H (2007) Proteasome-independent functions of ubiquitin in endocytosis and signaling. Science 315:201-205.
Muller O, Sattler T, Flotenmeyer M, Schwarz H, Plattner H, Mayer A (2000) Autophagic tubes: vacuolar invaginations involved in lateral membrane sorting and inverse vesicle budding. J Cell Biol 151:519-528.
Nakamura K, Jeong SY, Uchihara T, Anno M, Nagashima K, Nagashima T, Ikeda S, Tsuji S, Kanazawa I (2001) SCA17, a novel autosomal dominant cerebellar ataxia caused by an expanded polyglutamine in TATA-binding protein. Hum Mol Genet 10:1441-1448.
Namgung U, Xia Z (2001) Arsenic induces apoptosis in rat cerebellar neurons via activation of JNK3 and p38 MAP kinases. Toxicol Appl Pharmacol 174:130-138.
Navon A, Goldberg AL (2001) Proteins are unfolded on the surface of the ATPase ring before transport into the proteasome. Mol Cell 8:1339-1349.
Nishitoh H, Matsuzawa A, Tobiume K, Saegusa K, Takeda K, Inoue K, Hori S, Kakizuka A, Ichijo H (2002) ASK1 is essential for endoplasmic reticulum stress-induced neuronal cell death triggered by expanded polyglutamine repeats. Genes Dev 16:1345-1355.
Nishitoh H, Kadowaki H, Nagai A, Maruyama T, Yokota T, Fukutomi H, Noguchi T, Matsuzawa A, Takeda K, Ichijo H (2008) ALS-linked mutant SOD1 induces ER stress- and ASK1-dependent motor neuron death by targeting Derlin-1. Genes Dev 22:1451-1464.
Noda T, Ohsumi Y (1998) Tor, a phosphatidylinositol kinase homologue, controls autophagy in yeast. J Biol Chem 273:3963-3966.
Nucifora FC, Jr., Sasaki M, Peters MF, Huang H, Cooper JK, Yamada M, Takahashi H, Tsuji S, Troncoso J, Dawson VL, Dawson TM, Ross CA (2001) Interference by huntingtin and atrophin-1 with cbp-mediated transcription leading to cellular toxicity. Science 291:2423-2428.

Nunomura A, Moreira PI, Lee HG, Zhu X, Castellani RJ, Smith MA, Perry G (2007) Neuronal death and survival under oxidative stress in Alzheimer and Parkinson diseases. CNS Neurol Disord Drug Targets 6:411-423.
Ono K, Han J (2000) The p38 signal transduction pathway: activation and function. Cell Signal 12:1-13.
Orlowski M, Cardozo C, Michaud C (1993) Evidence for the presence of five distinct proteolytic components in the pituitary multicatalytic proteinase complex. Properties of two components cleaving bonds on the carboxyl side of branched chain and small neutral amino acids. Biochemistry 32:1563-1572.
Orr HT (2000) The Ins and Outs of a Polyglutamine Neurodegenerative Disease: Spinocerebellar Ataxia Type 1 (SCA1). Neurobiology of Disease 7:129-134.
Orr HT (2001) Beyond the Qs in the polyglutamine diseases. Genes Dev 15:925-932.
Orr HT, Chung MY, Banfi S, Kwiatkowski TJ, Jr., Servadio A, Beaudet AL, McCall AE, Duvick LA, Ranum LP, Zoghbi HY (1993) Expansion of an unstable trinucleotide CAG repeat in spinocerebellar ataxia type 1. Nat Genet 4:221-226.
Ortega Z, Diaz-Hernandez M, Maynard CJ, Hernandez F, Dantuma NP, Lucas JJ (2010) Acute polyglutamine expression in inducible mouse model unravels ubiquitin/proteasome system impairment and permanent recovery attributable to aggregate formation. J Neurosci 30:3675-3688.
Osaka H, Wang YL, Takada K, Takizawa S, Setsuie R, Li H, Sato Y, Nishikawa K, Sun YJ, Sakurai M, Harada T, Hara Y, Kimura I, Chiba S, Namikawa K, Kiyama H, Noda M, Aoki S, Wada K (2003) Ubiquitin carboxy-terminal hydrolase L1 binds to and stabilizes monoubiquitin in neuron. Hum Mol Genet 12:1945-1958.
Palacino JJ, Sagi D, Goldberg MS, Krauss S, Motz C, Wacker M, Klose J, Shen J (2004) Mitochondrial dysfunction and oxidative damage in parkin-deficient mice. J Biol Chem 279:18614-18622.
Pankiv S, Clausen TH, Lamark T, Brech A, Bruun JA, Outzen H, Overvatn A, Bjorkoy G, Johansen T (2007) p62/SQSTM1 binds directly to Atg8/LC3 to facilitate degradation of ubiquitinated protein aggregates by autophagy. J Biol Chem 282:24131-24145.
Papa FR, Amerik AY, Hochstrasser M (1999) Interaction of the Doa4 Deubiquitinating Enzyme with the Yeast 26S Proteasome. Mol Biol Cell 10:741-756.
Papoutsaki M, Moretti F, Lanza M, Marinari B, Sartorelli V, Guerrini L, Chimenti S, Levrero M, Costanzo A (2005) A p38-dependent pathway regulates DeltaNp63 DNA binding to p53-dependent promoters in UV-induced apoptosis of keratinocytes. Oncogene 24:6970-6975.
Park J, Lee SB, Lee S, Kim Y, Song S, Kim S, Bae E, Kim J, Shong M, Kim JM, Chung J (2006) Mitochondrial dysfunction in Drosophila PINK1 mutants is complemented by parkin. Nature 441:1157-1161.
Pasinelli P, Brown RH (2006) Molecular biology of amyotrophic lateral sclerosis: insights from genetics. Nat Rev Neurosci 7:710-723.
Passos JF, Nelson G, Wang C, Richter T, Simillion C, Proctor CJ, Miwa S, Olijslagers S, Hallinan J, Wipat A, Saretzki G, Rudolph KL, Kirkwood TB, von Zglinicki T (2010) Feedback between p21 and reactive oxygen production is necessary for cell senescence. Mol Syst Biol 6:347.
Paul C, Manero F, Gonin S, Kretz-Remy C, Virot S, Arrigo AP (2002) Hsp27 as a negative regulator of cytochrome C release. Mol Cell Biol 22:816-834.

Perutz MF, Johnson T, Suzuki M, Finch JT (1994) Glutamine repeats as polar zippers: their possible role in inherited neurodegenerative diseases. Proc Natl Acad Sci U S A 91:5355-5358.

Perutz MF, Pope BJ, Owen D, Wanker EE, Scherzinger E (2002) Aggregation of proteins with expanded glutamine and alanine repeats of the glutamine-rich and asparagine-rich domains of Sup35 and of the amyloid beta-peptide of amyloid plaques. Proc Natl Acad Sci U S A 99:5596-5600.

Pickart CM, Cohen RE (2004) Proteasomes and their kin: proteases in the machine age. Nat Rev Mol Cell Biol 5:177-187.

Pickford F, Masliah E, Britschgi M, Lucin K, Narasimhan R, Jaeger PA, Small S, Spencer B, Rockenstein E, Levine B, Wyss-Coray T (2008) The autophagy-related protein beclin 1 shows reduced expression in early Alzheimer disease and regulates amyloid beta accumulation in mice. J Clin Invest 118:2190-2199.

Picklo MJ, Montine TJ, Amarnath V, Neely MD (2002) Carbonyl toxicology and Alzheimer's disease. Toxicol Appl Pharmacol 184:187-197.

Pikkarainen M, Hartikainen P, Soininen H, Alafuzoff I (2011) Distribution and Pattern of Pathology in Subjects with Familial or Sporadic Late-Onset Cerebellar Ataxia as Assessed by p62/Sequestosome Immunohistochemistry. Cerebellum.

Poirier MA, Li H, Macosko J, Cai S, Amzel M, Ross CA (2002) Huntingtin spheroids and protofibrils as precursors in polyglutamine fibrilization. J Biol Chem 277:41032-41037.

Poizat C, Puri PL, Bai Y, Kedes L (2005) Phosphorylation-dependent degradation of p300 by doxorubicin-activated p38 mitogen-activated protein kinase in cardiac cells. Mol Cell Biol 25:2673-2687.

Polymeropoulos MH, Lavedan C, Leroy E, Ide SE, Dehejia A, Dutra A, Pike B, Root H, Rubenstein J, Boyer R, Stenroos ES, Chandrasekharappa S, Athanassiadou A, Papapetropoulos T, Johnson WG, Lazzarini AM, Duvoisin RC, Di Iorio G, Golbe LI, Nussbaum RL (1997) Mutation in the alpha-synuclein gene identified in families with Parkinson's disease. Science 276:2045-2047.

Preville X, Salvemini F, Giraud S, Chaufour S, Paul C, Stepien G, Ursini MV, Arrigo AP (1999) Mammalian small stress proteins protect against oxidative stress through their ability to increase glucose-6-phosphate dehydrogenase activity and by maintaining optimal cellular detoxifying machinery. Exp Cell Res 247:61-78.

Proctor CJ, Gray DA (2008) Explaining oscillations and variability in the p53-Mdm2 system. BMC Syst Biol 2:75.

Proctor CJ, Lorimer IA (2011) Modelling the role of the Hsp70/Hsp90 system in the maintenance of protein homeostasis. PLoS One 6:e22038.

Proctor CJ, Tsirigotis M, Gray DA (2007) An in silico model of the ubiquitin-proteasome system that incorporates normal homeostasis and age-related decline. BMC Syst Biol 1:17.

Proctor CJ, Soti C, Boys RJ, Gillespie CS, Shanley DP, Wilkinson DJ, Kirkwood TB (2005) Modelling the actions of chaperones and their role in ageing. Mech Ageing Dev 126:119-131.

Quintanilla RA, Johnson GV (2009) Role of mitochondrial dysfunction in the pathogenesis of Huntington's disease. Brain Res Bull 80:242-247.

Raoul C, Estevez AG, Nishimune H, Cleveland DW, deLapeyriere O, Henderson CE, Haase G, Pettmann B (2002) Motoneuron death triggered by a specific pathway downstream of Fas. potentiation by ALS-linked SOD1 mutations. Neuron 35:1067-1083.

Ravikumar B, Duden R, Rubinsztein DC (2002) Aggregate-prone proteins with polyglutamine and polyalanine expansions are degraded by autophagy. Hum Mol Genet 11:1107-1117.

Ravikumar B, Vacher C, Berger Z, Davies JE, Luo S, Oroz LG, Scaravilli F, Easton DF, Duden R, O'Kane CJ, Rubinsztein DC (2004) Inhibition of mTOR induces autophagy and reduces toxicity of polyglutamine expansions in fly and mouse models of Huntington disease. Nat Genet 36:585-595.

Ravikumar B, Futter M, Jahreiss L, Korolchuk VI, Lichtenberg M, Luo S, Massey DC, Menzies FM, Narayanan U, Renna M, Jimenez-Sanchez M, Sarkar S, Underwood B, Winslow A, Rubinsztein DC (2009) Mammalian macroautophagy at a glance. J Cell Sci 122:1707-1711.

Rideout HJ, Lang-Rollin I, Stefanis L (2004) Involvement of macroautophagy in the dissolution of neuronal inclusions. Int J Biochem Cell Biol 36:2551-2562.

Robinson MJ, Cobb MH (1997) Mitogen-activated protein kinase pathways. Curr Opin Cell Biol 9:180-186.

Rodriguez KA, Gaczynska M, Osmulski PA (2010) Molecular mechanisms of proteasome plasticity in aging. Mech Ageing Dev 131:144-155.

Rogalla T, Ehrnsperger M, Preville X, Kotlyarov A, Lutsch G, Ducasse C, Paul C, Wieske M, Arrigo AP, Buchner J, Gaestel M (1999) Regulation of Hsp27 oligomerization, chaperone function, and protective activity against oxidative stress/tumor necrosis factor alpha by phosphorylation. J Biol Chem 274:18947-18956.

Rose C, Menzies FM, Renna M, Acevedo-Arozena A, Corrochano S, Sadiq O, Brown SD, Rubinsztein DC (2010) Rilmenidine attenuates toxicity of polyglutamine expansions in a mouse model of Huntington's disease. Hum Mol Genet 19:2144-2153.

Rosen DR, Siddique T, Patterson D, Figlewicz DA, Sapp P, Hentati A, Donaldson D, Goto J, O'Regan JP, Deng HX, et al. (1993) Mutations in Cu/Zn superoxide dismutase gene are associated with familial amyotrophic lateral sclerosis. Nature 362:59-62.

Ross CA (2002) Polyglutamine pathogenesis: emergence of unifying mechanisms for Huntington's disease and related disorders. Neuron 35:819-822.

Ross CA, Poirier MA (2004) Protein aggregation and neurodegenerative disease. Nat Med 10 Suppl:S10-17.

Rubinsztein DC (2006) The roles of intracellular protein-degradation pathways in neurodegeneration. Nature 443:780-786.

Ryu K-Y, Garza JC, Lu X-Y, Barsh GS, Kopito RR (2008) Hypothalamic neurodegeneration and adult-onset obesity in mice lacking the Ubb polyubiquitin gene. Proceedings of the National Academy of Sciences 105:4016-4021.

Saeki Y, Kudo T, Sone T, Kikuchi Y, Yokosawa H, Toh-e A, Tanaka K (2009) Lysine 63-linked polyubiquitin chain may serve as a targeting signal for the 26S proteasome. Embo J 28:359-371.

Saigoh K, Wang YL, Suh JG, Yamanishi T, Sakai Y, Kiyosawa H, Harada T, Ichihara N, Wakana S, Kikuchi T, Wada K (1999) Intragenic deletion in the gene encoding ubiquitin carboxy-terminal hydrolase in gad mice. Nat Genet 23:47-51.

Sanchez I, Mahlke C, Yuan J (2003) Pivotal role of oligomerization in expanded polyglutamine neurodegenerative disorders. Nature 421:373-379.
Sarkar S, Krishna G, Imarisio S, Saiki S, O'Kane CJ, Rubinsztein DC (2008) A rational mechanism for combination treatment of Huntington's disease using lithium and rapamycin. Hum Mol Genet 17:170-178.
Saudou F, Finkbeiner S, Devys D, Greenberg ME (1998) Huntingtin acts in the nucleus to induce apoptosis but death does not correlate with the formation of intranuclear inclusions. Cell 95:55-66.
Schaffar G, Breuer P, Boteva R, Behrends C, Tzvetkov N, Strippel N, Sakahira H, Siegers K, Hayer-Hartl M, Hartl FU (2004) Cellular Toxicity of Polyglutamine Expansion Proteins: Mechanism of Transcription Factor Deactivation. Molecular Cell 15:95-105.
Schubert U, Anton LC, Gibbs J, Norbury CC, Yewdell JW, Bennink JR (2000) Rapid degradation of a large fraction of newly synthesized proteins by proteasomes. Nature 404:770-774.
Selkoe DJ (1994) Cell biology of the amyloid beta-protein precursor and the mechanism of Alzheimer's disease. Annu Rev Cell Biol 10:373-403.
Selkoe DJ (2001) Alzheimer's disease: genes, proteins, and therapy. Physiol Rev 81:741-766.
Selkoe DJ (2004) Cell biology of protein misfolding: the examples of Alzheimer's and Parkinson's diseases. Nat Cell Biol 6:1054-1061.
Seong IS, Ivanova E, Lee JM, Choo YS, Fossale E, Anderson M, Gusella JF, Laramie JM, Myers RH, Lesort M, MacDonald ME (2005) HD CAG repeat implicates a dominant property of huntingtin in mitochondrial energy metabolism. Hum Mol Genet 14:2871-2880.
Setsuie R, Wang YL, Mochizuki H, Osaka H, Hayakawa H, Ichihara N, Li H, Furuta A, Sano Y, Sun YJ, Kwon J, Kabuta T, Yoshimi K, Aoki S, Mizuno Y, Noda M, Wada K (2007) Dopaminergic neuronal loss in transgenic mice expressing the Parkinson's disease-associated UCH-L1 I93M mutant. Neurochem Int 50:119-129.
Shaulian E, Karin M (2001) AP-1 in cell proliferation and survival. Oncogene 20:2390-2400.
Shibata M, Lu T, Furuya T, Degterev A, Mizushima N, Yoshimori T, MacDonald M, Yankner B, Yuan J (2006) Regulation of intracellular accumulation of mutant Huntingtin by Beclin 1. J Biol Chem 281:14474-14485.
Shimura H, Schlossmacher MG, Hattori N, Frosch MP, Trockenbacher A, Schneider R, Mizuno Y, Kosik KS, Selkoe DJ (2001) Ubiquitination of a new form of alpha-synuclein by parkin from human brain: implications for Parkinson's disease. Science 293:263-269.
Shimura H, Hattori N, Kubo S, Mizuno Y, Asakawa S, Minoshima S, Shimizu N, Iwai K, Chiba T, Tanaka K, Suzuki T (2000) Familial Parkinson disease gene product, parkin, is a ubiquitin-protein ligase. Nat Genet 25:302-305.
Simeoni S, Mancini MA, Stenoien DL, Marcelli M, Weigel NL, Zanisi M, Martini L, Poletti A (2000) Motoneuronal cell death is not correlated with aggregate formation of androgen receptors containing an elongated polyglutamine tract. Hum Mol Genet 9:133-144.
Simmons DA, Casale M, Alcon B, Pham N, Narayan N, Lynch G (2007) Ferritin accumulation in dystrophic microglia is an early event in the development of Huntington's disease. Glia 55:1074-1084.

Singleton AB, Farrer M, Johnson J, Singleton A, Hague S, Kachergus J, Hulihan M, Peuralinna T, Dutra A, Nussbaum R, Lincoln S, Crawley A, Hanson M, Maraganore D, Adler C, Cookson MR, Muenter M, Baptista M, Miller D, Blancato J, Hardy J, Gwinn-Hardy K (2003) alpha-Synuclein locus triplication causes Parkinson's disease. Science 302:841.

Smith DM, Kafri G, Cheng Y, Ng D, Walz T, Goldberg AL (2005) ATP binding to PAN or the 26S ATPases causes association with the 20S proteasome, gate opening, and translocation of unfolded proteins. Mol Cell 20:687-698.

Smith MA, Richey Harris PL, Sayre LM, Beckman JS, Perry G (1997) Widespread peroxynitrite-mediated damage in Alzheimer's disease. J Neurosci 17:2653-2657.

Soboleva TA, Baker RT (2004) Deubiquitinating enzymes: their functions and substrate specificity. Curr Protein Pept Sci 5:191-200.

Sohal RS (2002) Role of oxidative stress and protein oxidation in the aging process. Free Radic Biol Med 33:37-44.

Song W, Chen J, Petrilli A, Liot G, Klinglmayr E, Zhou Y, Poquiz P, Tjong J, Pouladi MA, Hayden MR, Masliah E, Ellisman M, Rouiller I, Schwarzenbacher R, Bossy B, Perkins G, Bossy-Wetzel E (2011) Mutant huntingtin binds the mitochondrial fission GTPase dynamin-related protein-1 and increases its enzymatic activity. Nat Med 17:377-382.

Songyang Z, Blechner S, Hoagland N, Hoekstra MF, Piwnica-Worms H, Cantley LC (1994) Use of an oriented peptide library to determine the optimal substrates of protein kinases. Curr Biol 4:973-982.

Songyang Z, Lu KP, Kwon YT, Tsai LH, Filhol O, Cochet C, Brickey DA, Soderling TR, Bartleson C, Graves DJ, DeMaggio AJ, Hoekstra MF, Blenis J, Hunter T, Cantley LC (1996) A structural basis for substrate specificities of protein Ser/Thr kinases: primary sequence preference of casein kinases I and II, NIMA, phosphorylase kinase, calmodulin-dependent kinase II, CDK5, and Erk1. Mol Cell Biol 16:6486-6493.

Spillantini MG, Crowther RA, Jakes R, Hasegawa M, Goedert M (1998) alpha-Synuclein in filamentous inclusions of Lewy bodies from Parkinson's disease and dementia with lewy bodies. Proc Natl Acad Sci U S A 95:6469-6473.

Spilman P, Podlutskaya N, Hart MJ, Debnath J, Gorostiza O, Bredesen D, Richardson A, Strong R, Galvan V (2010) Inhibition of mTOR by rapamycin abolishes cognitive deficits and reduces amyloid-beta levels in a mouse model of Alzheimer's disease. PLoS One 5:e9979.

Steffan JS, Bodai L, Pallos J, Poelman M, McCampbell A, Apostol BL, Kazantsev A, Schmidt E, Zhu YZ, Greenwald M, Kurokawa R, Housman DE, Jackson GR, Marsh JL, Thompson LM (2001) Histone deacetylase inhibitors arrest polyglutamine-dependent neurodegeneration in Drosophila. Nature 413:739-743.

Stokoe D, Engel K, Campbell DG, Cohen P, Gaestel M (1992) Identification of MAPKAP kinase 2 as a major enzyme responsible for the phosphorylation of the small mammalian heat shock proteins. FEBS Lett 313:307-313.

Strong TV, Tagle DA, Valdes JM, Elmer LW, Boehm K, Swaroop M, Kaatz KW, Collins FS, Albin RL (1993) Widespread expression of the human and rat Huntington's disease gene in brain and nonneural tissues. Nat Genet 5:259-265.

Subramaniam S, Unsicker K (2006) Extracellular signal-regulated kinase as an inducer of non-apoptotic neuronal death. Neuroscience 138:1055-1065.

Subramaniam S, Unsicker K (2010) ERK and cell death: ERK1/2 in neuronal death. Febs J 277:22-29.
Subramaniam S, Zirrgiebel U, von Bohlen Und Halbach O, Strelau J, Laliberte C, Kaplan DR, Unsicker K (2004) ERK activation promotes neuronal degeneration predominantly through plasma membrane damage and independently of caspase-3. J Cell Biol 165:357-369.
Sugars KL, Brown R, J. Cook L, Swartz J, Rubinsztein DC (2004a) Decreased cAMP Response Element-mediated Transcription: AN EARLY EVENT IN EXON 1 AND FULL-LENGTH CELL MODELS OF HUNTINGTON'S DISEASE THAT CONTRIBUTES TO POLYGLUTAMINE PATHOGENESIS
10.1074/jbc.M310226200. J Biol Chem 279:4988-4999.
Sugars KL, Brown R, Cook LJ, Swartz J, Rubinsztein DC (2004b) Decreased cAMP response element-mediated transcription: an early event in exon 1 and full-length cell models of Huntington's disease that contributes to polyglutamine pathogenesis. J Biol Chem 279:4988-4999.
Sullivan PG, Dragicevic NB, Deng JH, Bai Y, Dimayuga E, Ding Q, Chen Q, Bruce-Keller AJ, Keller JN (2004) Proteasome inhibition alters neural mitochondrial homeostasis and mitochondria turnover. J Biol Chem 279:20699-20707.
Sun A, Liu M, Nguyen XV, Bing G (2003) P38 MAP kinase is activated at early stages in Alzheimer's disease brain. Exp Neurol 183:394-405.
Sun XM, Butterworth M, MacFarlane M, Dubiel W, Ciechanover A, Cohen GM (2004) Caspase activation inhibits proteasome function during apoptosis. Mol Cell 14:81-93.
Sun Z-W, Allis CD (2002) Ubiquitination of histone H2B regulates H3 methylation and gene silencing in yeast. Nature 418:104-108.
Suzuki K, Kirisako T, Kamada Y, Mizushima N, Noda T, Ohsumi Y (2001) The pre-autophagosomal structure organized by concerted functions of APG genes is essential for autophagosome formation. Embo J 20:5971-5981.
Suzuki N, Cheung TT, Cai XD, Odaka A, Otvos L, Jr., Eckman C, Golde TE, Younkin SG (1994) An increased percentage of long amyloid beta protein secreted by familial amyloid beta protein precursor (beta APP717) mutants. Science 264:1336-1340.
Swayne LA, Chen L, Hameed S, Barr W, Charlesworth E, Colicos MA, Zamponi GW, Braun JEA (2005) Crosstalk between huntingtin and syntaxin 1A regulates N-type calcium channels. Molecular and Cellular Neuroscience 30:339-351.
Tabrizi SJ, Workman J, Hart PE, Mangiarini L, Mahal A, Bates G, Cooper JM, Schapira AH (2000) Mitochondrial dysfunction and free radical damage in the Huntington R6/2 transgenic mouse. Ann Neurol 47:80-86.
Takahashi T, Katada S, Onodera O (2010) Polyglutamine diseases: where does toxicity come from? what is toxicity? where are we going? J Mol Cell Biol 2:180-191.
Takahashi T, Kikuchi S, Katada S, Nagai Y, Nishizawa M, Onodera O (2008) Soluble polyglutamine oligomers formed prior to inclusion body formation are cytotoxic. Hum Mol Genet 17:345-356.
Tan JM, Wong ES, Dawson VL, Dawson TM, Lim KL (2007) Lysine 63-linked polyubiquitin potentially partners with p62 to promote the clearance of protein inclusions by autophagy. Autophagy 4.

Tan Y, Rouse J, Zhang A, Cariati S, Cohen P, Comb MJ (1996) FGF and stress regulate CREB and ATF-1 via a pathway involving p38 MAP kinase and MAPKAP kinase-2. Embo J 15:4629-4642.

Tare M, Modi RM, Nainaparampil JJ, Puli OR, Bedi S, Fernandez-Funez P, Kango-Singh M, Singh A (2011) Activation of JNK Signaling Mediates Amyloid-ss-Dependent Cell Death. PLoS One 6:e24361.

Taylor JP, Tanaka F, Robitschek J, Sandoval CM, Taye A, Markovic-Plese S, Fischbeck KH (2003) Aggresomes protect cells by enhancing the degradation of toxic polyglutamine-containing protein. Hum Mol Genet 12:749-757.

Terman A, Brunk UT (2004) Myocyte aging and mitochondrial turnover. Exp Gerontol 39:701-705.

Thrower JS, Hoffman L, Rechsteiner M, Pickart CM (2000) Recognition of the polyubiquitin proteolytic signal. Embo J 19:94-102.

Tobias J, Varshavsky A (1991) Cloning and functional analysis of the ubiquitin-specific protease gene UBP1 of Saccharomyces cerevisiae. J Biol Chem 266:12021-12028.

Tournier C, Hess P, Yang DD, Xu J, Turner TK, Nimnual A, Bar-Sagi D, Jones SN, Flavell RA, Davis RJ (2000) Requirement of JNK for stress-induced activation of the cytochrome c-mediated death pathway. Science 288:870-874.

Trushina E, Dyer RB, Badger JD, 2nd, Ure D, Eide L, Tran DD, Vrieze BT, Legendre-Guillemin V, McPherson PS, Mandavilli BS, Van Houten B, Zeitlin S, McNiven M, Aebersold R, Hayden M, Parisi JE, Seeberg E, Dragatsis I, Doyle K, Bender A, Chacko C, McMurray CT (2004) Mutant huntingtin impairs axonal trafficking in mammalian neurons in vivo and in vitro. Mol Cell Biol 24:8195-8209.

Tsai CC, Kao HY, Mitzutani A, Banayo E, Rajan H, McKeown M, Evans RM (2004) Ataxin 1, a SCA1 neurodegenerative disorder protein, is functionally linked to the silencing mediator of retinoid and thyroid hormone receptors. Proc Natl Acad Sci U S A 101:4047-4052.

Tsai YC, Fishman PS, Thakor NV, Oyler GA (2003) Parkin facilitates the elimination of expanded polyglutamine proteins and leads to preservation of proteasome function. J Biol Chem 278:22044-22055.

Tsirigotis M, Baldwin RM, Tang MY, Lorimer IA, Gray DA (2008) Activation of p38MAPK contributes to expanded polyglutamine-induced cytotoxicity. PLoS ONE 3:e2130.

Tsirigotis M, Tang MY, Beyers M, Zhang M, Woulfe J, Gray DA (2006) Delayed spinocerebellar ataxia in transgenic mice expressing mutant ubiquitin. Neuropathol Appl Neurobiol 32:26-39.

Tsuda H, Jafar-Nejad H, Patel AJ, Sun Y, Chen H-K, Rose MF, Venken KJT, Botas J, Orr HT, Bellen HJ, Zoghbi HY (2005) The AXH Domain of Ataxin-1 Mediates Neurodegeneration through Its Interaction with Gfi-1/Senseless Proteins. Cell 122:633-644.

Tsvetkov AS, Miller J, Arrasate M, Wong JS, Pleiss MA, Finkbeiner S (2010) A small-molecule scaffold induces autophagy in primary neurons and protects against toxicity in a Huntington disease model. Proc Natl Acad Sci U S A 107:16982-16987.

Uchihara T, Fujigasaki H, Koyano S, Nakamura A, Yagishita S, Iwabuchi K (2001) Non-expanded polyglutamine proteins in intranuclear inclusions of hereditary ataxias--triple-labeling immunofluorescence study. Acta Neuropathol 102:149-152.

Ulrich HD, Walden H (2010) Ubiquitin signalling in DNA replication and repair. Nat Rev Mol Cell Biol 11:479-489.
Valente EM, Abou-Sleiman PM, Caputo V, Muqit MM, Harvey K, Gispert S, Ali Z, Del Turco D, Bentivoglio AR, Healy DG, Albanese A, Nussbaum R, Gonzalez-Maldonado R, Deller T, Salvi S, Cortelli P, Gilks WP, Latchman DS, Harvey RJ, Dallapiccola B, Auburger G, Wood NW (2004) Hereditary early-onset Parkinson's disease caused by mutations in PINK1. Science 304:1158-1160.
Vassar R, Citron M (2000) Abeta-generating enzymes: recent advances in beta- and gamma-secretase research. Neuron 27:419-422.
Venkatraman P, Wetzel R, Tanaka M, Nukina N, Goldberg AL (2004) Eukaryotic proteasomes cannot digest polyglutamine sequences and release them during degradation of polyglutamine-containing proteins. Mol Cell 14:95-104.
Verhoef LG, Lindsten K, Masucci MG, Dantuma NP (2002) Aggregate formation inhibits proteasomal degradation of polyglutamine proteins. Hum Mol Genet 11:2689-2700.
Vernace VA, Schmidt-Glenewinkel T, Figueiredo-Pereira ME (2007) Aging and regulated protein degradation: who has the UPPer hand? Aging Cell 6:599-606.
Vives-Bauza C, Zhou C, Huang Y, Cui M, de Vries RL, Kim J, May J, Tocilescu MA, Liu W, Ko HS, Magrane J, Moore DJ, Dawson VL, Grailhe R, Dawson TM, Li C, Tieu K, Przedborski S (2010) PINK1-dependent recruitment of Parkin to mitochondria in mitophagy. Proc Natl Acad Sci U S A 107:378-383.
Waelter S, Boeddrich A, Lurz R, Scherzinger E, Lueder G, Lehrach H, Wanker EE (2001) Accumulation of Mutant Huntingtin Fragments in Aggresome-like Inclusion Bodies as a Result of Insufficient Protein Degradation. Mol Biol Cell 12:1393-1407.
Wang H, Lim PJ, Karbowski M, Monteiro MJ (2009a) Effects of overexpression of huntingtin proteins on mitochondrial integrity. Hum Mol Genet 18:737-752.
Wang QJ, Ding Y, Kohtz DS, Mizushima N, Cristea IM, Rout MP, Chait BT, Zhong Y, Heintz N, Yue Z (2006) Induction of autophagy in axonal dystrophy and degeneration. J Neurosci 26:8057-8068.
Wang T, Lao U, Edgar BA (2009b) TOR-mediated autophagy regulates cell death in Drosophila neurodegenerative disease. J Cell Biol 186:703-711.
Wang X, McGowan CH, Zhao M, He L, Downey JS, Fearns C, Wang Y, Huang S, Han J (2000) Involvement of the MKK6-p38gamma cascade in gamma-radiation-induced cell cycle arrest. Mol Cell Biol 20:4543-4552.
Waters S, Marchbank K, Solomon E, Whitehouse C, Gautel M (2009) Interactions with LC3 and polyubiquitin chains link nbr1 to autophagic protein turnover. FEBS Lett 583:1846-1852.
Webb JL, Ravikumar B, Atkins J, Skepper JN, Rubinsztein DC (2003) Alpha-Synuclein is degraded by both autophagy and the proteasome. J Biol Chem 278:25009-25013.
Webber JL, Tooze SA (2010) Coordinated regulation of autophagy by p38alpha MAPK through mAtg9 and p38IP. Embo J 29:27-40.
Williams AJ, Paulson HL (2008) Polyglutamine neurodegeneration: protein misfolding revisited. Trends Neurosci 31:521-528.
Wong E, Cuervo AM (2010) Autophagy gone awry in neurodegenerative diseases. Nat Neurosci 13:805-811.

Wooten MW, Geetha T, Babu JR, Seibenhener ML, Peng J, Cox N, Diaz-Meco MT, Moscat J (2008) Essential role of sequestosome 1/p62 in regulating accumulation of Lys63-ubiquitinated proteins. J Biol Chem 283:6783-6789.
Woulfe J (2008) Nuclear bodies in neurodegenerative disease. Biochim Biophys Acta 1783:2195-2206.
Woulfe JM (2007) Abnormalities of the nucleus and nuclear inclusions in neurodegenerative disease: a work in progress. Neuropathol Appl Neurobiol 33:2-42.
Wyttenbach A, Sauvageot O, Carmichael J, Diaz-Latoud C, Arrigo A-P, Rubinsztein DC (2002) Heat shock protein 27 prevents cellular polyglutamine toxicity and suppresses the increase of reactive oxygen species caused by huntingtin
10.1093/hmg/11.9.1137. Hum Mol Genet 11:1137-1151.
Wyttenbach A, Carmichael J, Swartz J, Furlong RA, Narain Y, Rankin J, Rubinsztein DC (2000) Effects of heat shock, heat shock protein 40 (HDJ-2), and proteasome inhibition on protein aggregation in cellular models of Huntington's disease. Proc Natl Acad Sci U S A 97:2898-2903.
Xia Z, Dickens M, Raingeaud J, Davis RJ, Greenberg ME (1995) Opposing effects of ERK and JNK-p38 MAP kinases on apoptosis. Science 270:1326-1331.
Yamamoto A, Lucas JJ, Hen R (2000) Reversal of neuropathology and motor dysfunction in a conditional model of Huntington's disease. Cell 101:57-66.
Yan L, Vatner DE, O'Connor JP, Ivessa A, Ge H, Chen W, Hirotani S, Ishikawa Y, Sadoshima J, Vatner SF (2007) Type 5 adenylyl cyclase disruption increases longevity and protects against stress. Cell 130:247-258.
Yang D, Wang CE, Zhao B, Li W, Ouyang Z, Liu Z, Yang H, Fan P, O'Neill A, Gu W, Yi H, Li S, Lai L, Li XJ (2010) Expression of Huntington's disease protein results in apoptotic neurons in the brains of cloned transgenic pigs. Hum Mol Genet 19:3983-3994.
Ye Y, Rape M (2009) Building ubiquitin chains: E2 enzymes at work. 10:755-764.
Yeste-Velasco M, Folch J, Pallas M, Camins A (2009) The p38(MAPK) signaling pathway regulates neuronal apoptosis through the phosphorylation of the retinoblastoma protein. Neurochem Int 54:99-105.
Yoo SY, Pennesi ME, Weeber EJ, Xu B, Atkinson R, Chen S, Armstrong DL, Wu SM, Sweatt JD, Zoghbi HY (2003) SCA7 knockin mice model human SCA7 and reveal gradual accumulation of mutant ataxin-7 in neurons and abnormalities in short-term plasticity. Neuron 37:383-401.
Yorimitsu T, Klionsky DJ (2005) Autophagy: molecular machinery for self-eating. Cell Death Differ 12 Suppl 2:1542-1552.
Yue S, Serra HG, Zoghbi HY, Orr HT (2001) The spinocerebellar ataxia type 1 protein, ataxin-1, has RNA-binding activity that is inversely affected by the length of its polyglutamine tract. Hum Mol Genet 10:25-30.
Zhang DX, Gutterman DD (2007) Mitochondrial reactive oxygen species-mediated signaling in endothelial cells. Am J Physiol Heart Circ Physiol 292:H2023-2031.
Zhang H, Li Q, Graham RK, Slow E, Hayden MR, Bezprozvanny I (2008) Full length mutant huntingtin is required for altered Ca2+ signaling and apoptosis of striatal neurons in the YAC mouse model of Huntington's disease. Neurobiol Dis 31:80-88.
Zhang J, Campbell RE, Ting AY, Tsien RY (2002a) Creating new fluorescent probes for cell biology. Nat Rev Mol Cell Biol 3:906-918.

Zhang S, Xu L, Lee J, Xu T (2002b) Drosophila atrophin homolog functions as a transcriptional corepressor in multiple developmental processes. Cell 108:45-56.
Zhang X, Li L, Chen S, Yang D, Wang Y, Wang Z, Le W (2011) Rapamycin treatment augments motor neuron degeneration in SOD1(G93A) mouse model of amyotrophic lateral sclerosis. Autophagy 7:412-425.
Zhou G, Bao ZQ, Dixon JE (1995) Components of a new human protein kinase signal transduction pathway. J Biol Chem 270:12665-12669.
Zhu X, Rottkamp CA, Boux H, Takeda A, Perry G, Smith MA (2000) Activation of p38 kinase links tau phosphorylation, oxidative stress, and cell cycle-related events in Alzheimer disease. J Neuropathol Exp Neurol 59:880-888.
Zhu X, Mei M, Lee HG, Wang Y, Han J, Perry G, Smith MA (2005) P38 activation mediates amyloid-beta cytotoxicity. Neurochem Res 30:791-796.
Zhu X, Rottkamp CA, Hartzler A, Sun Z, Takeda A, Boux H, Shimohama S, Perry G, Smith MA (2001) Activation of MKK6, an upstream activator of p38, in Alzheimer's disease. J Neurochem 79:311-318.
Zhuchenko O, Bailey J, Bonnen P, Ashizawa T, Stockton DW, Amos C, Dobyns WB, Subramony SH, Zoghbi HY, Lee CC (1997) Autosomal dominant cerebellar ataxia (SCA6) associated with small polyglutamine expansions in the alpha 1A-voltage-dependent calcium channel. Nat Genet 15:62-69.
Zimmerman MC, Oberley LW, Flanagan SW (2007) Mutant SOD1-induced neuronal toxicity is mediated by increased mitochondrial superoxide levels. J Neurochem 102:609-618.
Zu T, Duvick LA, Kaytor MD, Berlinger MS, Zoghbi HY, Clark HB, Orr HT (2004) Recovery from polyglutamine-induced neurodegeneration in conditional SCA1 transgenic mice. J Neurosci 24:8853-8861.

STATEMENT OF CONTRIBUTION TO COLLABORATORS

All computer modeling results were generated by Dr. Carole Proctor at the University of Newcastle, Newcastle upon Tyne, United Kingdom. Drs. Maria Tsirigotis and R. Mitchell Baldwin assisted in the western blot analysis for phospho-p38MAPK, ERK and AFP. The NIH-3T3 GFP^{u} stable cell line was generated by Dr. Maria Tsirigotis. Cell survival by MTT analysis was either performed or assisted by Dr. R. Mitchell Baldwin. Mei Zhang assisted in the immunohistochemistry described in the thesis. Madison Gray assisted with the glutathione analysis. Schematic representation of the stochastic computer model, and the proposed model of expanded polyglutamine induced cytotoxicity were created in Adobe Illustrator by Dr. Douglas Gray.

APPENDIX 1. Stochastic model supplemental information

1.1 Fitting the model to experimental data

The model has 47 parameters but only a small set of these were used to fit the model to experimental data. These parameters are listed in Appendix 1 Table 4. The table also indicates which parameters effect aggregation kinetics, cell death or mRFPu levels. We began by fitting the model under normal conditions (addition of PolyQ without any other treatments) to the time course data for inclusion formation. Since the data corresponds to proportions of many cells, we ran the model 100 times initially and calculated the proportion of "simulated cells" with inclusions at the same time points. This was repeated many times until the best set of parameters was found. The parameters for cell death were adjusted to fit the experimental data in a similar way to the aggregation kinetic parameters. Finally we used the kinetic data for the levels of $mRFP^u$. In order to establish the level of $mRFP^u$ detection, we ran the model without PolyQ as under these conditions $mRFP^u$ is undetectable. The mean level of $mRFP^u$ is 300 but due to random fluctuations it can vary between 200 and 400. So we set a value of 400 as the threshold for detection.

After finding the best fit of the model to the data of untreated cells we mimicked the experiments of inhibiting the proteasome at 24h by adding an event to the model (see Appendix 1 Table S3). We then compared the model outcome with the experimental data. Originally the model did not closely match this data and so we adjusted parameters that affected inclusion formation and cell death, concentrating on those that were particularly affected by the proteasome e.g. rate of proteasome binding by aggregates. When we obtained a reasonable match we then redid the simulations with simulated untreated cells to check. Finally we validated the model with data for p38MAPK inhibition. In the initial stages of model building we did not include a feedback loop from p38MAPK to ROS i.e. the reaction for ROS generation by p38MAPK was not included. However, we found that we could not initially fit the model to the data with p38MAPK. A recent paper showed that a feedback between p38MAPK and ROS is necessary for cell senescence and so we decided to try and include this reaction in our current model. This enabled us to fit the data for all experimental conditions. In order to verify that this additional reaction is necessary, we also fitted the model without the loop to the experimental data for the addition of HttQ103 without any treatments and then ran the model for the inhibition experiments (Figure 34).

The model fitting was quite time-consuming to do but we plan to use a more automated approach in future using Bayesian approaches with the Calibayes system which has been developed at Newcastle University. Currently the system handles fitting model parameters to data for single cell time course experiments but it will be possible to adapt the software to handle population kinetic data.

1.2 Parameter values not used for model fitting.

The majority of parameter values were obtained from the literature or based on previous models and as they were not directly involved in aggregation or cell death pathways we did not use these to fit the model. We will now give a brief description of these parameters.

The parameters for the turnover of PolyQ and mRFP^{u} were set according to their half-lives which we assumed to be 20 hours and 30 minutes respectively when the proteasome is not inhibited. We assume that PolyQ is more difficult for the proteasome to degrade than mRFPu so that $k_{degPolyQ} < k_{degmRFPu}$. The parameter which has most affect on the half-life is the rate of binding of the protein to the proteasome ($k_{binPolyQProt}$ and $k_{binmRFPuProt}$). We set the synthesis rate of each protein to zero and adjusted the parameters for proteasome binding to achieve the desired half-life. Then we set the parameters for protein synthesis so that protein levels remain constant over time (there will be variability in the levels due to stochastic simulation but the mean level is constant). We also include a pool of generic protein which may misfold and either be refolded or degraded. We assumed that half-life of this protein pool was about 10 hours, that refolding and degradation occurred at about the same order of magnitude with slightly more refolding taking place. With these assumptions we were able to set the parameters for misfolding, refolding, binding to the proteasome and degradation. We also assumed that misfolded protein could aggregate but only if levels of misfolded protein are high, so that the rate of aggregation is set very low (three orders of magnitude lower than PolyQ). We assume that there is basal turnover of ROS and set the parameters for generation and removal of ROS so that the half-life is about 1 hour and the mean level of basal ROS (under conditions of no aggregation) is 10.

There are three dummy parameters in the model. First we include a parameter called k_{alive} in every reaction so that when cell death occurs the value of this parameter is changed from 1 to zero. This prevents any further reactions occurring after a cell death. The parameter $k_{proteff}$ is present in all the protein degradation reactions and is initially set to 1. The value of this parameter is reduced by a SBML event (see Appebdix 1 Table S3) to mimic a reduction in proteasome efficiency when proteasome inhibitor is added. Finally the parameter k_{p38act} allows p38MAPK activity to be reduced when p38 inhibitor is added. In the computer experiments for p38MAPK inhibition we set k_{p38act}=0.05 at the beginning of the simulation.

1.3 Comparison of model output to data by Olshina et al.

A study has recently been published in which the authors tracked mutant huntingtin aggregation in cells using sedimentation velocity analysis. They found that mutant huntingtin formed three major pools: monomers, oligomers and inclusion bodies. Interestingly, they found that the oligomer pool in proportion of total huntingtin did not

change over 3 days although monomers continued to be converted to inclusion bodies. In our model, monomers of huntingtin are represented by the species PolyQ, oligomers by AggPolyQ[i] (i=1-5) and inclusion bodies by SeqAggP. Therefore we selected cells from our simulations and tracked the levels of each pool over time and used the sum of the AggPolyQ[i]s to represent the pool of oligomers. As in the experimental data, we also found that after the initial increase in levels of AggPolyQ (since it was initially set to zero), levels remained fairly constant over time and were similar even when the pool of monomers was depleted and inclusion bodies formed (Appendix 1 Figure S1). The reason for the invariant size of the oligomeric pool in the model is that we assumed that once inclusion bodies have formed, monomers could be directly sequestered into these, whereas the oligomers were unable to be sequestered in this way. We based this assumption on a number of aggregation studies and kinetic models which suggest that inclusion bodies grow in size by the addition of monomers although other mechanisms have been proposed. Therefore, oligomers persist whether or not inclusion bodies are formed and these are the most toxic species since they interfere with the cellular machinery. Olshina et al found that the chaperone Hsc70 decreases oligomeric pools by increasing the flux of monomers to inclusion bodies. We could extend our current model to include the role of chaperones to examine this further. Since we have already built an SBML model of the chaperone system [5], this would be fairly straightforward to do.

Appendix 1 Table S1 List of Species

Species description	Name	Database term	Initial amount
Polyglutamine-containing protein	PolyQ	P42858	1000
red fluorescent protein	mRFPu	-	300
26S Proteasome	Proteasome	GO:0000502	1000
PolyQ bound to proteasome	PolyQ_Proteasome	-	0
mRFPu bound to proteasome	mRFPu_Proteasome	-	0
PolyQ aggregate of size i (i= 1-5)	AggPolyQi	-	0
Inclusion	SeqAggP	-	0
Aggregated protein bound to proteasome	AggP_Proteasome	-	0
Reactive oxygen species	ROS	CHEBI:26523	10
Active p38MAPK	p38_P	Q16539	0
Inactive p38MAPK	p38	Q16539	100
Generic pool of native protein	NatP	-	19,500
Misfolded protein	MisP	-	0
Misfolded protein bound to proteasome	MisP_Proteasome	-	0
Small aggregate of size i (i= 1-5)	AggPi	-	0
Dummy species to record cell death due to proteasome inhibition	PIdeath	-	0
Dummy species to record cell death due to p38MAPK activation	p38death	-	0

Appendix 1 Table S2 List of reactions

No.[a]	Reaction name	Reaction	Rate law[b]	Parameter value
1	PolyQ synthesis	Source → PolyQ	$k_{synPolyQ}$	7.0 E-3 molecule s^{-1}
2	PolyQ/proteasome binding	PolyQ + Proteasome → PolyQ_Proteasome	$k_{binPolyQ}$[#PolyQ][#Proteasome]	5.0 E-8 $molecule^{-1}$ s^{-1}
3	PolyQ/proteasome release	PolyQ_Proteasome → PolyQ + Proteasome	$k_{relPolyQ}$[#PolyQ_Proteasome]	1.0 E-9 s^{-1}
4	PolyQ degradation	PolyQ_Proteasome → Proteasome	$k_{degPolyQ}$*$k_{proteff}$ [#PolyQ_Proteasome]	2.5 E-3 s^{-1}
5	mRFPu synthesis	Source → mRFPu	$k_{synmRFPu}$	1.38 E-1 molecule s^{-1}
6	mRFPu / proteasome binding	mRFPU + Proteasome → mRFPu_Proteasome	$k_{binmRFPu}$[#mRFPu][#Proteasome]	5.0 E-7 $molecule^{-1}$ s^{-1}
7	mRFPu / proteasome release	mRFPu_Proteasome → mRFPU + Proteasome	$k_{relmRFPu}$[#mRFPu_Proteasome]	1.0 E-8 s^{-1}
8	mRFPu degradation	mRFPu_Proteasome → Proteasome	$k_{degmRFPu}$*$k_{proteff}$ [#mRFPu_Proteasome]	5.0 E-3 s^{-1}
9	PolyQ aggregation1	2PolyQ+ROS → AggPolyQ1+ROS	$k_{aggPolyQ}$[#PolyQ][#PolyQ-1]* ([#ROS^2]/(10^2+[#ROS^2]))	5.0 E-8 $molecule^{-1}$ s^{-1}
10	PolyQ aggregation[i+1] (i=1-4)	AggPolyQi+PolyQ+ROS → AggPolyQ(i+1)+ROS	$k_{aggPolyQ}$[#AggPolyQi][#PolyQ]* ([#ROS^2]/(10^2+[#ROS^2]))	5.0E-8 $molecule^{-1}$ s^{-1}
11	PolyQDisaggregation1	AggPolyQ1→2AggPolyQ	$k_{disaggPolyQ1}$[#AggPolyQ1]	5.0E-7 s^{-1}
12	PolyQDisaggregation2	AggPolyQ2→AggPolyQ1 +PolyQ	$k_{disaggPolyQ2}$[#AggPolyQ2]	4.0E-7 s^{-1}
	PolyQDisaggregation3	AggPolyQ3→AggPolyQ3 +PolyQ	$k_{disaggPolyQ3}$[#AggPolyQ3]	3.0E-7 s^{-1}
	PolyQDisaggregation4	AggPolyQ4→AggPolyQ3 +PolyQ	$k_{disaggPolyQ4}$[#AggPolyQ4]	2.0E-7 s^{-1}
	PolyQDisaggregation5	AggPolyQ5→AggPolyQ4 +PolyQ	$k_{disaggPolyQ5}$[#AggPolyQ5]	1.0E-7 s^{-1}
13	Inclusion formation	AggPolyQ5+PolyQ → *7*SeqAggP	$k_{aggPolyQ}$[#AggPolyQ5][#PolyQ]	5.0 E-8 $molecule^{-1}$ s^{-1}
	Inclusion growth	SeqAggP + PolyQ → 2SeqAggP	$k_{seqPolyQ}$[#SeqAggP][#PolyQ]	8.0 E-7 $molecule^{-1}$ s^{-1}
14	Proteasome inhibition by aggregates[i] (i=1-5)	AggPolyQi + Proteasome → AggP_Proteasome	$k_{inhprot}$[#AggPolyQ[i]] [#Proteasome]	5.0 E-9 $molecule^{-1}$ s^{-1}
15	Basal ROS production	Source → ROS	k_{genROS}	1.7 E-3 molecule s^{-1}
16	ROS removal	ROS → Sink	k_{remROS}[#ROS]	2.0 E-4 s^{-1}
17	ROS generation AggPolyQ[i] (i=1-5)	AggPolyQ[i]→AggPolyQ[i]+ ROS	$k_{genROSAggP}$ [#AggPolyQ[i]]	5.0 E-6 s^{-1}
18	ROS generation AggP_Proteasome	AggP_Proteasome → AggP_Proteasome + ROS	$k_{genROSAggP}$[#AggP_Proteasome]	5.0 E-6 s^{-1}
19	p38MAPK activation	ROS + p38 → ROS + p38_P	k_{actp38}[#ROS][#p38]	5.0 E-6 $molecule^{-1}$ s^{-1}
20	p38MAPK inactivation	p38_P → p38	$k_{inactp38}$[#p38_P]	2.0 E-3 s^{-1}
	AggP_Proteasome sequestering	AggP_Proteasome+SeqAggP →2SeqAggP	$k_{seqAggPProt}$[#AggP_Proteasome] [#SeqAggP]	5.0E-7 $molecule^{-1}$ s^{-1}
	PolyQ_Proteasome sequestering	PolyQ_Proteasome+SeqAggP →2SeqAggP	$k_{seqPolyQProt}$[#PolyQ_Proteasome] [#SeqAggP]	5.0e-7 $molecule^{-1}$ s^{-1}
	Protein synthesis	Source → NatP	$k_{synNatP}$	2.4 molecule s^{-1}
	Protein misfolding	NatP+ROS→MisP+ROS	$k_{misfold}$[#NatP][#ROS]	2.0E-6 $molecule^{-1}$ s^{-1}
	Protein refolding	MisP→NatP	k_{refold}[#MisP]	8.0E-5 s^{-1}

	MisP/Proteasome binding	MisP+Proteasome→ MisP_Proteasome	$k_{binMisPProt}$[#MisP][#Proteasome]	5.0E-8 molecule^{-1} s^{-1}
	MisP_Proteasome release	MisP_Proteasome→ MisP+Proteasome	$k_{relMisPProt}$[#MisP_Proteasome]	1.0E-8 s^{-1}
	Degradation of misfolded protein	MisP_Proteasome→ Proteasome	$k_{degMisP}$*$k_{proteff}$ [#MisP_Proteasome]	1.0E-2 s^{-1}
	MisP aggregation	2MisP → AggP1	$k_{aggMisP}$[#MisP][#MisP-1]/2.0	1.0E-11 molecule^{-1} s^{-1}
	MisP aggregation [i] (i=1-4)	AggP[i] + MisP → AggP[i+1]	$k_{agg2MisP}$[#MisP][#AggP[i]]	1.0E-10 molecule^{-1} s^{-1}
	MisP disaggregation1	AggP1→2MisP	$k_{disaggMisP1}$[#AggP1]	5.0E-7 s^{-1}
	MisP disaggregation2	AggP2→AggP1+MisP	$k_{disaggMisP2}$[#AggP2]	4.0E-7 s^{-1}
	MisP disaggregation3	AggP3→AggP2+MisP	$k_{disaggMisP3}$[#AggP3]	3.0E-7 s^{-1}
	MisP disaggregation4	AggP4→AggP3+MisP	$k_{disaggMisP4}$[#AggP4]	2.0E-7 s^{-1}
	MisP idsaggregation5	AggP5→AggP4+MisP	$k_{disaggMisP5}$[#AggP5]	1.0E-7 s^{-1}
	MisP Inclusion formation	AggP5 + MisP → 7SeqAggP	$k_{agg2MisP}$[#AggP5][#MisP]	1.0E-10 molecule^{-1} s^{-1}
	MisP Inclusion growth	SeqAggP+ MisP → 2SeqAggP	$k_{seqmisp}$[#SeqAggP][#MisP]	1.0E-9 molecule^{-1} s^{-1}
	MisP_Proteasome sequestering	MisP_Proteasome+SeqAggP→ 2SeqAggP	$k_{seqMisPProt}$[#MisP_Proteasome] [#SeqAggP]	5.0e-7 molecule^{-1} s^{-1}
	mRFPu_Proteasome sequestering	mRFPu_Proteasome+SeqAggP →2SeqAggP	$k_{seqmRFPuProt}$[#mRFPu_Proteasome] [#SeqAggP]	5.0e-7 molecule^{-1} s^{-1}
	mRFPu sequestering	mRFPu+SeqAggP→2SeqAggP	$k_{seqPolyQProt}$[#mRFPu][#SeqAggP]	1.0e-10 molecule^{-1} s^{-1}
	Proteasome inhibition AggP[i] (i=1-5)	AggP[i]+Proteasome→ AggP_Proteasome	$k_{inhprot}$[#AggP[i]][#Proteasome]	5.0E-9 molecule^{-1} s^{-1}
	ROS generation AggP[i] (i=1-5)	AggP[i] → AggP[i] + ROS	$k_{genROSAggP}$[#AggP[i]]	5.0E-6 s^{-1}
21	p38 ROS generation	p38_P→p38_P+ROS	$k_{genROSp38}$*k_{p38act}[#p38_P]	7.0E-4 s^{-1}
	SeqAggP ROS generation	SeqAggP→SeqAggP+ROS	$k_{genROSSeqAggP}$[#SeqAggP]	1.0E-7 s^{-1}
22	P38 cell death	p38_P→p38_P+p38death	$k_{p38death}$*k_{p38act} [#p38_P]	9.0E-8 s^{-1}
23	PI cell death	AggP_Proteasome→ AggP_Proteasome+PIdeath	$k_{PIdeath}$[#AggP_Proteasome]	2.5E-8 s^{-1}

[a]Numbers refer to reactions shown in Figure 32. [b]All rate laws contain a dummy parameter k_{alive}=1. [c]$k_{proteff}$=1 is a dummy parameter to allow proteasome efficiency to be reduced when proteasome inhibitor is added. . [d]k_{p38act}=1 is a dummy parameter to allow p38 activity to be reduced when p38 inhibitor is added.

Appendix 1 Table S3 List of events

Event name	Trigger	Assignments
PI Cell Death	PIdeath>0	$k_{alive} = 0$
p38 Cell Death	p38death>0	$k_{alive} = 0$
Proteasome Inhibition	t>86400.0	$k_{proteff}$=0.05

Appendix 1 Table S4 List of parameters used for fitting the model

Parameter name	Experimental data used in model fitting		
	% Cell Death	% Inclusion bodies	mRFPu levels
$k_{aggPolyQ}$		x	
$k_{seqPolyQ}$		x	
$k_{inhprot}$	x		x
$k_{genROSAggP}$	x	x	
k_{actp38}	x		
$k_{seqAggPProt}$		x	
$k_{seqPolyQProt}$		x	
$k_{genROSp38}$	x	x	
$k_{p38death}$	x		
$k_{PIdeath}$	x		

Appendix 1 Figure S1

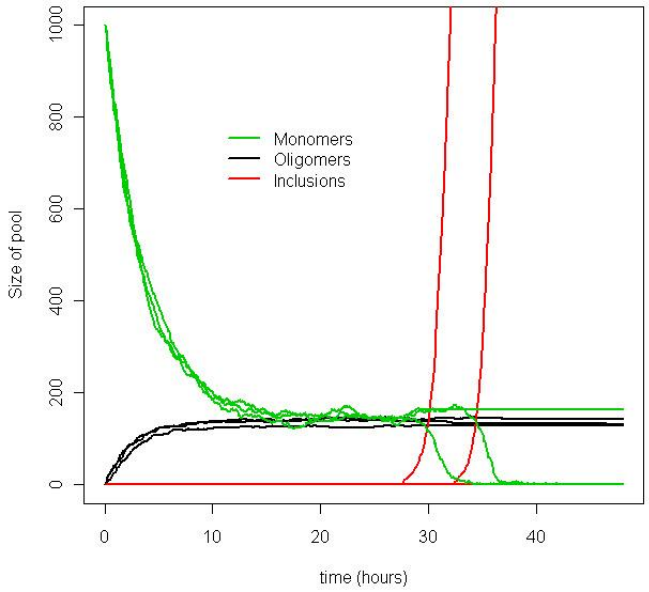

Figure S1 - Distribution of polyQ monomers, oligomers and inclusion bodies. Simulation output from 3 runs of the model showing that the size of the oligomeric pool remains constant even when inclusions form.

APPENDIX 2. Supplemental Figures

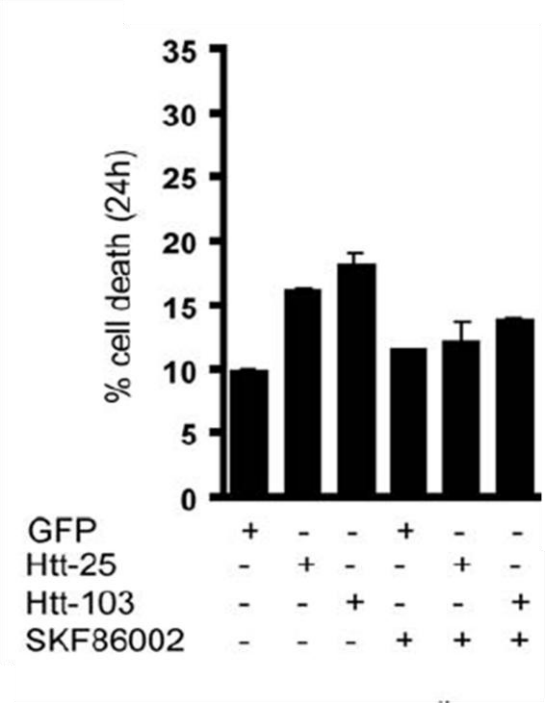

Supplemental Figure 1. Cell death analysis of polyglutamine-expressing cells treated with SKF86002

Inhibition of p38MAPK activation by treatment with SKF86002 rescues cells from expanded polyglutamine cytotoxicity. U87MG cells were treated with SKF86002 for 2 hours prior to transfection with GFP, HttQ25, or HttQ103. Cell survival was assessed by the flow cytometry using propidium iodide exclusion 24 hours post-transfection. The analysis revealed an increase in cell death of HttQ103-expressing cells compared to cells expressing GFP or HttQ25, which was reversed by treatment with SKF86002.

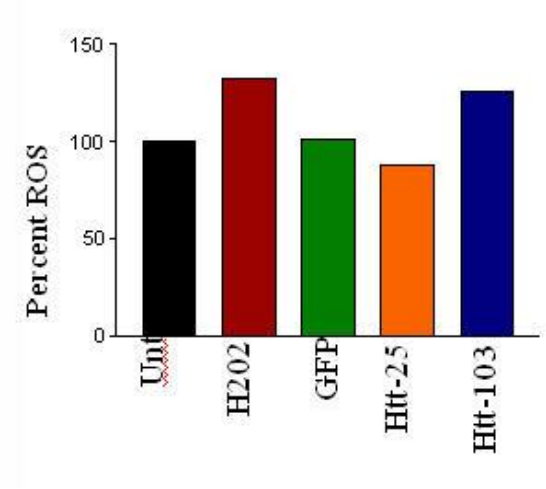

Supplemental Figure 2. Analysis of ROS in cells expressing polyglutamine proteins

Expression of expanded polyglutamine proteins generate reactive oxygen species (ROS) equivalent to hydrogen peroxide in a flow cytometric analysis using the ROS-sensitive fluor hydroxyphenyl fluorescein.

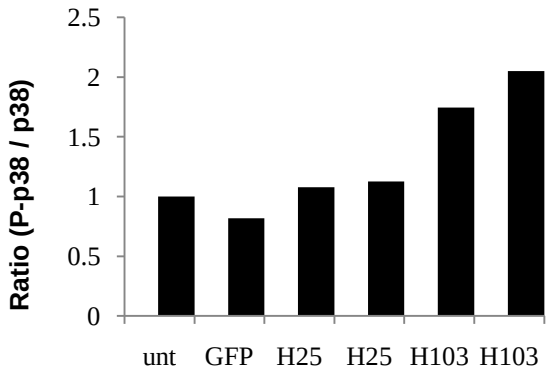

Supplemental Figure 3. Quantification of Western blot analysis of phosphorylated-p38MAPK protein levels from cells expressing polyglutamine proteins

Quantification of Western blot analysis of duplicate cell extracts from U87MG cells expressing GFP, HttQ25, or HttQ103 with the phospho-p38MAPK antibody. Relative intensities for each sample were determined by dividing the densitometry values for p38MAPK by the densitometry values of Total p38MAPK. Each value was then normalized to the untransfected control. Densitometry analysis reveal a 1.1 fold increase of phospho-p38MAK levels in HttQ25-expressing cells and a 1.8 fold increase of phospho-p38MAPK in HttQ103-expressing cells 24 hours post-transfection relative untransfected controls. Intensity values were normalized to Total p38MAPK levels.

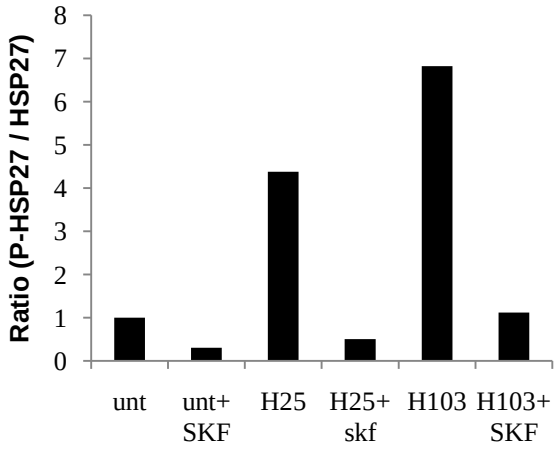

Supplemental Figure 4. Quantification of Western blot analysis of phosphorylated-HSP-27 protein levels from polyglutamine-expressing cells

Quantification of Western blot analysis of protein levels of phospho-HSP27 from lysates of U87MG cell expressing HttQ25 or HttQ103 with or without the p38MAPK inhibitor SKF86002. Relative intensities for each sample were determined by dividing the densitometry values for phospho-HSP27 by the densitometry values of Total HSP27. Each value was then normalized to the untransfected control. Densitometry analysis reveal a 4.3 fold increase of phospho-HSP27 in HttQ25-expressing cells and a 6.8 fold increase in of phospho-HSP27 in HttQ103-expressing cells relative to untransfected controls.

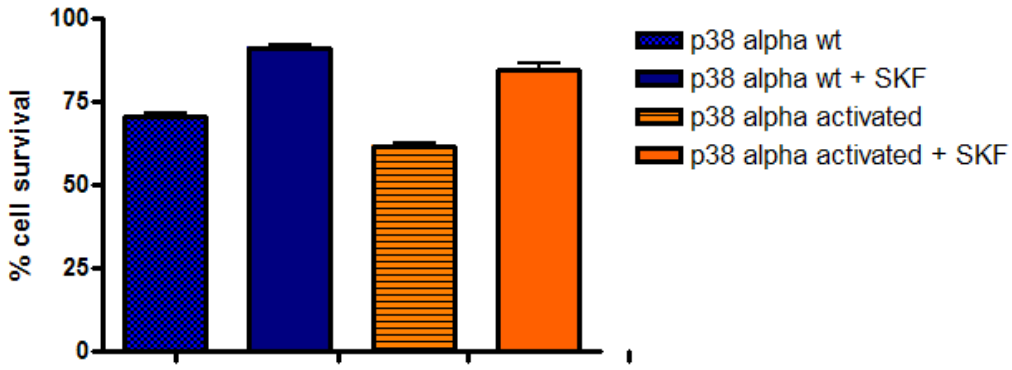

Supplemental Figure 5. Cell viability analysis of p38Wt and p38Active-expressing cells treated with SKF86002

U87MG cells were treated with or without SKF86002 for 2 hours prior to transfection with constructs encoding the alpha isoform of p38Wt or p38Acitive. Cell survival was assessed by the the MTT assay 24 hours post-transfection. The analysis revealed a ~30% decrease in cell survival in p38Wt expressing cells, and a ~40% decrease in cell survival in p38Active-expressing cells, which was reversed by treatment with SKF86002.

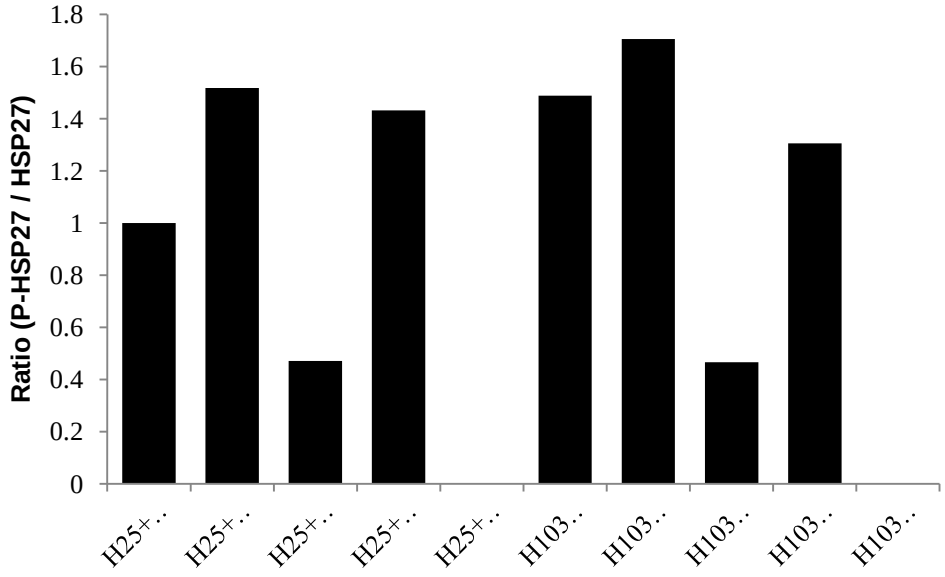

Supplemental Figure 6. Quantification of Western blot analysis of phosphorylated-HSP-27 protein levels in cells co-transfected with polyglutamine and p38MAPK expression constructs

Quantification of Western blot analysis with the phospho-HSP27 antibody of cell extracts from U87MG cells co-transfected with pcDNA empty vector (pcDNA), wild-type p38MAPK (p38 Wt), kinase-dead p38MAPK (p38 KD), or hyper-active p38MAPK (p38 Active) expression constructs in cells expressing HttQ25 or HttQ103. Relative intensities of each sample were determined by dividing the densitometry values for phospho-HSP27 by the densitometry values of Total HSP27. Each value was then normalized to cells co-transfected with HttQ25 and pcDNA. Densitometry analysis revealed that phospho-HSP27 levels were reduced by 2.1 fold in extracts from HttQ25- or HttQ103-expressing cells co-transfected with p38 KD when compared to co-transfection with pcDNA. A complete abrogation of HSP27 phosphorylation was shown in cells treated with SKF86002. Cells co-transfected with HttQ103 and p38Wt was found to have the highest levels (1.7 fold increase) of phospho-HSP27 when compared to cells co-transfected with HttQ103 and pcDNA.

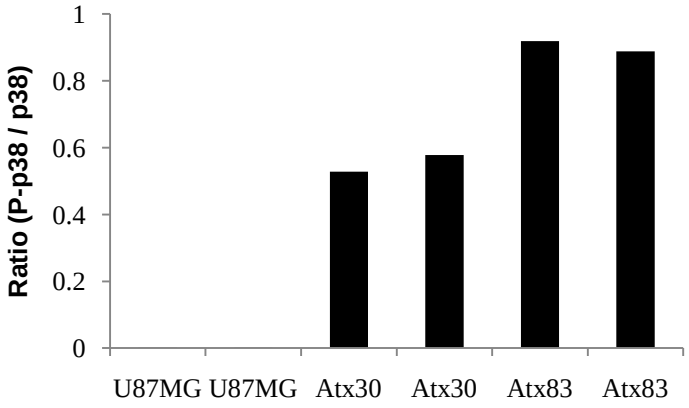

Supplemental Figure 7. Quantification of Western blot analysis of phosphorylated-p38MAPK protein levels from cells expressing expanded ataxin-1 protein

Quantification of Western blot analysis of duplicate cell extracts from U87MG cells expressing AtxQ30 or AtxQ83 with the phospho-p38MAPK antibody. Relative intensities for each sample were determined by dividing the densitometry values for phospho-p38MAPK by the densitometry values of Total p38MAPK. Densitometry analysis revealed a 1.6 fold increase in phospho-p38MAPK in Atx83-expressing cells relative to Atx30-expressing cells.

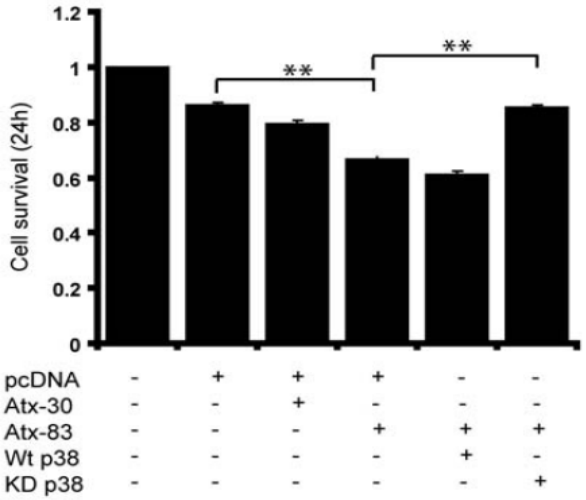

Supplemental Figure 8. Genetic modulation of p38MAPK increases cell survival of cell expressing Atx83

U87MG cells were co-transfected with Atx-103 and either empty vector alone (pcDNA) or expression constructs encoding p38MAPK wild-type (p38Wt) or dominant-negative p38MAPK (p38KD) alpha. 24 hours post-transfection, cells were analyzed by MTT which revealed a statistically significant increase in survival in cells co-expressing Atx-83 and p38KD (** $p<0.01$). The survival of cells expressing empty vector control alone or co-expressing Atx-30 with empty vector was not significantly different.

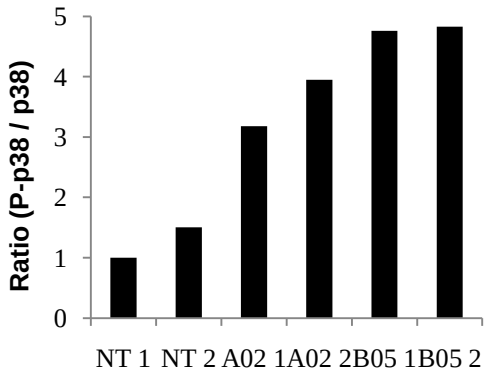

Supplemental Figure 9. Quantification of Western blot analysis of phosporylated-p38MAPK in the cerebella of 3-month-old SCA-1 mice

Quantification of Western blot analysis of duplicate cerebellar extracts from 3-month-old non-transgenic (NT), A02, and B05 mice with the phospho-p38MAPK antibody. Relative intensities for each sample were determined by dividing the densitometry values for phospho-p38MAPK by the densitometry values of Total p38MAPK. Densitometry analysis revealed a 5 fold increase in phospho-p38MAPK protein levels from extracts from B05 mice when compared to NT.

APPENDIX 3. Activation of p38MAPK Contributes to Expanded Polyglutamine-induced Cytotoxiciy

OPEN ACCESS Freely available online

PLoS one

Activation of p38MAPK Contributes to Expanded Polyglutamine-Induced Cytotoxicity

Maria Tsirigotis[1☯], R. Mitchell Baldwin[1,2☯], Matthew Y. Tang[1,2], Ian A. J. Lorimer[1,2], Douglas A. Gray[1,2]*

1 Centre for Cancer Therapeutics, Ottawa Health Research Institute, Ottawa, Ontario, Canada, **2** Department of Biochemistry, Microbiology and Immunology, University of Ottawa, Ottawa, Ontario, Canada

Abstract

Background: The signaling pathways that may modulate the pathogenesis of diseases induced by expanded polyglutamine proteins are not well understood.

Methodologies/Principal Findings: Herein we demonstrate that expanded polyglutamine protein cytotoxicity is mediated primarily through activation of p38MAPK and that the atypical PKC iota (PKCι) enzyme antagonizes polyglutamine-induced cell death through induction of the ERK signaling pathway. We show that pharmacological blockade of p38MAPK rescues cells from polyglutamine-induced cell death whereas inhibition of ERK recapitulates the sensitivity observed in cells depleted of PKCι by RNA interference. We provide evidence that two unrelated proteins with expanded polyglutamine repeats induce p38MAPK in cultured cells, and demonstrate induction of p38MAPK in an *in vivo* model of neurodegeneration (spinocerebellar ataxia 1, or SCA-1).

Conclusions/Significance: Taken together, our data implicate activated p38MAPK in disease progression and suggest that its inhibition may represent a rational strategy for therapeutic intervention in the polyglutamine disorders.

Citation: Tsirigotis M, Baldwin RM, Tang MY, Lorimer IAJ, Gray DA (2008) Activation of p38MAPK Contributes to Expanded Polyglutamine-Induced Cytotoxicity. PLoS ONE 3(5): e2130. doi:10.1371/journal.pone.0002130

Editor: Nick Gay, University of Cambridge, United Kingdom

Received February 7, 2008; **Accepted** March 27, 2008; **Published** May 7, 2008

Funding: The work was funded by Canadian Institutes of Health Research (grant number 57737 and 62797 awarded DAG and IAJL respectively) and the National Cancer Institute of Canada (grant number 015343 awarded IAJL). RMB is a Research Student of The Terry Fox Foundation through an award from the National Cancer Institute of Canada. MYT is the recipient of an Ontario Graduate Scholarship.

Competing Interests: The authors have declared that no competing interests exist.

* E-mail: dgray@ohri.ca

☯ These authors contributed equally to this work.

Introduction

The polyglutamine diseases encompass at least 9 different disorders including Huntington's disease (HD) and five spinocerebellar ataxias (SCA-1, SCA-2, SCA-3, SCA-6 and SCA-7 (reviewed in [1]). These are dominantly inherited diseases typically detected in the third or fourth decade of life. No effective therapeutic interventions are currently available, and the polyglutamine diseases are generally fatal. Polyglutamine disorders arise from expansion of a CAG repeat within the coding region of genes such that the length of the encoded polyglutamine stretch exceeds a critical threshold. At the ultrastructural level, disease progression features heat shock protein (HSP)-containing nuclear ubiquitinated inclusions [2] that have accumulated an assortment of cellular host components in association with the polyglutamine-containing protein [3]. There is evidence from experiments performed in cultured mammalian cells and animal models of disease that polyglutamine expanded proteins adversely affect basic biological processes (reviewed in [4]). Their expression has been associated with impaired proteolysis [5], loss of transcriptional control mechanisms [6] and with altered regulation of cell death/survival pathways (reviewed in [7]).

The mitogen-activated protein kinases (MAPK) are involved in the integration and processing of multiple extracellular signals and their induction triggers diverse biological responses (reviewed in [8,9]). While the activation of the extracellular regulated kinase 1/2 (hereafter referred to as ERK) by mitogenic and proliferative stimuli is coupled to cell survival [10], stress inducible kinases JNK and p38MAPK respond to environmental stress and their sustained activation transduces signals leading to cell death (reviewed in [11]). Protein kinase C (PKCs) family members have been positioned upstream of ERK and are potent modulators of its activation (reviewed in [12]). With the current exception of the stress-inducible kinase JNK whose excessive activation has been well documented in neurodegenerative diseases [13] and reviewed in [14], the mechanistic relationship between the stress inducible host signaling pathways and expanded polyglutamine-induced toxicity remain controversial. It has been shown, for example, that the mutant huntingtin (Htt) protein causes aberrant activation of epidermal growth factor receptor (EGFR) signaling [15], a finding which has been contradicted by more recent reports in which EGFR signaling was disrupted by expression of the expanded polyglutamine protein [16,17]. In a *Drosophila* model of polyglutamine toxicity, the mutant Htt protein has been shown to disrupt EGFR signaling through interference with the ERK cascade [18] while in a cell culture model it has been shown to activate the pro-survival pathway mediated through ERK [19]. All these anomalies are consistent with gain of function effects of expanded polyglutamine proteins. There is ample evidence from experimental systems that a simple polyglutamine tract can be toxic

without the context of its natural surrounding protein sequence [20,21] but possible loss of function effects in polyglutamine proteins must also be considered. The normal huntingtin protein, for example, has been shown to increase transcription of brain-derived neurotrophic factor (BDNF), which is required for survival of striatal neurons [22,23]. Loss of this activity in the mutant protein may therefore contribute to neuronal loss in diseased individuals. Insulin-like growth factor I also has neuroprotective activity in the context of polyglutamine-induced cytotoxicity [24,25], and like BDNF activates the survival pathway mediated through the phosphoinositide 3-kinase (PI3-K) [26–28]. Kinases activated downstream in this pathway include PKB/Akt and the atypical protein kinase C iota (PKCι) [29,30,31–34]. The toxicities of huntingtin and ataxin-1 gene products are modulated by their phosphorylation states [35,36], but while the role of PKB/Akt activity has been studied in this context nothing is known of the role of PKCι.

As a starting point the current study sought to address the role of MAPK signaling pathways in polyglutamine disorders including Huntington's disease and SCA-1. Our findings suggest that expanded polyglutamine proteins mediate adverse effects through activation of p38MAPK signaling and that this cytotoxicity is antagonized by PKCι, which enhances protective signaling through the ERK pathway. We show that pharmacological inhibition of p38MAPK rescues cells from polyglutamine-induced cell death whereas inhibition of ERK signaling or depletion of PKCι by RNA interference enhances cytotoxicity.

Methods

Reagents and antibodies

Custom RNA interference duplexes were synthesized by Dharmacon RNA Technologies Inc. (Lafayette, CO, USA). A control duplex having the following sense RNA sequence AUUCUAUCACUAGCGUGACUU (non-specific control duplex) was purchased from Dharmacon Research, Inc and used as a control. RNA duplex concentrations were determined by measuring absorbance at 260 nm and calculating concentrations using extinction coefficients provided by the manufacturer. Propidium iodide and MTT reagents were purchased from Sigma-Aldrich Canada Ltd. (Oakville, ON, Canada). P38MAPK inhibitors, SKF86002 and SB202190 were purchased from Calbiochem (San Diego, CA, USA) and Biosource (Camarillo, CA, USA) respectively. The MEK inhibitor U0126 was from Promega (Madison, WI, USA). The goat polyclonal antibodies nPKCæ (used to detect PKCι) and ataxin-1 were from Santa Cruz Biotechnology Inc. (Santa Cruz, CA, USA). The mouse monoclonal phospho-p38MAPK and phospho-ERK 1/2 antibodies and the rabbit polyclonal p38MAPK antibody were from Cell Signaling Technology (Beverly, MA, USA). Pan ERK monoclonal antibody was from Transduction Laboratories (Lexington, KY, USA). GFP, Htt-25 and Htt-103 were detected with a mouse monoclonal AFP antibody purchased from Quantum Biotechnologies Inc.(Montréal, Québec, Canada). Phospho-ATF2 and total ATF2 levels were detected with rabbit polyclonal antibodies purchased from Cell Signaling Technology (Beverly, MA, USA). The mouse monoclonal actin antibody was purchased from Sigma-Aldrich Canada (Oakville, ON).

Expression constructs and transgenic mice

The pEGFP-N1 expression construct which served as a control in transient transfection experiments was purchased from Clontech (Palo Alto, California, USA). The Htt-25 and Htt-103 expression constructs (gifts from Dr. Ron Kopito) contain a synthetic insert encoding exon 1 of human Huntingtin containing a polyglutamine tract of either 25Q or 103Q fused to the yellow fluorescent reporter protein (YFP). The plasmids encoding the full length human ataxin-1 proteins with a polyglutamine tract of 30Q or 83Q were a gift from Dr. Huda Zoghbi. The origin of the B05 transgenic line carrying a mutant Ataxin-1 allele with 82 CAG repeats and the A02 line with a CAG repeat of 30 codons was described in a paper from the laboratory of Dr. Harry Orr [37], from whom these lines were obtained.

Cell culture and transfections

The human U87MG cell line (a gift from Dr. W. Cavenee, Ludwig Institute for Cancer Research, La Jolla, CA) was maintained at 37°C and 5% CO_2 in Dulbecco's modified Eagle's medium (DMEM) supplemented with 100 units/ml penicillin, 100 μg/ml streptomycin, 2 mM glutamine and 10% (v/v) of a 2:1 mixture of donor bovine serum and fetal bovine serum. For RNA interference experiments, cells were transfected using Oligofectamine (Invitrogen Canada, Inc., Burlington, ON) as per the supplier's protocol. Final concentrations of RNA in the transfections were 5.3 nM for siPKCιA and 20 nM for siPKCιB. Control RNA concentrations were matched to the specific siRNA duplex used in the experiment. For transient transfections, cells were plated in either 96- or 6 well dishes 24 hours prior to transfections. Subsequently, they were transfected using GeneJuice Transfection Reagent (Novagen, Madison, WI, USA) as per the supplier's protocol. 0.5 μg of plasmid DNA was used in each well of a 96 well dish. A total amount of 3 μg of plasmid DNA was used in each well of a 6 well dish. For p38MAPK inhibition experiments using SKF86002 and SB202190, cells in 96 well plates were transfected with RNA duplexes. 24 hours post-transfection, cells were pre-treated for 2 h with 20 μM of the respective inhibitor. ERK inhibition experiments were performed in a similar manner using the MEK inhibitor U0126 at a final concentration of 20 μM. Following this incubation period cells were transiently transfected with various expression constructs.

Survival assays

Survival assays were performed by MTT, trypan blue exclusion and flow cytometry. For MTT assays, cells in 96 well microtitre plates were transfected with RNA duplexes as described above. 6 h post-transfection, they were transiently transfected with the GFP control vector, Htt-25, Htt-103, Atx-30 or Atx-83 as indicated. 24 h post-transfection of the plasmid DNA cell survival was assessed using the MTT (3-(4,5-cimethylthiazol-2-yl)-2,5-diphenyl tetrazolium bromide) assay as described previously [38]. Background values were determined by carrying out the assay in wells containing media without cells. Toxicity was measured by trypan blue exclusion in pooled fractions consisting of attached and detached cells. For flow cytometry experiments, adherent and non-adherent cells were harvested and fixed with 70% (v/v) ethanol in PBS. Cell nuclei were stained with propidium iodide. DNA content was analyzed by flow cytometry using a BD LSR flow cytometer (Becton Dickinson, San Jose, CA). Data was acquired using Cell Quest software (Becton Dickinson, San Jose, CA) and were analyzed using Mod Fit LT software (Verity Software House, Inc., Sopsham, ME).

Western blot analysis

U87MG cells were harvested in protein lysis buffer consisting of 100 mM Tris pH 6.8, 20 mM DTT, 4% SDS, 5% glycerol. Protein concentrations were determined using the Bradford assay reagents (Bio-Rad, Hercules, CA, USA). Reduced proteins were separated through 4–12% bis-tris polyacrylamide gels using an

Xcell II min cell system (Invitrogen, San Diego, CA, USA). Proteins were transferred onto PVDF nylon membranes (Amersham Pharmacia Biotech, Buckinghamshire, UK) and stained with amido black prior to probing with the appropriate primary antibody. Proteins were detected using the HRP method and SuperSignal West Pico Chemiluminescent Substrate reagents (Pierce, Rockford, IL, USA). Proteins were visualized using the GeneGnome (Syngene, Frederick, MD,USA). Sequential probing of membranes was performed after stripping with the use of Western Blot Stripping Buffer (Pierce, Rockford, IL, USA) for 30 min at room temperature. Mouse cerebella were harvested by homogenization in protein lysis buffer (20 mM Tris-HCl pH 7.5, 150 mM NaCl, 0.5 mM EDTA, 1% NP-40 and 20% glycerol) containing the following protease and phosphatase inhibitors: 200 μg/ml phenylmethylsulfonyl fluoride, 5 μg/ml leupeptin, 2 μg/ml aprotinin, 200 μM NaF, 200 μM NaPPi and 10 mM NEM. Soluble protein was quantified as described above. Proteins were resolved on a 10% SDS-polyacrylamide gel and electroblotted onto a Hybond C nitrocellulose membrane (Amersham Biosciences Corp, Baie d'Urfé, QC). The membranes were stained with Ponceau S prior to immunoblotting with the appropriate primary antibody. Proteins were visualized as described above.

Immunohistochemistry

Cerebella from age-matched nontransgenic, A02 and B05 mice were excised and fixed in 10% phosphate-buffered formalin overnight at room temperature. Tissues were paraffin-embedded and sectioned sagitally using a microtome at a thickness of 5 μm. Deparaffinized sections were heated in a solution of 10 mM sodium citrate (pH 6.0) in 700W microwave for 10 minutes. Endogenous peroxidase activity was blocked by incubating in methanol containing 3% hydrogen peroxide for 20 minutes. Sections were washed with PBS (pH 7.4) and incubated for 30 minutes with 1.5% normal goat serum (Santa Cruz Biotechnologies Inc., SC, CA, USA) to block nonspecific binding. Sections were then incubated overnight at 4°C with the phospho-p38MAPK antibody (Cell Signaling Technology, Beverly, MA, USA). The reaction product was visualized with the ABC system (DAKO Diagnostics Canada Inc.). The use of animals in these experiments followed the guidelines of the Animal Care Committee of the University of Ottawa and was approved under protocol number ME-212.

Statistical analysis

Unless otherwise indicated, all values are represented as the average of three independent experiments performed in triplicate, with error bars indicating standard error of the mean. Statistical significance was determined by a two tailed Student's t-test. Values were considered significant when $P<0.05$.

Results

PKCι modulates the sensitivity of cells to polyglutamine-induced cellular death

We used a previously described siRNA strategy [38] to investigate the role of PKCι depletion in polyglutamine-induced cytotoxicity. This method specifically depletes PKCι RNA and protein with no effect on other PKC enzymes [38]. We used U87MG cells which have been shown to have an elevated basal ERK activity as a result of increased signaling through the EGFR pathway [39]. We reasoned that if ERK was protective such a cell model would be less sensitive to expanded polyglutamine induced toxicity. The use of cells from a glial as opposed to neuronal lineage is unlikely to be of consequence in that similar results were obtained in glioblastoma and neuroblastoma cell lines (as described below). To assess whether the depletion of PKCi would affect cell survival in the presence of an expanded polyglutamine protein, U87MG cells were transfected with a control or one of two siPKCι RNAs (siPKCιA and siPKCιB). Cells were then transiently transfected with either a GFP control plasmid or constructs encoding exon 1 of the Huntingtin protein containing a normal polyglutamine tract of 25Qs (hereafter referred to as Htt-25) or with a pathogenic tract of 103Qs (hereafter referred to as Htt-103) fused to the yellow fluorescent protein (YFP) reporter. Similar expression constructs encoding exon 1 of the Htt protein with an expanded polyglutamine tract have been previously used in cell culture models of polyglutamine toxicity [6,40] and in the generation of the well characterized R6/2 transgenic mouse line [41]; R6/2 mice develop a progressive neurological phenotype with motor symptoms resembling those in HD [42]. By phase contrast microscopy, a pronounced effect was observed in PKCι depleted cells expressing Htt-103 wherein a significant increase in the number of shrunken, rounded and detached cells was noted (Figure 1A). Analogous to other cell culture systems used in the study of polyglutamine biology (3T3, PC12, SHY-5Y cells, etc), U87MG cells expressing Htt-103 were found to accumulate visible nuclear inclusions as early as 24 hours post-transfection (Figure 1B). No such inclusions were observed in cells expressing GFP alone or Htt-25 (Figure 1B). Depletion of PKCι was assessed by Western blot analysis with an antibody recognizing PKCι in extracts from U87MG cells transfected with either the control or siPKCιA and siPKCιB; a reduction in the protein levels was observed at 24 and 48 hours post-transfection (Figure 1C). The transfection efficiency of the Htt proteins in U87MG cells was estimated at ~80% as assessed by fluorescence microscopy (Figure 1B). Similar levels of expression of GFP, Htt-25 and Htt-103 were confirmed by Western blot analysis of extracts from transfected cells with an antibody specific for the fluorescent protein reporter (Figure 1D). Quantification of survival with the use of a metabolic assay (MTT) revealed that the depletion of PKCι sensitized cells to the expression of Htt-103 such that survival was reduced by approximately 25% when compared to cells transfected with the control RNA (Figure 2B). The survival of U87MG cells transfected with an Htt-25 expression plasmid was no different then that of cells expressing GFP alone (Figure 2A). When compared to GFP transfectants, the depletion of PKCι mildly sensitized cells to the expression of Htt-25 but to a lesser extent than did expression of Htt-103 (Figure 2A and B). The data obtained by MTT analysis were consistent with survival as measured by the trypan-blue exclusion method (Figure 2C) and by flow cytometric analysis (Figure 2D) of Htt-103 transfected cells, both of which revealed an increase in cell death in PKCι depleted cells when compared to control RNA transfectants. These data suggested that the depletion of PKCι was sensitizing cells to the expression of expanded polyglutamine proteins. As assessed by MTT, the exogenous expression of flag-tagged PKCι was found to modestly increase the resistance of cells to the toxic effects associated with expression of Htt-103 (Figure 2E). The overexpression of PKCι in these stable transfectants was confirmed by Western blot analysis with both the PKCι and flag tag antibodies respectively (Figure 2F).

Impaired ERK activation sensitizes cells to polyglutamine-expanded proteins

It has been previously reported that PKCι is positioned upstream of the mitogen-regulated kinase ERK [43] and it was therefore conceivable that PKCι depletion would affect ERK activation. To test this hypothesis, we examined the basal levels of

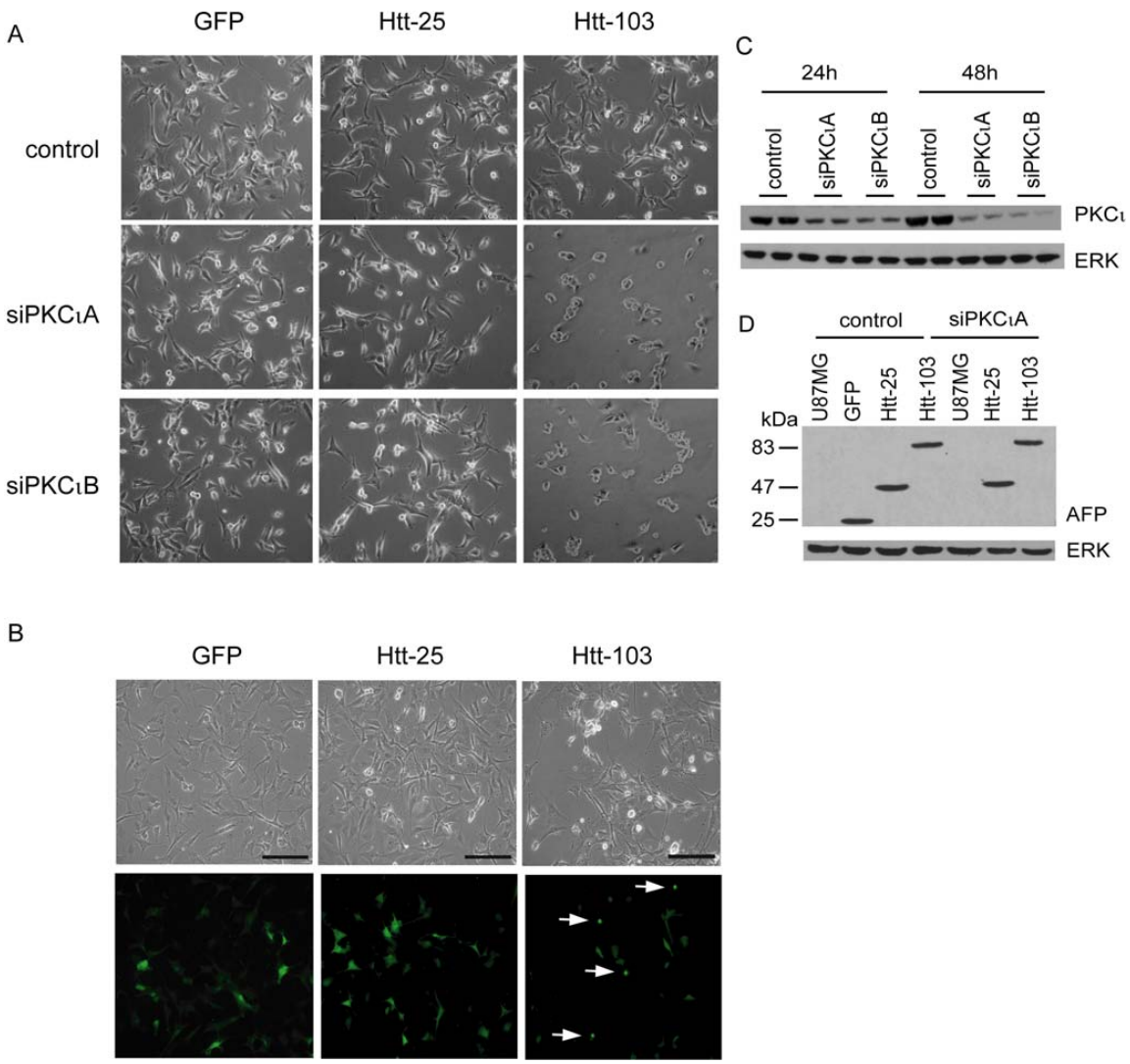

Figure 1. Morphological alterations in PKCι depleted cells expressing Htt-103. A) U87MG cells transfected with the control or with siPKCιA and siPKCιB were transiently transfected with plasmids encoding GFP, Htt-25 or Htt-103 for 24 hours. Cell morphology was assessed by phase contrast microscopy. An increase in the number of shrunken, rounded and detached cells was observed in PKCι depleted cells expressing Htt-103 when compared to control RNA transfected cells or cells expressing GFP or Htt-25. Magnification was 40×. B) U87MG cells expressing GFP, Htt-25 or Htt-103 for 24 hours were visualized under fluorescence (bottom panel) to assess transfection efficiency. Upper panels represent the same field of view visualized under white light. Arrowheads demonstrate nuclear inclusions in Htt-103 expressing cells. Scale bars represent 100 μm. C) Western blot analysis with a PKCι specific antibody of cell extracts from U87MG cells transfected in duplicate with either the control or siPKCιA and siPKCιB showing the reduction in the protein levels of PKCι at 24 and 48 hours post-transfection. The membrane was re-probed with an antibody directed against Pan-ERK which served as a loading control. D) Western blot analysis of cell extracts from cells transfected with either control or siPKCιA expressing GFP, Htt-25 or Htt-103 with an antibody raised against AFP. No significant difference in the protein levels of GFP, Htt-25 and Htt-103 were observed in extracts from control and PKCι transfected cells. The membrane was re-probed with an antibody directed against Pan-ERK which served as a loading control.
doi:10.1371/journal.pone.0002130.g001

activated ERK in PKCι depleted cells. Cell extracts from control or siPKCιA RNA transfected cells were analyzed by Western blot analysis with an antibody recognizing phospho-ERK. The analysis revealed a reduction in ERK phosphorylation in PKCι depleted cells when compared to the levels in U87MG cells transfected with the control RNA (Figure 3A). These data suggested that U87MG cells have elevated basal levels of activated ERK most probably due to the constitutively active EGFR pathway and that PKCι depletion affects ERK induction. To investigate specifically whether the loss of ERK signaling due to PKCι depletion was the basis for the increased sensitivity observed in PKCι depleted cells to expanded polyglutamine protein expression, we made use

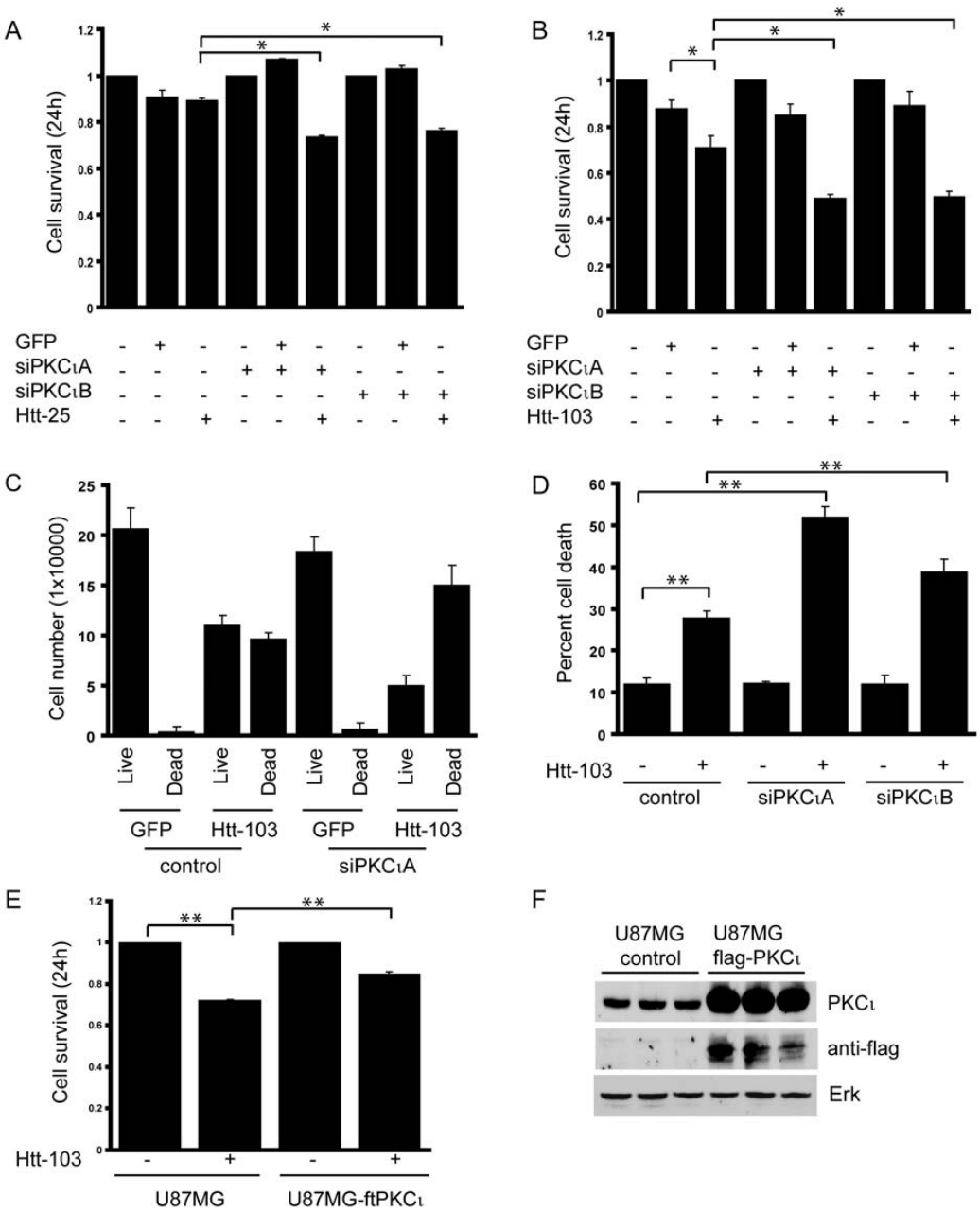

Figure 2. Depletion of PKCι sensitizes cells to polyglutamine induced toxicity. A) and B) U87MG cells transfected for 24 hours with either control or siPKCιA and PKCιB were plated in 96 well dishes. Subsequently, cells were transfected with expression constructs encoding GFP, Htt-25 (A) and Htt-103 (B) and cell survival was measured by MTT assay. A) The survival of mock RNA transfected cells expressing Htt-25 was comparable to cells expressing GFP alone. A slight decrease in cell survival was observed in PKCι depleted cells expressing Htt-25 when compared to GFP transfectants (* $p<0.05$). B) A marked decrease in cell survival was observed in control RNA transfected cells expressing Htt-103 that was further pronounced in PKCι depleted cells (* $p<0.05$). C) Survival as measured by trypan blue exclusion of U87MG cells transfected with control or siPKCιA in the presence or absence of Htt-103. In accordance with the MTT assay, an increase in the population of dead cells was observed in control transfected U87MG cells expressing Htt-103 which was further increased in PKCι depleted cells. D) Flow cytometric analysis of cells transfected with either the control or siPKCι expressing Htt-103 showing an increase in the number of dead cells in PKCι depleted cells when compared to control transfected cells. Data represents the average of three independent experiments, with error bars indicating standard deviation (** $p<0.01$). E) U87MG cells stably expressing flag epitope tagged PKCι (ftPKCι) were transiently transfected with the Htt-103 expression construct for 24 hours. Survival as assessed by MTT

analysis revealed a modest increase in survival in PKCι transfectants when compared to the parental U87MG cells (** $p<0.01$). F) Western blot analysis of triplicate cell extracts from untransfected U87MG and cells stably expressing flag-tagged PKCι with antibodies raised against PKCι and the flag epitope tag respectively. The flag tag specific antibody detected ectopically expressed PKCι in transfected cells, which was absent in the untransfected control cell extracts. The PKCι antibody detected endogenous and exogenous PKCι in lysates from U87MG cells and cells stably expressing PKCι. Pan-ERK served as the loading control. MTT and trypan blue data are represented as the average of three independent experiments performed in triplicate, with errors bars indicating standard error of the mean.
doi:10.1371/journal.pone.0002130.g002

of U0126, a specific inhibitor of MEK (positioned directly upstream of ERK). U87MG cells were either untreated or treated with U0126 prior to transfection with the GFP control vector, Htt-25 or Htt-103 plasmids. Twenty-four hours post-transfection, cell survival was assessed by the MTT assay. The data presented in figure 3B revealed that blockade of ERK recapitulated the findings in PKCι depleted cells: the survival of cells expressing Htt-103 was significantly compromised (Figure 3B). The survival of Htt-25 expressing cells treated with the inhibitor was comparable to that of GFP transfectants (Figure 3B). The efficient blockade of ERK activation in U0126 treated cells was confirmed by Western blot analysis of cell extracts from cells transfected with Htt-103 with the phospho-ERK specific antibody (Figure 3C). The data in Figure 3C also revealed that the expression of the expanded polyglutamine protein has no effect on ERK induction when compared to GFP transfectants. Taken together, they suggest that the status of ERK is strictly dependent on PKCι and not the expression of the expanded polyglutamine protein.

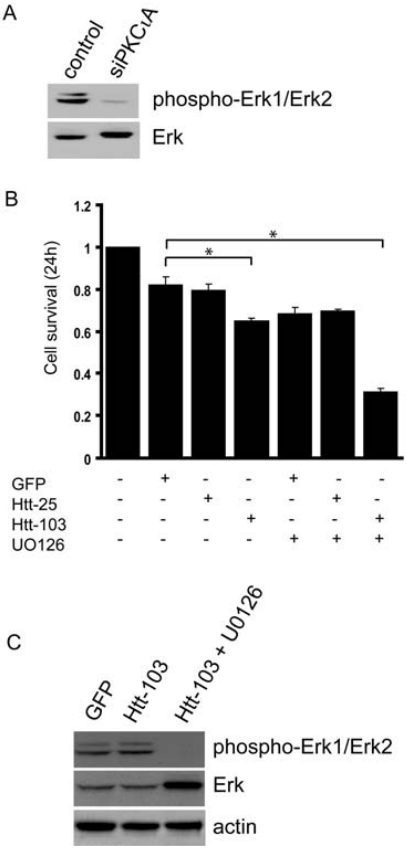

Figure 3. PKCι-mediated ERK activation protects cells from expanded polyglutamine-induced cytotoxicity. A) Western blot analysis of cell extracts from control and siPKCιA transfectants with the phospho-ERK specific antibody. The basal levels of ERK phosphoprotein were significantly reduced in PKCι depleted cells when compared to control RNA transfectants. Total ERK levels were assessed with the pan ERK antibody which also served as a loading control. B) U87MG cells were pre-treated with the MEK inhibitor U0126 for 2 hours prior to transfection with GFP, Htt-25 and Htt-103. Cell survival was assessed by MTT 24 hours post-transfection. Blockade of ERK in Htt-103 expressing cells resulted in a significant reduction in cell survival when compared to untreated Htt-103 expressing cells (* $p<0.05$). Data are represented as the average of three independent experiments performed in triplicate, with error bars indicating standard error of the mean. C) Western blot analysis of extracts from untreated and U0126 treated U87MG cells expressing Htt-103 with the phospho-ERK antibody confirming the blockade of ERK phosphorylation in U0126 treated cells. Pan-ERK was used to detect total ERK levels and actin served as a loading control.
doi:10.1371/journal.pone.0002130.g003

Expression of Htt-103 is associated with induction of p38MAPK and its pharmacological blockade rescues cells from polyglutamine-induced toxicity

Given that the blockade of ERK signaling preferentially sensitized Htt-103 expressing cells when compared to Htt-25 transfectants, we reasoned that the expanded polyglutamine may be affecting stress-inducible pro-apoptotic pathways. The activation of the p38MAPK pathway in response to environmental and genotoxic stress is well characterized [44–46] and its induction in response to amyloid beta treatment has been well documented [47,48]. Expanded polyglutamine proteins have recently been shown to induce death in cell culture models (reviewed in [49]) but the role of p38MAPK has not been investigated. To investigate the role of this kinase, we analyzed cell extracts from control and PKCι depleted cells expressing GFP, Htt-25 and Htt-103 by Western blot analysis with a phospho-p38MAPK antibody. The analysis revealed that the expression of Htt-103 resulted in a similar increase in p38MAPK phosphorylation in both the control and siPKCιA transfected cells. These data suggested that the status of PKCι has no effect on expanded polyglutamine induced p38MAPK activation (Figure 4A) and that the increased sensitivity observed in PKCι depleted cells was a reflection of a diminished activation of ERK. The levels of phospho-p38MAPK remained unchanged in GFP expressing cells and were minimally affected in Htt-25 transfectants (Figure 4A). This suggested that the activation of p38MAPK may be the basis for the increased cell death observed in Htt-103 expressing cells and that interfering with its phosphorylation may rescue cells from polyglutamine-induced toxicity. Inhibition of p38MAPK with the use of SKF86002, a specific p38MAPK inhibitor, resulted in a significant rescue of Htt-103 expressing U87MG control and siPKCιA transfected cells such that their survival was comparable to Htt-25 and GFP transfectants treated with the inhibitor (Figure 4B). Similar results were obtained by blockade of p38MAPK with the use of SB202190, a different p38MAPK inhibitor; its inhibition resulted in a statistically significant increase in cell survival of PKCι depleted cells expressing Htt-103 (Figure 4C). The efficient blockade of p38MAPK activation in SKF86002 treated cells was confirmed by Western analysis of cell extracts from Htt-103 expressing cells with a phospho-ATF2 antibody, a downstream

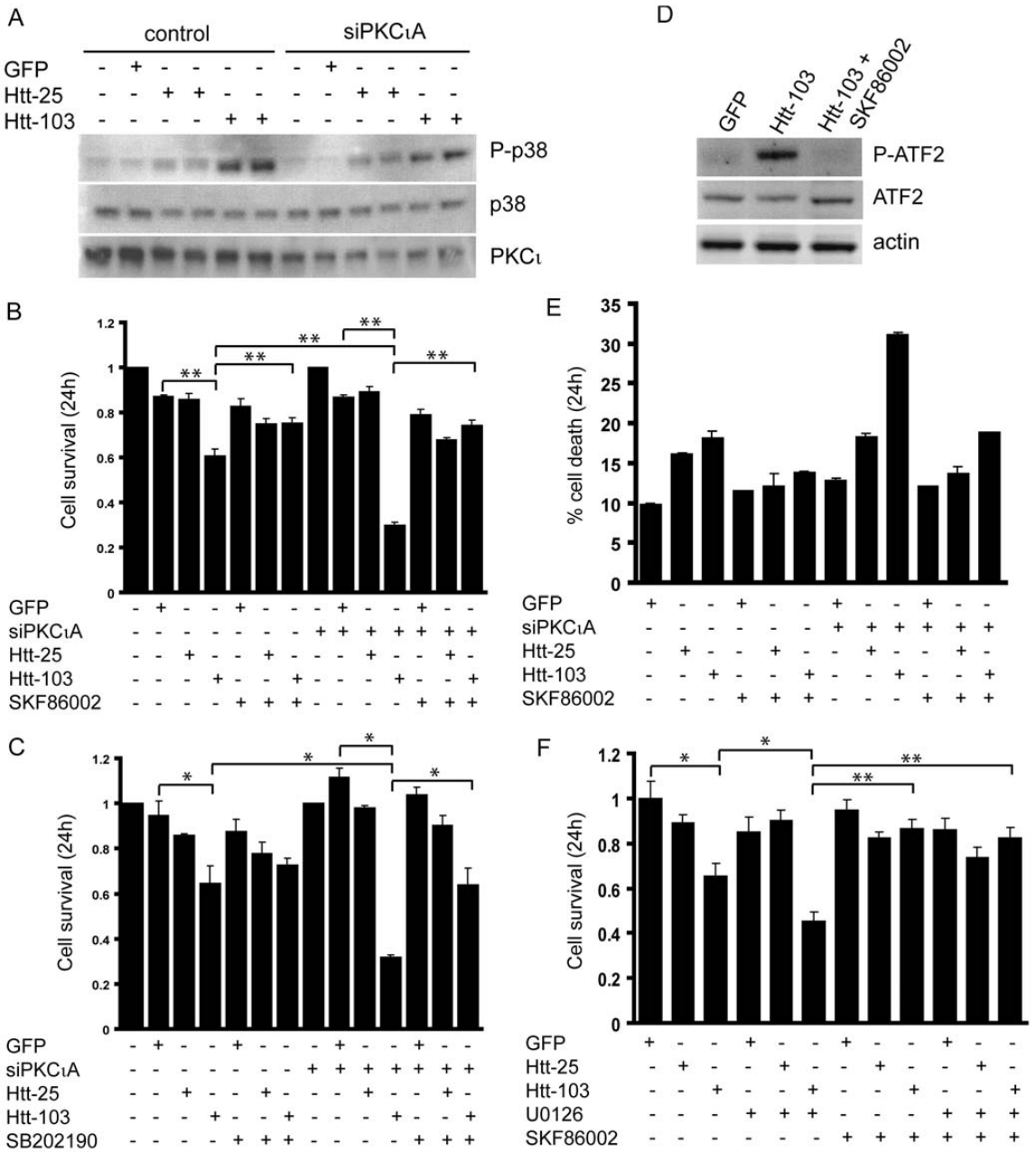

Figure 4. Expanded polyglutamine proteins induce p38MAPK. A) Western blot analysis of extracts from control and siPKCιA transfected cells expressing GFP, Htt-25 or Htt-103 with the phospho-38MAPK antibody showing the phosphorylation of p38MAPK in extracts from control and siPKCιA transfected cells expressing Htt-103. Phospho-p38MAPK levels were slightly increased in extracts from cells transfected with Htt-25 when compared to GFP transfectants. The levels of total p38MAPK remained unchanged in all extracts as assessed by Western blot analysis with the p38MAPK antibody. Efficient depletion of PKCι was confirmed by re-probing the membrane with the PKCι specific antibody. B) and C) Control or siPKCιA transfected cells were either left untreated or were pre-treated with p38MAPK inhibitors, SKF86002 (B) and SB202190 (C) for 2 hours prior to transfection with GFP, Htt-25 or Htt-103. 24 hours post-transfection, cell survival was assessed by MTT which revealed an increase in survival of Htt-103 expressing cells by treatment with SKF86002 in both control and siPKCιA transfected cells (** $p<0.01$). The survival of Htt-103 expressing cells treated with SB202190 was less pronounced when compared to SKF86002 treated cells but was still statistically increased in PKCι depleted cells when compared to the untreated counterparts (* $p<0.05$). D) Western blot analysis of cell extracts from cells expressing Htt-103 that were either untreated or treated with SKF86002 with the phospho-ATF2 antibody. The analysis revealed an abrogation of ATF2 phosphorylation in Htt-103 expressing cells treated with SKF86002. Re-probing the membrane with an ATF-2 antibody revealed no significant difference in the total levels of ATF2 protein. Actin

served as a loading control. E) Flow cytometric analysis of control and siPKCιA transfected cells expressing Htt-103 that were either left untreated or treated with SKF86002. The survival of SKF86002 treated, Htt-103 expressing cells was significantly improved when compared to the untreated counterparts and was comparable to the survival of GFP and Htt-25 transfectants in both the mock and PKCι depleted cells. Data is represented as the average of three independent experiments performed in duplicate with error bars indicating standard error of the mean. F) U87MG cells transfected with GFP, Htt-25 and Htt-103 were treated with SKF86002 in combination with U0126. Survival was assessed by MTT assay 24 hours post-transfection. As described above, treatment of Htt-103 expressing cells with U0126 resulted in reduced viability (* $p<0.05$) whereas treatment with SKF86002 alone or in combination with U0126 rescued cells from polyglutamine toxicity to a level that was similar to p38MAPK inhibition alone (** $p<0.01$). Data are represented as the average of three independent experiments performed in triplicate, with error bars indicating standard error of the mean.

doi:10.1371/journal.pone.0002130.g004

target of p38MAPK (Figure 4D). Flow cytometric analysis of Htt-103 expressing cells treated with SKF86002 revealed that inhibiting p38MAPK increased the survival of Htt-103 transfectants in both control and PKCι depleted cells (Figure 4E). To further dissect the relative importance of ERK and p38MAPK in polyglutamine-induced death, we treated GFP, Htt-25 and Htt-103 expressing U87MG cells with SKF86002 in combination with U0126. By MTT analysis, we found that pharmacological inhibition of p38MAPK alone or in combination with ERK inhibition resulted in a similar and significant rescue of cells from death associated with expression of Htt-103 (Figure 4F). These data suggest that the induction of p38MAPK contributes to polyglutamine-induced cytotoxicity and that whether in the presence or absence of activated ERK, its inhibition is sufficient to block cell death.

Full-length expanded human Ataxin-1 protein induces cell toxicity in a p38MAPK dependent manner

To investigate whether the depletion of PKCι and p38MAPK pathways represent a general mechanism of expanded polyglutamine toxicity, we transfected control or PKCι depleted cells with an expression construct encoding the full length ataxin-1 gene product with an expanded polyglutamine tract of 83Q (hereafter referred to as Atx-83). The length of the polyglutamine repeat in normal, unaffected humans is from 6 to 40 residues and mice expressing full length ataxin-1 with 30Qs (Atx-30) show no phenotype effects [37]; the Atx-30 expression was therefore a suitable control for the expanded (83Q) protein in our experiments. We were unable to detect expression of an ataxin-1 protein with only 2 glutamine residues and speculate that this variant may be unstable (data not shown). Western blot analysis of cell extracts from Atx-30 and Atx-83 transfected cells with the phospho-p38MAPK antibody revealed an increase in p38MAPK activation in Atx-83 expressing cells when compared to Atx-30 and parental U87MG cells (Figure 5A). Additionally, the ectopic expression of Atx-30 and Atx-83 resulted in an increase in total levels of p38MAPK as assessed by Western analysis of the same membrane with the antibody raised against total p38MAPK (Figure 5A). An increase in p38MAPK activation in response to ectopic expression of Atx-83 was also observed in NIH-3T3 fibroblasts and HT4 neuroblastoma cells suggesting that its induction represents a cell type independent mechanism of polyglutamine cytotoxicity (Figure 5B). By MTT assay, we found that the survival of control RNA transfected U87MG cells expressing Atx-83 was reduced when compared to cells expressing the non-expanded Atx-30 counterpart 24 hours post-transfection (Figure 5C). The sensitivity of cells expressing Atx-83 was significantly increased in PKCι depleted cells; survival was reduced by approximately 20% when compared to control RNA-transfected cells expressing an empty vector control (Figure 5C). Pharmacological inhibition of p38MAPK with the use of SKF86002 in Atx-83 expressing cells recapitulated the findings in Htt-103 transfectants; a statistically significant increase in cell survival was observed in control RNA transfectants and was more pronounced in PKCι depleted cells (Figure 5C). To confirm that the rescue observed in SKF86002 treated cells was attributable to blockade of p38MAPK signaling, we transiently co-transfected U87MG cells with the Atx-30 or Atx-83 plasmids in conjunction with constructs encoding either flag tagged wild-type p38 alpha (wt p38) or its dominant-negative kinase dead counterpart (KD p38). These expression constructs have previously been used to examine the contribution of p38MAPK signaling in cultured cells [50,51]. By MTT analysis we found that expression of the kinase dead p38MAPK increased survival of Htt-103 expressing cells in a similar manner to blockade with SKF86002 suggesting that the decrease in survival is due to activation of p38MAPK. The expression of wt p38 had no significant impact on survival of Atx-83 expressing cells (Figure 5D). The expression levels of Atx-30 and Atx-83 were similar as assessed by Western blot analysis with an ataxin-1 specific antibody (Figure 5E).

Expanded polyglutamine protein induced p38MAPK in the cerebella of SCA-1 transgenic mice

The *in vivo* induction of p38MAPK was examined in the previously characterized B05 mouse model of spinocerebellar ataxin-1 (SCA-1). In this model a human ataxin-1 cDNA with an expanded CAG tract encoding 82 glutamines is specifically expressed in Purkinje neurons (reviewed in [52]). The A02 transgenic strain expressing a similar construct with a non-pathological expansion of 30 glutamines served as a control. Western blot analysis of cerebellar extracts from aged-matched 3 month old mice with the phospho-p38MAPK antibody revealed phosphorylation of p38MAPK in extracts from nine B05 mice (five of which are shown in Figures 6A and B). In agreement with the findings in cultured cells, the phosphorylation of p38MAPK in lysates from A02 mice was lower than that detected in B05 extracts but slightly increased when compared to lysates from nontransgenic controls (Figure 6A). Contrary to what was observed in lysates from U87MG cells transfected with Atx-30 and Atx-83, re-probing the membrane with the antibody raised against total p38 revealed that total p38MAPK levels remained unchanged in A02 and B05 lysates when compared to nontransgenic control lysates (Figure 6A). We speculate that the induction of total p38MAPK levels may simply represent a response of cultured cells to the expression of Atx-30 and Atx-83. In B05 mice we observed a significant induction in p38MAPK phosphorylation at 3 months of age, while mice at 1 and 2 months of age show little or no detectable p38MAPK phosphorylation (Figure 6C). This activation correlates well with the onset of behavioral and anatomical anomalies in the mouse model of SCA-1. We examined the localization of phosphorylated p38MAPK by immunohistochemistry in cerebella of 3 month old nontransgenic and B05 mice. We found that phosphorylated p38MAPK was primarily localized to the cytoplasm and nucleus of Purkinje neurons (Figure 6D), showing that the increase in the levels of activated p38MAPK (as detected by Western analysis) could be attributed to expanded polyglutamine expression in those cells.

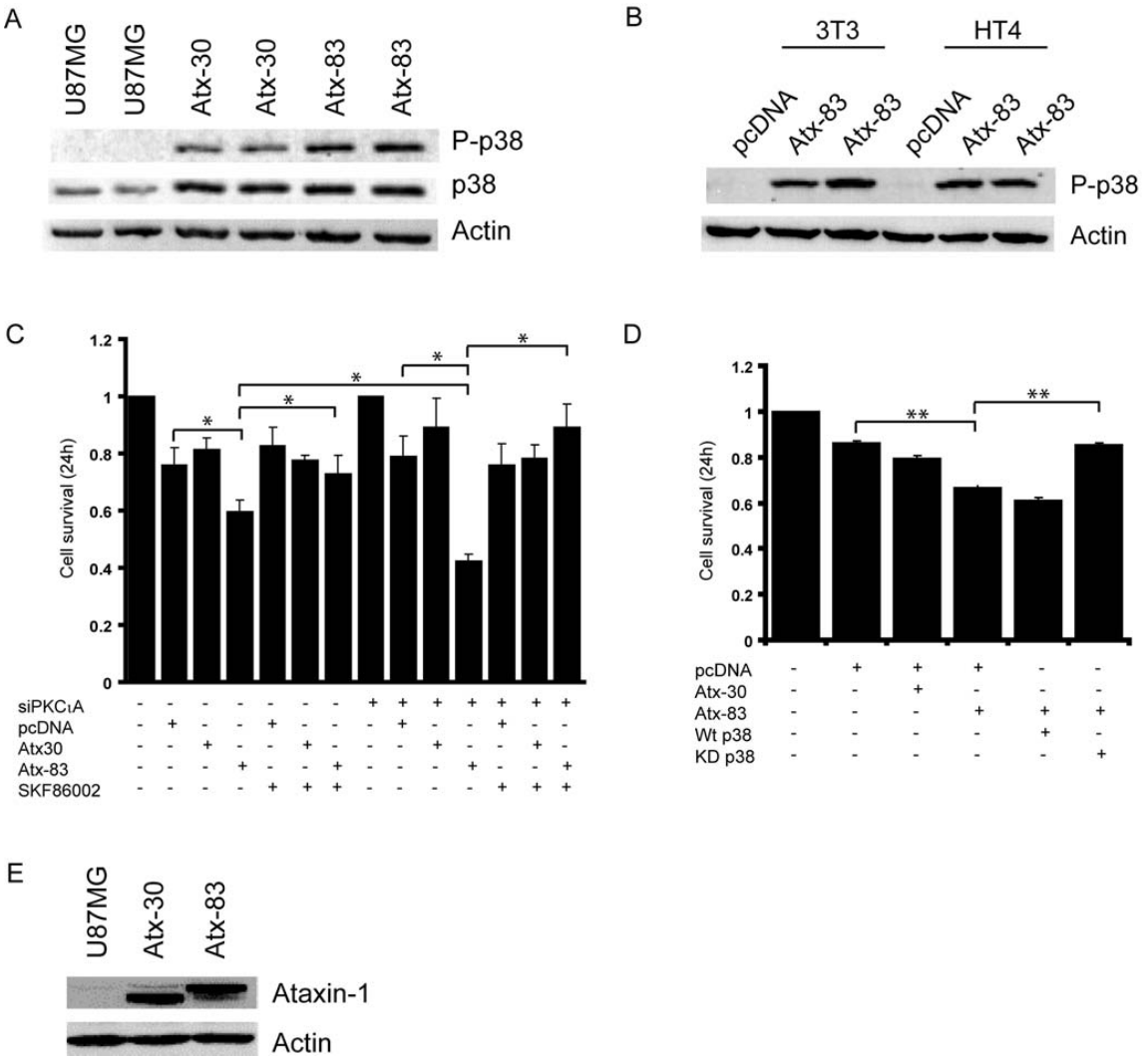

Figure 5. Expanded ataxin-1 toxicity is mediated through induction of p38MAPK. A) Western blot analysis of duplicate cell extracts from U87MG cells expressing Atx-30 and Atx-83 with the phospho-p38MAPK antibody. An increase in phosphorylated p38MAPK was observed in lysates from Atx-83 expressing cells when compared to lysates from mock transfected or cells expressing Atx-30. Total levels of p38MAPK were increased in lysates from cells transfected with either Atx-30 and Atx-83 when compared to mock transfected cells as assessed by re-probing of the membrane with the p38MAPK antibody. Actin served as a loading control. B) HT4 and NIH-3T3 cells were transiently transfected in duplicate with the Atx-83 expression construct. Cell extracts were analyzed by western blot analysis with the phospho-p38MAPK antibody. p38MAPK activation was observed in cell extracts from both NIH-3T3 and HT4 cells expressing Atx-83. The induction of p38MAPK was not observed in lysates from cells expressing an empty vector control. C) Untreated or SKF86002 treated control or siPKCιA transfected cells were transfected with Atx-30 or Atx-83 for 24 hours and cell survival was assessed by MTT. The analysis revealed a decrease in survival of Atx-83 expressing cells in control RNA transfected cells that was significantly more pronounced by PKCι depletion. Blockade of p38MAPK increased survival of Atx-83 expressing cells in both control and siPKCι transfectants such that it was comparable to the survival of Atx-30 expressing cells. Data represent the average of three independent experiments performed in triplicate, with error bars indicating standard error of the mean (* $p<0.05$). D) U87MG cells were co-transfected with Htt-103 and either empty vector alone or expression constructs encoding wild-type (wt p38) or dominant-negative (KD) p38MAPK alpha. 24 hours post-transfection, cells were analyzed by MTT which revealed a statistically significant increase in survival in cells co-expressing Htt-103 and dominant-negative p38MAPK alpha (** $p<0.01$). The survival of cells expressing empty vector control alone or co-expressing Htt-25 with empty vector was not significantly different. E) Western blot analysis of extracts from Atx-30 and Atx-83 transfected cells with an ataxin-1 specific antibody revealing a similar level of expression. Actin served as a loading control.
doi:10.1371/journal.pone.0002130.g005

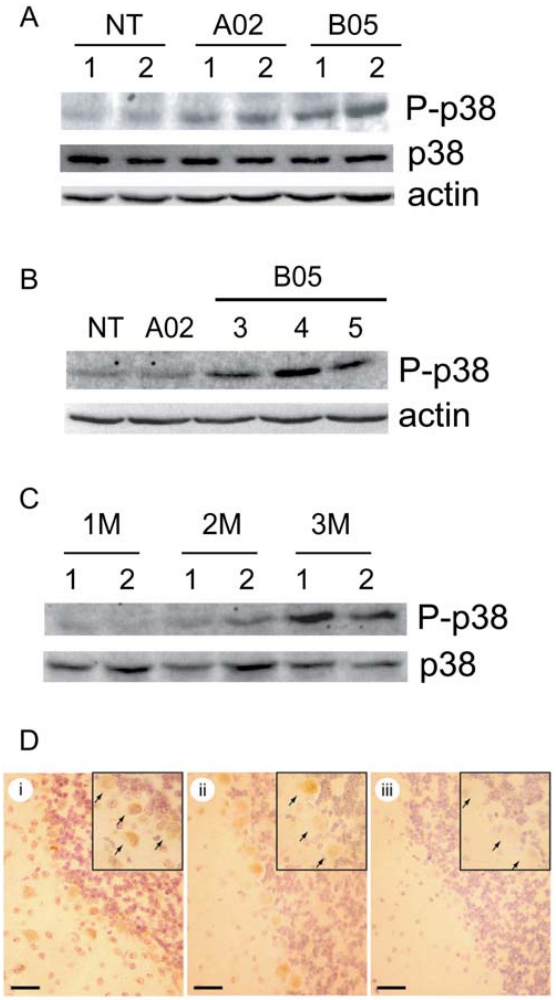

Figure 6. In vivo induction of p38MAPK in SCA-1 mice. A) and B) Western blot analysis of cerebellar extracts from 3 month-old non-transgenic, A02 and B05 mice with the phospho-p38MAPK antibody. An increase in the protein levels of phospho-p38 was detected in the extracts from B05 mice when compared to A02 and nontransgenic control extracts. Total p38MAPK levels were similar as assessed by re-probing the membrane with the p38MAPK antibody or actin. C) Western blot analysis of cerebellar extracts from B05 mice at 1,2 and 3 months of age with the phospho-p38MAPK antibody. The analysis revealed a detectable induction in p38MAPK activation in lysates from mice at 3 month of age. Total levels of p38MAPK were assayed by re-probing the membrane with the p38MAPK antibody which also served as a loading control. D) Immunohistochemistry of mouse cerebella with the phospho-p38MAPK antibody. Panel i) cerebellum of a B05 animal and panel ii) cerebellum of a nontransgenic animal. Immunoreactivity was observed in the cytoplasm and nucleus of Purkinje neurons in B05 and nontransgenic mice. Panel iii) section from a B05 animal stained with the secondary antibody alone demonstrating the absence of immunoreactivity by omission of the primary antibody. Scale bars represent 25 μm.
doi:10.1371/journal.pone.0002130.g006

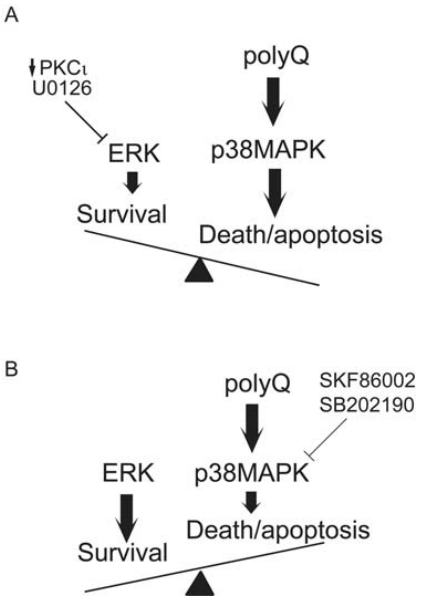

Figure 7. Model of polyglutamine induced toxicity. Activation p38MAPK signaling is counteracted by PKCι-mediated ERK activation in expanded polyglutamine expressing cells. The pharmacological blockade of ERK with U0126 or by PKCι depletion sensitizes cells to polyglutamine-induced death through a mechanism of exaggerated induction of p38MAPK (A). In contrast, inhibition of p38MAPK phosphorylation by SKF86002 or SB202190 rescues cells from polyglutamine toxicity (B). The blockade of both signaling pathways in cells expressing expanded polyglutamine proteins recapitulates blockade of p38MAPK (B) indicating a causative association between p38MAPK induction and polyglutamine induced death.
doi:10.1371/journal.pone.0002130.g007

Discussion

Clear evidence for the essential role of protein kinase C family members in neuronal homeostasis has been provided by neurodegeneration attributable to a loss of function mutation in the *PKCγ* gene in spinocerebellar ataxia type 14 (SCA-14, [53]). No such genetic disorder has been mapped to the *PKCι* gene, but evidence from overexpression studies indicates that PKCι can be protective against a variety of cytotoxic insults including UV damage and chemotherapy [38,54] and neurotoxic insults including beta amyloid [55]. Conversely, inhibition of PKCι and the closely related PKCζ by the prostate apoptosis-response 4 (PAR-4) protein has been recently shown to increase proteolytic processing of amyloid precursor protein [56,57] and to exacerbate Aβ accumulation and toxicity in mouse models of Alzheimer's disease [58,59] suggesting a role for PKCι in modulating survival.

Using specific MAP kinase inhibitors we have established that p38MAPK is activated in expanded polyglutamine expressing cells and that PKCι-mediated ERK activation can antagonize polyglutamine-induced cell death in a cell culture model. Our data are in accordance with a recent report demonstrating the protective effects of ERK activation in expanded polyglutamine expressing cells [19]. Based on our findings, we propose a mechanism (schematically depicted in Figure 7) wherein p38MAPK induction contributes significantly to the toxicity observed in expanded polyglutamine expressing cells while ERK activation serves to counteract its effects. The fate of cells

expressing polyglutamine proteins would therefore seem to be determined, in part, by comparing the activation state of the two signaling cascades. In this model the ERK cascade would generate a pro-survival signal in response to PKCι-mediated input. The p38MAPK cascade would generate a pro-death output specifically in response to the expanded polyglutamine protein. If the p38MAPK signal outweighed the ERK signal (as is the case by expression of expanded polyglutamine proteins or by blockade of ERK and/or PKCι signaling) the cell would respond by activating its cell death program. In the presence of expanded polyglutamine proteins the simultaneous blockade of both ERK and p38MAPK signaling pathways was found to be functionally equivalent to blockade of p38MAPK alone suggesting that the inhibition of p38MAPK was sufficient to block cell death regardless of the presence or absence of activated ERK (Figure 4F). To promote the survival of neurons in neurodegenerative disorders it may therefore suffice to block p38MAPK signaling (there may be no added therapeutic benefit in promoting the ERK-mediated survival signal, despite previously published evidence that ERK activation promotes survival of polyQ-expressing PC12 cells [19]). Consistent with our supposition that p38MAPK blockade should be the therapeutic objective is recent evidence demonstrating that the promotion of ERK-mediated signaling may ultimately compromise neuronal viability ([60–62] and reviewed in [63,64]).

A recent report has implicated activated stress inducible JNK in a cell culture model of HD [19] and its pharmacological blockade resulted in a statistically significant but partial inhibition of cell death [19]. Our data do not allow us to formally exclude a role for JNK, and it is conceivable that the concerted action of both these pathways mediate adverse effects on polyglutamine expressing cells. Whether or not this is the case the almost complete rescue of cell death by inhibition of p38MAPK under our experimental design suggests a significant contribution of this kinase in mediating toxicity.

The model presented in Figure 7 is based on data from polyglutamine tracts in two quite different contexts (an expanded polyglutamine tract appended to exon 1 of the huntingtin protein and the pathogenic form of full length ataxin-1), suggesting that it may have applicability to expanded polyglutamine proteins in general. The activation of p38MAPK was detected in cultured mammalian cells of different origins (glioblastoma, fibroblasts and cells of neural lineage) and more importantly in cerebellar Purkinje neurons of transgenic mice expressing the neuropathogenic ataxin-1 cDNA at the age of onset of pathology (Figure 6 and [65]). In conjunction with recent reports demonstrating p38MAPK induction in cellular [66] and animal models of Alzheimer's disease [67,68] and amyotrophic lateral sclerosis [69–71], our data suggest that blockade of p38MAPK may have broad utility in delaying the progress of neurodegenerative diseases, even those that do not involve expanded polyglutamine proteins. Consistent with this supposition is the finding that inhibition of p38MAPK is beneficial in mouse models of disease [72,73] and in the suppression of human inflammatory conditions [74–76]. Here we demonstrate that pharmacological blockade of p38MAPK may potentially be an efficacious intervention for the polyglutamine disorders. Such an intervention may not only attenuate regional inflammation (reviewed in [77]) and decrease the phosphorylation of HSP27 (a downstream target of p38/MAPKAP 2/3 whose phosphorylation status has been shown to modulate the cytotoxity of polyglutamine expressing cells, [78]), but may delay or preclude the otherwise inexorable neuronal loss that is associated with these diseases.

Other therapeutic modalities may become apparent as the events downstream of p38 MAPK activation by polyglutamine proteins become known. At this point it is not at all clear how many and which of the several pathogenic mechanisms might be affected by p38MAPK signaling. One plausible scenario is that p38MAPK activation leads to transcriptional dysregulation through negative effects on pivotal transcriptional regulators. For example, the levels of the p300/CBP histone acetyltransferase enzymes are known to be affected by expanded polyglutamine proteins [6,79–81], and their loss correlates with reduced expression of a set of target genes whose importance to neuronal homeostasis is well established [79,82]. It has recently been shown that p300 is degraded by the proteasome in response to p38MAPK activation [83] and that partial inhibition of proteolysis may delay the loss of p300/CBP in the SCA-1 model [84]. Consistent with this model, inhibitors of histone deacetylases (HDACs) have been shown to have beneficial effects in counteracting polyglutamine protein toxicity [85–88] and recently reviewed in [89]. The histone acetyltransferases would therefore seem promising as downstream targets of p38MAPK, and we are currently seeking a deeper understanding of this relationship.

Acknowledgments

We thank Dr. Ron Kopito for the Htt-expression constructs, Dr. Huda Zoghbi for the pcDNA human-ataxin-1 plasmids, and Dr. Harry Orr for the A02 and B05 transgenic strains.

Author Contributions

Conceived and designed the experiments: MT RB. Performed the experiments: MT RB MT. Analyzed the data: DG MT RB MT IL. Contributed reagents/materials/analysis tools: DG IL. Wrote the paper: DG MT RB MT IL.

References

1. Everett CM, Wood NW (2004) Trinucleotide repeats and neurodegenerative disease. Brain 127: 2385–2405.
2. Jana NR, Nukina N (2003) Recent advances in understanding the pathogenesis of polyglutamine diseases: involvement of molecular chaperones and ubiquitin-proteasome pathway. J Chem Neuroanat 26: 95–101.
3. Ross CA (1997) Intranuclear neuronal inclusions: a common pathogenic mechanism for glutamine-repeat neurodegenerative diseases? Neuron 19: 1147–1150.
4. Landles C, Bates GP (2004) Huntingtin and the molecular pathogenesis of Huntington's disease. Fourth in molecular medicine review series. EMBO Rep 5: 958–963.
5. Rangone H, Pardo R, Colin E, Girault JA, Saudou F, et al. (2005) Phosphorylation of arfaptin 2 at Ser260 by Akt Inhibits polyQ-huntingtin-induced toxicity by rescuing proteasome impairment. J Biol Chem 280: 22021–22028.
6. Sugars KL, Brown RJ, Cook L, Swartz J, Rubinsztein DC (2004) Decreased cAMP response element-mediated transcription: an early event in exon 1 and full-length cell models of Huntington's disease that contributes to polyglutamine pathogenesis. J Biol Chem 279: 4988–4999.
7. Sherman MY, Goldberg AL (2001) Cellular defenses against unfolded proteins: a cell biologist thinks about neurodegenerative diseases. Neuron 29: 15–32.
8. Kuida K, Boucher DM (2004) Functions of MAP kinases: insights from gene-targeting studies. J Biochem (Tokyo) 135: 653–656.
9. Johnson GL, Lapadat R (2002) Mitogen-activated protein kinase pathways mediated by ERK, JNK, and p38 protein kinases. Science 298: 1911–1912.
10. Torii S, Nakayama K, Yamamoto T, Nishida E (2004) Regulatory mechanisms and function of ERK MAP kinases. J Biochem (Tokyo) 136: 557–561.
11. Harper SJ, LoGrasso P (2001) Signalling for survival and death in neurones: the role of stress-activated kinases, JNK and p38. Cell Signal 13: 299–310.
12. Kolch W (2005) Coordinating ERK/MAPK signalling through scaffolds and inhibitors. Nat Rev Mol Cell Biol 6: 827–837.
13. Hunot S, Vila M, Teismann P, Davis RJ, Hirsch EC, et al. (2004) JNK-mediated induction of cyclooxygenase 2 is required for neurodegeneration in a mouse model of Parkinson's disease. Proc Natl Acad Sci U S A 101: 665–670.
14. Silva RM, Kuan CY, Rakic P, Burke RE (2005) Mixed lineage kinase-c-jun N-terminal kinase signaling pathway: a new therapeutic target in Parkinson's disease. Mov Disord 20: 653–664.

15. Song C, Perides G, Liu YF (2002) Expression of full-length polyglutamine-expanded Huntingtin disrupts growth factor receptor signaling in rat pheochromocytoma (PC12) cells. J Biol Chem 277: 6703–6707.
16. Li SH, Cheng AL, Li H, Li XJ (1999) Cellular defects and altered gene expression in PC12 cells stably expressing mutant huntingtin. J Neurosci 19: 5159–5172.
17. Charroux B, Freeman M, Kerridge S, Baonza A (2006) Atrophin contributes to the negative regulation of epidermal growth factor receptor signaling in Drosophila. Dev Biol 291: 278–290.
18. Lievens J-C, Rival T, Iche M, Chneiweiss H, Birman S (2005) Expanded polyglutamine peptides disrupt EGF receptor signaling and glutamate transporter expression in Drosophila. Hum Mol Genet 14: 713–724.
19. Apostol BL, Illes K, Pallos J, Bodai L, Wu J, et al. (2006) Mutant huntingtin alters MAPK signaling pathways in PC12 and striatal cells: ERK1/2 protects against mutant huntingtin-associated toxicity. Hum Mol Genet 15: 273–285.
20. Miller VM, Nelson RF, Gouvion CM, Williams A, Rodriguez-Lebron E, et al. (2005) CHIP suppresses polyglutamine aggregation and toxicity in vitro and in vivo. J Neurosci 25: 9152–9161.
21. Senut MC, Suhr ST, Kaspar B, Gage FH (2000) Intraneuronal aggregate formation and cell death after viral expression of expanded polyglutamine tracts in the adult rat brain. J Neurosci 20: 219–229.
22. Gauthier LR, Charrin BC, Borrell-Pages M, Dompierre JP, Rangone H, et al. (2004) Huntingtin controls neurotrophic support and survival of neurons by enhancing BDNF vesicular transport along microtubules. Cell 118: 127–138.
23. Miyashita T, Tabuchi A, Fukuchi M, Hara D, Kisukeda T, et al. (2005) Interference with activity-dependent transcriptional activation of BDNF gene depending upon the expanded polyglutamines in neurons. Biochem Biophys Res Commun 333: 1241–1248.
24. Humbert S, Bryson EA, Cordelieres FP, Connors NC, Datta SR, et al. (2002) The IGF-1/Akt Pathway Is Neuroprotective in Huntington's Disease and Involves Huntingtin Phosphorylation by Akt. Developmental Cell 2: 831–837.
25. Vig PJS, Subramony SH, D'Souza DR, Wei J, Lopez ME (2006) Intranasal administration of IGF-I improves behavior and Purkinje cell pathology in SCA1 mice. Brain Research Bulletin 69: 573–579.
26. Laurino L, Wang XX, de la Houssaye BA, Sosa L, Dupraz S, et al. (2005) PI3K activation by IGF-1 is essential for the regulation of membrane expansion at the nerve growth cone. J Cell Sci 118: 3653–3662.
27. Pearse RN, Swendeman SL, Li Y, Rafii D, Hempstead BL (2005) A neurotrophin axis in myeloma: TrkB and BDNF promote tumor-cell survival. Blood 105: 4429–4436.
28. Zheng W-H, Quirion R (2004) Comparative signaling pathways of insulin-like growth factor-1 and brain-derived neurotrophic factor in hippocampal neurons and the role of the PI3 kinase pathway in cell survival. Journal of Neurochemistry 89: 844–852.
29. Yu X-R, Jia G-R, Gao G-D, Wang S-H, Han Y, et al. (2006) Neuroprotection of Insulin against Oxidative Stress-induced Apoptosis in Cultured Retinal Neurons: Involvement of Phosphoinositide 3-kinase/Akt Signal Pathway. Acta Biochimica et Biophysica Sinica 38: 241–248.
30. Li B-S, Ma W, Jaffe H, Zheng Y, Takahashi S, et al. (2003) Cyclin-dependent Kinase-5 Is Involved in Neuregulin-dependent Activation of Phosphatidylinositol 3-Kinase and Akt Activity Mediating Neuronal Survival. J Biol Chem 278: 35702–35709.
31. Nakazawa T, Shimura M, Tomita H, Akiyama H, Yoshioka Y, et al. (2003) Intrinsic activation of PI3K/Akt signaling pathway and its neuroprotective effect against retinal injury. Current Eye Research 26: 55–63.
32. Campbell CSG, Caperuto LC, Hirata AE, Araujo EP, Velloso LA, et al. (2004) The phosphatidylinositol/AKT/atypical PKC pathway is involved in the improved insulin sensitivity by DHEA in muscle and liver of rats in vivo. Life Sciences 76: 57–70.
33. Antonella Muscella SG, Maria Giovanna Elia, Carlo Storelli, Santo Marsigliante (2004) Differential signalling of purinoceptors in HeLa cells through the extracellular signal-regulated kinase and protein kinase C pathways. Journal of Cellular Physiology 200: 428–439.
34. Bandyopadhyay G, Standaert ML, Sajan MP, Kanoh Y, Miura A, et al. (2004) Protein Kinase C-{lambda} Knockout in Embryonic Stem Cells and Adipocytes Impairs Insulin-Stimulated Glucose Transport. Mol Endocrinol 18: 373–383.
35. Warby SC, Chan EY, Metzler M, Gan L, Singaraja RR, et al. (2005) Huntingtin phosphorylation on serine 421 is significantly reduced in the striatum and by polyglutamine expansion in vivo. Hum Mol Genet 14: 1569–1577.
36. Kaytor MD, Byam CE, Tousey SK, Stevens SD, Zoghbi HY, et al. (2005) A cell-based screen for modulators of ataxin-1 phosphorylation. Hum Mol Genet 14: 1095–1105.
37. Burright EN, Clark HB, Servadio A, Matilla T, Feddersen RM, et al. (1995) SCA1 transgenic mice: a model for neurodegeneration caused by an expanded CAG trinucleotide repeat. Cell 82: 937–948.
38. Baldwin RM, Garratt-Lalonde M, Parolin DAE, Krzyzanowski PM, Andrade MA, et al. (2005) Protection of glioblastoma cells from cisplatin cytotoxicity via protein kinase C[iota]-mediated attenuation of p38 MAP kinase signaling. Oncogene 25: 2909–2919.
39. Wu C-j, Chen Z, Ullrich A, Greene MI, O'Rourke DM (2000) Inhibition of EGFR-mediated phosphoinositide-3-OH kinase (PI3-K) signaling and glioblastoma phenotype by Signal-Regulatory Proteins (SIRPs). Oncogene 19: 3999.
40. Swayne LA, Chen L, Hameed S, Barr W, Charlesworth E, et al. (2005) Crosstalk between huntingtin and syntaxin 1A regulates N-type calcium channels. Molecular and Cellular Neuroscience 30: 339–351.
41. Cha J-HJ, Kosinski CM, Kerner JA, Alsdorf SA, Mangiarini L, et al. (1998) Altered brain neurotransmitter receptors in transgenic mice expressing a portion of an abnormal human Huntington disease gene. Proceedings of the National Academy of Sciences 95: 6480–6485.
42. Carter RJ, Lione LA, Humby T, Mangiarini L, Mahal A, et al. (1999) Characterization of Progressive Motor Deficits in Mice Transgenic for the Human Huntington's Disease Mutation. J Neurosci 19: 3248–3257.
43. Regala RP, Weems C, Jamieson L, Khoor A, Edell ES, et al. (2005) Atypical protein kinase C iota is an oncogene in human non-small cell lung cancer. Cancer Res 65: 8905–8911.
44. Colognato R, Laurenza I, Fontana I, Coppede F, Siciliano G, et al. (2006) Modulation of hydrogen peroxide-induced DNA damage, MAPKs activation and cell death in PC12 by ergothioneine. Clin Nutr 25: 135–145.
45. Papoutsaki M, Moretti F, Lanza M, Marinari B, Sartorelli V, et al. (2005) A p38-dependent pathway regulates DeltaNp63 DNA binding to p53-dependent promoters in UV-induced apoptosis of keratinocytes. Oncogene 24: 6970–6975.
46. Nolan Y, Vereker E, Lynch AM, Lynch MA (2003) Evidence that lipopolysaccharide-induced cell death is mediated by accumulation of reactive oxygen species and activation of p38 in rat cortex and hippocampus. Exp Neurol 184: 794–804.
47. Bodles AM, Barger SW (2005) Secreted beta-amyloid precursor protein activates microglia via JNK and p38-MAPK. Neurobiol Aging 26: 9–16.
48. Puig B, Gomez-Isla T, Ribe E, Cuadrado M, Torrejon-Escribano B, et al. (2004) Expression of stress-activated kinases c-Jun N-terminal kinase (SAPK/JNK-P) and p38 kinase (p38-P), and tau hyperphosphorylation in neurites surrounding betaA plaques in APP Tg2576 mice. Neuropathol Appl Neurobiol 30: 491–502.
49. Lipinski MM, Yuan J (2004) Mechanisms of cell death in polyglutamine expansion diseases. Curr Opin Pharmacol 4: 85–90.
50. Ge B, Gram H, Di Padova F, Huang B, New L, et al. (2002) MAPKK-Independent Activation of p38alpha Mediated by TAB1-Dependent Autophosphorylation of p38alpha. Science 295: 1291–1294.
51. Wang X, McGowan CH, Zhao M, He L, Downey JS, et al. (2000) Involvement of the MKK6-p38gamma Cascade in gamma -Radiation-Induced Cell Cycle Arrest. Mol Cell Biol 20: 4543–4552.
52. Orr HT (2000) The ins and outs of a polyglutamine neurodegenerative disease: spinocerebellar ataxia type 1 (SCA1). Neurobiol Dis 7: 129–134.
53. van de Warrenburg BP, Verbeek DS, Piersma SJ, Hennekam FA, Pearson PL, et al. (2003) Identification of a novel SCA14 mutation in a Dutch autosomal dominant cerebellar ataxia family. Neurology 61: 1760–1765.
54. Chuanshu Huang JL, Nanyue Chen, Wei-ya Ma, G. Tim Bowden, Zigang Dong (2000) Inhibition of atypical PKC blocks ultraviolet-induced AP-1 activation by specifically inhibiting ERKs activation. Molecular Carcinogenesis 27: 65–75.
55. Xie J, Guo Q, Zhu H, Wooten MW, Mattson MP (2000) Protein kinase C iota protects neural cells against apoptosis induced by amyloid [beta]-peptide. Molecular Brain Research 82: 107–113.
56. Xie J, Guo Q (2005) PAR-4 is involved in regulation of beta-secretase cleavage of the Alzheimer amyloid precursor protein. J Biol Chem 280: 13824–13832.
57. Guo Q, Xie J, Chang X, Du H (2001) Prostate Apoptosis Response-4 Enhances Secretion of Amyloid beta Peptide 1-42 in Human Neuroblastoma IMR-32 Cells by a Caspase-dependent Pathway. J Biol Chem 276: 16040–16044.
58. Guo Q, Xie J (2004) AATF Inhibits Aberrant Production of Amyloid {beta} Peptide 1-42 by Interacting Directly with Par-4. J Biol Chem 279: 4596–4603.
59. Xie J, Chang X, Zhang X, Guo Q (2001) Aberrant induction of Par-4 is involved in apoptosis of hippocampal neurons in presenilin-1 M146V mutant knock-in mice. Brain Research 915: 1–10.
60. Monteiro FA, Sousa MM, Cardoso I, do Amaral JB, Guimaraes A, et al. (2006) Activation of ERK1/2 MAP kinases in familial amyloidotic polyneuropathy. J Neurochem 97: 151–161.
61. Subramaniam S, Unsicker K (2006) Extracellular signal-regulated kinase as an inducer of non-apoptotic neuronal death. Neuroscience 138: 1055–1065.
62. Subramaniam S, Zirrgiebel U, von Bohlen und Halbach O, Strelau J, Laliberte C, et al. (2004) ERK activation promotes neuronal degeneration predominantly through plasma membrane damage and independently of caspase-3. J Cell Biol 165: 357–369.
63. Cheung ECC, Slack RS (2004) Emerging Role for ERK as a Key Regulator of Neuronal Apoptosis. Sci STKE 2004: pe45-.
64. Luca Colucci-D'Amato CP-C, Umberto di Porzio (2003) Chronic activation of ERK and neurodegenerative diseases. BioEssays 25: 1085–1095.
65. Skinner PJ, Vierra-Green CA, Clark HB, Zoghbi HY, Orr HT (2001) Altered trafficking of membrane proteins in purkinje cells of SCA1 transgenic mice. Am J Pathol 159: 905–913.
66. Tamagno E, Robino G, Obbili A, Bardini P, Aragno M, et al. (2003) H2o2 and 4-hydroxynonenal mediate amyloid [beta]-induced neuronal apoptosis by activating jnks and p38mapk. Experimental Neurology 180: 144–155.
67. Sahara N, Vega IE, Ishizawa T, Lewis J, McGowan E, et al. (2004) Phosphorylated p38MAPK specific antibodies cross-react with sarkosyl-insoluble hyperphosphorylated tau proteins. Journal of Neurochemistry 90: 829–838.
68. Giovannini MG, Scali C, Prosperi C, Bellucci A, Vannucchi MG, et al. (2002) [beta]-Amyloid-Induced Inflammation and Cholinergic Hypofunction in the Rat Brain in Vivo: Involvement of the p38MAPK Pathway. Neurobiology of Disease 11: 257–274.

69. Tortarolo M, Veglianese P, Calvaresi N, Botturi A, Rossi C, et al. (2003) Persistent activation of p38 mitogen-activated protein kinase in a mouse model of familial amyotrophic lateral sclerosis correlates with disease progression. Mol Cell Neurosci 23: 180–192.
70. Holasek SS, Wengenack TM, Kandimalla KK, Montano C, Gregor DM, et al. (2005) Activation of the stress-activated MAP kinase, p38, but not JNK in cortical motor neurons during early presymptomatic stages of amyotrophic lateral sclerosis in transgenic mice. Brain Research 1045: 185–198.
71. Ackerley S, Grierson AJ, Banner S, Perkinton MS, Brownlees J, et al. (2004) p38[alpha] stress-activated protein kinase phosphorylates neurofilaments and is associated with neurofilament pathology in amyotrophic lateral sclerosis. Molecular and Cellular Neuroscience 26: 354–364.
72. Hildesheim J, Awwad RT, Fornace AJ Jr. (2004) p38 Mitogen-activated protein kinase inhibitor protects the epidermis against the acute damaging effects of ultraviolet irradiation by blocking apoptosis and inflammatory responses. J Invest Dermatol 122: 497–502.
73. Jochen Zwerina SH, Kurt Redlich, Klaus Bobacz, Giorgos Kollias, Josef S. Smolen, Georg Schett (2006) Activation of p38 MAPK is a key step in tumor necrosis factor-mediated inflammatory bone destruction. Arthritis & Rheumatism 54: 463–472.
74. Branger J, van den Blink B, Weijer S, Gupta A, van Deventer SJ, et al. (2003) Inhibition of coagulation, fibrinolysis, and endothelial cell activation by a p38 mitogen-activated protein kinase inhibitor during human endotoxemia. Blood 101: 4446–4448.
75. Branger J, van den Blink B, Weijer S, Madwed J, Bos CL, et al. (2002) Anti-inflammatory effects of a p38 mitogen-activated protein kinase inhibitor during human endotoxemia. J Immunol 168: 4070–4077.
76. van den Blink B, Branger J, Weijer S, Gupta A, van Deventer SJ, et al. (2004) P38 mitogen activated protein kinase is involved in the downregulation of granulocyte CXC chemokine receptors 1 and 2 during human endotoxemia. J Clin Immunol 24: 37–41.
77. Block ML, Hong JS (2005) Microglia and inflammation-mediated neurodegeneration: multiple triggers with a common mechanism. Prog Neurobiol 76: 77–98.
78. Wyttenbach A, Sauvageot O, Carmichael J, Diaz-Latoud C, Arrigo AP, et al. (2002) Heat shock protein 27 prevents cellular polyglutamine toxicity and suppresses the increase of reactive oxygen species caused by huntingtin. Hum Mol Genet 11: 1137–1151.
79. Nucifora FC Jr., Sasaki M, Peters MF, Huang H, Cooper JK, et al. (2001) Interference by Huntingtin and Atrophin-1 with CBP-Mediated Transcription Leading to Cellular Toxicity. Science 291: 2423–2428.
80. McCampbell A, Taylor JP, Taye AA, Robitschek J, Li M, et al. (2000) CREB-binding protein sequestration by expanded polyglutamine. Hum Mol Genet 9: 2197–2202.
81. Cong S-Y, Pepers BA, Evert BO, Rubinsztein DC, Roos RAC, et al. (2005) Mutant huntingtin represses CBP, but not p300, by binding and protein degradation. Molecular and Cellular Neuroscience 30: 12–23.
82. Chiang M-C, Lee Y-C, Huang C-L, Chern Y (2005) cAMP-response Element-binding Protein Contributes to Suppression of the A2A Adenosine Receptor Promoter by Mutant Huntingtin with Expanded Polyglutamine Residues. J Biol Chem 280: 14331–14340.
83. Poizat C, Puri PL, Bai Y, Kedes L (2005) Phosphorylation-Dependent Degradation of p300 by Doxorubicin-Activated p38 Mitogen-Activated Protein Kinase in Cardiac Cells. Mol Cell Biol 25: 2673–2687.
84. Tsirigotis M, Tang MY, Beyers M, Zhang M, Woulfe J, et al. (2006) Delayed spinocerebellar ataxia in transgenic mice expressing mutant ubiquitin. Neuropathology and Applied Neurobiology 32: 26–39.
85. Kariya S, Hirano M, Uesato S, Nagai Y, Nagaoka Y, et al. (2006) Cytoprotective effect of novel histone deacetylase inhibitors against polyglutamine toxicity. Neuroscience Letters 392: 213–215.
86. Minamiyama M, Katsuno M, Adachi H, Waza M, Sang C, et al. (2004) Sodium butyrate ameliorates phenotypic expression in a transgenic mouse model of spinal and bulbar muscular atrophy. Hum Mol Genet 13: 1183–1192.
87. Hockly E, Richon VM, Woodman B, Smith DL, Zhou X, et al. (2003) Suberoylanilide hydroxamic acid, a histone deacetylase inhibitor, ameliorates motor deficits in a mouse model of Huntington's disease. PNAS 100: 2041–2046.
88. Steffan JS, Bodai L, Pallos J, Poelman M, McCampbell A, et al. (2001) Histone deacetylase inhibitors arrest polyglutamine-dependent neurodegeneration in Drosophila. 413: 739–743.
89. Rouaux C, Loeffler J-P, Boutillier A-L (2004) Targeting CREB-binding protein (CBP) loss of function as a therapeutic strategy in neurological disorders. Biochemical Pharmacology Proceedings from the 6th and 7th international conferences, Signal Transduction 2004 and Chromatin 2004 68: 1157–1164.

APPENDIX 4. Experimental and Computational Analysis of Polyglutamine-Mediated Cytotoxicity

OPEN ACCESS Freely available online PLoS COMPUTATIONAL BIOLOGY

Experimental and Computational Analysis of Polyglutamine-Mediated Cytotoxicity

Matthew Y. Tang[1,2], Carole J. Proctor[3], John Woulfe[1,2], Douglas A. Gray[1,2,3]*

1 Ottawa Hospital Research Institute, Ottawa, Ontario, Canada, **2** Department of Biochemistry, Microbiology and Immunology, University of Ottawa, Ottawa, Ontario, Canada, **3** Centre for Integrated Systems Biology of Ageing and Nutrition, Institute for Ageing and Health, Newcastle University, Newcastle upon Tyne, United Kingdom

Abstract

Expanded polyglutamine (polyQ) proteins are known to be the causative agents of a number of human neurodegenerative diseases but the molecular basis of their cytoxicity is still poorly understood. PolyQ tracts may impede the activity of the proteasome, and evidence from single cell imaging suggests that the sequestration of polyQ into inclusion bodies can reduce the proteasomal burden and promote cell survival, at least in the short term. The presence of misfolded protein also leads to activation of stress kinases such as p38MAPK, which can be cytotoxic. The relationships of these systems are not well understood. We have used fluorescent reporter systems imaged in living cells, and stochastic computer modeling to explore the relationships of polyQ, p38MAPK activation, generation of reactive oxygen species (ROS), proteasome inhibition, and inclusion body formation. In cells expressing a polyQ protein inclusion, body formation was preceded by proteasome inhibition but cytotoxicity was greatly reduced by administration of a p38MAPK inhibitor. Computer simulations suggested that without the generation of ROS, the proteasome inhibition and activation of p38MAPK would have significantly reduced toxicity. Our data suggest a vicious cycle of stress kinase activation and proteasome inhibition that is ultimately lethal to cells. There was close agreement between experimental data and the predictions of a stochastic computer model, supporting a central role for proteasome inhibition and p38MAPK activation in inclusion body formation and ROS-mediated cell death.

Citation: Tang MY, Proctor CJ, Woulfe J, Gray DA (2010) Experimental and Computational Analysis of Polyglutamine-Mediated Cytotoxicity. PLoS Comput Biol 6(9): e1000944. doi:10.1371/journal.pcbi.1000944

Editor: Reinhard Schneider, EMBL Heidelberg, Germany

Received May 3, 2010; **Accepted** August 27, 2010; **Published** September 23, 2010

Funding: This research was supported by a grant from the Institute of Aging, Canadian Institutes of Health Research (www.cihr.ca), to D.A.G. and J.W. M.Y.T. is the recipient of an Ontario Graduate Scholarship in Science and Technology (www.osap.gov.on.ca). C.J.P. is funded by a Research Fellowship from Alzheimer Scotland (www.alzscot.org)and the Alzheimer's Research Trust UK (www.alzheimers-research.org.uk). C.J.P. was also funded by The Royal Society International Outgoing Short Visit scheme (www.royalsociety.org). The funders had no role in study design, data collection and analysis, decision to publish, or preparation of the manuscript.

Competing Interests: The authors have declared that no competing interests exist.

* E-mail: Doug.Gray@ncl.ac.uk

Introduction

A hallmark feature of human neurodegenerative diseases is the accumulation of misfolded or otherwise abnormal proteins which become concentrated into large aggregates. Inclusion bodies are large nuclear or cytoplasmic protein aggregates whose predominant constituents may be characteristic of particular diseases. In many cases inclusion bodies (IB) are immunoreactive for ubiquitin and proteasome components [1], indicative of abortive or incomplete proteolysis. The sustained expression of mutant protein with the propensity to misfold may ultimately overwhelm the ubiquitin/proteasome system (UPS) and promote the formation of inclusions. This process may be accelerated by an age-related decline in UPS efficiency (discussed in [2]), which may explain why genetically transmitted neurodegenerative disorders typically affect older individuals. Consistent with the proteasome impairment hypothesis, IB form in the neurons of mice in which proteasome function has been genetically compromised [3]. Because misfolded, damaged, or genetically abnormal proteins are aggregation-prone their sequestration into inclusion bodies may actually alleviate the load on the UPS and promote neuronal survival, at least in the short term. Time lapse microscopy of a fluorescent proteasome reporter in cultured neurons has indicated that the UPS load is partially alleviated upon IB formation [4], and there is evidence that cultured cells forming such inclusions have a survival benefit [5] over the course of the experiment. In the longer term, however, it is possible that deleterious effects from IB formation would become pronounced. Apart from potential physical perturbations imposed by large proteinaceous inclusions (in axons, for example) these entities may wreak havoc by depleting essential cellular components (reviewed in [6]) or by biochemical means. In Huntington's disease, IB form when a polyglutamine tract in the N-terminal region of the huntingtin protein exceeds the threshold length of approximately forty glutamine residues; early onset and severe disease are correlated with very long tracts, whereas huntingtin proteins with polyglutamine tracts shorter than the threshold do not form IB and are not pathogenic [7]. The nuclear IB formed by the mutant huntingtin protein are generators of reactive oxygen species [8], and expression of such an expanded polyglutamine protein results in sustained and ultimately cytotoxic activation of p38MAPK [9]. It is likely that proteasome inhibition, ROS generation, and p38MAPK activation all feature in the death of cells containing IB, but their relative importance and potentially complex

Author Summary

Neurodegenerative diseases feature concentration of misfolded or damaged proteins into inclusion bodies. There is controversy over whether these entities are protective, detrimental, or relatively benign. The formation of inclusion bodies may be accelerated by inefficient protein degradation and may promote activation of stress signalling pathways. Each of these events may promote the generation of reactive oxygen species which may exacerbate the problem by damaging more proteins, possibly damaging components of the UPS itself, but in either case further impeding the function of cellular proteolytic systems. To determine how these events are related and which are critical, we generated a live cell imaging system in which inclusion formation and proteolytic efficiency can be evaluated, and created a stochastic computer model incorporating the same components. Laboratory data and computer simulations were found to be in close agreement, supporting a mechanism wherein misfolded protein induced a vicious cycle of stress kinase activation, ROS generation, and proteasome inhibition which was ultimately cytotoxic. Inclusion body formation partially alleviated the burden on the proteolytic system, but may not provide long term benefit. Pharmacological blockade of a stress-activated kinase was effective in breaking the vicious cycle, as predicted by the computer model and confirmed experimentally.

interdependencies are poorly understood. We have combined live cell imaging with mathematical modeling to explore such relationships. Our data point to a positive feedback loop between IB formation and p38MAPK activation that likely involves ROS. The existence of this loop is supported by the close agreement of laboratory data and simulations generated by a stochastic computer model.

Results

p38MAPK inhibition rescues cells from polyglutamine-induced cell death

We have previously demonstrated sustained activation of p38MAPK in cultured mammalian cells expressing expanded polyglutamine proteins and in a transgenic mouse model of expanded-polyglutamine disease [9]. This activation could be abrogated by treatment with the specific p38MAPK inhibitor SKF86002. To confirm the activation of p38MAPK and its inhibition by SKF86002 we performed western blot analysis of U87MG cells expressing HttQ103 (an amino terminal fragment of the human huntingtin protein containing a 103 glutamine tract). Expression of the expanded polyglutamine protein resulted in extensive phosphorylation of HSP-27, a downstream target of p38MAPK (Figure 1A). Reduced phosphorylation of HSP-27 was detected in cells expressing HttQ25 and HSP-27 phosphorylation was undetectable in untransfected control cells. Although the HttQ25 protein contains a polyglutamine tract below the threshold length for pathogenicity, its overexpression upon transfection may be sufficient to activate p38MAPK at a low and nontoxic level as we have documented previously [9]. The phosphorylation of HSP-27 was precluded by pre-treatment of transfected cells with a pharmacological inhibitor of p38MAPK (Figure 1A) or by co-expression with a dominant-negative (kinase dead) variant of p38MAPK (Figure S1) confirming that the phosphorylation of HSP-27 was due to the activation of the p38MAPK pathway by Htt103.

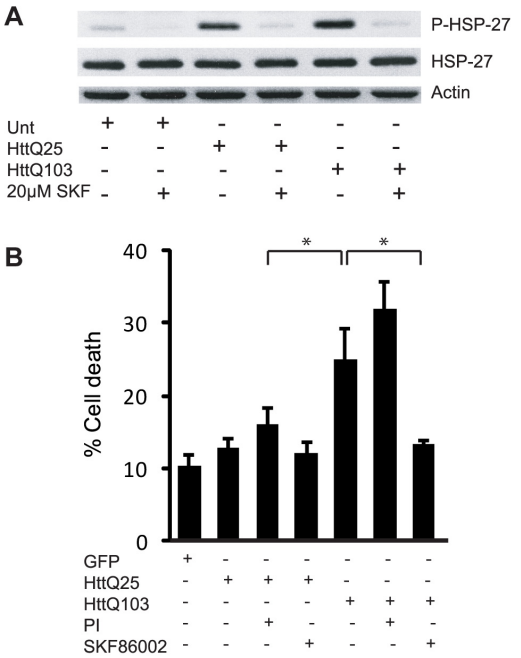

Figure 1. SKF86002 rescues cells from expanded-polyglutamine induced cell death. A) Western blot analysis with an antibody specific for phospho-HSP-27 in extracts from U87MG cells expressing HttQ25 or HttQ103. Cells were untreated or were treated with the p38MAPK inhibitor SKF86002. Expression of expanded HttQ103 activated p38MAPK and resulted in phosphorylation of HSP-27, a downstream target of p38MAPK. The analysis revealed a significant reduction of HSP-27 phosphorylation in HttQ25 and HttQ103 expressing cells treated with SKF86002. Re-probing the membrane with an antibody raised against total-HSP-27 revealed no significant difference in the total levels of HSP-27 protein. Actin served as a loading control. B) Cell viability of U87MG cells expressing GFP, HttQ25 or HttQ103 treated with proteasome inhibitor (PI) or p38MAPK inhibitor (SKF86002) was assessed by flow cytometry analysis using propidium iodide exclusion. The survival of SKF86002 treated HttQ103 expressing cells was significantly improved when compared to untreated counterparts. Treatment with PI resulted in a significant increase in cell death in cells expressing HttQ103 when compared to HttQ25 expressors. Error bars indicate the standard error of the mean (*$p<0.05$).
doi:10.1371/journal.pcbi.1000944.g001

To determine if blockade of p38MAPK activity affects cell survival, we transfected U87MG cells with either HttQ25, HttQ103 or a GFP control plasmid. At 30 hours post-transfection, flow cytometry was performed using propidium iodide exclusion, and revealed that HttQ103 expressing cells exhibited the highest levels of death (25%, Figure 1B) whereas the death associated with Htt25 expression was similar to that of GFP (10–12%). Pre-treatment of HttQ25 and HttQ103cells with SKF86002 resulted in a decrease in cell death that was most pronounced in cells expressing HttQ103 (Figure 1B). The HttQ103 protein is known to inhibit proteasome activity in a cell-based assay [10]; to determine if the cytotoxicity of the expanded-polyglutamine proteins could be enhanced by further proteasome inhibition a pharmacological proteasome inhibitor (PI) was added to HttQ25 and HttQ103 transfected cells. Cells were pre-treated with PI for 6 hours prior to assessing cellular death by flow cytometry. PI-

treated U87MG cells expressing HttQ103 exhibited a significant increase in cell death when compared to their untreated counterparts (Figure 1B), and was 15% greater than PI treated HttQ25 expressing cells. Under the same experimental conditions the amount of cell death induced by PI in untransfected cells was approximately 5% (not shown), roughly equivalent to the increase in cell death mediated by PI in cells expressing HttQ25 and HttQ103. Under our conditions proteasomes cannot therefore be fully inhibited by expression of the polyQ proteins alone. The pharmacological data support the argument that the cytotoxicity of misfolded proteins is mediated by proteasome inhibition and p38MAPK activation, but do not reveal whether these activities are independent.

IB formation is promoted by p38MAPK activity, and proteasome dysfunction

To simultaneously assess functioning of the UPS and inclusion body (IB) formation at a single cell level we created a bicistronic construct that encodes an expanded polyglutamine protein and fluorescent proteasome substrate on the same transcript (see schematic diagram in Figure 2A). This construct was designed to investigate the temporal order of events leading to HttQ103 induced cellular and proteasome toxicities and to dissect the role of p38MAPK in these events.

U87MG cells were transfected with HttQ103YFP-pIRES-mRFP^u and were imaged at 10 minute intervals from 24 to 48 hours post-transfection. The time lapse images revealed formation of IB at 36 hours post-transfection in cells expressing HttQ103 (Figure 2B, first panel; time lapse videos are provided as Videos S1 to S8). Values of mRFP^u intensity were graphed as a function of time revealing an increase in mRFP^u fluorescence prior to the formation of an IB, followed by a period of constant mRFP^u intensity. The single cell analysis revealed that HttQ103-induced cellular death is preceded by gradual UPS impairment. Once this impairment reaches a threshold level, IBs begin to form and their formation correlates with a momentary recovery of UPS efficiency as measured by mRFP^u intensity. These results are consistent with previously published findings in primary neuron cultures [4].

To examine the extent to which IB formation was dependent on UPS dysfunction U87MG cells expressing HttQ103YFP-pIRES-mRFP^u were treated with proteasome inhibitor. As expected PI treatment resulted in a rapid and persistent increase in mRFP^u intensity. Under these conditions IB formation was accelerated relative to untreated controls (Figure 2B, second panel). These data suggest an immediate relationship between proteasomal inhibition and IB formation.

Damaged proteins are normally eliminated by the UPS, and we speculated that an increase in cellular ROS levels would lead to oxidative damage to proteins and inflict an additional burden on proteasomes that may affect the kinetics of IB formation. To test this hypothesis, we depleted reduced glutathione levels in HttQ103YFP-pIRES-mRFP^u tranfected cells by treating cells with buthionine sulphoximine (BSO) at 24 hours post-transfection. In BSO treated cells we observed a constant increase in mRFP^u intensity (Figure 2B, third panel) consistent with a cumulative UPS burden.

Having previously established that the activation of p38MAPK in HttQ103 expressing cells contributes to cytotoxicity, we sought to determine what effects inhibition of p38MAPK signalling pathway would have on IB formation and UPS dysfunction. U87MG cells expressing HttQ103YFP-pIRES-mRFP^u were therefore treated with SKF86002. These cells exhibited a low level of mRFP^u fluorescence along with a delay in IB formation (Figure 2B, fourth panel). The mRFP^u fluorescence remained low and did not feature a rapid increase as seen in the untreated counterparts. These data suggest that inhibition of the p38MAPK pathway decouples the proteasome inhibition from HttQ103 protein expression, resulting in delayed formation of IB.

We quantified IB formation by recording the number of cells with IB at 6 hour intervals starting at 24 hours post-transfection. The percentage of cells with IB was graphed as a function of time (Figure 3A). PI treatment generated the greatest number of IB compared to untreated cells while SKF86002-treated cells were found to have the fewest IB. Comparative single-cell analysis of IB formation corresponded to time-points in which 40% of transfected cells had formed IB. Similarly, we quantified average mRFP^u fluorescence from many cells and graphed the fluorescence intensities as a function of time. Treatment with PI and BSO generated the highest amounts of mRFP^u fluorescence, while SKF86002 treatment resulted in the lowest levels of mRFP^u in comparison to untreated cells (Figure 3B). Findings from multiple cells were consistent with the mRFP^u fluorescence levels observed in the single cell analysis.

The critical role of p38MAPK is supported by mathematical modeling

We have previously used stochastic computer modeling to study the age-related decline of proteolysis [11], and have adapted this model to incorporate p38MAPK in an effort to better understand polyglutamine-mediated cell death. Our objective was to determine if a relatively simple mathematical model incorporating the components thought to be critical for polyQ-mediated cytotoxicity could recapitulate our laboratory findings; if not some critical component must have been overlooked or one or more of the starting assumptions must be invalid. Conversely, a good fit would suggest that the assumptions are valid and no critical elements have been overlooked. The stochastic computer model is represented schematically in Figure 4. The model was constructed using the Systems Biology Markup Language as described in the Materials and Methods section; details of molecular species and reactions are given in Text S1. The model predicted that treatment with PI would lead to reduced cell death at 30 hours (Figure 5A), a short term benefit from reduced levels of small aggregates binding to proteasomes (the consequence of which would be reduced by concentration of aggregates into IB). The experimental data, however, indicated a slight increase in the proportion of cell deaths under PI suggesting that the situation is more complex than is currently accounted for in the model. On the other hand, the model predicted that inhibition of p38MAPK activity should lead to much lower cell death, in close agreement with the experimental data. Also in agreement with the experimental findings described above, the model predicted that proteasome inhibition should lead to an increase in the rate of IB formation compared to untreated cells (Figure 5B). When p38MAPK activity is inhibited the model predicts a lower rate of IB formation at early time-points (Figure 5B) although from 36–48h, the rate of increase is similar to untreated cells (note lines are parallel for polyglutamine and p38MAPK inhibition during this time interval). The later increase in inclusion formation when p38MAPK activity is inhibited is probably due to ROS generation via the aggregated protein. The computer model predicts that much higher levels of mRFP^u will be observed in PI treated cells than in untreated cells, as expected for a proteasome substrate (Figure 5C). Critically, inhibition of p38MAPK activity reduced the accumulation of mRFP^u in the computer model. Overall the simulations and experimental data are in good agreement, indicating that the model describes the important molecular relationships of the system as portrayed in Figure 4.

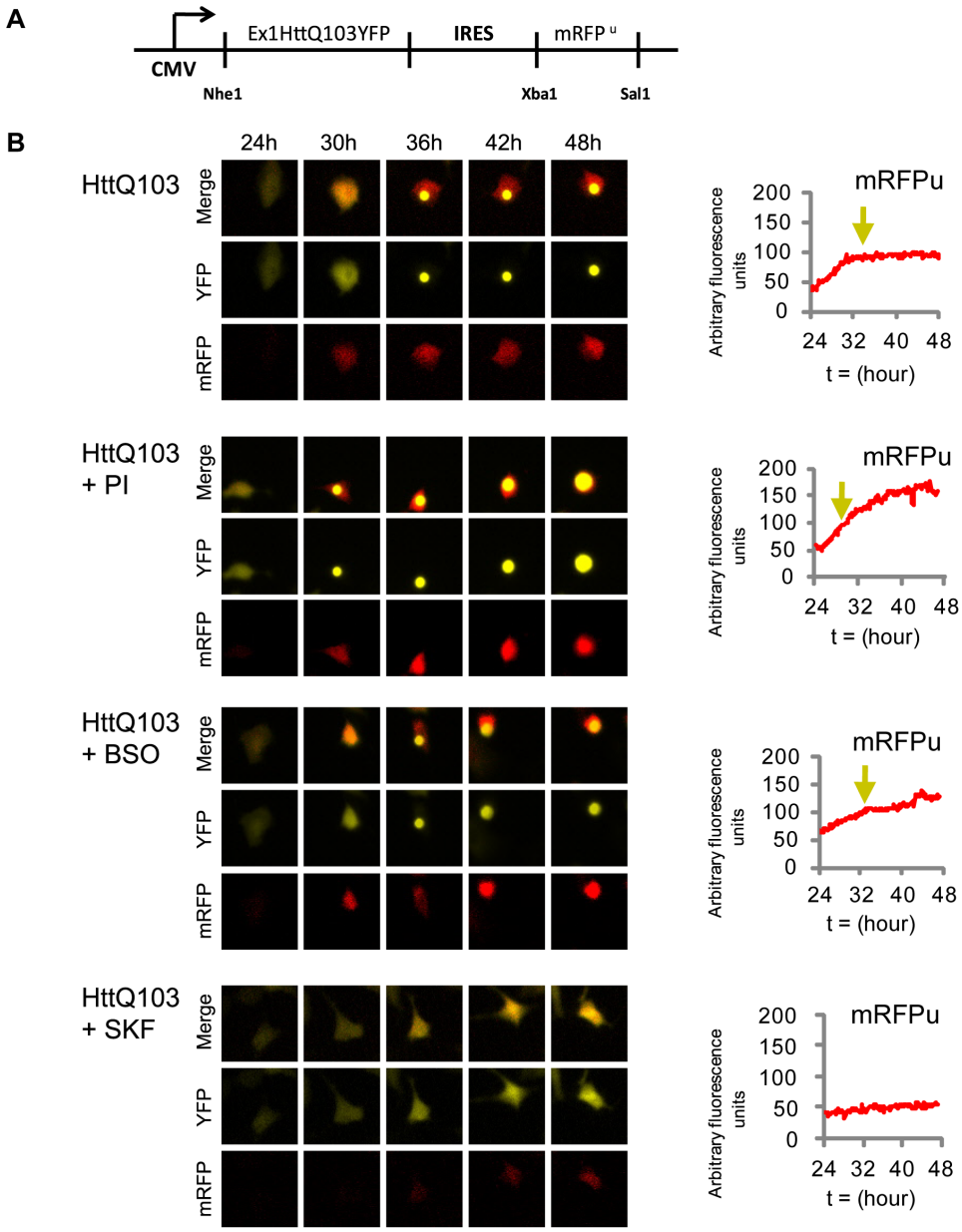

Figure 2. Expression of HttQ103 results in the formation of inclusion bodies (IB) that are preceded by increased levels of the proteasome reporter protein mRFP^{u}. A) Schematic representation of the bicistronic expression construct engineered to simultaneously express the huntingtin-derived protein HttQ103 fused to the yellow fluorescent protein (YFP) and an intrinsic proteasome activity reporter (mRFP^{u}) downstream of an internal ribosome entry site (IRES). B) Single cell analysis of IB formation and UPS impairment induced by the expression of the HttQ103 protein. U87MG cells expressing HttQ103YFP-pIRES-mRFP^{u} were imaged over the course of 24 hours to simultaneously follow IB formation and UPS impairment. Cells were either left untreated (panel 1) or treated with proteasome inhibitor (panel 2), buthionine sulphoximine (BSO, panel 3) or the p38MAPK inhibitor (SKF86002, panel 4) and visualized under fluorescence at 10 minute intervals. Over time accumulation of mRFP^{u} was graphed using densitometry values from a single cell for each condition which revealed detectible levels of mRFP^{u} prior to the formation of an IB (represented by the yellow arrow). Treatment with PI resulted in IB formation at an earlier time-point and correlated with increased levels of mRFP^{u}. BSO treatment also increased mRFP^{u} levels but did not significantly accelerate the timing of IB formation. Treatment with SKF86002 resulted in overall lower levels of mRFP^{u} and a delay in inclusion body formation. Single cells were isolated from the population of cells described in Figure 3.
doi:10.1371/journal.pcbi.1000944.g002

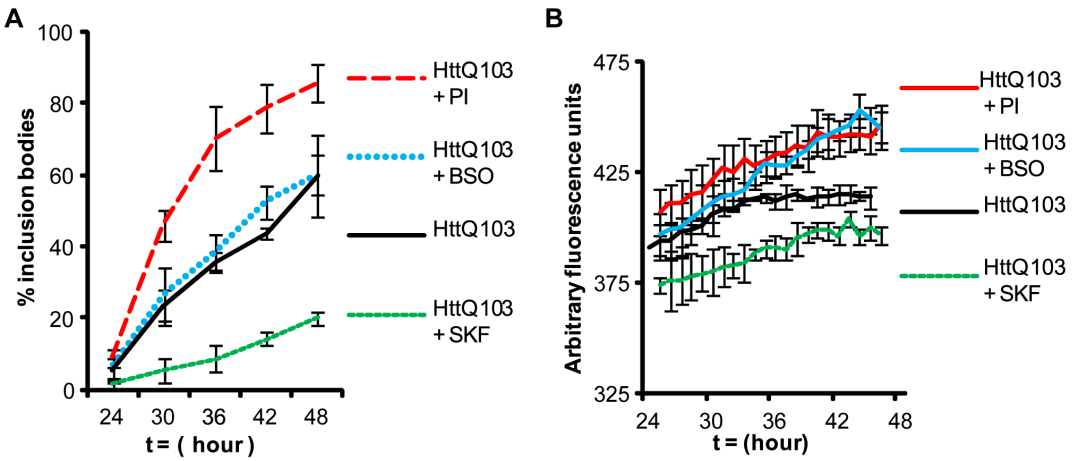

Figure 3. Data from multiple live cell analyses of IB formation and proteasome inhibition. A) The percentage of IB formation for each treatment was recorded every 6 hours beginning at 24 hours post-transfection. B) Average mRFP^u intensity values for multiple cells over time. Experiments were performed in triplicate with over 50 cells analyzed in each condition. Error bars indicate standard error of the mean.
doi:10.1371/journal.pcbi.1000944.g003

Activation of p38MAPK contributes to ROS production but not direct proteasome inhibition

Based on our single-cell analysis data, we speculated that the activation of p38MAPK and UPS impairment were contributing to the production of reactive oxygen species (ROS) and that SKF86002 may be counteracting this cellular response. A genetic approach was adopted to test this hypothesis, utilizing transfection of cells with expression vectors encoding wild type or kinase dead versions of p38MAPK. Whereas pharmacological inhibition may affect multiple p38MAPK isoforms any modulation of cellular response observed with the genetic approach would be attributable to the alpha isoform of p38MAPK exclusively. We first confirmed that in our U87MG cell system the expression vectors were capable of modulating p38MAPK activity using phosphorylation of HSP27 as a proxy marker (Figure S1). Cells were then transfected with the p38MAPK expression vectors or with an empty vector control construct and lysates were assayed for reduced glutathione (GSH) content, a marker of oxidative status within cells. We found that overexpression of wild type p38MAPK resulted in a significant decrease in GSH levels whereas the GSH content in cells expressing kinase dead p38MAPK was less affected in comparison to controls (Figure 6A). To determine if overexpression of wild type p38MAPK resulted in dysfunction of the UPS, we transfected the p38MAPK expression constructs into a cell line stably expressing GFP^u, a well characterized proteasome sensor [10]. For these experiments we made use of a stable NIH 3T3 cell line we had previously generated; the GFP^u reporter is expressed at a lower level in the stable line and does not accumulate as an artefact of transfection-mediated overexpression. By flow cytometric analysis, we found that cells overexpressing wild type p38MAPK exhibited the highest levels of GFP^u intensity whereas the levels of GFP^u in cells expressing the kinase dead p38MAPK or the empty vector were similar (Figure 6B). These data suggested that the activation of p38MAPK was negatively affecting UPS function. To test whether this inhibition of the proteasome was a direct affect of p38MAPK activation, we transfected cells with the same set of plasmids and assayed their proteasome activity using fluorogenic substrates. No significant differences were noted (Figure S1). Taken together, the data indicate that the expression of p38MAPK does affect the oxidative status of cells but does not directly inhibit the proteasome.

Since aggregated protein leads to increased levels of ROS, inhibition of p38MAPK may simply delay cell death and thereby allow more aggregation to take place. To determine the predicted outcome should p38MAPK *not* be involved in generating more ROS we removed the reaction for ROS generation via p38MAPK from the model and repeated the computer simulations. Without p38MAPK-generated ROS less cell death was predicted under all conditions (Figure 7A). With the feedback loop broken in this way the model also predicted that there would be no significant difference in the numbers of inclusions at each time point between untreated cells and cells treated with a p38MAPK inhibitor (Figure 7B). We also refitted the model for HttQ103 without treatments and no feedback loop using the experimental data for cell death and inclusion formation (Figure 7C–D). Since the model predicted less cell deaths and lower levels of inclusions than the data, we increased the parameters for inclusion formation ($k_{aggPolyQ}$) and cell death ($k_{p38death}$ and $k_{PIdeath}$). We also increased the parameter for ROS generation via p38MAPK ($k_{genROSp38}$) since this had the effect of increasing both the levels of inclusions and the number of cell deaths. We then ran the model with the treatment for proteasome inhibition and p38MAPK inhibition. The model was not able to reproduce the decline in cell death or the lower levels of inclusions when p38MAPK is inhibited (evident from the comparison of Figure 7C–D with Figure 5A–B). Therefore the model indicates that a feedback loop from p38MAPK to ROS is required to explain the experimental data.

Discussion

Based on the experimental data and the computer simulations reported herein we propose a vicious cycle mechanism of polyglutamine-mediated cytotoxicity (Figure 8). In the proposed mechanism the initiating event is the inhibition of the proteasome by small aggregates of misfolded protein. It has been previously shown that proteasome inhibition leads to the generation of ROS (reviewed in [12]) and the activation of MKK3 and MKK6 kinases

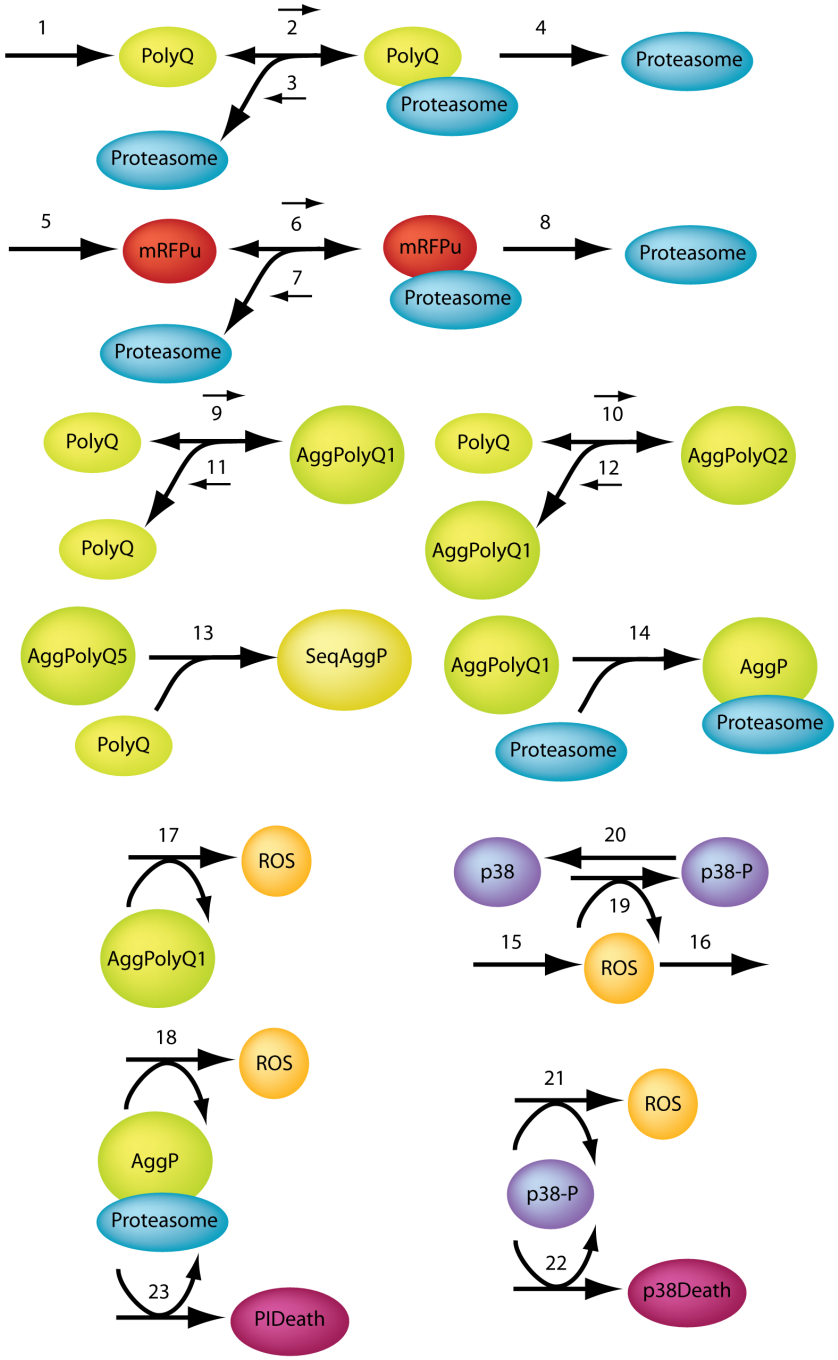

Figure 4. Diagram of molecular relationships simulated in the computer model. The model assumptions are presented in Text S1, along with lists of molecular species (Table S1 in Text S1) and reaction parameters (Table S2 in Text S1).
doi:10.1371/journal.pcbi.1000944.g004

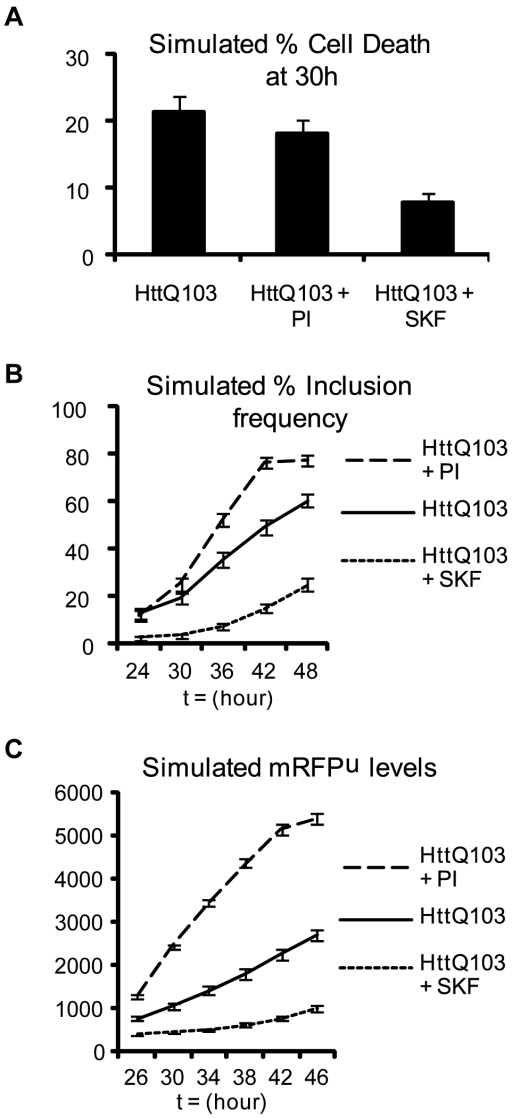

Figure 5. Simulations generated by a stochastic computer model of polyglutamine-mediated cytotoxicity. A) Model predictions for cell death at 30 hours. Results show percentage of cells that died by 30 hours in 300 simulations of each computer experiment. B) Model predictions for kinetics of inclusion formation. Results show percentage of cells with inclusions at each time point from 300 simulations for each computer experiment. C) Model predictions for accumulation of $mRFP^u$. The mean level of $mRFP^u$ for 300 simulations of each computer experiment was calculated for each of the time-points shown. The y-axis shows the number of molecules predicted by the simulations. Error bars for the model predictions represent standard error of the mean.
doi:10.1371/journal.pcbi.1000944.g005

upstream of the stress kinase p38MAPK [13,14]. Activation of p38MAPK by its upstream regulators may exacerbate the problem by promoting downstream ROS production (through a mechanism discussed below). By damaging other cellular proteins the reactive oxygen would provide an additional burden to the UPS, which is normally charged with the proteolytic degradation of damaged or abnormal proteins. Increasing proteasome inhibition would lead to further accumulation of misfolded proteins, ultimately coalescing into inclusion bodies. By reducing local concentrations of the small aggregates that are thought to be most inhibitory to the proteasome the IBs may temporarily alleviate proteasome inhibition, but by concentrating iron they may promote the further generation of ROS, ensuring yet more damage and the conditions that will sustain p38MAPK activation. Whether or not there is self-amplification of the vicious cycle as a consequence of increasing ROS production we postulate that it is sustained p38MAPK activity and proteasome inhibition that will ultimately lead to cell death.

The mathematical model was based on our previous model of the ubiquitin/proteasome system which we modified and extended to include turnover and aggregation of polyglutamine proteins. The model predictions were in close agreement with the experimental data indicating that the proposed network in Figure 4 captures the important components in the system. However, we found that there were some discrepancies between the model predictions and experimental data regarding cell death at early time-points under conditions of proteasome inhibition. This suggests that there is something missing from the model. Since proteasome inhibition affects all protein turnover, the missing part could be a pro-apoptotic protein. One such candidate is the transcription factor p53 which is normally rapidly turned over by the proteasome. A future extension of our current model to include a pro-apoptotic protein would be fairly straightforward as we have previously modelled the p53 system [15]. An advantage of modelling over laboratory experiments is that it is easy to manipulate the system on a computer, whereas the same experiments in the laboratory may be impossible or very costly to do. For example, although it would be difficult to prove experimentally that ROS generation by p38MAPK is required to explain the experimental data, the hypothesis could easily be tested in the mathematical model by simply removing the reaction of p38MAPK-dependent ROS generation and repeating the simulations. The model confirmed that p38MAPK is involved in generating more ROS since with the feedback loop broken the model output no longer fitted the experimental data.

We have previously shown that pharmacological blockade of p38MAPK can protect cells from polyglutamine-mediated cell death [9], and the current experimental data and mathematical modeling provide an explanation for the efficacy of this intervention: by breaking the vicious cycle the p38MAPK inhibitor precludes further damage and proteasome inhibition. The data we present herein support a central role for ROS in the proposed cycle of p38MAPK activation, proteasome inhibition, and protein aggregation that ultimately leads to cell death. The importance of ROS in protein misfolding disorders is not a new concept; indeed the cytotoxicity of elevated ROS generated by mutant huntingtin has been convincingly demonstrated by the laboratory of Rubinsztein [16]. Intriguingly, the proteasome is itself an important regulator of oxidative damage in neurons and proteasome inhibition is known to induce mitochondrial dysfunction and promote oxidative damage to DNA and protein (reviewed in [12]). Once some threshold of polyQ-mediated proteasome inhibition is reached it seems entirely plausible that a self-perpetuating loop of ROS generation and p38MAPK activation could lock the cell into a dysfunctional state. Indeed, a directly analogous positive feedback loop involving ROS and p38MAPK activation was recently proposed for the induction of senescence in

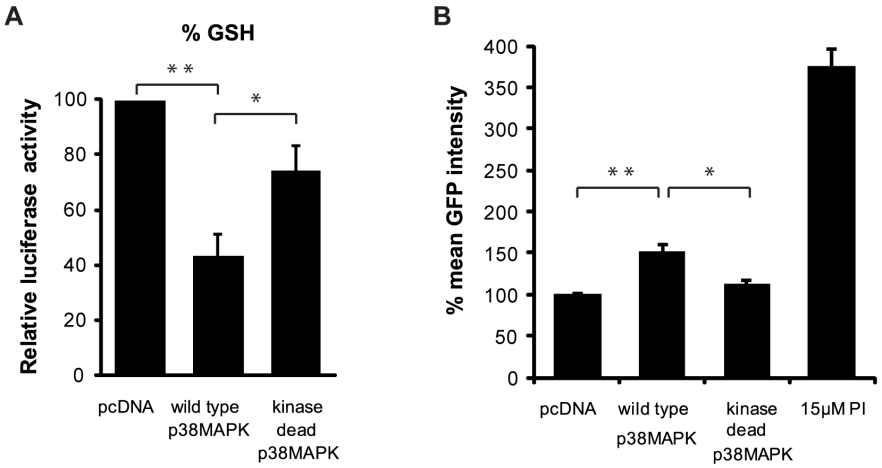

Figure 6. Effects of p38MAPK activity on GSH and GFP^u levels. A) Lysates from cells expressing either wild type p38MAPK, kinase dead p38MAPK, or pcDNA control plasmids were assayed for reduced GSH content 48 hours post transfection. Cells transfected with wild type p38MAPK had lower levels of reduced GSH when compared to the pcDNA empty vector control (**$p<0.05$) and kinase dead p38MAPK expressing cells (*$p = 0.06$). B) Activation of the p38MAPK pathway leads to proteasomal inhibition. Wild type p38MAPK or kinase dead p38MAPK were transfected into 3T3 cells stably expressing the proteasome reporter GFP^u. Cells were collected at 48 hours post-transfection and GFP^u intensity was analyzed by flow cytometric analysis. Cells over-expressing wild type p38MAPK had significantly higher levels of GFP^u accumulation when compared to cells expressing kinase dead p38MAPK (*$p<0.05$) or pcDNA empty vector control (**$p<0.01$). PI treatment served as a positive control.
doi:10.1371/journal.pcbi.1000944.g006

mammalian cells. By combining bioinformatics, stochastic computer modeling, and direct experimental interventions Passos et al. have provided convincing evidence that sustained activation of p38MAPK is required for generation of mitochondrial ROS, which by generating DNA damage ensures the continued activation of p38MAPK in senescent cells [17]. The ROS generated as a consequence of proteasome inhibition also appears to be of mitochondrial origin [18], so the cascade of events in cells expressing misfolded protein may be very similar to that in cells in which the initiating event is exposure to ionizing radiation (as was the case in the Passos paper). If a similar loop were operating in cells expressing expanded polyglutamine proteins one might expect to find ROS-mediated DNA damage leading to activation of ATM and phosphorylation of histone H2AX, as has indeed been documented in cells from Huntington's disease and SCA-2 patients [19]. The activation of ATM and formation of H2AX repair foci appears to precede the formation of IB [20], but may be coincident with p38MAPK activation and the generation of ROS. If our model is correct pretreatment of cells with the p38MAPK inhibitor should reduce the number of H2AX foci in cells expressing HttQ103. We are currently testing this hypothesis.

Enhanced levels of autophagy may also contribute to the protective effects of the p38MAPK inhibitor we have observed. Although the effects may be dependent on cell type, there is evidence that the alpha isoform of p38MAPK inhibits autophagy [21] [note that this is the same isoform utilized in our genetic experiments, and may be the target of primary importance to all of the interventions described herein]. Low level inhibition of the proteasome is known to promote autophagy [22], but as proteasome inhibition increases the activation of p38MAPK may limit autophagic clearance of protein aggregates. Enhancement of autophagy has been proposed as a therapeutic strategy for the treatment of polyglutamine disorders such as Huntington's disease [23], and pharmacological blockade of p38MAPK may provide benefit by multiple mechanisms. It may break the vicious cycle of ROS generation while promoting autophagy-mediated clearance of aggregates in cells already compromised for proteasome function.

We have performed the current set of experiments in U87MG cells, a human glioblastoma cell line. These cells were chosen for their ease of handling, including their high transfection efficiency. Because the critical components of the proposed vicious cycle are universally present in mammalian cells (including p38MAPK, proteasomes, and ROS from mitochondria) it is likely that a self-perpetuating loop could be triggered by expanded polyglutamine proteins in any cell type, and we have previously demonstrated the protective effect of a p38MAPK inhibitor in normal and transformed cells of both human and mouse origin [9]. We nevertheless recognize that the kinetics of the events we have described may be markedly different for neurons *in situ*.

Although the short term benefit of IB formation (through improved proteasome function) has been demonstrated in cultured neurons [4,5] the longer term implications of IB in neurodegenerative diseases must be considered. A transient alleviation by IB of the polyglutamine-mediated proteasome burden was recently demonstrated *in vivo* in an inducible model of Huntington's disease [24], but no long term impairment of proteasome function was observed in the brains of these mice. If the IB concentrates iron and promotes ROS generation through Fenton chemistry [8] the IB, once formed, might ensure the perpetuation of the vicious cycle proposed in Figure 3C. The failure to detect this effect in older mice expressing a polyQ protein may relate to the inability of the reporter system to detect less than a 40% decrease in proteasome inhibition [24] or may relate to differences between the mouse model and the human disease. In human polyglutamine disorders the disease may progress over years if not decades, and the later consequences of IB formation might therefore be more severe. Clinical evidence supports a deleterious role for IB in human disease. In polyglutamine repeat diseases such as HD, frontotemporal lobar degeneration, and RNA-mediated diseases

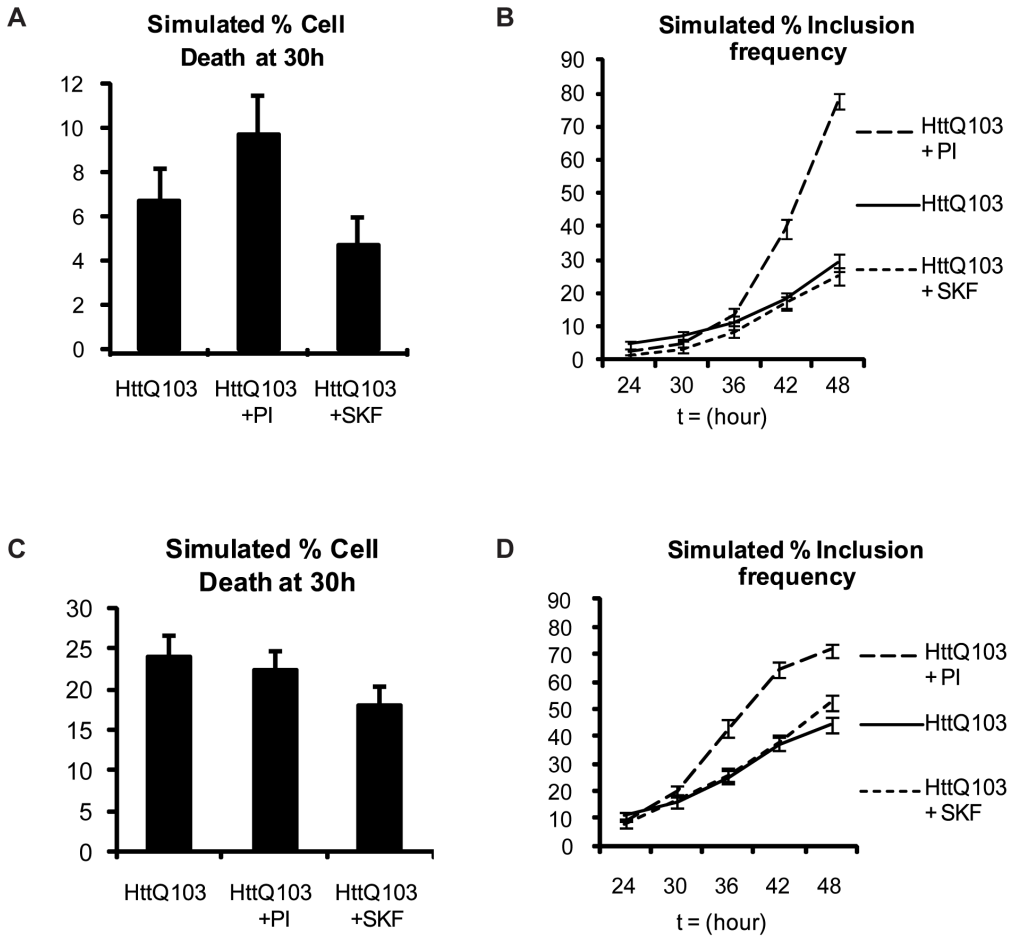

Figure 7. Simulated effects of p38MAPK activation without ROS generation. A) When the feedback loop is broken by eliminating ROS production the model predicts that cell death will be reduced under all conditions. B) Under ROS-free conditions the model predicts no significant difference in the numbers of inclusions at each time point between untreated polyglutamine-expressing cells or cells treated with a p38MAPK inhibitor. Similarly, no significant difference is predicted in the number of inclusions at early time points between untreated cells or cells treated with a proteasome inhibitor. At later time points (> = 42h) more inclusions are predicted for the PI treated cells due to the accumulation of misfolded protein which cannot be degraded. C) Model re-fitted to data of untreated poly-glutamine-expressing cells predicts more cell deaths but still no significant differences between treatments. D) Model re-fitted to data of untreated poly-glutamine-expressing cells shows no significant differences between untreated and treated cells at early time points. At 48h, the model predicts a small but significant increase in the number of inclusions for cells treated with p38MAPK inhibitor indicating that the model no longer fits the data. The error bars represent the standard error of the percentage given by $\sqrt{p(100-p)/n}$ where n is the number of simulation runs (n = 300) and p is the percentage of cells.
doi:10.1371/journal.pcbi.1000944.g007

such as myotonic dystrophy, inclusion-mediated titration of transcription factors (like CBP), tar DNA-binding protein 43 (TDP-43), and RNA splicing factors (for example muscleblind), respectively, may represent an important molecular mechanism of disease [6]. Added to these effects would be the deleterious effects we ascribe to the ROS-mediated vicious cycle.

Materials and Methods

Expression constructs

The pEGFP-N1 expression construct was purchased from Clontech (Palo Alto, California, USA). Htt-Q25 and Htt-Q103 expression constructs containing a synthetic insert encoding exon 1 or human Huntingtin containing a polyglutamine tract of either 25Q or 103Q fused to the yellow fluorescent reporter protein (YFP) were generous gifts from Dr. Ron Kopito (Stanford University). These are designated HttQ25YFP or HttQ103YFP. A red fluorescent proteasome reporter was generated by PCR-mediated transfer of the degron sequence from the GFP^{U} reporter (Bence et al.; the gift of Dr. Ron Kopito) to the C terminus of the monomeric red fluorescent protein (the gift of Dr. Robert Campbell, University of Alberta). Under normal conditions, $mRFP^{u}$ is quickly degraded by the 26S proteasome, but during conditions of proteasomal impairment, turnover of

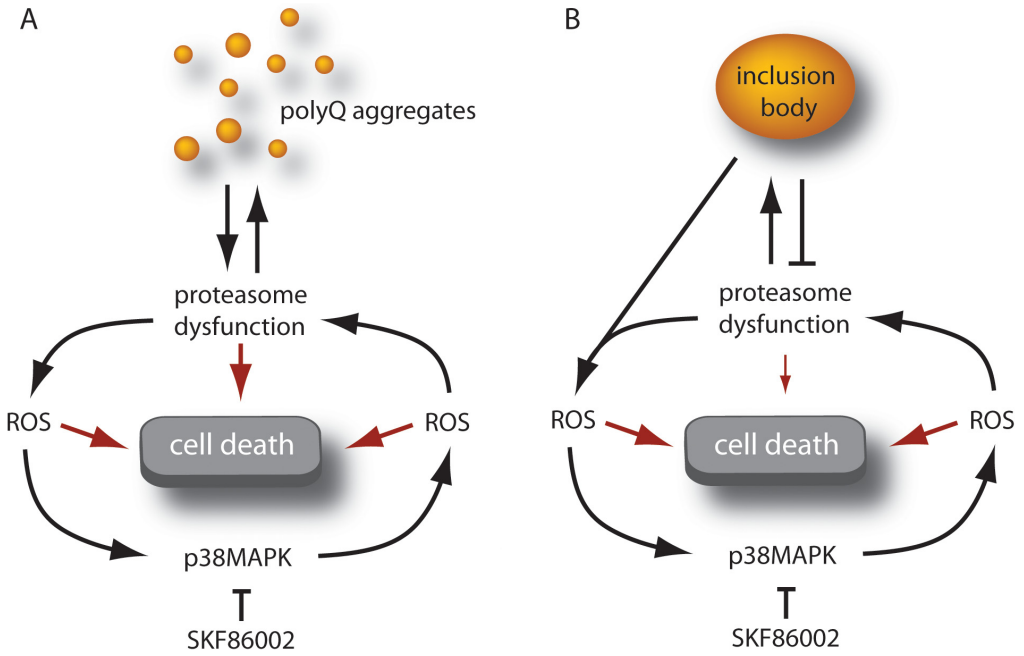

Figure 8. Proposed model of expanded-polyglutamine induced toxicity. A) Expression of expanded-polyglutamine proteins leads to proteasome inhibition, promoting the generation of ROS. This in turn leads to p38MAPK activation (which can be blocked by pretreatment of cells with SKF86002) and the further generation of ROS through a mechanism which is likely to involve mitochondria. An increased burden of oxidatively damaged proteins leads to further proteasome impairment, and yet more ROS generation. B) Proteasome impairment ultimately leads to inclusion formation, which temporarily reduces UPS dysfunction. IBs perpetuate ROS production through concentration of iron, ensuring continued activation of p38MAPK. Pharmocological inhibitors of p38MAPK such as SKF86002 can preclude the initiation of the vicious cycle or potentially interrupt it at a later stage.
doi:10.1371/journal.pcbi.1000944.g008

mRFP^u is reduced, leading to an accumulation of mRFP^u that is visible by fluorescent microscopy. To simultaneously express the expanded YFP-tagged polyglutamine proteins and the red fluorescent proteasome reporter the former was inserted into NheI site upstream of the internal ribosome entry site (IRES) in the vector pIRES (Clontech, Palo Alto, California, USA) and the latter was inserted between the Xba I and Sal I sites downstream of the IRES element. The wild type and kinase dead p38MAPK variants were generous gifts from Dr. J. Han (The Scripps Research Institute, La Jolla, CA). The hyper-active p38MAPK construct was a gift from Dr. Oded Livnah (The Hebrew University of Jerusalem).

Cell culture and transfections

The human U87MG glioblastoma cells (a gift from Dr. I. Lorimer at the Ottawa Hospital Research Institute) were maintained in Dulbecco's modified Eagle's medium (DMEM) and supplemented with 10% FBS and maintained in a 37°C incubator with 5% CO_2. For transient transfections, cells were plated in either 96- or 6 well dishes 24hours prior to transfections. Subsequently, they were transfected using GeneJuice Transfection Reagent (Novagen, Madison, WI, USA) as per the supplier's protocol. 0.5µg or 3.0µg of plasmid DNA was used in each well of a 96 or 6 well dish. For p38MAPK inhibition experiments, cells were pre-treated for 2h with 20µM SKF86002 (Calbiochem) prior to transfection with various expression constructs.

Western blot analysis

U87MG cells were harvested in protein lysis buffer consisting of 100mM Tris pH 6.8, 20mM DTT, 4% SDS, 5% glycerol. Protein concentrations were determined using the Bradford assay reagents (Bio-Rad, Hercules, CA, USA). Reduced proteins were resolved on a 10% SDS-polyacrylamide gel and electro-blotted onto a Hybond C nitrocellulose membrane (Amersham Bioscience Corp, Baie d'Urfé, QC). The membranes were stained with Ponceau S prior to immunoblotting with phospho-HSP-27 (polyclonal rabbit), total HSP-27 (rabbit polyclonal) (Cell Signaling, Danvers, MA), or Actin (Sigma-Aldrich). Proteins were detected using the HRP method and SuperSignal West Pico Chemiluminescent Substrate reagents (Pierce, Rockford, IL, USA). Proteins were visualized using the GeneGnome (Syngene, Frederick, MD, USA).

Survival assays

Cell viability was assessed by flow cytometry using propidium iodide exclusion. Adherent and non-adherent cells were transfected with various constructs for 30 hours, harvested and stained with Propidium Iodide. For p38MAPK inhibition experiments, cells were pre-treated for 2h with 20µM SKF86002 (Calbiochem) prior to transfection with various expression constructs. For proteasome inhibition experiments, cells were treated with Proteasome Inhibitor I (Calbiochem) 24h post-transfection at a final concentration of 25µM. Fluorescent detection was analyzed by flow cytometry using a Beckman Coulter Quanta SC MPL. Data and

analysis were done using Quanta Analysis software (Beckman Coulter, Inc., Brea, CA, USA).

Live-cell imaging

75 000 U87MG glioblastoma cells were seeded onto a Delta T4 culture dish system (Bioptechs, Butler, PA) and maintained in a 37°C incubator with 5% CO_2 for 24h hours. Cells were transfected with 2ug of plasmid DNA encoding HttQ103YFP-pIRES-mRFP^u for 24 hours before being transferred onto a heated stage maintained at 37°C and at 5% CO_2 using a Delta T4 culture dish temperature controller and cell perfusion system (Bioptechs, Butler, PA). For p38MAPK inhibition experiments, cells were pre-treated for 2h with SKF86002 for a final concentration of 20μM to preclude kinase activation upon transfection. For proteasome inhibition experiments, cells were treated with Proteasome Inhibitor I (Calbiochem) 24h post-transfection at a final concentration of 25μM (treatment with PI prior to transfection is not possible due to its immediate toxicity). For buthionine sulphoximide (BSO)-induced depletion of glutathione experiments, cells were treated 24h post-transfection with BSO (Sigma) 24h post-transfection at a final concentration of 5mM. Microscopy was performed 24 hours post-transfection on a Zeiss Axiovert 200M inverted fluorescent microscope for a total of 24 hours. Fully automated multidimensional acquisition was controlled using Axiovision 4.8 software. Images were acquired using a 10× objective (EC Plan-Neofluar) with a side-mounted AxiocamHRm camera. Yellow fluorescent protein or red fluorescent protein was excited using the Zeiss Colibri LED illumination system (LEDmodule 505nm or LED module 590nm) and detected using the appropriate filters (46HEYFP or 61HEGFP/HcRED, respectively). Fixed exposure times were as follows: Brightfield phase contrast 1ms; YFP 100ms; RFP 188ms. Images were taken at 10 minute intervals for 48 hours and compiled into video files using Axiovision 4.8 software (Carl Zeiss, Thornwood, NY).

Glutathione assay

Cell lysates from U87MG cells over-expressing wild type p38MAPK or kinase dead p38MAPK were analyzed for reduced GSH content using a luciferase kit (GSH-Glo) from Promega (Madison, WI). 10,000 cells were seeded in 96-well plates and transfected with 0.5μg of DNA for 48 hours. Cells were collected and analyzed for GSH following the manufacture's protocol.

Proteasome inhibition analysis

Mouse NIH 3T3 cells were co-transfected with GFP^u and a PGK-driven puromycin resistance gene (gift of Dr. M. McBurney, Ottawa Hospital Research Institute). Cells stably expressing the proteasome reporter GFP^u were selected over 2 weeks in a final concentration of 2.0μg/ml. For proteasome assays, wild type p38MAPK, kinase dead p38MAPK, or pcDNA were transfected into 3T3-GFP^u cells for 48 hours. Cells were collected and analyzed for GFP^u expression by flow cytometry (Beckman Coulter Quanta SC MPL). Mean GFP intensity was analyzed using the Quanta Analysis software and subsequently graphed using Excel (Microsoft).

Statistical analysis

Statistical significance was determined by a two tailed Student's t-test. Unless otherwise indicated, values were considered significant when $p<0.05$.

Mathematical model

The model was developed to mimic the experimental system so that simulations could be performed to see which parameters affected the different cellular outcomes. The model was initially fitted to experimental data where HttQ103 had been added to cells but without any inhibitors. The model was then used to mimic the experimental treatments and the model predictions were compared to the experimental results. If there were discrepancies between the model predictions and experimental results, the model was modified (either by changing parameter values or by the addition of further reactions). The model was then re-run for the experiment without any treatments to check that it still fitted the experimental data. If the model did not fit, further adjustments were made and the procedure repeated. We originally started with a model that did not contain a feedback loop from p38MAPK to ROS but found that it was necessary to include this loop in order to get the model to fit both the data for the treatment with p38MAPK inhibitor and the data without the treatment. Further details are given in Text S1.

The model was encoded in the Systems Biology Markup Language (SBML) as this standard allows models to be easily shared, modified and extended [25]. SBML is a way of representing a network of interactions so that it can be simulated on a computer and the evolution of the system over time can be followed. SBML shorthand was used to create the SBML code which was then converted into full SBML [26]. The network diagram is given in Figure 4, and Tables S1 and S2 in Text S1 give details of the species and reactions respectively. Text S1 also contains more detail of events and parameter values (Tables S3 and S4 in Text S1). Since there is large variability in cellular outcomes in terms of both inclusion formation and cell death, we used stochastic simulation. This was based on the Gillespie algorithm [27] which assumes that collisions of molecules occur within a reaction vessel and that at most only two molecules can collide. We chose this method of simulation as there are low copy numbers of many of the species and random effects play a major role in this model, as can be seen by the cell to cell variability of the model output. It should be noted that we have a few reactions which have more than two molecules in the list of reactants. These are the reactions for the aggregation of polyQ where we assume that ROS affects the reaction kinetics although ROS itself is not consumed by the reaction (and so also appears in the list of products). We use a function of ROS in the kinetic law so that we have a pseudo second order reaction rather than a third order reaction. Although this may seem to be a violation of the assumptions of the Gillespie algorithm, this provides a simple way to allow for the effects of ROS on the aggregation process rather than adding many more reactions and parameters. The model is available from the Biology of Ageing e-Science Simulation and Integration (BASIS) system ([28,29]) and the Biomodels database (ID:MODEL1002250000) [30].

Model Assumptions

We assume that the addition of the polyQ gene to the cell resulted in continuous synthesis of the polyQ protein. It is also degraded by the proteasome so that total levels remain fairly constant with a half-life of about 20 hours [31]. We set the levels of polyQ sythesis and degradation so that the half-life would be 20 hours if the proteasome did not become inhibited by aggregates. Two molecules of polyQ interact to form a small aggregate (AggPolyQ1). We assume that ROS affects the aggregation kinetics if it rises above basal levels. The aggregate can grow in size by the addition of further polyQ proteins in a reversible manner. However, when the aggregate reaches a certain threshold size, we assume that disaggregation can no longer take place and that instead an inclusion forms (SeqAggP). This threshold represents the seed and is assumed to be of size six

based on data for amyloid fibril polymerization [32]. Since mutant huntingtin forms amyloid-like filaments, it is reasonable to assume that it has similar aggregation kinetics [33,34]. A very recent study shows that mutant huntingtin forms three major pools: monomers, oligomers and inclusion bodies [35]. Interestingly, the study showed that the pool of oligomers as a proportion of total huntingtin did not change over a time period of 3 days despite continued conversion of monomer to inclusion bodies. We also compared the levels of oligomers (represented by the species AggPolyQ[i], where $i = 1–5$) in our simulation output in cells which formed inclusion bodies (Figure S2) and discuss the results in the Text S1 section. It has been shown that small aggregates bind to proteasomes and inhibit proteasomal function [36]. Therefore, we assume that AggPolyQ can bind to the proteasome and so reduce the pool of available proteasomes. However we assume that inclusions do not interfere with the degradation machinery. We also include a species to represent mRFPu and assume that this is turned over with a half-life of about 30 minutes [36]. We assume that ROS is continuously generated and removed with a half-life of 1 hour [37] but that basal levels are low (about 10 molecules). We assume that small aggregates may generate ROS, so that the level of ROS is dependent on the amount of small aggregates (either bound to the proteasome or free pools). We also assume that the presence of inclusions will increase levels of ROS but with a much smaller effect than small aggregates. We represent p38MAPK in two forms: unphosphorylated (p38) and phosphorylated (p38-P) with p38-P being the active state. We assume that high levels of ROS activate p38MAPK and that high levels of p38-P initiate a signalling cascade that results in cell death. We set the rate of this reaction so that it is unlikely to occur when p38-P levels are low and the probability of the reaction occurring increases with increasing levels of p38-P. However, since the model is stochastic, it is possible that even low levels of p38-P will occasionally signal for cell death. We also assume that if the level of proteasomes bound by aggregates increases above a threshold of about 50%, then another signalling pathway leads to cell death due to the accumulation of the pro-apoptotic protein p53. As in the p38 death pathway, cell death due to aggregates inhibiting the proteasome may occur even when levels of AggP Proteasome are fairly low. The reactions for the cell death pathways are shown in Table S2 in Text S1. After cell death occurs, a dummy parameter k_{alive} is set to zero to prevent further reactions occurring, and a dummy species to record the cause of cell death is set to 1. This makes it possible to plot the time of cell death, the cause of death and to count the number of cell deaths of each type in multiple simulations.

We also assume that proteasomes bound by AggP, polyQ or mRFPu may be sequestered into inclusions if degradation does not take place. If AggP is sequestered into inclusions, then this will help alleviate the increase in ROS due to protein aggregation, since we assume that small aggregates lead to greater ROS generation than inclusions.

We also include a generic pool of protein (NatP) which can misfold to become (MisP). We assume that misfolded protein can be either refolded, ubiquitinated and degraded or at high concentrations it may start to aggregate. Once an inclusion forms, misfolded protein may be sequestered into the inclusion body, including MisP bound to proteasomes.

Supporting Information

Figure S1 A)Western blot analysis with the phospho-HSP-27 antibody of cell extracts from U87MG cells co-transfected with pcDNA empty vector, wild type p38 MAPK, kinase dead p38MAPK, or hyper-active p38 MAPK expression constructs in cells expressing HttQ25 or HttQ103. The analysis revealed that phospho-Hsp27 levels were reduced in extracts from cells co-transfected with kinase dead p38MAPK and showed a complete abrogation of HSP-27 phosphorylation in cells treated with SKF86002. The antibody raised against total HSP-27 was used to detect total HSP-27 levels and actin served as a loading control. B) Expression of p38 MAPK does not directly inhibit the proteasome. Cells were transfected with either wild type p38 MAPK, kinase dead p38MAPK, or pcDNA control plasmids and assayed for their ability to process a peptidylglutamyl- or chymotrypsin-specific fluorogenic substrate. Cells were lysed 48 hours post-transfection and assayed in triplicates. The relative activity of the proteasome was measured 12 hours after the addition of the substrates. PI added to lysates was used as a control to demonstrate the specificity of the PI inhibitor for the chymotrypsin-like activity of the proteasome. Data was normalized to the proteasome activity in lysates from cells transfected with a pcDNA control vector. Experiments were performed in triplicate. Error bars represent standard deviation of the mean.
Found at: doi:10.1371/journal.pcbi.1000944.s001 (0.28 MB TIF)

Figure S2 Distribution of polyQ monomers, oligomers and inclusion bodies. Simulation output from 3 runs of the model showing that the size of the oligomeric pool remains constant even when inclusions form.
Found at: doi:10.1371/journal.pcbi.1000944.s002 (1.26 MB TIF)

Text S1 Model details.
Found at: doi:10.1371/journal.pcbi.1000944.s003 (0.14 MB DOC)

Video S1 Time-lapse imaging of IB formation and UPS dysfunction in U87MG cells transfected with HttQ103YFP-pIRES-mRFP^u. Live cell imaging was initiated at 24 hours post-transfection and images were acquired every 10 minutes. Cells were visualized under white light, and filters that detect YFP or RFP. The brightfield and fluorescence emanating from the YFP and RFP channels were merged to create a movie file. Images were acquired using a 10× objective for a total of 24 hours. At the beginning of the movie HttQ103 is expressed throughout the cell. At 36 hours (the half way point) many cells have formed an inclusion body and have notable accumulation of the red reporter protein (indicative of proteasome inhibition). Note that based on their morphology many cells with IB appear to be viable at the end of the movie.
Found at: doi:10.1371/journal.pcbi.1000944.s004 (5.79 MB MOV)

Video S2 Time-lapse imaging of IB formation and UPS dysfunction in U87MG cells transfected with HttQ103YFP-pIRES-mRFP^u. Live cell imaging was initiated at 24 hours post-transfection and images acquired every 10 minutes. Cells were visualized using filters that detect YFP or RFP. Fluorescent images were merged to create a movie file. Images were acquired using a 10× objective for a total of 24 hours. At the beginning of the movie HttQ103 is expressed throughout the cell. At 36 hours (the half way point) many cells have formed an inclusion body and have notable accumulation of the red reporter protein (indicative of proteasome inhibition). Note that based on their morphology many cells with IB appear to be viable at the end of the movie.
Found at: doi:10.1371/journal.pcbi.1000944.s005 (5.63 MB MOV)

Video S3 Time-lapse imaging of U87MG cells transfected with HttQ103YFP-pIRES-mRFP^u treated with PI 24 hours post-

transfection showing an increase of IB formation and UPS dysfunction. Cells were visualized under white light, and filters that detect YFP or RFP. The brightfield and fluorescence emanating from the YFP and RFP channels were merged to create a movie file. Images were acquired every 10 minutes using a 10× objective for a total of 24 hours. The movie shows rapid and progressive accumulation of the mRFP^u reporter protein (red colour) after the addition of PI. This coincides with the formation of IB at an earlier time point (30 hours). At the conclusion of the movie there are considerably more IB and cell death events as compared to untreated cells (videos S1 and S2).
Found at: doi:10.1371/journal.pcbi.1000944.s006 (6.83 MB MOV)

Video S4 Time-lapse imaging of U87MG cells expressing HttQ103YFP-pIRES-mRFP^u treated with PI 24 hours post-transfection. Cells were visualized using filters that detect YFP or RFP. Fluorescence emanating from the YFP and RFP channels was merged to create a movie which shows an increase of IB formation and UPS dysfunction. Images acquired every 10 minutes using a 10× objective for a total of 24 hours. The movie shows rapid and progressive accumulation of the mRFP^u reporter protein (red colour) after the addition of PI. This coincides with the formation of IB at an earlier time point (30 hours). At the conclusion of the movie there are considerably more IB and cell death events as compared to untreated cells (videos S1 and S2).
Found at: doi:10.1371/journal.pcbi.1000944.s007 (4.26 MB MOV)

Video S5 Time-lapse imaging of U87MG cells transfected with HttQ103YFP-pIRES-mRFP^u treated with BSO 24 hours post-transfection. Treated cells displayed an increase in UPS dysfunction without IB formation. Cells were visualized under white light and filters that detect YFP or RFP. The brightfield and fluorescence emanating from the YFP and RFP channels was merged to create a movie file. Images were acquired every 10 minutes using a 10× objective for a total of 24 hours. Cells treated with BSO display a rapid and progressive accumulation of the mRFP^u reporter protein (red colour), but the frequency of IB formation is not notably different than in untreated cells (videos S1 and S2).
Found at: doi:10.1371/journal.pcbi.1000944.s008 (4.76 MB MOV)

Video S6 Time-lapse imaging of U87MG cells transfected with HttQ103YFP-pIRES-mRFP^u treated with BSO 24 hours post-transfection showing an increase in UPS dysfunction without IB formation. Cells were visualized using filters that detect YFP or RFP. Fluorescence emanating from the YFP and RFP channels was merged to create a movie file. Images were acquired every 10 minutes using a 10× objective for a total of 24 hours. Cells treated with BSO display a rapid and progressive accumulation of the mRFPu reporter protein (red colour), but the frequency of IB formation is not notably different than in untreated cells (videos S1 and S2).
Found at: doi:10.1371/journal.pcbi.1000944.s009 (1.85 MB MOV)

Video S7 Time-lapse imaging of U87MG cells transfected with HttQ103YFP-pIRES-mRFP^u pre-treated with SKF86002 two hours prior to transfection. The movie shows a decrease in IB formation and UPS dysfunction. Live cell imaging was initiated at 24 hours post-transfection, with images acquired every 10 minutes. Cells were visualized under white light, and filters that detect YFP or RFP. The brightfield and fluorescence emanating from the YFP and RFP channels were merged to create a movie file. Images were acquired using a 10× objective for a total of 24 hours. Throughout the movie there are fewer cells with IBs (relative to untreated cells in movies S1 and S2). The levels of the mRFPu reporter protein (red colour) remain lower than in untreated cells and do not increase until late in the movie.
Found at: doi:10.1371/journal.pcbi.1000944.s010 (5.95 MB MOV)

Video S8 Time-lapse imaging of U87MG cells transfected with HttQ103YFP-pIRES-mRFP^u pre-treated with SKF86002 two hours prior to transfection. The movie shows a decrease in IB formation and UPS dysfunction. Live cell imaging was initiated at 24 hours post-transfection and images were acquired every 10 minutes. Cells were visualized using filters that detect YFP or RFP. Fluorescence emanating from the YFP and RFP channels was merged to create a movie file. Images were acquired using a 10× objective for a total of 24 hours. Throughout the movie there are fewer cells with IBs (relative to untreated cells in videos S1 and S2). The levels of the mRFPu reporter protein (red colour) remain lower than in untreated cells and do not increase until late in the movie.
Found at: doi:10.1371/journal.pcbi.1000944.s011 (1.17 MB MOV)

Acknowledgments

We are indebted to Drs. Ian Lorimer and Maria Tsirigotis for useful suggestions and insights. We are grateful to Drs. Ron Kopito, Robert Campbell, Oded Livnah, and Jiahuai Han for the gift of reagents mentioned in the text.

Author Contributions

Conceived and designed the experiments: MYT CJP DAG. Performed the experiments: MYT. Analyzed the data: MYT CJP JW DAG. Contributed reagents/materials/analysis tools: CJP. Wrote the paper: MYT CJP JW DAG.

References

1. Lowe J, Mayer J, Landon M, Layfield R (2001) Ubiquitin and the molecular pathology of neurodegenerative diseases. Adv Exp Med Biol 487: 169–186.
2. Gray DA, Tsirigotis M, Woulfe J (2003) Ubiquitin, proteasomes, and the aging brain. Sci Aging Knowledge Environ 2003: RE6.
3. Bedford L, Hay D, Devoy A, Paine S, Powe DG, et al. (2008) Depletion of 26S proteasomes in mouse brain neurons causes neurodegeneration and Lewy-like inclusions resembling human pale bodies. J Neurosci 28: 8189–8198.
4. Mitra S, Tsvetkov AS, Finkbeiner S (2009) Single neuron ubiquitin-proteasome dynamics accompanying inclusion body formation in huntington disease. J Biol Chem 284: 4398–4403.
5. Arrasate M, Mitra S, Schweitzer ES, Segal MR, Finkbeiner S (2004) Inclusion body formation reduces levels of mutant huntingtin and the risk of neuronal death. Nature 431: 805–810.
6. Woulfe JM (2007) Abnormalities of the nucleus and nuclear inclusions in neurodegenerative disease: a work in progress. Neuropathol Appl Neurobiol 33: 2–42.
7. Ross CA (1997) Intranuclear neuronal inclusions: a common pathogenic mechanism for glutamine-repeat neurodegenerative diseases? Neuron 19: 1147–1150.
8. Firdaus WJ, Wyttenbach A, Giuliano P, Kretz-Remy C, Currie RW, et al. (2006) Huntingtin inclusion bodies are iron-dependent centers of oxidative events. FEBS J 273: 5428–5441.
9. Tsirigotis M, Baldwin RM, Tang MY, Lorimer IA, Gray DA (2008) Activation of p38MAPK contributes to expanded polyglutamine-induced cytotoxicity. PLoS One 3: e2130.
10. Bence NF, Sampat RM, Kopito RR (2001) Impairment of the ubiquitin-proteasome system by protein aggregation. Science 292: 1552–1555.
11. Proctor CJ, Tsirigotis M, Gray DA (2007) An in silico model of the ubiquitin-proteasome system that incorporates normal homeostasis and age-related decline. BMC Syst Biol 1: 17.
12. Ding Q, Dimayuga E, Keller JN (2006) Proteasome regulation of oxidative stress in aging and age-related diseases of the CNS. Antioxid Redox Signal 8: 163–172.

13. Fernandes AF, Bian Q, Jiang JK, Thomas CJ, Taylor A, et al. (2009) Proteasome inactivation promotes p38 mitogen-activated protein kinase-dependent phosphatidylinositol 3-kinase activation and increases interleukin-8 production in retinal pigment epithelial cells. Mol Biol Cell 20: 3690–3699.
14. Ho AK, McNeil L, Terriff D, Price DM, Chik CL (2005) Role of protein turnover in the activation of p38 mitogen-activated protein kinase in rat pinealocytes. Biochem Pharmacol 70: 1840–1850.
15. Proctor CJ, Gray DA (2008) Explaining oscillations and variability in the p53-Mdm2 system. BMC Syst Biol 2: 75.
16. Wyttenbach A, Sauvageot O, Carmichael J, Diaz-Latoud C, Arrigo AP, et al. (2002) Heat shock protein 27 prevents cellular polyglutamine toxicity and suppresses the increase of reactive oxygen species caused by huntingtin. Hum Mol Genet 11: 1137–1151.
17. Passos JF, Nelson G, Wang C, Richter T, Simillion C, et al. (2010) Feedback between p21 and reactive oxygen production is necessary for cell senescence. Mol Syst Biol 6: 347.
18. Sullivan PG, Dragicevic NB, Deng JH, Bai Y, Dimayuga E, et al. (2004) Proteasome inhibition alters neural mitochondrial homeostasis and mitochondria turnover. J Biol Chem 279: 20699–20707.
19. Giuliano P, De Cristofaro T, Affaitati A, Pizzulo GM, Feliciello A, et al. (2003) DNA damage induced by polyglutamine-expanded proteins. Hum Mol Genet 12: 2301–2309.
20. Illuzzi J, Yerkes S, Parekh-Olmedo H, Kmiec EB (2009) DNA breakage and induction of DNA damage response proteins precede the appearance of visible mutant huntingtin aggregates. J Neurosci Res 87: 733–747.
21. Webber JL, Tooze SA (2010) Coordinated regulation of autophagy by p38alpha MAPK through mAtg9 and p38IP. EMBO J 29: 27–40.
22. Ding Q, Dimayuga E, Martin S, Bruce-Keller AJ, Nukala V, et al. (2003) Characterization of chronic low-level proteasome inhibition on neural homeostasis. J Neurochem 86: 489–497.
23. Sarkar S, Krishna G, Imarisio S, Saiki S, O'Kane CJ, et al. (2008) A rational mechanism for combination treatment of Huntington's disease using lithium and rapamycin. Hum Mol Genet 17: 170–178.
24. Ortega Z, Diaz-Hernandez M, Maynard CJ, Hernandez F, Dantuma NP, et al. (2010) Acute polyglutamine expression in inducible mouse model unravels ubiquitin/proteasome system impairment and permanent recovery attributable to aggregate formation. J Neurosci 30: 3675–3688.
25. Hucka M, Finney A, Sauro HM, Bolouri H, Doyle JC, et al. (2003) The systems biology markup language (SBML): a medium for representation and exchange of biochemical network models. Bioinformatics 19: 524–531.
26. Wilkinson D (2006) Stochastic Modelling for Systems Biology Chapman & Hall/CRC Press.
27. Gillespie DT (1977) Exact stochastic simulation of coupled chemical reactions. J Phys Chem 31: 2340–2361.
28. Gillespie CS, Wilkinson DJ, Proctor CJ, Shanley DP, Boys RJ, et al. (2006) Tools for the SBML Community. Bioinformatics 22: 628–629.
29. Kirkwood TB, Boys RJ, Gillespie CS, Proctor CJ, Shanley DP, et al. (2003) Towards an e-biology of ageing: integrating theory and data. Nat Rev Mol Cell Biol 4: 243–249.
30. Le Novere N, Bornstein B, Broicher A, Courtot M, Donizelli M, et al. (2006) BioModels Database: a free, centralized database of curated, published, quantitative kinetic models of biochemical and cellular systems. Nucleic Acids Res 34: D689–691.
31. Turnbull VJ, Storey E, Tarlac V, Walsh R, Stefani D, et al. (2004) Different ataxin-2 antibodies display different immunoreactive profiles. Brain Research 1027: 103–116.
32. Shoghi-Jadid K, Barrio JR, Kepe V, Wu H-M, Small GW, et al. (2005) Imaging b-amyloid fibrils in Alzheimer's disease: a critical analysis through simulation of amyloid fibril polymerization. Nucl Med Biol 32: 337–351.
33. Diaz-Hernandez M, Moreno-Herrero F, Gomez-Ramos P, Moran MA, Ferrer I, et al. (2004) Biochemical, ultrastructural, and reversibility studies on huntingtin filaments isolated from mouse and human brain. J Neurosci 24: 9361–9371.
34. Huang X, Atwood CS, Hartshorn MA, Multhaup G, Goldstein LE, et al. (1999) The Ab peptide of Alzheimer's disease directly produces hydrogen peroxide through metal ion reduction. Biochemistry 38: 7609–7616.
35. Olshina MA, Angley LM, Ramdzan YM, Tang J, Bailey MF, et al. Tracking mutant huntingtin aggregation kinetics in cells reveals three major populations that include an invariant oligomer pool. J Biol Chem 285: 21807–21816.
36. Bence NF, Sampat RM, Kopito RR (2001) Impairment of the ubiquitin-proteasome system by protein aggregation. Science 292: 1552–1555.
37. Garg T, Chang J (2004) 15-deoxy-delta 12, 14-Prostaglandin J2 prevents reactive oxygen species generation and mitochondrial membrane depolarization induced by oxidative stress. BMC Pharmacol 4: 6.